



POLITECHNIKA KRAKOWSKA
im. Tadeusza Kościuszki
WYDZIAŁ INŻYNIERII I TECHNOLOGII CHEMICZNEJ

**PRACA
DOKTORSKA**

**Katalizator CrO_x/SiO₂ – modelowanie form
powierzchniowych oraz studia nad mechanizmem
polimeryzacji etylenu**

mgr inż. Maciej Gierada

PROMOTOR: **dr hab. inż. Jarosław Handzlik, prof. PK**

KRAKÓW 2018



Praca zrealizowana została w Katedrze Technologii Organicznej i Procesów Rafineryjnych Instytutu Chemii i Technologii Organicznej na Wydziale Inżynierii i Technologii Chemicznej Politechniki Krakowskiej im. Tadeusza Kościuszki. W części była ona finansowana z grantu NCN PRELUDIUM 10 nr UMO-2015/19/N/ST4/00007 „Od prekursora tlenkowego do centrum aktywnego – teoretyczne badania mechanizmu polimeryzacji etylenu na katalizatorze Phillipsa”, którego byłem/jestem kierownikiem jak również w ramach dotacji ze środków MNiSW na badania naukowe w ramach działalności statutowej, temat nr C-2/294/2016/DS-M „Badanie mechanizmu redukcji katalizatora Phillipsa”

Obliczenia kwantowo-chemiczne zostały wykonane z zastosowaniem Infrastruktury PL-Grid – Polska (granty mg1-mg5, jh1-jh4), CYFRONET AGH – Polska (granty MNiSW/IBM_BC_HS21/PK/003/2013 i MNiSW/IBM_BC_HS21/PK/037/2014)) oraz GENCI-[CCRT/CINES/IDRIS] – Francja (grant 2015-[x2015082022]). Część obliczeń prowadzona była również na serwerze obliczeniowym znajdującym się na Wydziale Inżynierii i Technologii Chemicznej Politechniki Krakowskiej. Został on zakupiony ze środków finansowych grantu NCN UMO-2015/19/N/ST4/00007.



Spis treści

1. Streszczenie.....	4
2. Abstract.....	5
3. Wstęp.....	6
4. Cel i zakres pracy doktorskiej.....	11
5. Lista publikacji będących podstawą pracy doktorskiej.....	12
6. Opis dokonania badawczego	13
6.1 Modelowanie struktury form tlenkowych chromu na powierzchni amorficznej krzemionki [D2]	15
6.2. Studia nad mechanizmem polimeryzacji etylenu [D3, D4]	19
6.3. Badanie mechanizmu redukcji katalizatora Phillipsa [D5]	25
7. Podsumowanie i wnioski.....	32
8. Literatura.....	34
9. Pełne teksty artykułów będących podstawą pracy doktorskiej.....	39
Artykuł D1.....	39
Artykuł D2.....	46
Artykuł D3.....	61
Artykuł D4.....	77
Artykuł D5.....	93
10. Deklaracje współautorów	105
11. Wykaz dorobku naukowego.....	110

1. Streszczenie

Katalizator Phillipsa (CrO_x/SiO₂) to jeden z najczęściej stosowanych w przemyśle układów katalitycznych umożliwiających otrzymanie polietylenu wysokiej gęstości (HDPE). Pomimo wielu lat intensywnych prac badawczych wiele kwestii związanych z jego naturą chemiczną nie zostało w pełni zrozumianych. Struktura form tlenkowych chromu na powierzchni utlenionego i zredukowanego katalizatora nie jest jednoznacznie zdefiniowana. Ponadto, nieznany jest mechanizm redukcji katalizatora oraz powstawania centrów aktywnych polimeryzacji etylenu. Celem badań teoretycznych (DFT) prowadzonych w ramach tej pracy doktorskiej było poznanie tych mechanizmów oraz struktury form tlenkowych katalizatora CrO_x/SiO₂.

W pierwszej części pracy badano strukturę form tlenkowych chromu na powierzchni amorficznej krzemionki. Otrzymane wyniki wskazują, że formy dimeryczne są mniej stabilne termodynamicznie w porównaniu do form monomerycznych, stąd te drugie powinny dominować na powierzchni badanego katalizatora. Redukcja niektórych formy monomerycznych może przebiegać z wytworzeniem formy Cr(IV), niemniej, w większości przypadków prowadzi do Cr(II). Cr(III) może natomiast powstawać na skutek hydrolizy wiązań Cr-O-Si form powierzchniowych lub podczas hydratacji potencjalnych form dimerycznych.

W kolejnej części pracy badano mechanizm polimeryzacji etylenu w obecności układu CrO_x/SiO₂. Analizowano potencjalne mechanizmy generowania centrów aktywnych z udziałem form Cr(II), Cr(III) oraz Cr(V), w tym kilka nowych, niepostulowanych w literaturze. W przypadku form Cr(II) najniższe bariery aktywacji związane są z powstawaniem cyklicznych produktów przejściowych. Dla form Cr(III) wyznaczone bariery analogicznych przekształceń są wyższe. Mechanizm polimeryzacji zaproponowany w oparciu o formę Cr(III)-OH, do tej pory nie postulowaną w literaturze, charakteryzuje się najniższą całkowitą barierą aktywacji. W pierwszym etapie tego mechanizmu dochodzi do wytworzenia centrum aktywnego Cr(III)-CH=CH₂. Analizowano również możliwą rolę rodnikowych defektów powierzchniowych w generowaniu centrów aktywnych oraz w przekształcaniu form monomerycznych Cr(II) do Cr(III).

W ostatniej części pracy badano różne potencjalne mechanizmy redukcji katalizatora CrO_x/SiO₂ etylenem. Otrzymane wyniki wskazują, że najkorzystniejsza kinetycznie jest redukcja formy diokso Cr(VI) przebiegająca z wytworzeniem centrum Cr(II) oraz dwóch cząsteczek HCHO. Formaldehyd może następnie ulegać utlenieniu do CO₂ i H₂O. Mniej prawdopodobne jest jego przekształcenie do estru.

2. Abstract

The Phillips CrO_x/SiO₂ catalyst is one of the most commonly used systems in the industrial production of high-density polyethylene (HDPE). Despite many years of intensive investigations, several aspects about its chemical nature still remains unknown. Among others, structure of the chromium oxide species on the surface of the oxidized and reduced catalyst is not well defined. Likewise, a mechanism of the catalyst reduction and active site formation is the subject of an ongoing debate. The goal of this PhD thesis was to establish these mechanisms and to determine structure of the chromium oxide species supported on the amorphous silica using theoretical approach (DFT).

In the first part of this thesis, a molecular structure of the CrO_x/SiO₂ catalyst was studied. It was found that dimeric species are less thermodynamically stable than the monomeric ones. Hence, the latter should dominate on the catalyst surface. Some monomeric Cr(VI) oxide species can be reduced to Cr(IV), however, in general, reduction leads to Cr(II). Cr(III) can be formed as a result of Cr-O-Si bond hydrolysis or during hydration of the potential dimeric Cr species.

In the next part of the thesis, a large number of different mechanisms of the active sites formation were calculated to find the most probable ones. Among others, mechanisms involving Cr(II), Cr(III) and Cr(V) were analyzed. Assuming Cr(II) species as the precursors of the active sites, it was showed that the lowest activation barriers are associated with formation of cyclic intermediates. For Cr(III), the corresponding computed barriers are higher. According to the obtained results, the most kinetically accessible pathway of ethylene polymerization can start from the Cr(III)-OH oxide precursors and involve Cr(III)-CH=CH₂ formation. The potential role of radical surface defects was considered in Cr(II) to Cr(III) transformation. It was concluded that these surface defects may also facilitate the active sites formation.

The last part of the PhD thesis is focused on the mechanisms of the Phillips catalyst reduction by ethylene. The obtained results indicate that reduction involving dioxo Cr(VI) oxide species and resulting in formation of Cr(II) together with two HCHO molecules is the most probable pathway of the reaction. Formaldehyde can be subsequently oxidized to CO₂ and H₂O. The pathway leading to ester formation is less likely, as evidenced by the calculated activation barriers.

3. Wstęp

Tlenkowe formy chromu osadzone na powierzchni amorficznej krzemionki (CrO_x/SiO₂) stanowią efektywny układ katalityczny powszechnie stosowany w przemyśle chemicznym. Tego typu katalizator wykazuje aktywność między innymi w reakcji dehydroizomeryzacji i odwodornienia alkanów,^{1–4} utleniającego odwodornienia węglowodorów w obecności O₂^{5,6} oraz CO₂,^{7–9} jak również w licznych reakcjach selektywnego utleniania.^{10–14} Niemniej, układ CrO_x/SiO₂ znalazł główne zastosowanie jako katalizator niskociśnieniowej polimeryzacji etylenu prowadzącej do otrzymania polietylenu wysokiej gęstości (*ang. high-density polyethylene* – HDPE), polimeru, który jest powszechnie stosowany m.in. do produkcji opakowań.^{1,10,15–22} W kontekście wspomnianej reakcji układ ten zwykle nazywać się katalizatorem Phillipsa.¹⁸ Szacuje się, że 40–50% światowej produkcji HDPE jest związane z tym katalizatorem,²³ przy rocznej produkcji liniowego polietylenu (HDPE i LLDPE – *ang. linear low-density polyethylene*) wynoszącej około $60 \cdot 10^9$ kg.²⁴ Pokazuje to, jak ważny jest to układ katalityczny.

Powszechnie zastosowanie katalizatora Phillipsa w polimeryzacji etylenu jest związane z tym, że w przeciwieństwie do innych układów aktywnych w tej reakcji (np. katalizatory Zieglera-Natty lub układy metalocenowe) nie wymaga on obecności kokatalizatorów.^{10,16–20,25,26} Co więcej, jego preparatyka jest prosta. W trakcie osadzania fazy aktywnej na nośniku (najczęściej metodą impregnacji) dochodzi do reakcji pomiędzy grupami silanolowymi obecnymi na powierzchni amorficznej krzemionki a źródłem chromu, np. octanem chromu(III).^{10,17,25} Po przeprowadzeniu wysokotemperaturowej kalcynacji w atmosferze utleniającej na powierzchni obecne są głównie zdyspergowane formy Cr(VI).^{4,8,10,17,27–31} Dodatkowo, podczas tego etapu dochodzi do dehydroksylacji powierzchni na skutek kondensacji grup silanolowych. W kolejnym etapie, formy Cr(VI) przekształca się w aktywne katalitycznie zredukowane formy tlenkowe Cr, będące właściwymi prekursorami centrów aktywnych. Można to osiągnąć na dwa sposoby, które pod względem jakości otrzymywanej polietylenu są równoważne.²⁵

- (i) Zsyntezowany układ katalityczny poddaje się reakcji z etylenem w około 100°C. Po tzw. okresie indukcji, kiedy następuje redukcja form Cr(VI) i generowane są centra aktywne, rozpoczyna się polimeryzacja. Podczas tego etapu powstają również ubocznie tlenowe produkty transformacji etylenu. Ta droga przemian jest charakterystyczna dla procesów przemysłowych.

(ii) Zsyntezowany układ katalityczny poddaje się wstępnej redukcji z zastosowaniem CO, co prowadzi głównie do powstania form Cr(II). Tak wstępnie zredukowany katalizator wykazuje aktywność w polimeryzacji etylenu w temperaturze pokojowej, a okres indukcji ulega znaczącemu skróceniu. Jest to częsty sposób postępowania w badaniach laboratoryjnych.

Od odkrycia właściwości katalitycznych układu $\text{CrO}_x/\text{SiO}_2$ w latach 50. XX wieku³² wiele pracy włożono w ustalenie struktury form powierzchniowych chromu oraz mechanizmu polimeryzacji etylenu. Na powierzchni katalizatora obecne są różne formy Cr: utlenione – Cr(VI)^{1–6,8,10,17,27–30,33–35} oraz zredukowane: Cr(II), Cr(III) i niewielkie ilości Cr(V).^{1,3,4,6,8,10,11,17,29,36–40} Na podstawie badań z zastosowaniem metody UV-Vis DRS^{7–10,17,29,40–46} postuluje się, że Cr(VI) występuje na powierzchni w formie monomerycznej, dimerycznej i polimerycznej. Przy małych zawartościach chromu formy monomeryczne dominują na powierzchni lub są jedynymi typami centrów.^{5,6,13,14,17,27–30,43,47–50} Pośród form monomerycznych Cr(VI) wyróżnia się dominujące formy diokso Cr(VI)^{1–6,8,10,17,27–30,33,34} oraz będące w mniejszości formy monoookso Cr(VI).^{27–29,33–35} Te ostatnie formy często były ignorowane w badaniach układu $\text{CrO}_x/\text{SiO}_2$, jednak nie można wykluczyć, że mogą one odgrywać rolę w rozważanych przemianach. Ostatnio jednak pokazano,⁵¹ że wyniki badań spektroskopowych układu Cr(VI)/ SiO_2 mogą być wy tłumaczone wyłącznie w oparciu o formę diokso Cr(VI).

Dotychczasowe badania teoretyczne dotyczące struktury form powierzchniowych układu $\text{CrO}_x/\text{SiO}_2$ ograniczone były głównie do modelowania form Cr(VI) i przy założeniu monomerycznej struktury centrum. Guesmi i Tielens³⁴ pokazali, że na powierzchni uwodnionej można wyróżnić 3 rodzaje struktur. W niskich temperaturach stabilna jest hydroksylowa forma diokso Cr(VI). W wyższych temperaturach, typowych dla warunków pracy tego katalizatora, najstabilniejsze są formy diokso Cr(VI) oraz monoookso Cr(VI). W innej pracy³³ modelowano powierzchnię tego katalizatora m.in. symulując warunki wysokotemperaturowej kalcynacji. Otrzymane wyniki wskazują, że tetraedryczna forma diokso Cr(VI) jest stabilniejsza termodynamicznie od formy monoookso Cr(VI). Niemniej, stabilność różnych struktur Cr(VI) zależy od ich lokalizacji na powierzchni krzemionki.

Po wytworzeniu zredukowanych form Cr proces polimeryzacji etylenu następuje bardzo szybko. Ponadto, szacuje się, że zazwyczaj nie więcej niż 10% fazy zawierającej Cr jest aktywna katalitycznie,^{17,23} chociaż większe wartości (10 – 30%) są również postulowane, w

zależności od zastosowanej metody analizy i składu katalizatora.⁵² Stąd, jednocześnie badania eksperymentalne mechanizmu redukcji i polimeryzacji stanowią duże wyzwanie.^{17,23}

Zaskakująco niewiele opublikowano badań dotyczących samego mechanizmu redukcji katalizatora Phillipsa etylenem. Wczesne prace eksperymentalne Bakera i Carricka pokazały,⁵³ że podczas reakcji Cr(VI) z różnymi olefinami powstają związki karbonylowe. Zaproponowali oni również mechanizm, który przebiega poprzez pośredni kompleks dioksachromacyklopentanowy. W przypadku zastosowanie etylenu, jednym z postulowanych produktów tlenowych jest formaldehyd.^{53–55} Niemniej, inne prace wskazują na estry,^{56–58} aldehydy/ketony⁵⁶ lub oligomery etylenu.^{54,55} Produkty utleniania etylenu mogą pozostać zaadsorbowane na powierzchni i wpływać na aktywność katalizatora w polimeryzacji etylenu.^{17,23,58–60} W innej pracy pokazano,⁵⁶ że produkty tlenowe mogą finalnie prowadzić do powstawania CO_2 i H_2O , jednak w temperaturach dużo wyższych niż typowe dla procesu polimeryzacji.

Na uwagę zasługuje fakt, że w większości mechanizmów polimeryzacji etylenu postulowanych do tej pory w literaturze zakłada się *a priori* istnienie na powierzchni krzemionki izolowanych form tlenkowych Cr(II), Cr(III) lub ich alkilowych/winylowych pochodnych, nie tłumacząc reakcji prowadzących do ich wytworzenia z form Cr(VI) obecnych na powierzchni katalizatora po jego przygotowaniu.

Ponieważ Cr(II) dominuje na powierzchni wstępnie zredukowanego katalizatora,^{1,4,10,17,20,22,23,41} forma ta była powszechnie postulowana jako prekursor centrów aktywnych.^{17,61–73} Zaproponowano liczne mechanizmy z jej udziałem, zachodzące z wytworzeniem acyklicznego^{17,64,65,67,71,72} (w szczególności karbenowego^{17,64,66–71}) lub cyklicznego^{17,61–64,71,73} centrum aktywnego, gdzie Cr występuje formalnie na +2 lub +4 stopniu utlenienia. Zaproponowano również mechanizm uwzględniający dimeryczną formę Cr(II),⁷³ jednak ta propozycja wydaje się być mniej prawdopodobna, biorąc pod uwagę wysoką aktywność katalizatorów o małej zawartości Cr.⁷⁴ Forma Cr(III), obecna na powierzchni w szczególności gdy redukcję prowadzi się z zastosowaniem H_2 lub C_2H_4 ,^{1–4,6–8,10,11,17,29,36,40} również była proponowana jako centrum aktywne.^{65,75–85} Na szczególną uwagę zasługują najnowsze prace,^{65,76,77,85} które ukazały się równolegle do publikacji przedstawiających wyniki moich badań, gdzie autorzy proponują homolityczny rozpad wiązania Cr-C jako potencjalny mechanizm inicjacji. Propozycje te są o tyle interesujące, iż dotychczas zakładano, że mechanizm polimeryzacji etylenu na katalizatorze Phillipsa jest podobny do mechanizmu na katalizatorach Zieglera-Natty, w tym w szczególności, żaden z etapów nie ma charakteru reakcji rodnikowej. Niemniej, jak do tej pory, żaden z zaproponowanych mechanizmów nie

jest powszechnie zaakceptowany ani nie wydaje się być jednoznacznie udowodniony. Warto zaznaczyć, że większość z nich została zaproponowana na drodze analizy danych eksperymentalnych w oparciu o dowody nie odnoszące się bezpośrednio do struktury centrów aktywnych. Najnowsze prace teoretyczne sugerują,^{63–65,81,82,84} że w wielu przypadkach bariera aktywacji dla etapu inicjacji lub propagacji jest zbyt wysoka, stąd mechanizmy te nie mogą tłumaczyć obserwacji eksperymentalnych. W niektórych przypadkach, szybkość reakcji terminacji jest większa niż propagacji, stąd oligomery etylenu powinny być głównym produktem, a nie polimer. Ponadto, w niektórych mechanizmach terminacja wymaga ponownej inicjacji, co często wiąże się z pokonaniem dużej bariery aktywacji. Widać więc, że dotychczasowy stan wiedzy w zakresie reaktywności katalizatora $\text{CrO}_x/\text{SiO}_2$ jest niepełny i wciąż budzi wiele wątpliwości.

W ostatnich latach obserwuje się znaczący wzrost zainteresowania katalizatorem $\text{CrO}_x/\text{SiO}_2$, co potwierdza liczba artykułów w tym temacie^{12,24,31,36,51,56–58,64,65,76,77,82–95} autorstwa czołowych światowych zespołów badawczych, opublikowanych w latach 2015–2018 w najlepszych czasopismach naukowych z dziedziny katalizy i pokrewnych. Dowodzi to, że tematyka badań prowadzonych w ramach pracy doktorskiej jest bardzo aktualna.

Jako że badania eksperymentalne nie dostarczają jednoznacznych informacji o naturze katalizatora Phillipsa, bardzo pomocne okazują się być badania teoretyczne. Jak widać również z wymienionych wyżej przykładów, prace te mogą dostarczyć komplementarnych informacji o strukturze i reaktywności form powierzchniowych, nieosiągalnych przy zastosowaniu metod eksperymentalnych. Często również ułatwiają interpretację danych doświadczalnych. Mogą być zatem traktowane jako uzupełnienie badań eksperymentalnych, przy czym ważne jest, aby nie traktować nadzwiednie jednego podejścia wobec drugiego. Modelowanie komputerowe umożliwia bezpośrednią charakterystykę mechanizmów reakcji, gdyż każdy etap badanego procesu może być analizowany osobno i niezależnie, co często jest nieosiągalne w przypadku badań eksperymentalnych.

Teoretyczne badania procesów zachodzących na powierzchni katalizatorów heterogenicznych wciąż stanowią duże wyzwanie koncepcyjne, gdyż wymagają zastosowania uproszczeń zarówno na gruncie teorii jak i stosowanego modelu powierzchni. Wyróżnia się dwa różne sposoby modelowania powierzchni ciał stałych. W pierwszym z nich stosuje się tzw. modele klasterowe.^{20,63–65,71–73,82,85,95,96} W podejściu tym wycina się skończony fragment układu, który ma reprezentować powierzchnię. Oznacza to, że zakłada się *a priori* lokalny charakter oddziaływań w pobliżu centrum aktywnego. Pewnym problemem jest tutaj opis atomów peryferyjnych. Najczęściej zerwane wiązania wysyca się atomami wodoru. Modele

klasterowe są stosunkowo często stosowane w badaniach mechanizmów reakcji zachodzących na powierzchni katalizatorów heterogenicznych. Warto jednak zaznaczyć, iż w przeszłości, a w szczególności w kontekście katalizatora CrO_x/SiO₂, zwykle stosowano bardzo małe modele klasterowe, zbudowane z co najwyżej kilku atomów krzemu.^{20,63–65,71–73,82,85,95,96} Prosty model klasterowy nie oddaje jednak w pełni złożoności powierzchni oraz heterogeniczności centrów aktywnych.^{17,23}

Inny sposób teoretycznego opisu powierzchni ciał stałych opiera się na zastosowaniu modeli periodycznych.^{84,94,97–99} W tym przypadku, definiuje się komórkę elementarną, którą następnie powiela się z zastosowaniem periodycznych warunków brzegowych. Komórka elementarna musi być odpowiednio duża, aby uniknąć sztucznego oddziaływania pomiędzy badaną formą powierzchniową a jej periodycznym obrazem. Ponadto, rozmiar komórki elementarnej musi być również tak dobrany, aby modelowana powierzchnia nie była zbyt powtarzalna. Zaletą tego typu opisu układu jest uwzględnienie oddziaływań dalekozasięgowych i brak problemu z atomami peryferyjnymi. Jak dotąd, tylko w kilku pracach^{33,34,84,94} zastosowano modele periodyczne do badania układu CrO_x/SiO₂.

W związku z sukcesywnym wzrostem mocy obliczeniowej komputerów możliwe staje się coraz dokładniejsze badanie teoretyczne złożonych układów. W przypadku badania heterogenicznych układów katalitycznych zastosowanie teorii funkcjonału gęstości (*ang. density functional theory - DFT*) jest obecnie standardem, gdyż metody DFT dostarczają wyniki o akceptowalnej dokładności przy umiarkowanym zapotrzebowaniu na moc obliczeniową. Oprócz odpowiednio dobranej metody istotny wpływ ma również model powierzchni stosowany w symulacjach komputerowych. W kontekście katalizatora CrO_x/SiO₂ dąży się do tego, aby stosowane modele uwzględniały heterogeniczność centrów aktywnych lub ich prekursorów, tak jak ma to miejsce w przypadku rzeczywistego katalizatora.^{17,23,33,34} Można to osiągnąć stosując realistyczne modele amorficznej krzemionki.^{33,34} Takim modelem jest na przykład model periodyczny opracowany przez Tielensa i współpracowników¹⁰⁰ z późniejszymi modyfikacjami.^{33,101}

Jak przedstawiono wcześniej, dotychczasowe badania w zakresie ustalenia struktury oraz reaktywności katalizatora Phillipsa nie przyniosły jednoznacznych wyników. Wiele kwestii związanych z jego naturą chemiczną nadal budzi kontrowersje. W literaturze można znaleźć pewną liczbę prac teoretycznych^{20,63,96,64,65,71–73,82,85,95} dotyczących struktury zredukowanych form powierzchniowych chromu, jednak są one ograniczone do niewielkich i mało realistycznych modeli. Ponadto, nie analizowano dotychczas względnej stabilności form monomerycznych, dimerycznych i ewentualnie polimerycznych. W kontekście redukcji

katalizatora Phillipsa etylenem, tylko w jednej pracy¹⁰² teoretycznej badany jest mechanizm reakcji, przy czym autorzy ograniczyli się jedynie do analizy termodynamiki procesu (zmiana entalpii reakcji). Mechanizm powstawania centrów aktywnych polimeryzacji etylenu nadal nie jest dobrze poznany, pomimo intensywnych badań prowadzonych w tym temacie przez różne zespoły.

4. Cel i zakres pracy doktorskiej

Celem mojej pracy doktorskiej była analiza struktury form powierzchniowych układu CrO_x/SiO₂, ustalenie najbardziej prawdopodobnych mechanizmów powstawania centrów aktywnych polimeryzacji etylenu oraz ustalenie mechanizmu redukcji katalizatora Phillipsa etylenem. Zostało to zrealizowane poprzez wykonanie badań teoretycznych z zastosowaniem teorii funkcjonału gęstości.

Poniżej wyszczególnię w punktach zakres pracy doktorskiej:

1. Badanie struktury monomerycznych i dimerycznych form tlenkowych układu CrO_x/SiO₂ na różnym stopniu utlenienia z zastosowaniem zawansowanych periodycznych i klastrowych modeli amorficznej krzemionki oraz analiza ich redukcji z uwzględnieniem CO i H₂ jako czynników redukujących.
2. Badanie mechanizmu polimeryzacji etylenu (etap inicjacji, propagacji oraz terminacji) przy uwzględnieniu różnych form tlenkowych Cr jako prekursorów centrów aktywnych.
3. Badanie mechanizmu redukcji katalizatora Phillipsa etylenem i CO oraz analiza dalszych przekształceń ubocznych produktów tlenowych.

5. Lista publikacji będących podstawą pracy doktorskiej

Nr	Dane bibliograficzne ^a	Liczba cytowań (Scopus) ^b
D1	M. Gierada, ✉ J. Handzlik, <i>Zastosowanie oraz struktura form powierzchniowych układów katalitycznych Cr/SiO_2 Przem. Chem.</i> 94(6) (2015) 900-905, (IF = 0.399) http://dx.doi.org/10.15199/62.2015.6.8	0
D2	M. Gierada, P. Michorczyk,✉ F. Tielens, J. Handzlik,✉ <i>Reduction of chromia-silica catalyst: A molecular picture</i> J. Catal. 340 (2016) 122-135, (IF = 7.354) http://dx.doi.org/10.1016/j.jcat.2016.04.022	10
D3	A. Chakrabarti, M. Gierada , J. Handzlik, I. E. Wachs,✉ <i>Operando Molecular Spectroscopy During Ethylene Polymerization by Supported $\text{CrO}_x/\text{SiO}_2$ Catalysts: Active Sites, Reaction Intermediates, and Structure-Activity Relationship</i> Top. Catal. 59 (2016) 725-739, (IF = 2.355) http://dx.doi.org/10.1007/s11244-016-0546-6	13
D4	M. Gierada , J. Handzlik,✉ <i>Active sites formation and their transformations during ethylene polymerization by the Phillips $\text{CrO}_x/\text{SiO}_2$ catalyst</i> , J. Catal. 352 (2017) 314-328, (IF = 7.354) http://dx.doi.org/10.1016/j.jcat.2017.05.025	6
D5	M. Gierada , J. Handzlik,✉ <i>Computational insights into reduction of the Phillips $\text{CrO}_x/\text{SiO}_2$ catalyst by ethylene and CO</i> , J. Catal. 359 (2018) 261-271 (IF = 6.844) https://doi.org/10.1016/j.jcat.2018.01.014	0

^a IF z roku publikacji

^b dane na 28 V 2018

6. Opis dokonania badawczego

Cykl prac [**D1-D5**] pt. „*Katalizator $\text{CrO}_x/\text{SiO}_2$ – modelowanie form powierzchniowych oraz studia nad mechanizmem polimeryzacji etylenu*” stanowi podsumowanie moich kilkuletnich badań realizowanych w ramach pracy doktorskiej, której promotorem jest dr hab. inż. Jarosław Handzlik, prof. PK. W odróżnieniu od pełnych tekstów publikacji, informacje zawarte w niniejszym opracowaniu zawierają najważniejsze wyniki i skupiają się wyłącznie na badaniach wykonanych przeze mnie. Wszystkie prace (z wyjątkiem [**D1**]) są rozbudowane o informacje uzupełniające (*Supporting/Supplementary Data*), gdzie znajdują się dodatkowe szczegóły, nie uwzględnione w głównym tekście artykułów lub w tym opracowaniu. Oświadczenia współautorów o ich wkładzie w powstanie każdej z tych prac znajdują się w rozdziale 10 niniejszego opracowania.

Pierwsza praca [**D1**] to przegląd literatury, w którym znajdują się informacje na temat zastosowania układu $\text{CrO}_x/\text{SiO}_2$ oraz struktury form powierzchniowych chromu. Z perspektywy czasu informacje zawarte w pracy [**D1**] są niepełne, ze względu na ukazanie się kilku nowych, ważnych prac. Ponadto, nie ma tam informacji na temat mechanizmu redukcji katalizatora Phillipsa oraz mechanizmu polimeryzacji etylenu. Informacje te zostały uwzględnione w rozdziale 3 niniejszego opracowania.

Kolejna praca [**D2**] zawiera wyniki dotyczące struktury form powierzchniowych układu $\text{CrO}_x/\text{SiO}_2$. W pracy tej analizowałem stabilność termodynamiczną form monomerycznych i dimerycznych chromu, zarówno utlenionych jak i zredukowanych. Wykonane przeze mnie obliczenia teoretyczne zostały uzupełnione o materiał eksperymentalny, będący efektem współpracy z dr hab. inż. P. Michorczykiem, prof. PK (*Politechnika Krakowska*).

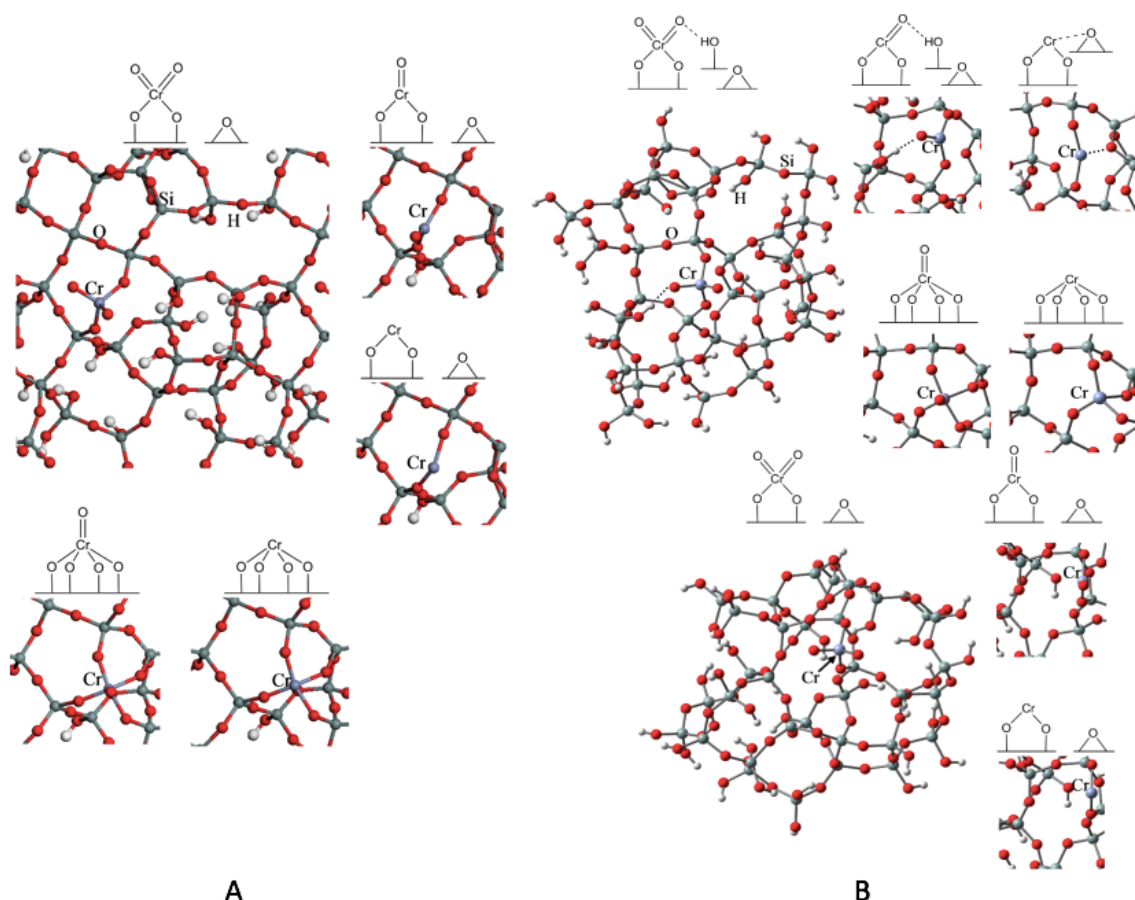
Dominującą częścią pracy [**D3**] jest materiał eksperymentalny, będący wynikiem prac zespołu prof. I.E. Wachsa (*Lehigh University*), z którym miałem przyjemność współpracować. Niemniej, w artykule tym znajdują się również moje wstępne wyniki obliczeń dotyczące mechanizmu polimeryzacji etylenu na katalizatorze Phillipsa. W szczególności, po raz pierwszy zaproponowane zostały dwa nowe mechanizmy reakcji, w tym jeden uwzględniający formę Cr(III) dotychczas niepostulowaną w literaturze.

Kolejna praca [**D4**] jest w całości pracą teoretyczną. Znajduje się w niej analiza licznych mechanizmów polimeryzacji etylenu na katalizatorze $\text{CrO}_x/\text{SiO}_2$. Dzięki przeprowadzeniu kompleksowych studiów teoretycznych możliwe było wskazanie najbardziej prawdopodobnych mechanizmów spośród wszystkich do tej pory zaproponowanych, zarówno w literaturze jak i przeze mnie.

W pracy [D5] zawarte zostały wyniki moich badań, w których przeanalizowałem liczne ścieżki redukcji katalizatora Phillipsa etylenem prowadzące do powstawania różnych ubocznych produktów tlenowych. Badałem również dalsze transformacje tych ostatnich. Dodatkowo, w pracy tej zaproponowany został mechanizm redukcji katalizatora z zastosowaniem CO. Praca ta jest pierwszym opracowaniem teoretycznym, w którym policzone zostały mechanizmy redukcji katalizatora Phillipsa, przy czym większość z nich została zaproponowana po raz pierwszy.

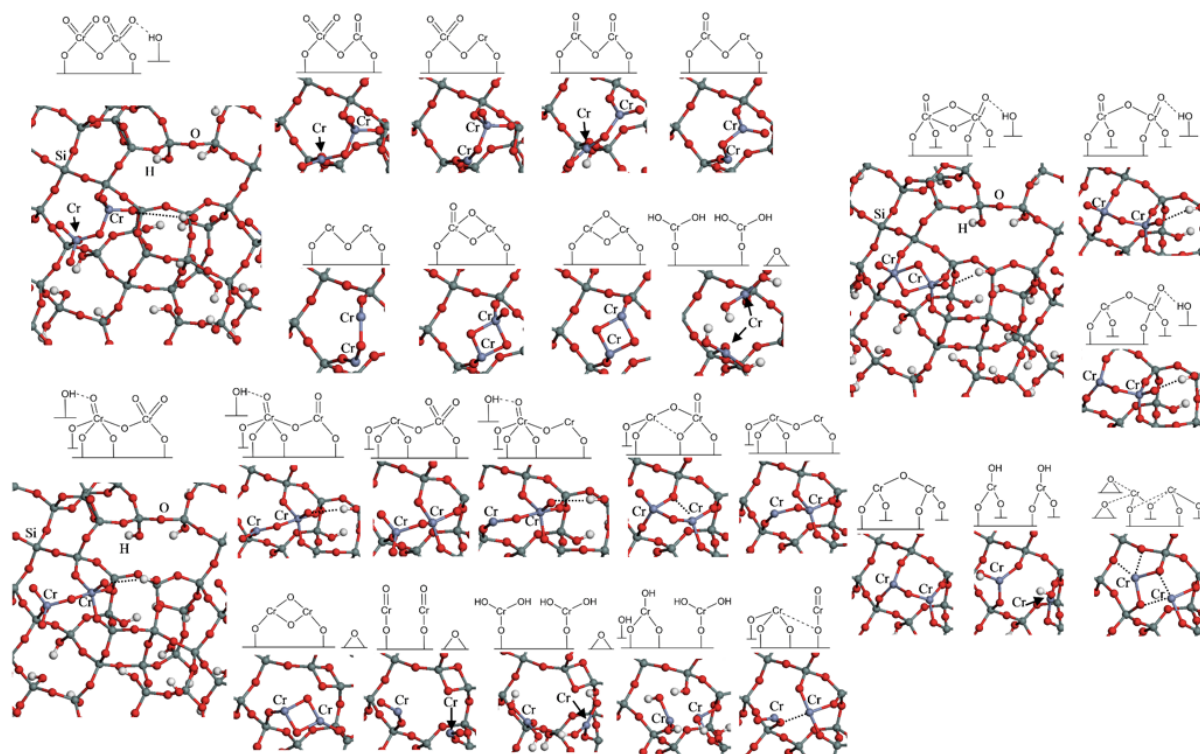
6.1 Modelowanie struktury form tlenkowych chromu na powierzchni amorficznej krzemionki [D2]

Celem badań opisanych w pracy [D2] była ocena stabilności termodynamicznej różnych struktur Cr na powierzchni amorficznej krzemionki, analiza reakcji redukcji form utlenionych do zredukowanych oraz ich hydrolizy. W obliczeniach zastosowano zaawansowane modele periodyczne i klasterowe na bazie modelu amorficznej krzemionki opracowanego przez Tielensa i współpracowników.¹⁰⁰ Monomeryczne struktury Cr(VI) są efektem wcześniejszych prac³³ i zostały zamieszczone tylko celem porównania otrzymanych wyników. Posłużyły one również do otrzymania odpowiednich form zredukowanych. W obliczeniach stosowano funkcjonał PW91¹⁰³ oraz bazy def2-SVP i def2-TZVPP.¹⁰⁴ Obliczenia przeprowadzono z użyciem programu Gaussian 09¹⁰⁵ i VASP 5^{106–108}. Szczegółowe informacje na temat stosowanej metodyki obliczeń znajdują się w pracy [D2].



Rys. 1 Przykładowe struktury form monomerycznych układu $\text{CrO}_x/\text{SiO}_2$ (A) – obliczenia periodyczne (B) obliczenia klasterowe [D2]. Modele Cr(VI) zaczerpnięto z pracy.³³

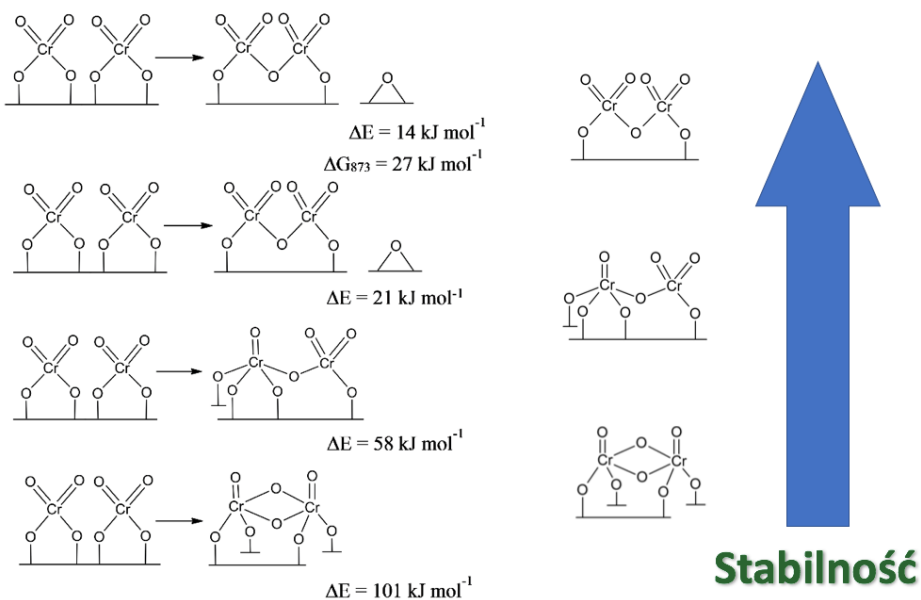
Przykładowe zoptymalizowane struktury form monomerycznych i dimerycznych układu $\text{CrO}_x/\text{SiO}_2$ zostały zaprezentowane odpowiednio na Rys. 1 i 2.



Rys. 2 Przykładowe struktury form dimerycznych układu $\text{CrO}_x/\text{SiO}_2$ – obliczenia periodyczne [D2].

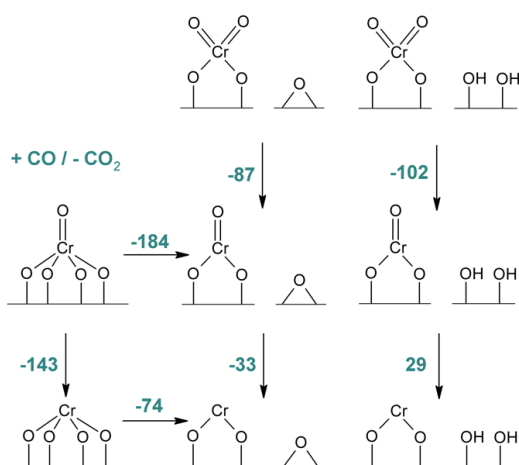
Zarówno w przypadku form monomerycznych jak i dimerycznych długość wiązania $\text{Cr}=\text{O}$ nie zmienia się w zależności od stopnia utlenienia Cr. Zaobserwowano natomiast korelację pomiędzy stopniem utlenienia Cr a długością wiązania $\text{Cr}-\text{OSi}$. Im niższy stopień utlenienia Cr, tym to wiązanie jest dłuższe. Otrzymane wyniki dobrze zgadzają się z wcześniejszymi sugestiami pojawiającymi się w literaturze^{16,17,42} oraz są zgodne z danymi EXAFS dla Cr(VI) ^{19,30} oraz Cr(II) .¹⁰⁹

Analiza stabilności różnych form tlenkowych Cr pozwoliła na stwierdzenie, że formy dimeryczne są mniej stabilne termodynamicznie od form monomerycznych (Rys. 3), stąd te ostatnie powinny dominować na powierzchni katalizatora. Wyniki te są zgodne z wieloma pracami eksperymentalnymi,^{17,28–30,48} ale kontrastują z innymi.^{10,45} Otrzymane wyniki mają istotne znaczenie w kontekście debaty na temat struktury molekularnej katalizatora $\text{CrO}_x/\text{SiO}_2$.^{10,17,28–30,43,45,48}



Rys. 3 Względne wartości energii (ΔE) i energii Gibbsa w $T = 873$ K (ΔG_{873}) dla monomerycznych i dimerycznych form Cr(VI) na krzemionce (obliczenia periodyczne i klasterowe) [D2].

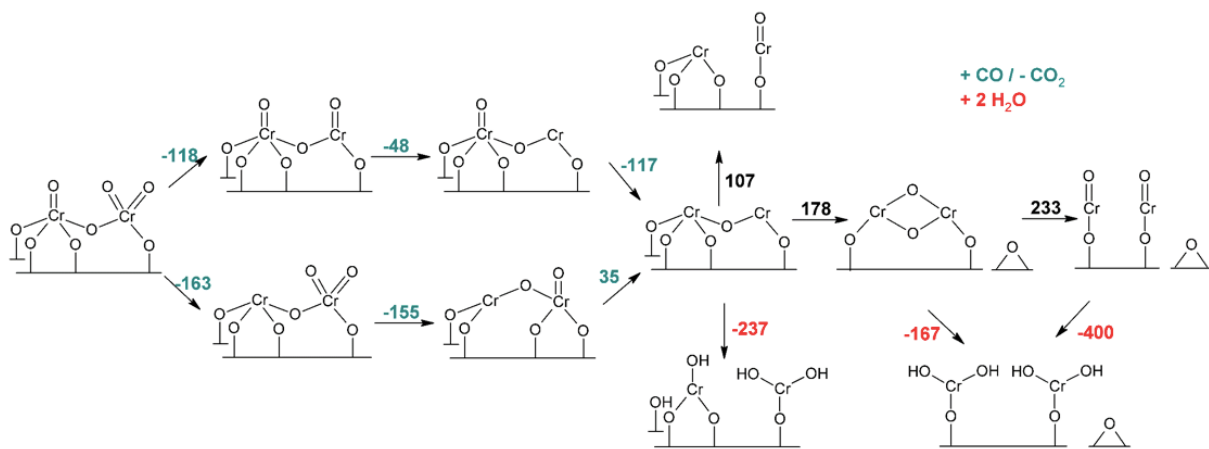
Dzięki zastosowaniu zaawansowanych periodycznych i klasterowych modeli amorficznej krzemionki (Rys. 1, 2) można było wykazać, że nie obserwuje się zależności pomiędzy rozmiarem pierścienia chromasiloksanowego a kątem O-Cr-O dla monomerycznych form Cr(II), inaczej niż sugerowano w literaturze.^{19,71} Jest to związane z oddziaływaniami centrów Cr(II) z grupami silanolowymi i mostkami siloksanowymi obecnymi na powierzchni oraz złożoną strukturą amorficznej krzemionki. Wyniki te pokazują, jak ważne w badaniach teoretycznych heterogenicznych układów katalitycznych jest dysponowanie realistycznymi i zaawansowanymi modelami powierzchni, które uwzględniają heterogeniczność form powierzchniowych.



Rys. 4 Energia Gibbsa w $T = 873$ K (ΔG_{873} , kJ mol^{-1}) redukcji monomerycznych form tlenkowych Cr(VI) na powierzchni krzemionki. Obliczenia klasterowe [D2].

Wyniki moich obliczeń pokazują, że pierwszy etap dwustopniowej redukcji monomerycznych form tlenkowych Cr(VI) z zastosowaniem CO, tj. $\text{Cr(VI)} \rightarrow \text{Cr(IV)}$ jest procesem egzoergicznym, podczas gdy efekt egzoergiczny drugiego etapu, tj. $\text{Cr(IV)} \rightarrow \text{Cr(II)}$ jest mniejszy (Rys. 4). Niemniej, w zależności od lokalizacji centrum monookso Cr(IV) na powierzchni, okazuje się, że nie zawsze drugi etap redukcji musi być procesem samorzutnym, stąd w niektórych warunkach forma monookso Cr(IV) może być stabilna termodynamicznie. Otrzymane wyniki są o tyle istotne, że w najnowszych badaniach eksperymentalnych^{83,110} taka forma prawdopodobnie została zaobserwowana. Forma Cr(III), często obserwowana eksperymentalnie, może powstawać na skutek hydrolizy wiązań Cr-O-Si powierzchniowych form Cr.

Redukcja dimerycznych form Cr(VI) przebiega przez liczne formy na różnych stopniach utlenienia, by finalnie dać Cr(II) i/lub Cr(III). W obecności H_2O niektóre formy dimeryczne mogą zostać przekształcone w formy monomeryczne. Woda może również reutleniać Cr(II) do Cr(III) [D2]. Schemat redukcji, hydratacji oraz przegrupowania wybranego periodycznego modelu dimerycznej formy Cr(VI) wraz z wartościami energii reakcji został zaprezentowany na Rys. 5.



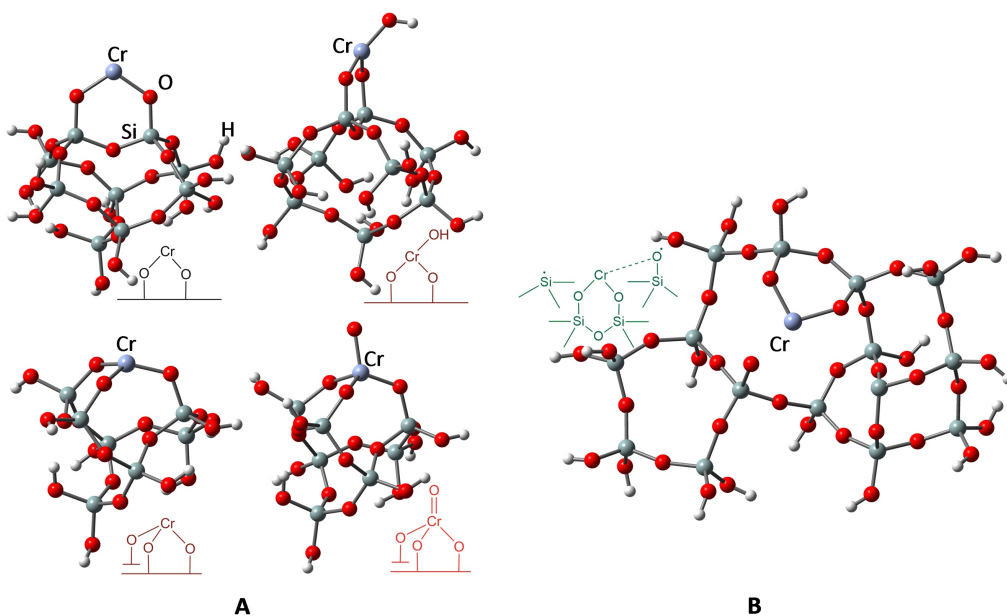
Rys. 5 Energia w T = 0 K (ΔE , kJ mol⁻¹) redukcji, hydratacji oraz przegrupowania dimerycznej formy tlenkowej Cr(VI) na powierzchni krzemionki. Obliczenia periodyczne [D2].

Przeprowadzenie symulacji widm IR oraz Ramana [D2] umożliwiło m.in. nową interpretację danych eksperymentalnych.^{27,110} Można było stwierdzić, że w zakresie drgań rozciągających Cr=O, przypisywanych drganiom formy monookso Cr(VI) i/lub asymetrycznym drganiom rozciągającym Cr(=O)₂ form diokso Cr(VI) (ok. 1020-1010 cm⁻¹) obserwowane są również drgania rozciągające Cr=O formy monookso Cr(IV). W przypadku

form dimerycznych Cr(VI) drgania $\nu_s(\text{O}=\text{Cr}=\text{O})$ oraz $\nu_{as}(\text{O}=\text{Cr}=\text{O})$ występują przy zbliżonych wartościach liczb falowych jak w przypadku monomerycznych form Cr(VI), podczas gdy dla zredukowanych form drgania te pojawiają się przy mniejszych wartościach liczby falowej. Drgania $\nu(\text{Cr}-\text{O}-\text{Si})$ form dimerycznych pojawiają się w podobnym zakresie jak w przypadku form monomerycznych. Jedynie drgania $\nu_s(\text{O}-\text{Cr}-\text{O})$ oraz $\nu_{as}(\text{O}-\text{Cr}-\text{O})$ umożliwiłyby rozróżnienie form monomerycznych od dimerycznych. Dla form Cr(VI) te pierwsze drgania powinny występować przy około $515\text{-}536 \text{ cm}^{-1}$, co dobrze koreluje z bardzo słabym drgiem przy 576 cm^{-1} obserwowanym eksperymentalnie.²⁷

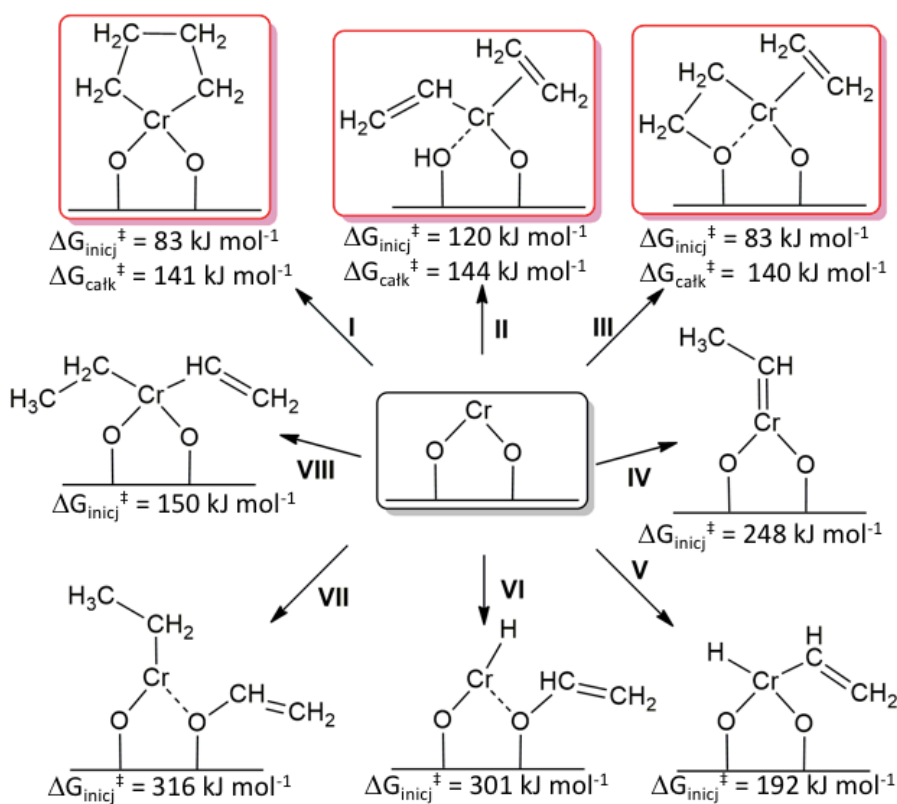
6.2. Studia nad mechanizmem polimeryzacji etylenu [D3, D4]

Celem badań prowadzonych w pracach [D3, D4] było poznanie pełnego mechanizmu polimeryzacji etylenu na katalizatorze Phillipsa, uwzględniającego etap inicjacji, propagacji oraz terminacji. Obliczenia prowadzono z zastosowaniem funkcjonału PBE0¹¹¹ oraz baz def2-SVP i def2-TZVPP.¹⁰⁴ W obliczeniach uwzględniono również poprawki na oddziaływanie dyspersyjne D3(BJ).^{112,113} Modele form powierzchniowych opracowano na bazie modelu β -krystobalitu,¹¹⁴ (Rys. 6 A) który często jest stosowany w celu symulacji powierzchni amorficznej krzemionki.^{20,35,98,115–119} Rozmiar użytych modeli umożliwia efektywne obliczenia wielu złożonych ścieżek reakcji. Ponadto, zastosowano również uproszczone i odpowiednio zmodyfikowane modele klastrowe układu $\text{CrO}_x/\text{SiO}_2$ uzyskane w poprzedniej pracy [D2] Rys. 6 B). Obliczenia wykonano w programie Gaussian 09. Szczegółowe informacje o stosowanej metodzie obliczeniowej znajdują się w pracach [D3, D4].



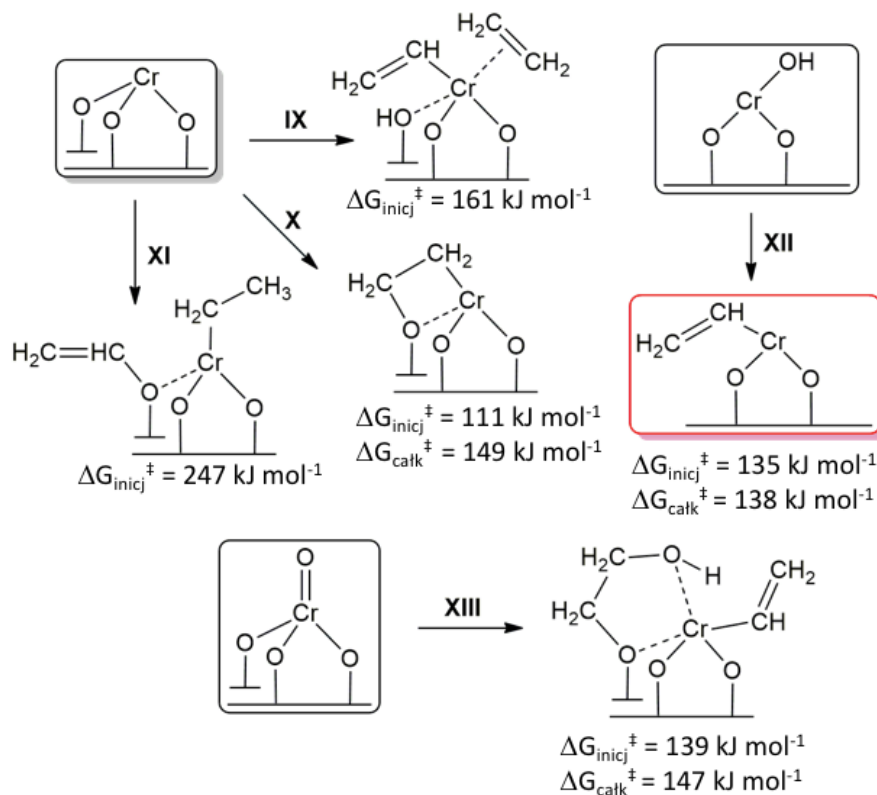
Rys. 6 Modele izolowanych form tlenkowych Cr na powierzchni krzemionki rozpatrywane jako prekursory centrów aktywnych w badaniach polimeryzacji etylenu [D3].

Jak wspomniałem we wstępie, forma Cr(II) dominuje na powierzchni wstępnie redukowanego katalizatora, stąd była ona często postulowana jako prekursor centrum aktywnego. Moim punktem wyjścia w badaniu mechanizmu polimeryzacji było zatem zweryfikowanie licznych mechanizmów z udziałem Cr(II), które dotychczas pojawiały się w literaturze. Dzięki temu możliwe było ich bezpośrednie porównanie, gdyż wszystkie zostały policzone stosując tą samą metodę obliczeniową. Na podstawie wykonanych obliczeń udało się także zaproponować nowe mechanizmy transformacji Cr(II) w formy aktywne. Otrzymane wyniki zostały sumarycznie zestawione na Rys. 7, gdzie dla wszystkich prezentowanych form $\Delta G_{\text{inicj}}^{\ddagger}$ oznacza barierę aktywacji związaną z powstawaniem danej formy aktywnej (reakcja inicjacji). Dla najmniejszych wartości $\Delta G_{\text{inicj}}^{\ddagger}$, pokazano również efektywne bariery aktywacji $\Delta G_{\text{całk}}^{\ddagger}$ związane z całą ścieżką reakcji, które oprócz etapu inicjacji uwzględniają również etap propagacji.



Rys. 7 Wyznaczone wartości barier aktywacji związane z powstawaniem danej formy aktywnej (reakcja inicjacji, $\Delta G_{\text{inicj}}^{\ddagger}$, T = 373 K) przy uwzględnieniu Cr(II) jako prekursora centrum aktywnego. Dla najniższych wartości $\Delta G_{\text{inicj}}^{\ddagger}$ pokazano dodatkowo efektywne bariery aktywacji ($\Delta G_{\text{całk}}^{\ddagger}$, T = 373 K) związane z całą ścieżką reakcji, które oprócz etapu inicjacji uwzględniają również etap propagacji.

Analiza otrzymanych danych [D4] wskazuje, że w wielu przypadkach (Rys. 7, IV-VIII) wyznaczona bariera aktywacji etapu inicjacji jest zbyt wysoka, by postulowana reakcja mogła tłumaczyć powstawanie centrów aktywnych. Jedynie w przypadku ścieżek I-III bariery inicjacji są relatywnie niskie. Na szczególną uwagę zasługuje reakcja prowadząca do kompleksu chromacyklopentanowego (Rys. 7 I) oraz oksachromacyklobutanowego (Rys. 7 III). W tym przypadku obie reakcje zachodzą z taką samą barierą inicjacji równą 83 kJ mol^{-1} , niemniej, reakcja I wymaga zmiany multipletowości. Alternatywna ścieżka II, generująca formę $(\text{HO})\text{Cr(II)}-\text{CH}=\text{CH}_2$, jest mniej preferowana termodynamicznie oraz kinetycznie. Rozpatrując jednocześnie inicjację i propagację, wszystkie trzy ścieżki (I-III) przewidują podobną efektywną barierę aktywacji. Jednak tylko w przypadku mechanizmu oksachromacyklicznego (III) propagacja jest bardziej korzystna kinetycznie w porównaniu do terminacji. Pełna analiza wszystkich ścieżek reakcji jest zamieszczona w pracy [D4].



Rys. 8 Wyznaczone wartości barier aktywacji związane z powstawaniem danej formy aktywnej (reakcja inicjacji, $\Delta G_{\text{inicj}}^{\ddagger}$, $T = 373 \text{ K}$) przy uwzględnieniu Cr(III) oraz Cr(V) jako prekursorów centrów aktywnych. Dla najniższych wartości $\Delta G_{\text{inicj}}^{\ddagger}$ pokazano dodatkowo efektywne bariery aktywacji ($\Delta G_{\text{całk}}^{\ddagger}$, $T = 373 \text{ K}$) związane z całą ścieżką reakcji, które oprócz etapu inicjacji uwzględniają również etap propagacji.

Formy Cr(III) również są obecne na powierzchni badanego katalizatora i były one ostatnio rozważane w innych pracach^{64,81,82,84} jako potencjalne prekursory centrów aktywnych.

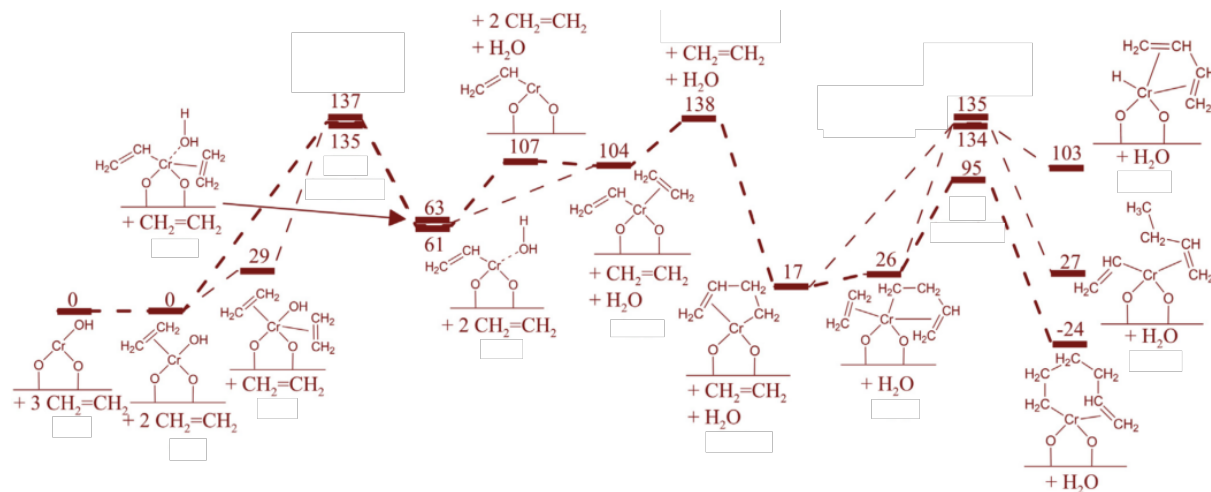
Wszystkie analizowane przeze mnie mechanizmy inicjacji (Rys. 8 IX-XI), przewidują wyższe bariery aktywacji niż w przypadku analogicznych mechanizmów dla form Cr(II). Gdy zastosuje się bardziej zaawansowane modele amorficznej krzemionki, bariera aktywacji może być znacznie obniżona. Podobny wniosek został ostatnio wyciągnięty w innej pracy teoretycznej.⁸⁴

Z racji tego, że niewielkie ilości form Cr(V) są wykrywane przy zastosowaniu technik XPS¹²⁰ oraz EPR,^{8,11,37–40} przeanalizowałem również ich potencjalną reaktywność względem etylenu (Rys. 8 XIII). Całkowita bariera aktywacji jest porównywalna jak w przypadku form Cr(III), jednak w zaproponowanym mechanizmie dochodzi do powstania nowego centrum aktywnego podczas etapu terminacji łańcucha polimerowego, przez co nie ma potrzeby ponownej inicjacji.

Najkorzystniejsze wyniki uzyskałem dla hydroksylowej formy Cr(III), tj. Cr(III)-OH (Rys. 8 XII). Mechanizm polimeryzacji zaproponowany w oparciu o tę formę przewiduje najniższą barierę aktywacji w porównaniu do innych analizowanych mechanizmów, dotychczas postulowanych w literaturze. W szczególności, struktura Cr(III)-OH powinna być aktywniejsza od Cr(III) (Rys. 8 IX-XI) [**D3, D4**].

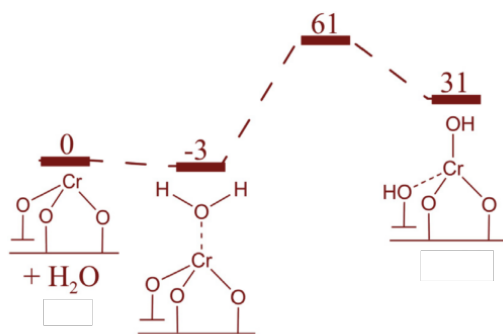
W pierwszym etapie zaproponowanego mechanizmu (Rys. 9) dochodzi do powstania formy Cr(III)-CH=CH₂ na drodze transferu protonu z etylenu do grupy hydroksylowej. Powstała forma jest właściwym centrum aktywnym. Wsparcie eksperymentalne [**D3**] dla istnienia takiego centrum uzyskałem współpracując z zespołem wybitnego eksperymentalisty w zakresie katalizy heterogenicznej – Israelem E. Wachsem (*Lehigh University*). Istnieją również inne ścieżki reakcji prowadzące do centrum Cr(III)-CH=CH₂, niemniej mechanizm zaproponowany na Rys. 9 wskazuje na najniższą barierę aktywacji pośród wszystkich analizowanych. W kolejnym etapie, po desorpcji cząsteczki H₂O będącej produktem reakcji, zachodzi adsorpcja kolejnej cząsteczki etylenu. Dalsze etapy propagacji przebiegają zgodnie z klasycznym mechanizmem typu Cossee-Arlman¹²¹ poprzez insercję etylenu pomiędzy wiązanie σ Cr-C. Na uwagę zasługuje to, że w postulowanym mechanizmie kinetycznie bardziej uprzywilejowana jest reakcja propagacji niż terminacji, stąd wzrost łańcucha polimerowego jest preferowany. Niemniej, nawet jeżeli dochodzi do terminacji na skutek oddziaływanego etylenu z alkilowym centrum Cr, to w efekcie powstaje nowe centrum aktywne Cr(III)-CH=CH₂, które łatwo katalizuje dalszą polimeryzację. W związku z tym, opisany tu mechanizm wydaje się być najlepszą propozycją wyjaśnienia polimeryzacji etylenu na katalizatorze Phillipsa, spośród analizowanych w tej pracy. Składa się na to szereg czynników: bariera inicjacji oraz propagacji jest najbardziej korzystna w porównaniu do innych badanych

ścieżek reakcji, propagacja jest zdecydowanie bardziej preferowana względem terminacji oraz podczas terminacji dochodzi do odtworzenia centrum aktywnego.



Rys. 9 Profil energii Gibbsa (ΔG , kJ mol^{-1}) w $T = 373\text{ K}$ dla mechanizmu polimeryzacji etylenu uwzględniającego formę Cr(III)-OH jako prekursor centrum aktywnego. Grubsza linia wskazuje bardziej preferowaną ścieżkę. Stan podstawowy wszystkich kompleksów to kwartet **[D4]**.

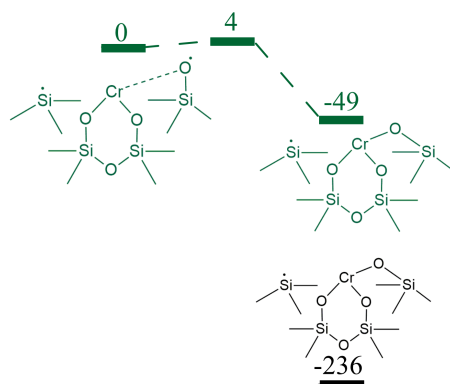
Z mechanizmem tym związany jest jednak problem braku dowodów eksperymentalnych wskazujących na istnienie formy Cr(III)-OH oraz wyjaśnienia sposobu powstawania takiej struktury. We wcześniejszej pracy pokazano **[D2]**, że takie formy mogą powstawać na skutek redukcji dimerycznych form Cr i późniejszej hydratacji. Inna możliwość to hydratacja monomerycznych form Cr(III) (Rys. 10). Zakładając nawet bardzo niskie ciśnienie cząstkowe wody ($p_{\text{H}_2\text{O}}=10^{-5}\text{ atm}$) oraz typową temperaturę procesu polimeryzacji ($T = 373\text{ K}$) reakcja ta wymaga pokonania niewielkiej bariery aktywacji ($\Delta G^\ddagger = 64\text{ kJ mol}^{-1}$). Woda może m.in. powstawać ubocznie podczas redukcji katalizatora Phillipsa w obecności etylenu.⁵⁶



Rys. 10 Profil energii Gibbsa (ΔG , kJ mol^{-1}) w $T = 373\text{ K}$ oraz przy $p_{\text{H}_2\text{O}} = 10^{-5}\text{ atm}$ dla hydratacji formy Cr(III) . Stan podstawowy wszystkich kompleksów to kwartet **[D4]**.

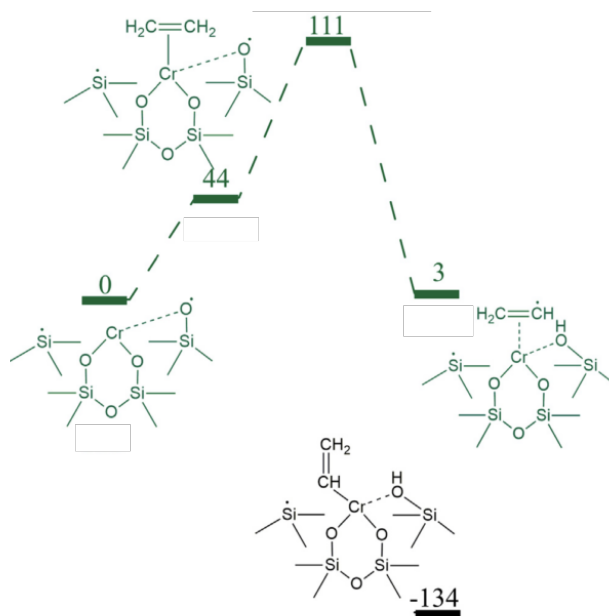
Warto w tym miejscu wspomnieć, że zaproponowany mechanizm inicjacji (Rys. 9) przewiduje powstawanie ubocznie tylko jednej cząsteczki H_2O na samym początku procesu. Powstała cząsteczka H_2O mogłaby następnie reagować z utworzeniem nowego centrum Cr(III)-OH (np. jak na Rys. 10). W związku z tym, liczba prekursorów centrów aktywnych mogłaby zwiększać się przy nawet bardzo małej zawartości H_2O . Zbyt duże ciśnienie cząstkowe wody doprowadziłoby do dezaktywacji katalizatora, ze względu na hydrolizę wiązań Cr-O-Si [D2].

Chociaż wiadomo, że formy Cr(III) istnieją w bardzo niewielkich ilościach na powierzchni katalizatora $\text{CrO}_x/\text{SiO}_2$ po przeprowadzeniu wysokotemperaturowej kalcynacji,^{17,23} to trudno wytlumaczyć, jak mogą one powstawać z początkowych form monomerycznych Cr(VI) na drodze redukcji z zastosowaniem dwuelektronowych reduktorów, takich jak CO , H_2 [D2] lub $\text{CH}_2=\text{CH}_2$ [D5]. Z drugiej strony wiadomo, że w strukturze powierzchni amorficznej krzemionki obecne są defekty, w szczególności po przeprowadzeniu wysokotemperaturowej kalcynacji.^{27,122–128} Nie można stąd jednoznacznie wykluczyć roli defektów powierzchniowych w generowaniu centrów aktywnych lub ich prekursorów. Co więcej, badania eksperymentalne pokazują, że wraz ze wzrostem temperatury kalcynacji rośnie aktywność katalityczna.^{17,23} Może być to związane z większą liczbą defektów powierzchniowych, których powstanie jest bardziej prawdopodobne w wysokich temperaturach. Biorąc powyższe pod uwagę, w pracy [D4] zaproponowano, że defekty w postaci $\equiv\text{SiO}^\bullet$ oraz $\equiv\text{Si}^\bullet$ mogą odgrywać rolę w przekształceniu Cr(II) do Cr(III) (Rys. 11). Obecność tego typu defektów na powierzchni SiO_2 była postulowana w pracach eksperymentalnych.^{122,124,125,128–130} Mogą one powstawać na skutek dehydroksylacji krzemionki zachodzącej w wysokich temperaturach.^{124,128–130} Model klastrowy formy Cr(II) sąsiadującej z defektem powierzchniowym otrzymano na bazie modelu periodycznego Cr(VI) .³³ W tym ostatnim, podczas optymalizacji geometrii doszło do spontanicznego wytworzenia takiego defektu.



Rys. 11 Profil energii Gibbsa (ΔG , kJ mol^{-1}) w $T = 373 \text{ K}$ otrzymywania Cr(III) z Cr(II) i sąsiedniego defektu powierzchniowego. Kolorem zielonym i czarnym oznaczono odpowiednio ścieżkę septetową oraz kwintetową [D4].

Otrzymane wyniki wskazują, że Cr(II) bardzo łatwo reaguje z sąsiadującym defektem powierzchniowym ($\Delta G^\ddagger = 4 \text{ kJ mol}^{-1}$), wskutek czego generowana jest forma Cr(III). Uwzględniając zmianę multipletowości, całkowita energia Gibbsa reakcji wynosi -236 kJ mol^{-1} . Na tej podstawie można przynajmniej częściowo wytlumaczyć mechanizm generowania Cr(III) z Cr(II).



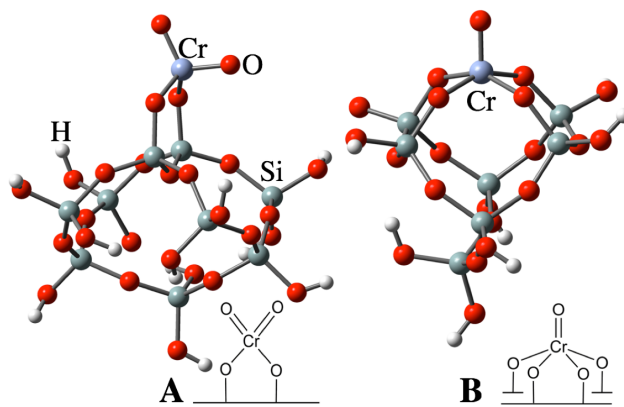
Rys. 12 Profil energii Gibbsa (ΔG , kJ mol^{-1}) w $T = 373 \text{ K}$ otrzymywania Cr(III)-CH=CH_2 na drodze dysocjacyjnej adsorpcji etylenu na Cr(II) i sąsiednim defekcie powierzchniowym. Kolorem zielonym i czarnym oznaczono odpowiednio ścieżkę septetową oraz kwintetową [D4].

Dysocjacyjna adsorpcja etylenu na monomerycznym centrum Cr(II) sąsiadującym z centrum $\equiv\text{SiO}^\bullet$ jest kolejną reakcją, w której defekty powierzchniowe mogą odgrywać rolę (Rys. 12). W pierwszym etapie zaproponowanego mechanizmu dochodzi do przeniesienia protonu z etylenu na $\equiv\text{SiO}^\bullet$, w efekcie czego powstaje nowa grupa silanolowa oraz centrum Cr(III)-CH=CH_2 . Bariera aktywacji związana z tą transformacją jest relatywnie niska ($\Delta G^\ddagger = 111 \text{ kJ mol}^{-1}$). Mechanizm ten może być alternatywną ścieżką, inną niż przedstawiona na Rys. 9, prowadzącą do struktury Cr(III)-CH=CH_2 wykrywanej eksperymentalnie [D3]. Podobny mechanizm może dodatkowo tłumaczyć powstawanie Cr(III)-OH , jeżeli zajdzie dysocjacyjna adsorpcja H_2O na monomerycznym centrum Cr(II) w sąsiedztwie $\equiv\text{SiO}^\bullet$.

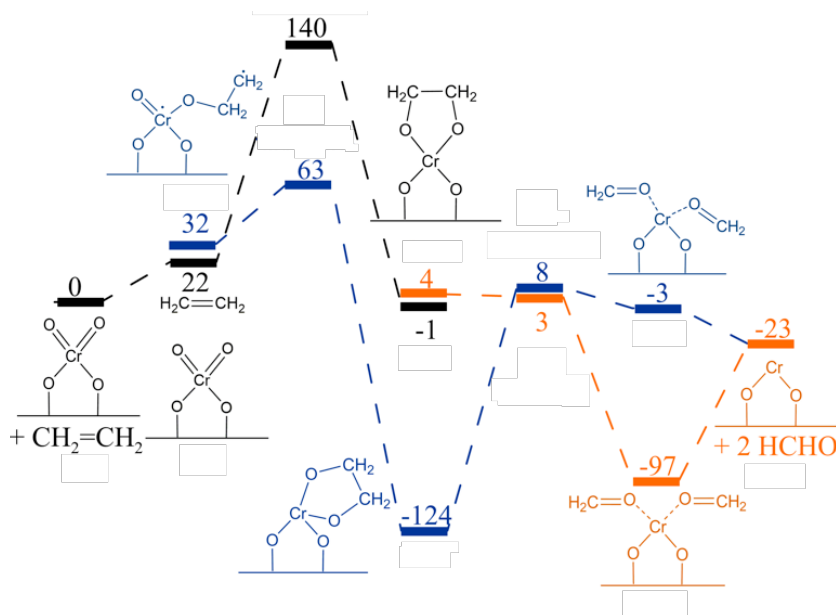
6.3. Badanie mechanizmu redukcji katalizatora Phillipsa [D5]

W tej części pracy głównym celem było poznanie mechanizmu redukcji katalizatora Phillipsa etylenem wraz z uwzględnieniem następujących transformacji ubocznych produktów

tlenowych. Zastosowano tu taką samą metodykę jak w przypadku badania mechanizmu polimeryzacji etylenu. Dzięki temu wyniki otrzymane w obu przypadkach mogą być bezpośrednio porównane. Ponadto, obliczono ścieżkę reakcji redukcji form Cr(VI) i Cr(IV) w obecności CO. Modele form powierzchniowych Cr(VI), stosowanych w tej części badań [D5] zostały zaprezentowane na Rys. 13. Są one analogiczne do tych na bazie struktury β -krystobalitu, które zostały opracowane i zastosowane w pracach [D3, D4].



Rys. 13 Modele izolowanych form tlenkowych Cr(VI) na powierzchni krzemionki stosowane w badaniach mechanizmu redukcji katalizatora Phillipsa: (A) model formy diokso, (B) model formy monoookso [D5].



Rys. 14 Profil energii Gibbsa (kJ mol^{-1}) w $T = 373 \text{ K}$ dla redukcji formy diokso Cr(VI) etylenem do Cr(II) oraz dwóch cząsteczek HCHO. Kolorem czarnym, niebieskim i pomarańczowym oznaczono odpowiednio ścieżkę singletową, trypletową oraz kwintetową [D5].

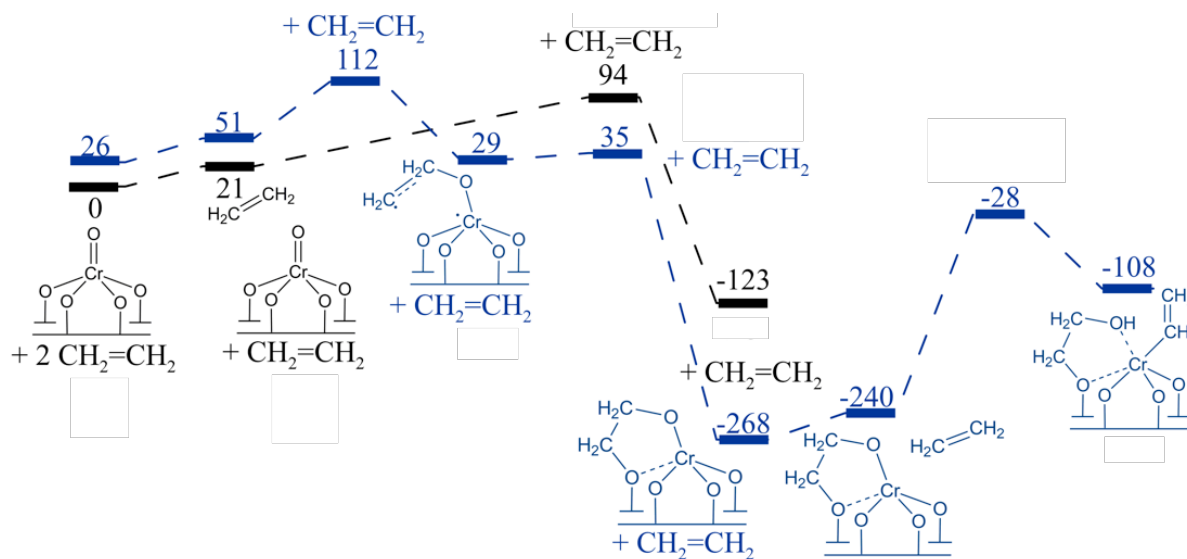
Otrzymane wyniki wskazują [D5], że najkorzystniejszą z termodynamicznego i kinetycznego punktu widzenia ścieżką redukcji katalizatora Phillipsa jest ta zamieszczona na Rys. 14. Mechanizm ten, w formie uproszczonej, został po raz pierwszy zaproponowany przez Bakera i Carricka⁵³ na podstawie analizy danych doświadczalnych. Jak do tej pory, tylko w jednej pracy teoretycznej¹⁰² był on analizowany, przy czym autorzy wyznaczyli jedynie całkowity efekt energetyczny przekształcania Cr(VI) w Cr(II) zakładając, że produktem utleniania etylenu jest formaldehyd.

W pierwszym etapie postulowanego mechanizmu (Rys. 14) zachodzi reduktywne sprzęganie etylenu z ligandami okso formy diokso Cr(VI), co prowadzi do pośredniej formy cyklicznej Cr(IV). Preferowanym stanem spinowym na tym etapie jest stan trypletowy, a proces jest dwustopniowy (pierwszy stopień, czyli tworzenie jednego wiązania O-C to ścieżka monotoniczna) i zachodzi z niską barierą aktywacji ($\Delta G^\ddagger = 63 \text{ kJ mol}^{-1}$). W przypadku jednostopniowej ścieżki singletowej bariera ta jest ponad dwa razy większa ($\Delta G^\ddagger = 140 \text{ kJ mol}^{-1}$). W związku z tym, jednoetapowa transformacja zaproponowana przez Bakera i Carricka jest dużo mniej prawdopodobna.

W kolejnym etapie postulowanego mechanizmu zachodzi reduktywny rozkład kompleksu dioksachromacyklicznego Cr(IV) z wytworzeniem dwóch cząsteczek HCHO oraz Cr(II). Na tym etapie ponownie dochodzi do zmiany multipletowości. Efektywna bariera aktywacji wynosi $\Delta G^\ddagger = 127 \text{ kJ mol}^{-1}$ (Rys. 14), co jest wartością nieco niższą w porównaniu do bariery aktywacji dla najkorzystniejszego mechanizmu polimeryzacji etylenu [D3, D4].

Desorpceja formaldehydu z powierzchni nie jest uprzywilejowana termodynamicznie w warunkach $p_{\text{HCHO}} = 1 \text{ atm}$ oraz $T = 373 \text{ K}$ ($\Delta G = 74 \text{ kJ mol}^{-1}$). Otrzymane wyniki są jakościowo zgodne z pracą Zhonga i współpracowników.⁶³ Dla niskiego ciśnienia cząstkowego HCHO, spodziewanego w warunkach procesu, reakcja ta staje się bardziej preferowana. Dla przykładu, dla $p_{\text{HCHO}} = 10^{-5}$ oraz 10^{-7} atm , odpowiednio $\Delta G = 46$ oraz 34 kJ mol^{-1} . Wartości te są porównywalne z wartością ΔG desorpceji etylenu z Cr(II) (34 kJ mol^{-1}) [D4]. W związku z tym, przy dużym nadmiarze etylenu, spodziewanym w warunkach reakcji, możliwa jest wymiana HCHO na etylen.

Inne warianty redukcji formy diokso Cr(VI), w których w inny sposób dochodzi do wytworzenia wiązania Cr-O lub Cr-C oraz generowane są inne produkty małocząsteczkowe (aldehyd octowy, tlenek etylenu), są mniej preferowane kinetycznie. Szczegółowe informację o tych ścieżkach znajdują się w pracy [D5].

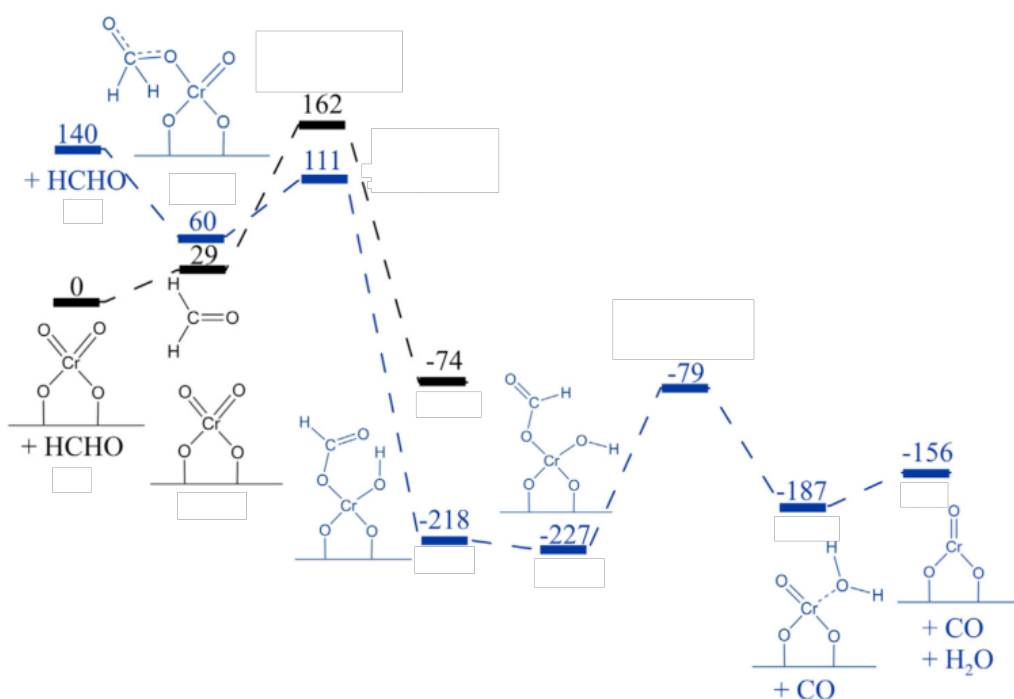


Rys. 15 Profil energii Gibbsa (kJ mol^{-1}) w $T = 373$ K dla redukcji formy monookso Cr(VI) etylenem i dalszej aktywacji do formy winylowej Cr(IV). Kolorem czarnym i niebieskim oznaczono odpowiednio ścieżkę singletową oraz trypletową [D5].

Ponieważ badania eksperymentalne sugerują, że forma monookso Cr(VI) (Rys. 13 B) może istnieć w mniejszości na powierzchni badanego katalizatora,^{27–29} postanowiłem przeanalizować jej potencjalną reaktywność względem etylenu (Rys. 15). Pomimo tego, że pierwszy etap reakcji pomiędzy etylenem a formą monookso Cr(VI) jest kinetycznie możliwy, generuje on bardzo stabilną strukturę cykliczną, która jest nieaktywna w dalszych potencjalnych przekształceniach (Rys. 15). Z drugiej strony, redukcja formy diokso Cr(VI), chociaż nieco mniej korzystna z kinetycznego i termodynamicznego punktu widzenia (Rys. 14) w porównaniu do pierwszego etapu mechanizmu przedstawionego na Rys. 15, generuje formę Cr(II) często postulowaną w literaturze jako prekursor centrów aktywnych polimeryzacji etylenu. Otrzymane wyniki mogą wyjaśnić dane eksperymentalne [D3], które wskazują, że forma diokso Cr(VI) szybciej ulega redukcji i aktywacji w porównaniu do formy monookso Cr(VI).

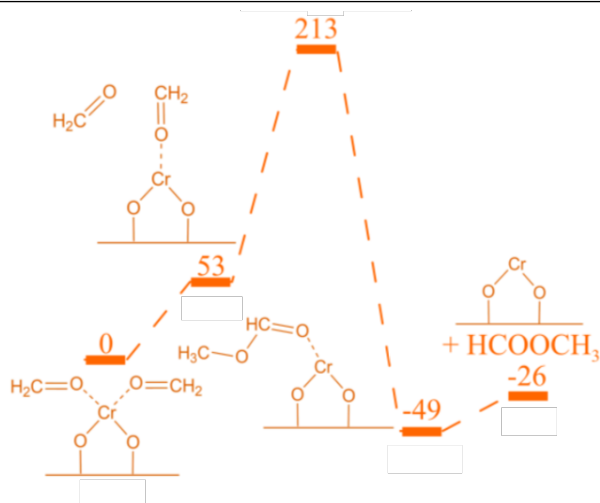
Z racji tego, że nie ma bezpośrednich eksperymentalnych dowodów na obecność HCHO w fazie gazowej po redukcji katalizatora Phillipsa etylenem, ulega on prawdopodobnie dalszym przekształceniom. Możliwą ścieżką reakcji może być utlenianie formaldehydu na centrum diokso Cr(VI), co zostało pokazane na Rys. 16. W pierwszym etapie proponowanego mechanizmu dochodzi do przeniesienia protonu z formaldehydu na ligand okso formy diokso Cr(VI) oraz wytworzenia wiązania C-O z udziałem drugiego ligantu okso. W drugim etapie zachodzi jednoczesne przeniesienie kolejnego protonu na nowo powstałą grupę hydroksylową

oraz zerwanie wiązania C–O, w efekcie czego powstaje forma monookso Cr(IV), cząsteczka H_2O oraz cząsteczka CO. Tlenek węgla(II) może następnie zostać utleniony do CO_2 na centrum Cr(VI) lub Cr(IV), co również zostało zaprezentowane w pracy [D5]. Tlenek węgla(IV) został wykryty w badaniach eksperymentalnych jako produkt redukcji katalizatora $\text{CrO}_x/\text{SiO}_2$ etylenem w wyższych temperaturach.⁵⁶ [D3] W związku z tym, zaproponowana kaskada reakcji tworzenia HCHO (Rys. 15) i następnie jego utleniania (Rys. 16) może przynajmniej częściowo tłumaczyć obserwacje eksperymentalne.



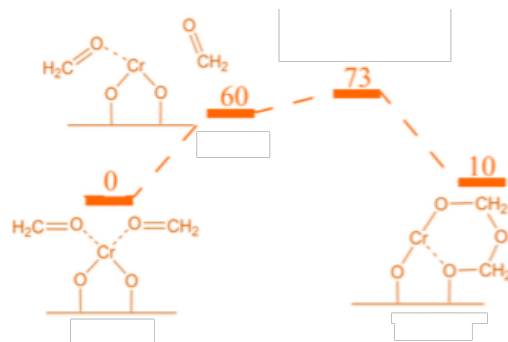
Rys. 16 Profil energii Gibbsa (kJ mol^{-1}) w $T = 373 \text{ K}$ dla utleniania formaldehydu na centrum diokso Cr(VI). Kolorem czarnym i niebieskim oznaczono odpowiednio ścieżkę singletową oraz trypletową [D5].

W najnowszych pracach Barzan i współpracownicy^{57,58} zaproponowali, że aldehydy powstałe podczas redukcji układu Cr(VI)/ SiO_2 olefinami ulegają dalszym przekształceniom do estrów. Te produkty tlenowe pozostają silnie zaadsorbowane na powierzchni katalizatora, co wpływa na jego aktywność w polimeryzacji etylenu. W związku z tym, jeżeli HCHO powstaje podczas redukcji katalizatora Phillipsa etylenem, to może ulec on dalszym przekształceniom do mrówczanu metylu. To skłoniło mnie do zbadania tej możliwości z teoretycznego punktu widzenia.



Rys. 17 Profil energii Gibbsa (kJ mol^{-1}) w $T = 373 \text{ K}$ dla jednoetapowego przekształcania formaldehydu do mrówczanu metylu (ścieżka kwintetowa) [D5].

Najkorzystniejszy obliczony mechanizm został zaprezentowany na Rys. 17. W tym jednoetapowym przekształceniu dwóch zaadsorbowanych cząsteczek HCHO na centrum Cr(II) dochodzi do jednoczesnego przeniesienia wodoru oraz wytworzenia wiązania C-O. W mechanizmie tym, w przeciwieństwie do innych badanych ścieżek [D5], stan kwintetowy jest stanem podstawowym dla wszystkich reagentów (Rys. 17). Niemniej, bariera aktywacji związana z tą transformacją jest bardzo wysoka ($\Delta G^\ddagger = 213 \text{ kJ mol}^{-1}$), co raczej wyklucza możliwość powstawania mrówczanu metylu zgodnie z tym mechanizmem w warunkach w jakich prowadzony jest proces polimeryzacji etylenu (ok. 373 K)



Rys. 18 Profil energii Gibbsa (kJ mol^{-1}) w $T = 373 \text{ K}$ dla mechanizmu powstawania formy dioksametylenowej z Cr(II) oraz dwóch cząsteczek HCHO (ścieżka kwintetowa) [D5].

Inny interesujący mechanizm związany z transformacją HCHO z udziałem Cr(II) został zaprezentowany na Rys. 18. Insercja dwóch cząsteczek HCHO pomiędzy wiązanie Cr-OSi generuje dioksametylenową formę cykliczną. Tego typu struktury były wykrywane eksperymentalnie na powierzchni różnych tlenków podczas adsorpcji HCHO.^{56,131}

Z przeprowadzonych obliczeń wynika, że pierwszym ubocznym, tlenowym produktem redukcji katalizatora Phillipsa etylenem jest formaldehyd. Jego dalsze utlenianie do CO/CO_2 oraz H_2O jest możliwe i, na co warto zwrócić szczególną uwagę, może być bardziej uprzywilejowane kinetycznie niż przekształcenie do estru. Wyniki te są zgodne z badaniami eksperymentalnymi [D3], w których wykryto jedynie CO_2 jako produkt utleniania etylenu w wyższych temperaturach.

W niedawnej pracy Barzan i współpracownicy⁵⁸ badali tlenowe produkty powstałe podczas redukcji katalizatora Phillipsa etylenem. Obserwowane pasma IR przypisane zostały zaadsorbowanym estrom, w szczególności mrówczanowi metylu. Jednak w oparciu o analizę obliczonych częstości drgań oscylacyjnych różnych organicznych form powierzchniowych [D5], które zlokalizowałem na badanych ścieżkach reakcji, można zaproponować, że różne ugrupowania mają wkład w drgania obserwowane eksperymentalnie. Wydaje się to być prawdopodobne, biorąc pod uwagę złożony proces redukcji katalizatora Phillipsa etylenem.

7. Podsumowanie i wnioski

Cykl prac [D1-D5] składający się na moją pracę doktorską dotyczył modelowania struktury oraz badania reaktywności układu CrO_x/SiO₂ w kontekście procesu polimeryzacji etylenu.

Wykonane prace prowadzą do następujących wniosków:

1. Formy dimeryczne Cr(VI) są mniej stabilne od form monomerycznych, stąd te drugie powinny dominować na powierzchni katalizatora CrO_x/SiO₂ [D2].
2. W przypadku form monomerycznych Cr(VI) pierwszy etap redukcji, tj. Cr(VI) → Cr(IV), jest procesem silnie egzoergicznym, podczas gdy efekt egzoergiczny drugiego etapu, tj. Cr(IV) → Cr(II), jest mniejszy. Redukcja dimerycznych form Cr(VI) może przebiegać poprzez formy na różnym stopniu utlenienia i finalnie prowadzi do Cr(II) i Cr(III). W obecności pary wodnej możliwa jest hydratacja niektórych form dimerycznych do monomerycznych. Woda może również utleniać Cr(II) do Cr(III) lub hydrolizować wiązania Cr-O-Si [D2].
3. W zakresie drgań rozciągających Cr=O, przypisywanych drganiom formy monookso Cr(VI) i/lub asymetrycznym drganiom rozciągającym Cr(=O)₂ form diokso Cr(VI), obserwowane są również drgania rozciągające Cr=O formy monookso Cr(IV) [D2].
4. Analiza licznych mechanizmów generowania centrów aktywnych polimeryzacji etylenu wskazuje, że dla form Cr(II) najniższe bariery aktywacji są związane z powstawaniem cyklicznych kompleksów typu oksachromacyklobutan i chromacyklopentan. Inne mechanizmy uwzględniające Cr(II) są mniej prawdopodobne [D4].
5. Mechanizmy z udziałem form Cr(III) wiążą się z wyższymi barierami aktywacji, w porównaniu do analogicznych mechanizmów dla form Cr(II). [D3, D4].
6. Mechanizm polimeryzacji zaproponowany w oparciu o formę Cr(III)-OH, do tej pory niepostulowaną w literaturze, charakteryzuje się najniższą całkowitą barierą aktywacji w porównaniu do pozostałych analizowanych ścieżek. Ponadto, etap propagacji jest bardziej preferowany kinetycznie od etapu terminacji. Co więcej, po dekoordynacji powstałego polimeru lub oligomeru odtwarzane jest nowe centrum aktywne, przez co ponowna inicjacja nie jest wymagana. W zaproponowanym mechanizmie, w pierwszym etapie dochodzi do wytworzenia struktury Cr(III)-CH=CH₂, która jest właściwym centrum aktywnym [D3, D4]. Wyniki te są zgodne z rezultatami badań

- eksperymentalnych [D3]. Forma Cr(III)-OH może powstawać na skutek redukcji dimerycznych form Cr i późniejszej hydratacji [D2] lub hydratacji monomerycznych form Cr(III) [D4].
7. Potencjalny mechanizm polimeryzacji zaproponowany dla formy monookso Cr(V) jest związany z nieco wyższą efektywną barierą aktywacji niż dla formy Cr(III)-OH, jednak również przewiduje on generowanie nowego centrum aktywnego po dekoordynacji rosnącego łańcucha polimerowego [D4].
 8. Defekty rodnikowe na powierzchni amorficznej krzemionki mogą ułatwiać powstawanie form monomerycznych Cr(III) z Cr(II) oraz generowanie centrów aktywnych polimeryzacji etylenu [D4].
 9. Najbardziej korzystna z kinetycznego punktu widzenia ścieżka redukcji katalizatora Phillipsa etylenem uwzględnia reakcję pomiędzy tym ostatnim a formą diokso Cr(VI) i prowadzi do powstania Cr(II) oraz dwóch cząsteczek formaldehydu. Redukcja formy monookso Cr(VI) prowadzi do stabilnej formy Cr(IV), nieulegającej dalszym przekształceniom [D5].
 10. Formaldehyd powstały podczas redukcji katalizatora Phillipsa etylenem może zostać utleniony do wykrywanych eksperymentalnie w wyższych temperaturach CO_2 i H_2O , zgodnie z postulowanym w tej pracy mechanizmem. Jego przekształcenia do estru (mrówczan metylu) jest mniej preferowane kinetycznie. Formaldehyd może również ulegać reakcji z Cr(II) generując cykliczne formy dioksometrylenowe oraz być zaadsorbowany na Cr(II), co dodatkowo może tłumaczyć, dlaczego nie jest on bezpośrednio wykrywany w badaniach eksperymentalnych [D5].
 11. Wiele różnych form powierzchniowych powstałych podczas redukcji katalizatora $\text{CrO}_x/\text{SiO}_2$ etylenem może mieć wkład w obserwowane eksperymentalnie pasma IR, opisane w literaturze i przypisane przez autorów zaadsorbowanemu estrowi [D5].

8. Literatura

- (1) Gaspar, A. B.; Brito, J. L. F.; Dieguez, L. C. *J. Mol. Catal. A Chem.* **2003**, 203, 251–266.
- (2) Hakuli, A.; Harlin, M. E.; Backman, L. B.; Krause, A. O. I. *J. Catal.* **1999**, 184, 349–356.
- (3) Pozan, G. S.; Tavman, A.; Boz, I. *Chem. Eng. J.* **2008**, 143, 180–185.
- (4) Sattler, J. J. H. B.; Ruiz-Martinez, J.; Santillan-Jimenez, E.; Weckhuysen, B. M. *Chem. Rev.* **2014**, 114, 10613–10653.
- (5) Ramani, N. C.; Sullivan, D. L.; Ekerdt, J. G.; Jehng, J.; Wachs, I. E. *J. Catal.* **1998**, 176, 143–154.
- (6) Cherian, M.; Rao, M. S.; Hirt, A. M.; Wachs, I. E.; Deo, G. *J. Catal.* **2002**, 211, 482–495.
- (7) Michorczyk, P.; Ogonowski, J.; Zeńczak, K. *J. Mol. Catal. A Chem.* **2011**, 349, 1–12.
- (8) Michorczyk, P.; Pietrzyk, P.; Ogonowski, J. *Micropor. Mesopor. Mater.* **2012**, 161, 56–66.
- (9) Botavina, M. A.; Martra, G.; Agafonov, Y. A.; Gaidai, N. A.; Nekrasov, N. V.; Trushin, D. V.; Coluccia, S.; Lapidus, A. L. *Appl. Catal. A Gen.* **2008**, 347, 126–132.
- (10) Weckhuysen, B. M.; Wachs, I. E.; Schoonheydt, R. A. *Chem. Rev.* **1996**, 96, 3327–3349.
- (11) Liotta, L. F.; Venezia, A. M.; Pantaleo, G.; Deganello, G.; Gruttaduria, M.; Noto, R. *Catal. Today* **2004**, 91–92, 231–236.
- (12) Somekawa, S.; Watanabe, H.; Oaki, Y.; Imai, H. *Catal. Commun.* **2015**, 72, 161–164.
- (13) Kim, D. S.; Tatibouet, J.-M.; Wachs, I. E. *J. Catal.* **1992**, 136, 209–221.
- (14) Kim, D. S.; Wachs, I. E. *J. Catal.* **1993**, 142, 166–171.
- (15) Weckhuysen, B. M.; Schoonheydt, R. A. *Catal. Today* **1999**, 51, 215–221.
- (16) Groppo, E.; Prestipino, C.; Cesano, F.; Bonino, F.; Bordiga, S.; Lamberti, C.; Thune, P.; Niemantsverdriet, J.; Zecchina, A. *J. Catal.* **2005**, 230, 98–108.
- (17) Groppo, E.; Lamberti, C.; Bordiga, S.; Spoto, G.; Zecchina, A. *Chem. Rev.* **2005**, 105, 115–183.
- (18) McDaniel, M. P.; Collins, K. S.; Benham, E. A.; Cymbaluk, T. H. *Appl. Catal. A Gen.* **2008**, 335, 252–261.
- (19) Demmelmaier, C. A.; White, R. E.; van Bokhoven, J. A.; Scott, S. L. *J. Catal.* **2009**, 262, 44–56.
- (20) Zhong, L.; Lee, M.-Y.; Liu, Z.; Wanglee, Y.-J.; Liu, B.; Scott, S. L. *J. Catal.* **2012**, 293, 1–12.
- (21) Gaspar, A. B.; Martins, R. L.; Schmal, M.; Dieguez, L. C. *J. Mol. Catal. A Chem.* **2001**, 169, 105–112.
- (22) Gaspar, A. B.; Dieguez, L. C. *Appl. Catal. A Gen.* **2002**, 227, 241–254.
- (23) McDaniel, M. P. In *Advances in Catalysis*; 2010; Vol. 53, pp 123–606.
- (24) Jayaratne, K. C.; Cymbaluk, T. H.; Jensen, M. D. *ACS Catal.* **2018**, 8, 602–614.
- (25) Zecchina, A.; Bordiga, S.; Groppo, E. *Selective Nanocatalysts and Nanoscience: Concepts for Heterogeneous and Homogeneous Catalysis*; Wiley-VCH, 2011.
- (26) McDaniel, M. P.; Clear, K. S. *Appl. Catal. A Gen.* **2016**, 527, 116–126.
- (27) Lee, E. L.; Wachs, I. E. *J. Phys. Chem. C* **2007**, 111, 14410–14425.
- (28) Lee, E. L.; Wachs, I. E. *J. Phys. Chem. C* **2008**, 112, 6487–6498.
- (29) Chakrabarti, A.; Wachs, I. E. *Catal. Lett.* **2015**, 145, 985–994.
- (30) Moisii, C.; Deguns, E. W.; Lita, A.; Callahan, S. D.; van de Burgt, L. J.; Magana, D.; Stiegman, A. E. *Chem. Mater.* **2006**, 18, 3965–3975.
- (31) McDaniel, M. P. *Appl. Catal. A Gen.* **2017**, 542, 392–410.
- (32) Hogan, J. P.; Banks, R. L. US Patent 2 825 721, 1958.

- (33) Handzlik, J.; Gryboś, R.; Tielens, F. *J. Phys. Chem. C* **2013**, 117, 8138–8149.
- (34) Guesmi, H.; Tielens, F. *J. Phys. Chem. C* **2012**, 116, 994–1001.
- (35) Handzlik, J.; Kurleto, K. *Chem. Phys. Lett.* **2013**, 561–562, 87–91.
- (36) Cicmil, D.; Meeuwissen, J.; Vantomme, A.; Wang, J.; Ravenhorst, I. K.; van der Bij, H. E.; Muñoz-Murillo, A.; Weckhuysen, B. M. *Angew. Chem. Int. Ed.* **2015**, 127, 13265–13271.
- (37) Cimino, A.; Cordischi, D.; Febbraro, S.; Gazzoli, D.; Indovina, V.; Occhiuzzi, M.; Valigi, M.; Bocuzzi, F.; Chiorino, A.; Ghiotti, G. *J. Mol. Catal.* **1989**, 55, 23–33.
- (38) Beck, D. D.; Lunsford, J. H. *J. Catal.* **1981**, 68, 121–131.
- (39) Ayscough, P. B.; Eden, C.; Steiner, H. *J. Catal.* **1965**, 4, 278–190.
- (40) Weckhuysen, B. M.; De Ridder, L. M.; Grobet, P. J.; Schoonheydt, R. A. *J. Phys. Chem.* **1995**, 99, 320–326.
- (41) Weckhuysen, B. M.; De Ridder, L. M.; Schoonheydt, R. A. *J. Phys. Chem.* **1993**, 97, 4756–4763.
- (42) Weckhuysen, B. M.; Schoonheydt, R. A.; Jehng, J.-M.; Wachs, I. E.; Cho, S. J.; Ryoo, R.; Kijlstra, S.; Poels, E. *J. Chem. Soc. Faraday Trans.* **1995**, 91, 3245–3253.
- (43) Zecchina, A.; Gropo, E.; Damin, A.; Prestipino, C. *Top. Organomet. Chem.* **2005**, 16, 1–35.
- (44) Weckhuysen, B. M.; Schoonheydt, R. A. *Catal. Today* **1999**, 49, 441–451.
- (45) Panchenko, V. N.; Zakharov, V. A.; Paukshtis, E. A. *Appl. Catal. A Gen.* **2006**, 313, 130–136.
- (46) Michorczyk, P.; Ogonowski, J. *Chem. Commun.* **2012**, 48, 7283–7285.
- (47) Vuurman, M. A.; Wachs, I. E.; Stufkens, D. J.; Oskam, A. *J. Mol. Catal.* **1993**, 80, 209–227.
- (48) Wachs, I. E.; Roberts, C. A. *Chem. Soc. Rev.* **2010**, 39, 5002–5017.
- (49) Dines, T. J.; Inglis, S. *Phys. Chem. Chem. Phys.* **2003**, 5, 1320–1328.
- (50) Gropo, E.; Damin, A.; Bonino, F.; Zecchina, A.; Bordiga, S.; Lamberti, C. *Chem. Mater.* **2005**, 17, 2019–2027.
- (51) Peek, N. M.; Jeffcoat, D. B.; Moisii, C.; van de Burgt, L.; Profeta Jr., S.; Scott, S. L.; Stiegman, A. E. *J. Phys. Chem. C* **2018**, 122, 4399–4358.
- (52) McDaniel, M. P.; Martin, S. J. *J. Phys. Chem.* **1991**, 95, 3289–3293.
- (53) Baker, L. M.; Carrick, W. L. *J. Org. Chem.* **1968**, 33, 616–618.
- (54) Liu, B.; Nakatani, H.; Terano, M. *J. Mol. Catal. A Chem.* **2002**, 184, 387–398.
- (55) Liu, B.; Nakatani, H.; Terano, M. *J. Mol. Catal. A Chem.* **2003**, 201, 189–197.
- (56) Potter, K. C.; Beckerle, C. W.; Jentoft, F. C.; Schwerdtfeger, E.; McDaniel, M. P. *J. Catal.* **2016**, 344, 657–668.
- (57) Barzan, C.; Damin, A. A.; Budnyk, A.; Zecchina, A.; Bordiga, S.; Gropo, E. *J. Catal.* **2016**, 337, 45–51.
- (58) Barzan, C.; Piovano, A.; Braglia, L.; Martino, G. A.; Lamberti, C.; Bordiga, S.; Gropo, E. *J. Am. Chem. Soc.* **2017**, 139, 17064–17073.
- (59) Choi, K. Y.; Tang, S. *J. Appl. Polym. Sci.* **2004**, 91, 2923–2927.
- (60) Choi, K. Y.; Tang, S.; Yoon, W. *J. Macromol. Theory Simul.* **2004**, 13, 169–177.
- (61) Rebenstorf, B.; Larsson, R. *J. Mol. Catal.* **1981**, 11, 247–256.
- (62) Gropo, E.; Lamberti, C.; Bordiga, S.; Spoto, G.; Zecchina, A. *J. Catal.* **2006**, 240, 172–181.
- (63) Zhong, L.; Liu, Z.; Cheng, R.; Tang, S.; Qiu, P.; He, X.; Terano, M.; Liu, B. *ChemCatChem* **2012**, 4, 872–881.
- (64) Fong, A.; Yuan, Y.; Ivry, S. L.; Scott, S. L.; Peters, B. *ACS Catal.* **2015**, 5, 3360–3374.
- (65) Fong, A.; Peters, B.; Scott, S. L. *ACS Catal.* **2016**, 6, 6073–6085.
- (66) Ghiotti, G.; Garrone, E.; Zecchina, A. *J. Mol. Catal.* **1988**, 46, 61–77.

- (67) Zielinski, P.; Dalla Lana, I. G. *J. Catal.* **1992**, 137, 368–376.
(68) Kantcheva, M.; Dalla Lana, I. G.; Szymura, J. A. *J. Catal.* **1995**, 154, 329–334.
(69) Scott, S. L.; Amor Nait Ajjou, J. *Chem. Eng. Sci.* **2001**, 56, 4155–4168.
(70) Amor Nait Ajjou, J.; Scott, S. L. *J. Am. Chem. Soc.* **2000**, 122, 8968–8976.
(71) Espelid, Ø.; Børve, K. J. *J. Catal.* **2000**, 195, 125–139.
(72) Espelid, Ø.; Børve, K. J. *J. Catal.* **2002**, 205, 366–374.
(73) Espelid, Ø.; Børve, K. J. *J. Catal.* **2002**, 206, 331–338.
(74) Budnyk, A.; Damin, A.; Barzan, C.; Groppo, E.; Lamberti, C.; Bordiga, S.; Zecchina, A. *J. Catal.* **2013**, 308, 319–327.
(75) Myers, D. L.; Lunsford, J. H. *J. Catal.* **1985**, 92, 260–271.
(76) Goldsmith, B. R.; Peters, B.; Johnson, J. K.; Gates, B. C.; Scott, S. L. *ACS Catal.* **2017**, 7, 7543–7557.
(77) Fong, A.; Vandervelden, C.; Scott, S. L.; Peters, B. *ACS Catal.* **2018**, 8, 1728–1733.
(78) Myers, D. L.; Lunsford, J. H. *J. Catal.* **1986**, 99, 140–148.
(79) Conley, M. P.; Delley, M. F.; Siddiqi, G.; Lapadula, G.; Norsic, S.; Monteil, V.; Safonova, O. V.; Copéret, C. *Angew. Chem. Int. Ed.* **2014**, 53, 1872–1876.
(80) Delley, M. F.; Conley, M. P.; Copéret, C. *Catal. Lett.* **2014**, 144, 805–808.
(81) Delley, M. F.; Nuñez-Zarur, F.; Conley, M. P.; Comas-Vives, A.; Siddiqi, G.; Norsic, S.; Monteil, V.; Safonova, O. V.; Copéret, C. *Proc. Natl. Acad. Sci. USA* **2014**, 111, 11624–11629.
(82) Conley, M. P.; Delley, M. F.; Nuñez-Zarur, F.; Comas-Vives, A.; Copéret, C. *Inorg. Chem.* **2015**, 54, 5065–5078.
(83) Brown, C.; Krzystek, J.; Achey, R.; Lita, A.; Fu, R.; Meulenberg, R. W.; Polinski, M.; Peek, N.; Wang, Y.; van de Burgt, L. J.; Profeta Jr., S.; Stiegman, A. E.; Scott, S. L. *ACS Catal.* **2015**, 5, 5574–5583.
(84) Floryan, L.; Borosy, A. P.; Nuñez-Zarur, F.; Comas-Vives, A.; Copéret, C. *J. Catal.* **2017**, 346, 50–56.
(85) Brown, C.; Lita, A.; Tao, Y.; Peek, N.; Crosswhite, M.; Mileham, M. L.; Krzystek, J.; Achey, R.; Fu, R.; Bindra, J. K.; Polinski, M.; Wang, Y.; van de Burgt, L.; Jeffcoat, D.; Profeta Jr., S.; Stiegman, A. E.; Scott, S. L. *ACS Catal.* **2017**, 7, 7442–7455.
(86) Ma, Y.; Wang, L.; Liu, Z.; Cheng, R.; Zhong, L.; Yang, Y.; He, X.; Fang, Y.; Terano, M.; Liu, B. *J. Mol. Catal. A Chem.* **2015**, 401, 1–12.
(87) Budnyk, A.; Damin, A.; Groppo, E.; Zecchina, A.; Bordiga, S. *J. Catal.* **2015**, 324, 79–87.
(88) Ma, Y.; Cheng, R.; Li, J.; Zhong, L.; Liu, Z.; He, X.; Liu, B. *J. Organomet. Chem.* **2015**, 791, 311–321.
(89) Zhang, J.; Qiu, P.; Liu, Z.; Liu, B.; Batrice, R. J.; Botoshansky, M.; Eisen, M. S. *ACS Catal.* **2015**, 5, 3562–3574.
(90) Cicmil, D.; van Ravenhorst, I. K.; Meeuwissen, J.; Vantomme, A.; Weckhuysen, B. M. *Catal. Sci. Technol.* **2016**, 6, 731–743.
(91) Barzan, C.; Bordiga, S.; Groppo, E. *ACS Catal.* **2016**, 6, 2918–2922.
(92) Cicmil, D.; Meeuwissen, J.; Vantomme, A.; Weckhuysen, B. M. *ChemCatChem* **2016**, 8, 1937–1944.
(93) Barzan, C.; Bordiga, S.; Quadrelli, E. A.; Groppo, E. *Top. Catal.* **2016**, 59, 1732–1739.
(94) Delley, M. F.; Praveen, C. S.; Borosy, A. P.; Nuñez-Zarur, F.; Comas-Vives, A.; Copéret, C. *J. Catal.* **2017**, 354, 223–230.
(95) Sun, Q.; Cheng, R.; Liu, Z.; He, X.; Zhao, N.; Liu, B. *ChemCatChem* **2017**, 9, 3364–3373.
(96) Liu, Z.; Cheng, R.; He, X.; Wu, X.; Liu, B. *J. Phys. Chem. A* **2012**, 116, 7538–7549.
(97) Cheng, Z.; Lo, C. S. *ACS Catal.* **2012**, 2, 341–349.

- (98) Handzlik, J.; Ogonowski, J. *J. Phys. Chem. C* **2012**, 116, 5571–5584.
- (99) Neyman, K. M.; Illas, F. *Catal. Today* **2005**, 105, 2–16.
- (100) Tielens, F.; Gervais, C.; Lambert, J. F.; Mauri, F.; Costa, D. *Chem. Mater.* **2008**, 20, 3336–3344.
- (101) Gierada, M.; Petit, I.; Handzlik, J.; Tielens, F. *Phys. Chem. Chem. Phys.* **2016**, 18, 32962–32972.
- (102) Liu, B.; Fang, Y.; Xia, W.; Terano, M. *Kinet. Catal.* **2006**, 47, 234–240.
- (103) Perdew, J.; Chevary, J.; Vosko, S.; Jackson, K.; Pederson, M.; Singh, D.; Fiolhais, C. *Phys. Rev. B* **1993**, 46, 6671–8867.
- (104) Weigend, F.; Ahlrichs, R. *Phys. Chem. Chem. Phys.* **2005**, 7, 3297–3305.
- (105) Frisch, M. J.; Trucks, G. W.; Schlegel, H. B.; Scuseria, G. E.; Robb, M. A.; Cheeseman, J. R.; Scalmani, G.; Barone, V.; Mennucci, B.; Petersson, G. A.; Nakatsuji, H.; Caricato, M.; Li, X.; Hratchian, H. P.; Izmaylov, A. F.; Bloino, J.; Zheng, G.; Sonnenberg, J. L.; Hada, M.; Ehara, M.; Toyota, K.; Fukuda, R.; Hasegawa, J.; Ishida, M.; Nakajima, T.; Honda, Y.; Kitao, O.; Nakai, H.; Vreven, T.; Montgomery, J. A. J.; Peralta, J. E.; Ogliaro, F.; Bearpark, M.; Heyd, J. J.; Brothers, E.; Kudin, K. N.; Staroverov, V. N.; Kobayashi, R.; Normand, J.; Raghavachari, K.; Rendell, A.; Burant, J. C.; Iyengar, S. S.; Tomasi, J.; Cossi, M.; Rega, N.; Millam, J. M.; Klene, M.; Knox, J. E.; Cross, J. B.; Bakken, V.; Adamo, C.; Jaramillo, J.; Gomperts, R.; Stratmann, R. E.; Yazyev, O.; Austin, A. J.; Cammi, R.; Pomelli, C.; Ochterski, J. W.; Martin, R. L.; Morokuma, K.; Zakrzewski, V. G.; Voth, G. A.; Salvador, P.; Dannenberg, J. J.; Dapprich, S.; Daniels, A. D.; Farkas, Ö.; Foresman, J. B.; Ortiz, J. V.; Cioslowski, J.; Fox, D. J. *Gaussian 09 Revision D.01*, Gaussian Inc., Wallingford CT, 2013.
- (106) Kresse, G.; Hafner, J. *Phys. Rev. B* **1993**, 47, 558–561.
- (107) Kresse, G.; Furthmüller, J. *Comput. Mater. Sci.* **1996**, 6, 15–50.
- (108) Kresse, G.; Furthmüller, J. *Phys. Rev. B* **1996**, 54, 11169–11186.
- (109) Gianolio, D.; Groppo, E.; Vitillo, J. G.; Damin, A.; Bordiga, S.; Zecchina, A.; Lamberti, C. *Chem. Commun.* **2010**, 46, 976–978.
- (110) Groppo, E.; Damin, A.; Arean, C. O.; Zecchina, A. *Chem. Eur. J.* **2011**, 17, 11110–11114.
- (111) Adamo, C.; Barone, V. *J. Chem. Phys.* **1999**, 110, 6158–6170.
- (112) Grimme, S.; Antony, J.; Ehrlich, S.; Krieg, H. *J. Chem. Phys.* **2010**, 132, 154104–154123.
- (113) Grimme, S.; Ehrlich, S.; Goerigk, L. *J. Comput. Chem.* **2011**, 32, 1456–1465.
- (114) Wright, A. F.; Leadbetter, A. J. *Philos. Mag.* **1975**, 31, 1391–1401.
- (115) Mortensen, J. J.; Parrinello, M. *J. Phys. Chem. B* **2000**, 104, 2901–2907.
- (116) Ceresoli, D.; Bernasconi, M.; Iarlori, S.; Parrinello, M.; Tosatti, E. *Phys. Rev. Lett.* **2000**, 84, 3887–3890.
- (117) Solans-Monfort, X.; Filhol, J.-S.; Copéret, C.; Eisenstein, O. *New J. Chem.* **2006**, 30, 842–850.
- (118) Mian, S. A.; Saha, L. C.; Jang, J.; Wang, L.; Gao, X.; Nagase, S. *J. Phys. Chem. C* **2010**, 114, 20793–20800.
- (119) Handzlik, J. *Chem. Phys. Lett.* **2009**, 469, 140–144.
- (120) Liu, B.; Šindelář, P.; Fang, Y.; Hasebe, K.; Terano, M. *J. Mol. Catal. A Chem.* **2005**, 238, 142–150.
- (121) Arlman, E.; Cossee, P. *J. Catal.* **1964**, 3, 99–104.
- (122) Rimola, A.; Costa, D.; Sodupe, M.; Lambert, J. F.; Ugliengo, P. *Chem. Rev.* **2013**, 113, 4216–4313.
- (123) Gao, X.; Bare, S. R.; Fierro, J. L. G.; Banares, M. A.; Wachs, I. E. *J. Phys. Chem. B* **1998**, 102, 5653–5666.

- (124) Inaki, Y.; Yoshida, H.; Yoshida, T.; Hattori, T. *J. Phys. Chem. B* **2002**, 106, 9098–9106.
- (125) Antonietti, M.; Michalski, M.; Heiz, U.; Jones, H.; Lim, K. H.; Rösch, N.; Vitto, A. Del; Pacchioni, G. *Phys. Rev. Lett.* **2005**, 94, 213402.
- (126) Giordano, L.; Sushko, P. V.; Pacchioni, G.; Shluger, A. L. *Phys. Rev. Lett.* **2007**, 99, 136801.
- (127) Musso, F.; Ugliengo, P.; Solans-Monfort, X.; Sodupe, M. *J. Phys. Chem. C* **2010**, 114, 16430–16438.
- (128) Zeleňák, V.; Zeleňáková, A.; Kováč, J. *Colloids and Surfaces A*: **2010**, 357, 97–104.
- (129) Glinka, Y. D.; Jaroniec, C. P.; Jaroniec, M. *J. Colloid Interface Sci.* **1998**, 201, 210–219.
- (130) Glinka, Y. D.; Lin, S.-H.; Hwang, L.-P.; Chen, Y.-T. *J. Phys. Chem. B* **2000**, 104, 8652–8663.
- (131) Busca, G.; Lamotte, J.; Lavalle, J.-C.; Lorenzelli, V. *J. Am. Chem. Soc.* **1987**, 109, 5197–5202.

9. Pełne teksty artykułów będących podstawą pracy doktorskiej

Artykuł D1

Zastosowanie oraz struktura form powierzchniowych układów katalitycznych Cr/SiO₂

Maciej Gierada,✉ Jarosław Handzlik

Przem. Chem. 94(6) (2015) 900-905

Use of the Cr/SiO₂ catalysts and structure of their surface species

Zastosowanie oraz struktura form powierzchniowych układów katalitycznych Cr/SiO₂

DOI: 10.15199/62.2015.6.8

A review, with 70 refs., of the title catalysts as used for polymn. of olefins, oxidn. of org. compds. and oxidative dehydrogenation of alkanes.

Tlenkowe formy chromu osadzone na powierzchni krzemionki to powszechnie stosowane układy katalityczne w przemyśle chemicznym. Jednak pomimo wielu lat badań, głównie eksperymentalnych, struktura form powierzchniowych oraz mechanizmy reakcji związane z tymi układami nie zostały jednoznacznie ustalone. Dokonano przeglądu literaturowego związanego z katalizatorem Cr/SiO₂. Opisano jego najważniejsze zastosowania w różnych procesach oraz przedstawiono bieżący stan badań nad ustaleniem struktury form powierzchniowych.

Po II Wojnie Światowej naukowcy pracujący w amerykańskich spółkach naftowych Phillips Petroleum i Standard Oil Company of Indiana rozpoczęli badania nad metodami konwersji olefin do paliw benzynowych i smarów. Celem było znalezienie zastosowania dla tychże węglowodorów nienasyconych, które otrzymywano jako produkty uboczne w różnych procesach rafinacji. Efektem tych prac było m.in. przypadkowe odkrycie katalizatorów polimeryzacji etylenu do liniowego polietylenu. Zsyntezowane układy katalityczne oparte były na

metalu przejściowym naniesionym na trwały termicznie nośnik. Wśród nich najważniejszą grupę stanowiły układy zawierające tlenek chromu osadzony na krzemionce, tzw. katalizatory Phillipsa odkryte przez Hogana i Banksa. Inną grupę stanowiły układy oparte na tlenku molibdenu naniesionym na tlenek glinu, które odkryte zostały przez Zletza i współprac. Katalizatory na bazie chromu szybko zyskały na znaczeniu, głównie dzięki intensywnej promocji Phillipsa (obecnie Chevron Phillips Chemical Company), natomiast odkryte przez Zletza i współprac. nie znalazły powszechnego zastosowania w procesach polimeryzacji¹⁾.

Celem pracy było przedstawienie bieżącej wiedzy na temat układu Cr/SiO₂, ze szczególnym uwzględnieniem jego zastosowań w przemyśle chemicznym. Przedyskutowano również obecny stan badań nad ustaleniem struktury tlenkowych form chromu na powierzchni krzemionki.

Polimeryzacja

Odkryte przez Hogana i Banksa układy katalityczne na bazie chromu zostały opatentowane we wczesnych latach pięćdziesiątych XX w.²⁾. Początkowo układy te stosowane były jedynie jako katalizatory w procesie otrzymywania polietylenu wysokiej gęstości PE-HD (*high-density polyethylene*). W następnych latach ich zastosowanie zostało rozszerzone do syntezy liniowego polietylenu niskiej gęstości PE-LLD (*linear low-density polyethylene*). Ten ostatni polimer otrzymuje się metodą kopolimeryzacji etylenu w obecności niewielkich ilości α-olefin, takich jak but-1-en, heks-1-en lub okt-1-en. Do dnia dzisiejszego w procesie polimeryzacji olefin, w tym głównie etylenu, powszechnie stosuje się układy Cr/SiO₂³⁻¹⁰⁾. Obecnie szacuje się, że



Mgr inż. Maciej GIERADA w roku 2014 ukończył studia na Wydziale Inżynierii i Technologii Chemicznej Politechniki Krakowskiej. Obecnie jest doktorantem w Katedrze Technologii Organicznej i Procesów Rafineryjnych tej uczelni. Specjalność – lekka technologia organiczna.

* Autor do korespondencji:

Katedra Technologii Organicznej i Procesów Rafineryjnych, Instytut Chemii i Technologii Organicznej, Politechnika Krakowska im. Tadeusza Kościuszki, ul. Warszawska 24, 31-155 Kraków, tel.: (12) 628-27-64, fax: (12) 628-20-37, email: mgierada@chemia.pk.edu.pl



Dr hab. inż. Jarosław HANDZLIK w roku 1993 ukończył studia na Wydziale Inżynierii i Technologii Chemicznej Politechniki Krakowskiej. Obecnie jest profesorem nadzwyczajnym Politechniki Krakowskiej, pracuje w Katedrze Technologii Organicznej i Procesów Rafineryjnych tej uczelni. Specjalność – kataliza, chemia teoretyczna.

katalizatory Phillipsa stosowane są w 40–50% światowej produkcji politylenu^{11, 12)}. Przy zastosowaniu tych katalizatorów otrzymuje się więcej niż 50 różnych odmian tego polimeru^{13, 14)}. Do głównych zalet układów odkrytych przez Hogana i Banksa należy zaliczyć brak potrzeby stosowania aktywatorów lub promotorów¹²⁾. Ponadto, zarówno synteza układu, jak i prowadzenie procesu polimeryzacji nie jest skomplikowane. Należy jednak zaznaczyć, że katalizatorów Phillipsa nie stosuje się w procesie otrzymywania politylenu niskiej gęstości PE-LD (*low-density polyethylene*). Ten typ politylenu otrzymuje się metodą wysokociśnieniowej/wysokotemperaturowej wolnorodnikowej polimeryzacji etylenu. Typowe warunki procesu produkcji PE-LD to temp. 350–450 K i ciśnienie powyżej 50 bar. Oprócz Cr/SiO₂ przy produkcji PE-HD i PE-LLD są stosowane także katalizatory homogeniczne^{1, 6)}.

Polimeryzację etylenu przy zastosowaniu katalizatorów Phillipsa w przemyśle prowadzi się wg jednego z trzech wariantów. Pierwsza odmiana polega na reakcji w roztworze. Jako substancję rozpuszczającą powstały polimer stosuje się inertne węglowodory należące do grupy cykloparafin, przede wszystkim cykloheksan. Proces prowadzony jest w temp. 400–450 K i pod ciśnieniem 20–30 bar. Z otrzymanego polimeru usuwa się monomer przez odparowanie, a zawiesinę katalizatora oddziela się w procesie filtracji. Innym wariantem jest proces znany jako Phillips Particle Form® (Phillips Petroleum). W procesie tym stosuje się ciekłe dyspergatory, głównie *n*-pentan, mające na celu utrzymanie zarówno politylenu, jak i układu katalitycznego w zawiesinie w trakcie prowadzenia polimeryzacji. Temperatura procesu nie powinna przekraczać 380 K, co ma na celu uniknięcie rozpuszczania polimeru. Inną odmianą prowadzenia polimeryzacji przy zastosowaniu katalizatorów Phillipsa jest proces znany pod nazwą Unipol® (Union Carbide). W tym wariantie reakcja przebiega w fazie gazowej, w reaktorze z fluidalnym złożem katalizatora. Proces prowadzi się w temp. ok. 370 K i pod ciśnieniem 20 bar. Odmienna ta nie wymaga stosowania żadnych rozpuszczalników i dyspergatorów, co znacznie obniża koszty produkcji polimeru^{3, 4, 6, 15)}.

Układy katalityczne oparte na Cr/SiO₂ wykazują dużą aktywność w procesie polimeryzacji olefin, w tym głównie etylenu. Można by przypuszczać, że układy te z powodzeniem stosuje się jako katalizatory polimeryzacji innych alkenów, np. propylenu. Okazuje się jednak, że ich zastosowanie w przypadku polimeryzacji tego ostatniego związku na skalę przemysłową nie przynosi zadowalających korzyści.

Niewiele prowadzono badań dotyczących polimeryzacji alkinów w obecności katalizatorów Phillipsa. Zecchina i współprac.¹⁶⁾ wykazali, że zachodzi jedynie cyklotrimeryzacja acetylenu lub metyoacetylenu (propynu), a produktem reakcji jest odpowiednio benzen lub 1,3,5-trimetylobenzen. W oparciu o dane spektroskopowe autorzy określili mechanizm tej reakcji. W ostatnich latach prowadzono również badania teoretyczne nad zastosowaniem układów Cr/SiO₂ w reakcji cyklotrimeryzacji acetylenu i metyoacetylenu^{14, 17)}, których efektem było m.in. zaproponowanie innych mechanizmów tych reakcji, niż w pracy Zecchiny i współprac.¹⁶⁾

Odwodornienie

Zastosowanie heterogenicznych układów katalitycznych opartych na chromie w reakcjach hydrogenacji i dehydrogenacji^{10, 18–21)} było przedmiotem intensywnych badań. Katalizatory te wykazują ponadto aktywność w reakcji dehydrocyklizacji²²⁾ i dehydroizomeryzacji alkanów²³⁾.

W literaturze dużą uwagę skupiono na katalitycznej dehydrogenacji lekkich alkanów. Idea procesu polega na pozyskaniu cenniejszych substancji o szerszym zastosowaniu (olefin) z dużo tańszego surowca, jakim są nasycone węglowodory. Katalityczne właściwości układów Cr/Al₂O₃ w procesie odwodorowania zostały po raz pierwszy odkryte przez Freya i Huppkego w 1933 r. i opatentowane 4 lata później²⁴⁾. Układy te obecnie znane są pod nazwą katalizatorów Houdry. Katalizują one konwersję etanu do etylenu, propanu do propenu, *n*-butanu do butadienu, izobutanu do izobutenu i etylobenzenu do sty-

renu w warunkach względnie wysokiej temp. (720–970 K) i niskiego ciśnienia (1–5 bar). Ze względu na liczne reakcje uboczne, takie jak kraking lub koksowanie, wynikające z obecności Al₂O₃ jako nośnika, układy te ulegają szybkiej dezaktywacji, co wymaga regeneracji katalizatora^{3, 10)}. Prowadzone były również badania nad innymi układami katalizującymi proces odwodorowania, w tym Cr/SiO₂. Miały one na celu identyfikację centrów aktywnych, określenie wpływu preparaty i warunków obróbki katalizatora na aktywność, selektywność i struktury powierzchniowe oraz wyjaśnienie mechanizmu reakcji dehydrogenacji²⁵⁾.

Pomimo tego, że układ Cr/SiO₂ również wykazuje aktywność w reakcjach odwodorowania, to w przemysłowych procesach zastosowanie znalazło głównie katalizator Cr/Al₂O₃. Od momentu odkrycia przez Freya i Huppkego aktywności katalitycznej układów opartych na chromie w reakcji odwodorowania, kilka koncernów chemicznych rozpoczęło badania nad ich zastosowaniem w warunkach przemysłowych. Główne problemy technologiczne, bez rozwiązania których prowadzenie procesu w warunkach ciągłych byłoby niemożliwe, to odpowiednie dostarczenie ciepła do przestrzeni reakcyjnej, kontrola temperatury zapewniająca minimalną degradację produktów, ale również maksymalny stopień konwersji oraz umożliwienie regeneracji układu katalitycznego. W zależności od firmy pojawiły się różne rozwiązania technologiczne. Proces Catofin® jest jednym z najlepiej rozwiniętych. Stosowany jest on w celu odwodorowania alkanów do alkenów. Składa się z serii połączonych ze sobą adiabatycznych reaktorów ze stałym złożem katalizatora, w których cyklicznie prowadzi się reakcję dehydrogenacji i regeneracji układu katalitycznego. Inne rozwiązanie technologiczne zastosowano w procesie Snamprogetti-Yarsitez®. W tej odmianie reakcję prowadzi się w reaktorze z fluidalnym złożem katalizatora. Do innych technologii stosowanych do przeprowadzenia odwodorowania należą procesy Catadiene® (dieny), LINDEBASF®, UOP®. We wszystkich tych procesach ciepło wydzielone podczas wypalania depozytu węglowego wykorzystywane jest do przeprowadzenia silnie endotermicznej reakcji odwodorowania²⁵⁾.

Proces odwodorowania przy zastosowaniu układów katalitycznych na bazie chromu może być prowadzony również w warunkach utleniających, zarówno w obecności O₂^{26–28)}, jak i CO₂^{29–31)} jako czynnika utleniającego. Podobnie jak w przypadku tradycyjnego procesu odwodorowania, główne zastosowanie znalazły układy oparte na Cr/Al₂O₃. Niemniej prowadzone były prace nad zastosowaniem innych nośników²⁷⁾. Badania procesu utleniającego odwodorowania propanu do propenu dowodzą, że aktywność i selektywność silnie uzależniona jest od zawartości chromu i rodzaju zastosowanego nośnika. Stopień konwersji propanu i selektywność otrzymywania propenu zwiększa się wraz z zawartością chromu, aż do pokrycia powierzchni monowarstwą fazy aktywnej. Aktywność katalityczna odniesiona do liczby centrów aktywnych na powierzchni TOF (*turnover frequency*) zmieniała się w zależności od zastosowanego nośnika i zwiększała się w szeregu: Cr/Al₂O₃ ≈ Cr/SiO₂–Al₂O₃ < Cr/SiO₂ ≈ Cr/TiO₂. Jednak dla każdego z zastosowanych układów katalitycznych wartość TOF była w danej temperaturze niezależna od stopnia pokrycia powierzchni fazą aktywną, aż do osiągnięcia monowarstwy.

Takahara i Saito³²⁾ badali proces odwodorowania propanu w obecności CO₂ przy zastosowaniu układów katalitycznych na bazie chromu niesionego na różne nośniki. Stwierdzono, że największą aktywność w tej reakcji wykazywał katalizator, w którym jako nośnik zastosowano SiO₂. Ponadto dowiedziono, że tylko w przypadku krzemionki CO₂ wywierał promujący efekt. Do podobnych konkluzji doszła inna grupa badaczy³³⁾, wykazując że charakter nośnika istotnie wpływał na aktywność katalityczną. Przy zastosowaniu Al₂O₃ selektywność otrzymywania propenu jest znaczco mniejsza niż w przypadku układu Cr/SiO₂. Inne badania³⁰⁾ wskazują, że największą aktywność, stabilność i selektywność wykazują układy o zawartości chromu ok. 5% mas.

Tego samego typu katalizatory znalazły również zastosowanie w reakcji uwodorowania^{19–21)}, jednakże ze względów termodynamicznych, procesy te prowadzi się w warunkach względnie niskiej temperatury i wysokiego ciśnienia.

Utlenianie

Procesy utleniania związków organicznych mogą być katalizowane przez układy na bazie chromu, przy czym w przemysłowych metodach zastosowanie znalazły głównie heterogeniczne systemy katalityczne, co wynika z łatwości regeneracji katalizatora oraz oddzielenia go od produktów reakcji. Prowadzenie reakcji w warunkach katalizy homogenicznej implikuje stosowanie najczęściej stochiometrycznych stężeń soli zawierającej Cr(VI), które zwykle nie ulegają regeneracji po procesie, co generuje wysokie koszty i toksyczne odpady³⁾.

Heterogeniczne układy tlenkowe oparte na chromie wykazują wysoką aktywność w różnych procesach selektywnego utleniania m.in. benzofenonu, difenylometanu i etanolu^{3, 34–36)} oraz olefin, np. but-1-enu²⁶⁾ i chlorowcopochodnych, np. chlorku metylenu³⁾. Jednak najszerzej prowadzone były badania procesu utleniania metanolu do formaldehydu przy zastosowaniu układów na bazie chromu naniesionego na różne nośniki^{35, 36)}. Stwierdzono, że selektywność otrzymywania formaldehydu zmienia się w zależności od zastosowanego nośnika oraz stopnia pokrycia powierzchni przez chrom. Nośniki charakteryzujące się mocnymi centrami kwasowymi typu Lewisa (np. Al_2O_3) zwiększą selektywność otrzymywania eteru dimetylowego, produktu ubocznego w tej reakcji. Natomiast nośniki posiadające słabe centra kwasowe typu Lewisa (np. SiO_2) lub centra redoksowe preferują powstawanie innego produktu ubocznego – mrówczanu metylu. Co więcej, selektywność otrzymywania produktów ubocznych zmniejsza się wraz ze wzrostem stopnia pokrycia powierzchni przez chrom. W przypadku układu Cr/SiO_2 powstawanie mrówczanu metylu może być ograniczone poprzez zmniejszenie liczby grup hydroksylowych na powierzchni SiO_2 . Efekt taki otrzymuje się przeprowadzając wysokotemperaturową kalcynację katalizatora. Im mniej grup hydroksylowych na powierzchni, tym bardziej ograniczona jest adsorpcja metanolu, który reagując z formaldehydem daje mrówczan metylu. Przeprowadzenie kalcynacji układu Cr/SiO_2 w temp. 920 K pozwala otrzymać formaldehyd metodą utleniania metanolu z selektywnością ok. 90%^{3, 35, 36)}.

Heterogeniczne układy katalityczne na bazie chromu są również aktywne w reakcjach całkowitego utleniania węglowodorów³⁷⁾. Badania porównawcze nad utlenianiem metanu w obecności różnych układów katalitycznych (Cr/SiO_2 , V/SiO_2 , Mo/SiO_2) wykazały, że aktywność ta zmienia się w szeregu $\text{Cr} > \text{V} > \text{Mo}$. Ponadto, zastosowanie układu Cr/SiO_2 pozwala prowadzić proces z największą selektywnością³⁾.

Katalizatory chromowe były również badane pod kątem zastosowania w procesach katalitycznego usuwania tlenku azotu, tlenku węgla i chlorowcopochodnych z gazów spalinowych. Selektynna katalityczna redukcja SCR (*selective catalytic reduction*) tlenków azotu jest jedną z najczęściej stosowanych metod kontroli emisji NO_x do atmosfery przez różne zakłady chemiczne. Najefektywniejszym układem katalizującym ten proces jest $\text{V}_2\text{O}_5/\text{TiO}_2$. Katalizator $\text{Cr}/\text{Al}_2\text{O}_3$ wykazuje aktywność w rozważanych reakcjach SCR, jednak optymalne parametry prowadzenia procesu, np. temp. reakcji ok. 470 K, uniemożliwiają jego zastosowanie w warunkach przemysłowych. Aktywność wykazuje również amorficzny i krystaliczny Cr_2O_3 , jednak przy zastosowaniu tego związku jako katalizatora, oprócz selektywnej redukcji NO_x do N_2 , zachodzi ubocznie niekorzystny proces utlenienia NH_3 , szczególnie w wyższych temperaturach. Prowadzone były również badania nad układem Cr/TiO_2 . Dowiedziono, że system ten jest aktywny w reakcji SCR w temp. poniżej 200 K, jednak wykazuje mniejszą selektywność w porównaniu z $\text{V}_2\text{O}_5/\text{TiO}_2$ ³⁾.

Preparatyka i aktywacja

Do wymagań stawianych heterogenicznym katalizatorom zawierającym Cr należy zaliczyć dużą odporność termiczną i mechaniczną gwarantującą stabilność pracy w warunkach reakcji, możliwość regeneracji i łatwość wydzielenia z produktów reakcji, wysoką aktywność, selektywność i wydajność, oraz łatwą preparatykę. Należy jednak zaznaczyć, że parametry preparatyki, w tym m.in. obróbka termiczna,

istotnie wpływają na strukturę fazy aktywnej na nośniku, a tym samym na właściwości katalityczne^{1, 3)}.

Katalizator Phillipsa to jeden z najprostszych jak dotąd zsyntezowanych układów stosowanych w polimeryzacji olefin. Jego preparatyka składa się z dwóch zasadniczych etapów. Pierwszy z nich polega na nanoszeniu substancji aktywnej na nośnik metodą impregnacji. Jako źródło chromu najczęściej stosuje się octan chromu(III), tlenek chromu(VI) lub azotan chromu(III). Po wysuszeniu, układ jest kalcynowany w temp. powyżej 770 K. Podczas kalcynacji powstają powierzchniowe struktury Cr(VI) i następuje częściowa dehydroksylacja powierzchni krzemionki. Typowa powierzchnia amorficznej krzemionki wynosi ok. 400 m²/g, stąd przy zawartości 0,5–1% mas. Cr odpowiada to^{13, 38–40)} ok. 0,2–0,4 atomów chromu na nm².

W praktyce przemysłowej proces kalcynacji katalizatora Cr/SiO_2 prowadzony jest w złożu fluidalnym, a na jej efektywność wpływa wiele czynników, m.in. temperatura procesu, wysokość złożu, objętościowe natężenie przepływu gazu, zawartość wilgoci oraz czas prowadzenie procesu³⁸⁾.

Katalizator Phillipsa poddaje się również aktywacji *in situ*. Proces ten może być przeprowadzony na dwa różne sposoby: (i) W warunkach przemysłowych układ katalityczny najczęściej wstępnie kontaktuje się z etylenem w temp. ok. 350–370 K. W okresie indukcji zachodzi proces redukcji wyjściowych form Cr(VI), czego wynikiem jest obecność struktur na niższych stopniach utlenienia, w tym głównie na 2+. Struktury te uważa się za formę aktywną katalizatora, choć najnowsze badania sugerują, że to Cr(III) jest formą aktywną^{11, 12, 41)}. (ii) Katalizator Cr/SiO_2 można wstępnie poddać redukcji do Cr(II) w temp. ok. 620 K w obecności CO, po której wykazuje on aktywność katalityczną w reakcji polimeryzacji etylenu już w temperaturze pokojowej. Pod względem wydajności oraz selektywności otrzymywania polietylenu oba wyżej opisane etapy aktywacji dają porównywalne wyniki, jednak wariant (i) jest mniej skomplikowany, stąd jego powszechnie zastosowanie w przemyśle⁴²⁾.

Struktura i właściwości

Powierzchniowe struktury heterogenicznych układów katalitycznych Cr/SiO_2 były obiektem szczegółowych, głównie eksperymentalnych badań w ciągu ostatnich 60 lat. Pomimo to, struktura form tlenkowych Cr nie jest jednoznacznie określona. W literaturze dyskutuje się nad różnymi konfiguracjami centrów aktywnych zarówno dla układu utlenionego – zawierającego centra Cr(VI), jak i zredukowanego – Cr(III) i Cr(II). Zainteresowanie naukowców tym tematem jest zrozumiałe. Bez jednoznacznego określenia struktur powierzchniowych nie można określić np. mechanizmu reakcji polimeryzacji olefin przy zastosowaniu katalizatorów Phillipsa³⁹⁾. Mechanizm ten do dnia dzisiejszego pozostaje nieustalony, pomimo wielu badań^{1, 6, 11, 12, 43–47)}. Obecnie, zarówno prace eksperymentalne, jak i modele teoretyczne stanowią podstawy określania struktur powierzchniowych katalizatorów heterogenicznych.

Układy utlenione Cr(VI)

Najwięcej opublikowanych prac dotyczy określenia struktur powierzchniowych form Cr(VI) w kalcynowanym katalizatorze Cr/SiO_2 , będących zwykle prekursorami centrów aktywnych. W zależności od wielu czynników, różne konfiguracje centrów są mniej lub bardziej prawdopodobne. Do najistotniejszych parametrów wpływających na powstawanie poszczególnych form Cr(VI) należy zaliczyć: rodzaj zastosowanego nośnika (typ krzemionki, porowatość), stężenie grup hydroksylowych, zawartość chromu, parametry preparatyki układu katalitycznego (temperatura, czas, atmosfera kalcynacji) i obecność ewentualnych domieszek innych substancji⁶⁾.

Dane otrzymane przy zastosowaniu spektroskopii UV-Vis wskazują na obecność monomerycznych, dimerycznych i polimerycznych form Cr(VI) (rys. 1). Stosunek form monomerycznych do dimerycznych zależy od rodzaju zastosowanej krzemionki i zawartości chromu^{3, 4, 6, 7, 30, 31, 48–52)}.

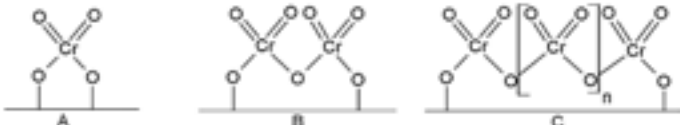


Fig. 1. Possible surface Cr(VI) oxide species on silica: A – monomeric, B – dimeric, C – polymeric for $n \geq 1$ ⁵⁷

Rys. 1. Możliwe struktury powierzchniowych form tlenkowych Cr(VI) na krzemionce: A – struktura monomeryczna, B – dimeryczna, C – polimeryczna dla $n \geq 1$ ⁵⁷

Starano się określić różnice pomiędzy strukturami monomerycznymi i dimerycznymi, badając zmianę zawartości grup hydroksylowych na powierzchni krzemionki podczas prowadzenia procesu osadzania substancji aktywnej na nośniku. Spodziewano się, że układy monomeryczne powinny powstawać wskutek reakcji dwóch grup hydroksylowych na jeden atom chromu, podczas gdy formy dimeryczne to produkty reakcji jednej grupy hydroksylowej na jeden atom chromu. Zastosowanie takiego podejścia nie przyniosło jednak jednoznacznych wyników. Zaobserwowano, że stosunek ubytku liczby grup hydroksylowych do liczby atomów chromu nie jest wielkością stałą. Zależy m.in. od temperatury kalcynacji⁶.

Spektroskopia Ramana to jedna z najważniejszych technik badawczych stosowana w badaniach struktury form powierzchniowych Cr na krzemionce. Otrzymane wyniki wskazują, że w przypadku niewielkich zawartości chromu dominującymi, a czasem jedynymi formami powierzchniowymi Cr(VI), są struktury monomeryczne^{6, 26, 27, 35, 36, 39, 48, 52–56}. Występowanie izolowanych form Cr(VI) potwierdzają również badania EXAFS-XANES^{5, 6, 8, 56}. Jak już zostało wspomniane, najczęściej stosuje się układy katalityczne poddane uprzednio procesowi wysokotemperaturowej kalcynacji. Zabieg taki w przeważającej większości powoduje formowanie się dobrze zdyspergowanych powierzchniowych form tlenkowych Cr(VI)^{3–10, 18, 23, 26–31, 34–37, 39, 48–57}, które są już centrami aktywnymi lub ich prekursorami^{3–10, 18, 26–28, 30, 31, 34–36, 48}.

Prawdopodobnie dominującą powierzchniową formą monomeryczną Cr(VI) jest struktura diokso o budowie tetraedrycznej, w której dwa atomy tlenu łączą chrom z powierzchnią krzemionki, natomiast dwa kolejne atomy tlenu stanowią ligandy okso (rys. 1A). Za obecnością takiej struktury przemawiają wyniki badań spektroskopii Ramana, EXAFS oraz XANES^{6, 8, 26, 27, 35, 36, 39, 48, 52–56}. Ponadto, niektóre prace^{52, 54–56} wskazują, że na powierzchni układu Cr/SiO₂ poddanego wcześniej procesowi kalcynacji w mniejszości obecna jest również konfiguracja monookso, w której atom chromu charakteryzuje się liczbą koordynacyjną równą 5. W tym przypadku występują 4 mostki tlenowe pomiędzy atomem chromu a powierzchnią krzemionki, natomiast jeden atom tlenu jest ligandem okso. Najnowsza praca Chakrabartiiego i Wachs⁴¹ wskazuje, że ok. 2/3 całej fazy aktywnej na powierzchni krzemionki stanowią formy diokso, natomiast ok. 1/3 to struktury monookso. Opierając się na metodzie H₂-TPSR oraz H₂-TP-Raman badano również kinetykę redukcji form Cr(VI). Wyniki otrzymane przez tych badaczy⁴¹ wskazują, że w temp. 773 K formy diokso ulegają redukcji ok. 37 razy szybciej niż struktury monookso. W niższych temperaturach różnica w szybkości redukcji poszczególnych form powierzchniowych jest jeszcze większa.

Komplementarnych informacji dotyczących powierzchniowych struktur w katalizatorach heterogenicznych dostarczają badania teoretyczne oparte na metodach obliczeniowych chemii kwantowej. Główną zaletą tego typu podejścia jest możliwość uzyskania informacji, które są nieosiągalne przy zastosowaniu metod doświadczalnych. Ponadto, porównanie wyników badań teoretycznych i doświadczalnych pozwala na weryfikację tych pierwszych oraz dokładniejszą interpretację tych drugich. Ciągle zwiększająca się moc obliczeniowa komputerów pozwala rozważać modele o coraz większej złożoności, odpowiadające w coraz większym stopniu rzeczywistości. Ma to szczególnie istotne znaczenie w przypadku badania struktury układu Cr/SiO₂, głównie ze względu na amorficzną naturę krzemionki^{58, 59}.

W ostatnim czasie ukazały się prace teoretyczne dotyczące struktur form powierzchniowych w układzie Cr(VI)/SiO₂, w których zastosowano teorię funkcjonału gęstości (DFT) i bardzo zaawansowane modele amorficznej krzemionki^{58, 59}. Celem badań Guesmi i Tielensa⁵⁸ było m.in. określenie najbardziej prawdopodobnej geometrii tlenkowych form Cr(VI) na powierzchni częściowo uwodnionej krzemionki. Rozważano kilka modeli połączonych jednym, dwoma, trzema i czterema mostkami tlenowymi z nośnikiem (rys. 2). Obliczenia wskazują, że w niskich temperaturach, najstabilniejszą formą jest struktura diokso C, połączona jednym atomem tlenu z krzemionką. Często proponowana w literaturze forma diokso F jest stabilna w szerokim zakresie temperatur, natomiast w wyższych temperaturach dominujący charakter ma struktura monookso I (rys. 2). We wszystkich układach obliczone długości wiązań Cr=O są podobne i wynoszą ok. 1,60 Å. Wynik ten jest zgodny z danymi EXAFS, na podstawie których Moisii i współprac. zaproponowali tetraedryczną strukturę diokso, jako tę, która najlepiej odpowiada danym doświadczalnym (rys. 2F)⁵⁶. Jest ona jednocześnie jedną z najbardziej stabilnych i prawdopodobnych konfiguracji wytypowanych w badaniach teoretycznych⁵⁸.

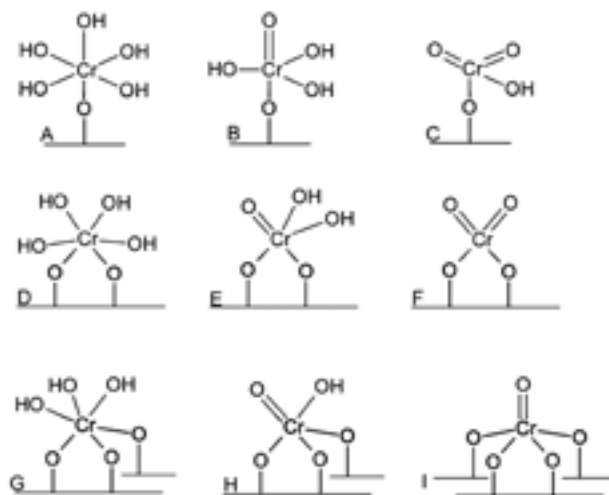


Fig. 2. Calculated surface Cr(VI) oxide species on the partially hydrated silica surface⁵⁸

Rys. 2. Struktury powierzchniowych form tlenkowych Cr(VI) na powierzchni częściowo uwodnionej krzemionki otrzymane w obliczeniach⁵⁸

W kolejnej pracy⁵⁹ głównym celem badań było określenie struktury monomerycznych form Cr(VI) na powierzchni odwodnionej krzemionki, a więc w warunkach odpowiadających kalcynacji katalizatora. Otrzymane wyniki prowadzą do wniosku, że niezależnie od zastosowanego modelu SiO₂, tetraedryczne struktury diokso Cr(VI) (rys. 2F) są bardziej stabilne od form monookso Cr(VI) (rys. 2I). Te ostatnie mogą jednak występować na powierzchni odwodnionej krzemionki, obok dominujących form diokso, co potwierdzają dane eksperymentalne^{41, 52, 54}. Ponadto, stwierdzono, że względne stabilności struktur Cr(VI) zależą od ich lokalizacji na powierzchni krzemionki⁵⁹.

Stosując bardzo uproszczone modele katalizatora Liu i współprac.⁶⁰ prowadzili obliczenia dla redukcji Cr(VI) → Cr(II) w obecności etylenu. Uważa się, że etap ten ma kluczowe znaczenie w procesie aktywacji katalizatora Phillipsa podczas polimeryzacji etylenu. Opierając się na wcześniejszych badaniach doświadczalnych zaproponowano, że redukcja zachodzi poprzez pośrednie stadium Cr(IV) z wydzieleniem następnie dwóch cząsteczek formaldehydu (rys. 3). W kolejnej pracy stwierdzono, że redukcja Cr(VI) do Cr(II) jest termodynamicznie bardziej korzystna przy zastosowaniu trietyloglinu i CO jako reduktorów, niż w przypadku użycia etylenu⁶¹.

Ostatnio, stosując technikę XPS oraz obliczenia DFT, badano wpływ modyfikacji glinem katalizatora Phillipsa na strukturę form

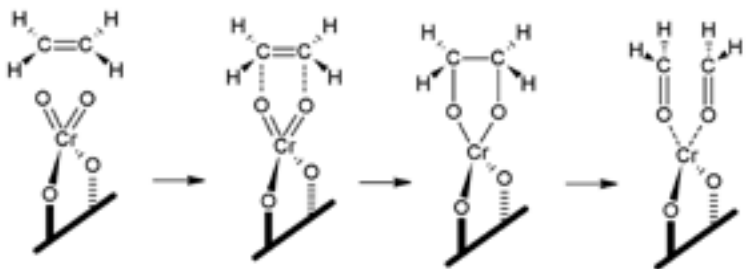


Fig. 3. Reaction between the ethylene molecule and the monomeric Cr(VI) oxide species on silica surface⁶⁰

Rys. 3. Reakcja cząsteczki etylenu z monomeryczną formą tlenkową Cr(VI) na powierzchni krzemionki⁶⁰

powierzchniowych oraz właściwości katalityczne⁴⁷). Zaobserwowano zwiększenie aktywności w polimeryzacji etylenu po wprowadzeniu glinu do układu katalitycznego. W tym przypadku wyliczona bariera aktywacji dla etapu inicjacji jest mniejsza niż dla niemodyfikowanego układu Cr/SiO₂, natomiast teoretyczna energia aktywacji dla etapów propagacji jest wyższa w przypadku katalizatora modyfikowanego glinem. Dodatek glinu wpływa również na właściwości powstającego polimeru.

Układy zredukowane Cr(III) i Cr(II)

Zredukowane formy chromu stanowią centra aktywne polimeryzacji olefin, a zatem znajomość ich struktury jest niezbędna do dokładnego określenia mechanizmu tego procesu. Na powierzchni katalizatora Phillipsa wykryto zredukowane struktury powierzchniowe chromu na 5+, 3+ i 2+ stopniu utlenienia^{3–6, 8–10, 18, 23, 26–31, 34, 35, 49–53, 57, 62, 63}. Przy wyższych zawartościach Cr obserwuje się ponadto formowanie klasterek Cr₂O₃.

Termiczna redukcja układu Cr(VI)/SiO₂ w atmosferze CO lub H₂ prowadzi do powstawania tlenkowych form powierzchniowych chromu na różnym stopniu utlenienia i o odmiennej geometrii⁶. Warunki prowadzenia redukcji istotnie wpływają na tworzące się struktury. Przeprowadzenie redukcji w temp. 620 K powoduje formowanie się układów na średnio 2+ stopniu utlenienia, przy czym wraz ze wzrostem zawartości chromu stopień ten zwiększa się⁵¹. Redukcja układu Cr/SiO₂ może być przeprowadzona również przy zastosowaniu innych substancji. Jeżeli proces ten przeprowadzi się w obecności C₂H₄, reakcja polimeryzacji zachodzi natychmiast i badania struktur powierzchniowych są znacznie utrudnione⁶⁴. Inne znane z literatury metody otrzymywania zredukowanych układów Cr/SiO₂ polegają na: (i) fotochemicznej redukcji Cr(VI)/SiO₂ w atmosferze H₂ lub CO, (ii) substytucji powierzchniowych grup hydroksylowych krzemionki związkami metaloorganicznymi zawierającym zredukowany Cr, (iii) redukcji trietyloglinem oraz (iv) wymianie jonowej w wodnym roztworze zawierającym jony Cr³⁺. Przewagą metod opierających się na termicznej redukcji w atmosferze CO jest formowanie się struktur monomerycznych o małej liczbie koordynacyjnej chromu, które można badać z zastosowaniem metod spektroskopowych (spektroskopia ramanowska, UV-Vis DRS, IR, EXAFS, XANES)^{6, 61, 64}.

Pomiary z zastosowaniem spektroskopii UV-Vis DRS^{22, 49, 50} wskazują na występowanie trzech zasadniczych form powierzchniowych zredukowanego chromu. Są to pseudooktaedryczne i pseudotetraedryczne formy Cr(II) oraz pseudooktaedryczne formy Cr(III). Względna zawartość poszczególnych struktur zależy m.in. od temperatury redukcji i rodzaju zastosowanego nośnika. Wykrywane są również śladowe zawartości Cr(V). Niektórzy autorzy^{5, 6} sugerują także obecność struktur Cr(IV). Wyniki badań z użyciem spektroskopii IR oraz EXAFS^{6, 39, 51} wskazują, że centra Cr(II) i Cr(III) są niewyscone koordynacyjnie. Na podstawie analizy danych EXAFS określono wartości liczb koordynacyjnych chromu w zredukowanych strukturach powierzchniowych, wynoszące odpowiednio 2,5 oraz 3,4 dla układów

Cr/SiO₂ i Cr/Al₂O₃. Metoda IR ponadto pozwala określić różnice pomiędzy odmiennymi formami powierzchniowymi Cr(II). Badając adsorpcję CO w zredukowanym układzie Cr(II)/SiO₂ w temperaturze pokojowej stwierdzono występowanie trzech różnych konfiguracji Cr(II) różniących się reaktywnością^{6, 39, 64}.

Badania z zastosowaniem techniki ESR^{3, 25, 65–67} wskazują na obecność na powierzchni trzech różnych zredukowanych form tlenkowych Cr: izolowanych Cr(V), klasterycznych Cr(III) i dobrze zdyspergowanych Cr(III). Pomiary z zastosowaniem spektroskopii XPS^{25, 57} potwierdzają występowanie na powierzchni SiO₂ zredukowanych form powierzchniowych chromu na 5+, 3+ i 2+ stopniu utlenienia.

Jedną z chemicznych metod stosowanych do analizy struktur powierzchniowych jest technika TPR⁵¹. Wyniki otrzymane przy zastosowaniu tej metody do badania układu Cr/SiO₂-Al₂O₃ wskazują, że stopień utlenienia Cr po przeprowadzeniu procesu redukcji jest tym większy, im wyższą zawartością Al charakteryzuje się nośnik glinokrzemianowy. W przypadku zastosowania krzemionki proces redukcji zachodzi najgłębiej. Ponadto, redukcji do Cr(II) ulegają najłatwiej dobrze zdyspergowane formy powierzchniowe chromu. Przy większych zawartościach chromu w układzie, jego stopień dyspersji na powierzchni jest niewielki i powstaje głównie Cr₂O₃, jako że jest to najbardziej stabilny tlenek chromu. Prace Weckhuysena i współprac.⁵¹ wskazują, że przy zastosowaniu krzemionki jako nośnika redukcja z 6+ na 2+ stopień utlenienia jest reakcją najbardziej uprzywilejowaną. Świadczy to o silnym związaniu chromu z powierzchnią.

Badania mechanizmu redukcji Cr(VI) prowadzone przez Bensalema i współprac.⁶⁸ wskazały, że jest to proces dwuetapowy. Początkowo CO ulega adsorpcji na centrum aktywnym, skutkując wytworzeniem formy aktywnej. W kolejnym etapie zachodzi proces redukcji, który rozpoczyna się w temp. 370 K.

Jednym z celów teoretycznych badań nad układami Cr(II)/SiO₂ była interpretacja danych spektroskopowych otrzymanych z analizy widm UV-Vis^{69, 70}. Badano m.in. struktury monomeryczne Cr(II) o geometrii pseudotetraedrycznej (rys. 4A), pseudooktaedrycznej (rys. 4B) oraz pośredniej (rys. 4C). Najlepszą zgodność z wynikami eksperymentalnymi otrzymano dla pierwszej z nich, stąd stwierdzono, że obserwowane widma mogą być wyjaśnione w oparciu o strukturę pseudotetraedryczną monomerycznych form Cr(II).

Niewysycenie koordynacyjne zredukowanych układów Cr/SiO₂ wiąże się ze zdolnością do adsorpcji różnych cząsteczek, np. O₂ (odtworzony zostanie wówczas utleniony układ Cr(VI)/SiO₂), N₂, CO i NO^{6, 64}. Wytworzone addukty można następnie badać z zastosowaniem metod spektroskopowych. Teoretyczne prace Zecchiny, Damina i współprac.⁶⁴ dotyczyły modelowania procesu adsorpcji N₂ i CO na zredukowanych strukturach powierzchniowych chromu. Starano się głównie wyjaśnić dane otrzymane z badań eksperymentalnych, otrzymując jednak niejednoznaczne wyniki.

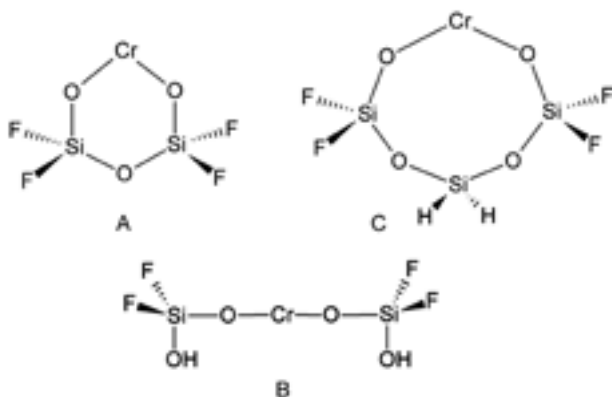


Fig. 4. Models of the Cr(II) species on the silica surface^{69, 70}

Rys. 4. Modele struktur Cr(II) na powierzchni krzemionki^{69, 70}

Obecność form tlenkowych Cr(III) na powierzchni SiO_2 została dowiedziona w licznych pracach^{3–6, 8–10, 23, 26–31, 49–52, 57)}, jednak ich struktura molekularna nadal nie jest jednoznacznie określona. Najczęściej proponowane w literaturze konfiguracje przedstawiono na rys. 5⁵⁷⁾.



Fig. 5. Possible surface Cr(III) species on silica⁵⁷⁾

Rys. 5. Możliwe struktury powierzchniowe form Cr(III) na krzemionce⁵⁷⁾

Podsumowanie

Przedstawiony przegląd literatury nie wyczerpuje w pełni zagadnień związań z katalizatorem Cr/SiO₂, skupiając się przede wszystkim na aspektach przemysłowych oraz strukturze tego układu. Jest on stosowany przede wszystkim jako przemysłowy katalizator polimeryzacji etylenu, ale wykazuje aktywność również w innych, ważnych z praktycznego punktu widzenia, procesach chemicznych. Liczne prace potwierdziły, że redukcja form chromu na 6+ stopniu utlenienia prowadzi do różnorodnych struktur na 5+, 3+ i 2+ stopniu utlenienia. Wszystkie zredukowane układy badane były głównie eksperymentalnie z zastosowaniem wielu metod spektroskopowych. Uzupełnieniem badań doświadczalnych są prace teoretyczne, dostarczające często komplementarnych informacji na temat struktury i reaktywności powierzchniowych form chromu. Pomimo to, prezentowane w literaturze wyniki nie pozwalają na razie na jednoznaczne określenie ani struktury centów aktywnych ani mechanizmów reakcji katalitycznych przebiegających w układzie Cr/SiO₂. Wynika stąd konieczność i sens prowadzenia dalszych badań w tym kierunku.

Otrzymano: 26-01-2015

LITERATURA

- D.B. Malpass, *Introduction to industrial polyethylene. Properties, catalysts, and processes*, 45, Wiley, 2010.
- Pat. USA 2 825 721* (1958).
- B.M. Weckhuysen, I.E. Wachs, R.A. Schoonheydt, *Chem. Rev.* 1996, **96**, 3327.
- B.M. Weckhuysen, R.A. Schoonheydt, *Catal. Today* 1999, **51**, 215.
- E. Gropo, C. Prestipino, F. Cesano, F. Bonino, S. Bordiga, C. Lamberti, P. Thüne, J. Niemantsverdriet, A. Zecchina, *J. Catal.* 2005, **230**, 98.
- E. Gropo, C. Lamberti, S. Bordiga, G. Spoto, A. Zecchina, *Chem. Rev.* 2005, **105**, 115.
- V. Panchenko, V. Zakharov, E. Paukshtis, *Appl. Catal. A: Gen.* 2006, **313**, 130.
- C.A. Demmelmair, R.E. White, J.A. van Bokhoven, S.L. Scott, *J. Catal.* 2009, **262**, 44.
- A. Gaspar, L. Dieguez, *Appl. Catal. A: Gen.* 2002, **227**, 241.
- A. Gaspar, J. Brito, L. Dieguez, *J. Mol. Catal. A: Chem.* 2003, **203**, 251.
- M.P. Conley, M.F. Delley, G. Siddiqi, G. Lapadula, S. Norsic, V. Monteil, O.V. Safanova, C. Copéret, *Angew. Chem. Int. Ed. Engl.* 2014, **53**, 1872.
- M.F. Delley, M.P. Conley, C. Copéret, *Catal. Lett.* 2014, **144**, 805.
- M. McDaniel, *Adv. Catal.* 1985, **33**, 47.
- Z. Liu, R. Cheng, X. He, X. Wu, B. Liu, *J. Phys. Chem. A* 2012, **116**, 7538.
- B.M. Weckhuysen, L.M. De Ridder, P.J. Grobet, R.A. Schoonheydt, *J. Phys. Chem.* 1995, **99**, 320.
- A. Zecchina, S. Bertarione, A. Damin, D. Scarano, C. Lamberti, C. Prestipino, G. Spoto, S. Bordiga, *Phys. Chem. Chem. Phys.* 2003, **5**, 4414.
- Z. Liu, R. Cheng, X. He, B. Liu, *ACS Catal.* 2013, **3**, 1172.
- A. Hakuli, M.E. Harlin, L.B. Backman, A.O.I. Krause, *J. Catal.* 1999, **184**, 349.
- R.L. Burwell Jr, A.B. Littlewood, M. Cardew, G. Pass, C.T.H. Stoddart, *J. Am. Chem. Soc.* 1960, **82**, 6272.
- M. Cardew, R.L. Burwell Jr, *J. Am. Chem. Soc.* 1960, **82**, 6289.
- A.B. Littlewood, R.L. Burwell Jr, *J. Am. Chem. Soc.* 1960, **82**, 6287.
- B.M. Weckhuysen, I.E. Wachs, R.A. Schoonheydt, *Stud. Surf. Sci. Catal.* 1995, **91**, 151.
- G.S. Pozan, A. Tavman, I. Boz, *Chem. Eng. J.* 2008, **143**, 180.
- Pat. USA 2 098 959* (1937).
- B.M. Weckhuysen, R.A. Schoonheydt, *Catal. Today* 1999, **51**, 223.
- N.C. Ramani, D.L. Sullivan, J.G. Ekerdt, J.-M. Jehng, I.E. Wachs, *J. Catal.* 1998, **176**, 143.
- M. Cherian, M.S. Rao, A.M. Hirt, I.E. Wachs, G. Deo, *J. Catal.* 2002, **211**, 482.
- B.Y. Jibril, N.O. Elbashir, S.M. Al-Zahrani, A.E. Abasaeed, *Chem. Eng. Process.* 2005, **44**, 835.
- S. Wang, K. Murata, T. Hayakawa, S. Hamakawa, F. Suzuki, *Appl. Catal. A: Gen.* 2000, **196**, 1.
- M.A. Botavina, G. Martra, Y.A. Agafonov, N.A. Gaidai, N.V. Nekrasov, D.V. Trushin, S. Coluccia, A.L. Lapidus, *Appl. Catal. A: Gen.* 2008, **347**, 126.
- P. Michorczyk, J. Ogonowski, K. Zeńczak, *J. Mol. Catal. A: Chem.* 2011, **349**, 1.
- I. Takahara, W.C. Chang, N. Mimura, M. Saito, *Catal. Today* 1998, **45**, 55.
- M. Kocoń, P. Michorczyk, J. Ogonowski, *Catal. Lett.* 2005, **101**, 53.
- L.F. Liotta, A.M. Venezia, G. Pantaleo, G. Deganello, M. Gruttaduria, R. Noto, *Catal. Today* 2004, **91**, 231.
- D.S. Kim, J.M. Tatibouet, I.E. Wachs, *J. Catal.* 1992, **136**, 209.
- D.S. Kim, I.E. Wachs, *J. Catal.* 1993, **142**, 166.
- C. Pradier, F. Rodrigues, P. Marcus, M. Landau, M. Kaliya, A. Gutman, M. Herskowitz, *Appl. Catal. B: Env.* 2000, **27**, 73.
- M. McDaniel, K. Collins, E. Benham, T. Cymbaluk, *Appl. Catal. A: Gen.* 2008, **335**, 252.
- E. Gropo, A. Damin, F. Bonino, A. Zecchina, S. Bordiga, C. Lamberti, *Chem. Mater.* 2005, **17**, 2019.
- W. Jóźwiak, W. Ignaczak, D. Dominiak, T. Maniecki, *Appl. Catal. A: Gen.* 2004, **258**, 33.
- A. Chakrabarti, I.E. Wachs, *Catal. Lett.* 2014, 1.
- A. Zecchina, S. Bordiga, E. Gropo, *Selective nanocatalysts and nanoscience. Concepts for heterogeneous and homogeneous catalysis*, John Wiley & Sons, 2011.
- L. Zhong, Z. Liu, R. Cheng, S. Tang, P. Qiu, X. He, M. Terano, B. Liu, *ChemCatChem* 2012, **4**, 872.
- E. Gropo, A. Damin, C. Otero Arean, A. Zecchina, *Chem. Eur. J.* 2011, **17**, 11110.
- P. Qiu, R. Cheng, Z. Liu, B. Liu, B. Tumanskii, M.S. Eisen, *J. Organomet. Chem.* 2012, **699**, 48.
- N. Zhao, R. Cheng, X. He, Z. Liu, B. Liu, *Macromol. Chem. Phys.* 2014, **215**, 1753.
- Y. Ma, L. Wang, Z. Liu, R. Cheng, L. Zhong, Y. Yang, X. He, Y. Fang, M. Terano, B. Liu, *J. Mol. Catal. A: Chem.* 2015, **401**, 1.
- A. Zecchina, E. Gropo, A. Damin, C. Prestipino, *Surface and interfacial organometallic chemistry and catalysis*, Springer 2005.
- B.M. Weckhuysen, L.M. De Ridder, R.A. Schoonheydt, *J. Phys. Chem.* 1993, **97**, 4756.
- B.M. Weckhuysen, A.A. Verberckmoes, A.L. Buttens, R.A. Schoonheydt, *J. Phys. Chem.* 1994, **98**, 579.
- B.M. Weckhuysen, R.A. Schoonheydt, J.-M. Jehng, I.E. Wachs, S.J. Cho, R. Ryoo, S. Kijlstra, E. Poels, *J. Chem. Soc., Faraday Trans.* 1995, **91**, 3245.
- E.L. Lee, I.E. Wachs, *J. Phys. Chem. C* 2007, **111**, 14410.
- M.A. Vuurman, I.E. Wachs, D.J. Stufkens, A.D. Oskam, *J. Mol. Catal.* 1993, **80**, 209.
- E.L. Lee, I.E. Wachs, *J. Phys. Chem.* 2008, **112**, 6487.
- T.J. Dines, S. Inglis, *Phys. Chem. Chem. Phys.* 2003, **5**, 1320.
- C. Moisii, E.W. Deguns, A. Lita, S.D. Callahan, L.J. van de Burgt, D. Magana, A.E. Stiegman, *Chem. Mat.* 2006, **18**, 3965.
- B. Liu, M. Terano, *J. Mol. Catal. A: Chem.* 2001, **172**, 227.
- H. Guesmi, F. Tielen, *J. Phys. Chem. C* 2011, **116**, 994.
- J. Handzlik, R. Grybos, F. Tielen, *J. Phys. Chem. C* 2013, **117**, 8138.
- B. Liu, Y. Fang, M. Terano, *Mol. Simulat.* 2004, **30**, 963.
- B. Liu, Y. Fang, W. Xia, M. Terano, *Kinet. Catal.* 2006, **47**, 234.
- S.L. Scott, J. Amor Nait Ajijou, *Chem. Eng. Sci.* 2001, **56**, 4155.
- E. Gropo, C. Lamberti, G. Spoto, S. Bordiga, G. Magnacca, A. Zecchina, *J. Catal.* 2005, **236**, 233.
- A. Damin, J.G. Vitillo, G. Ricchiardi, S. Bordiga, C. Lamberti, E. Gropo, A. Zecchina, *J. Phys. Chem. A* 2009, **113**, 14261.
- B.M. Weckhuysen, R.A. Schoonheydt, *Stud. Surf. Sci. Catal.* 1994, **84**, 965.
- B.M. Weckhuysen, R.R. Rao, P. Bodart, G. Debras, O. Collart, P. van der Voort, R. Schoonheydt, E. Vansant, *Chem. Eur. J.* 2000, **6**, 2960.
- B.M. Weckhuysen, R.A. Schoonheydt, *Catal. Today* 1999, **49**, 441.
- A. Bensalem, B.M. Weckhuysen, R.A. Schoonheydt, *J. Chem. Soc., Faraday Trans.* 1997, **93**, 4065.
- Ø. Espelid, K.J. Børve, *J. Catal.* 2002, **205**, 177.
- Ø. Espelid, K. Børve, *Catal. Lett.* 2001, **75**, 49.

Artykuł **D2**

Reduction of chromia-silica catalyst: A molecular picture

Maciej Gierada, Piotr Michorczyk,✉ Frederik Tielens, Jarosław Handzlik✉

J. Catal. 340 (2016) 122-135



Reduction of chromia–silica catalysts: A molecular picture

Maciej Gierada ^a, Piotr Michorczyk ^{a,*}, Frederik Tielens ^b, Jarosław Handzlik ^{a,*}

^a Faculty of Chemical Engineering and Technology, Cracow University of Technology, ul. Warszawska 24, 31-155 Kraków, Poland

^b Sorbonne Universités, UPMC Univ Paris 06, UMR 7574, Laboratoire Chimie de la Matière Condensée, Collège de France, 11 place Marcelin Berthelot, 75231 Paris Cedex 05, France

ARTICLE INFO

Article history:

Received 7 January 2016

Revised 2 April 2016

Accepted 27 April 2016

Keywords:

Chromium

Silica

Reduction

DFT

UV-vis

DRS

Vibrational frequencies

Phillips catalyst

ABSTRACT

The nature of reduced Cr species on silica is still under debate. In this work, combined DFT and *in situ* UV-vis DRS investigations of reduction of chromia–silica catalyst have been done. Advanced periodic and cluster models of amorphous silica are applied to reproduce the heterogeneity of surface Cr species. Geometrical parameters, vibrational frequencies, excitation energies, and relative stabilities of Cr sites are determined. It is predicted that reduction of monomeric Cr(VI) species to Cr(IV) sites is highly exergonic, whereas deep reduction to Cr(II) is less thermodynamically favored. Dimeric Cr(VI) species can finally be reduced to Cr(III) or Cr(II). *In situ* UV-vis DRS studies indicate that Cr(VI) species are selectively converted to Cr(II) under CO in dry conditions, whereas reduction with dry H₂ leads to formation of Cr(III) and Cr(II). For both reducing agents, the presence of water hampers deep reduction to Cr(II), which can be explained by reoxidation/hydrolysis processes.

© 2016 Elsevier Inc. All rights reserved.

1. Introduction

Chromium oxide species supported on silica are efficient heterogeneous catalytic systems widely used in the chemical industry. They are mainly known as Phillips catalysts for ethylene polymerization at relatively low pressures [1–11]. Moreover, these catalysts also show activity in other important reactions—among others, dehydroisomerization and dehydrogenation of alkanes [11–14], oxidative dehydrogenation of hydrocarbons in the presence of oxygen [15,16] or CO₂ [17–19], and various selective oxidation reactions [1,20–22]. Despite many years of extensive, mainly experimental investigations, the structure of the surface chromium species has not been unambiguously determined. The same fundamental questions are still being debated, i.e., what is the nature of the surface Cr species (monomeric, dimeric, or polymeric) and how do the initial oxidized Cr(VI) species transform into reduced Cr(III) and Cr(II) species, which are the active sites or their precursors in most of the reactions mentioned above.

Several spectroscopic techniques have been employed to clarify the surface chromium chemistry, including UV-vis DRS, IR, EPR, XPS, EXAFS, XANES, and Raman spectroscopy. There is a general consensus that detectable oxidation states of chromium oxide species are (i) oxidized Cr(VI) [1–38] and (ii) reduced Cr(V), Cr(III), and

Cr(II) [1–14,17–19,21–27,32,34,35,37–44]. CO is the most commonly used reducing agent to study silica-supported chromium oxide species in lower oxidation states [1–5,8,10,24–27,32,34,35,38–40,43–46]. The UV-vis DRS data indicate the presence of three different types of reduced chromium oxide species: (pseudo)tetrahedral Cr(II), (pseudo)octahedral Cr(II), and (pseudo)octahedral Cr(III) [1,24–26]. The ratio between different forms depends on the temperature of reduction and the kind (or composition) of the support. Upon interaction of the Cr(VI)/SiO₂ system with CO, the major surface species is Cr(II), but Cr(III) is also present in a minority [1,24–27]. It is worth noting here that at high loadings and low Cr dispersions, reduction of initial Cr(VI) oxide species produces mostly Cr₂O₃, whereas at low loadings and high dispersions, reduction leads mainly to surface Cr(II) site formation. Reduction of the Cr(VI)/SiO₂ system with H₂ was also investigated [9–13,16–18,22,29,32,46], but the nature of the reduced Cr species was rarely directly characterized. On the basis of H₂ TPR experiments followed by UV-vis DRS measurements, it was concluded that Cr(VI) species are reduced to Cr(III) [9,32]. Monitoring of the oxidation state of chromium oxide species on SBA-1 during H₂ TPR experiments indicated the formation of both Cr(III) and Cr(II) species [18].

The data obtained with IR spectroscopy of adsorbed probe molecules (CO, NO) show three different types of Cr(II) oxide species, which differ in ability to coordinate small molecules [1,4,34,35,39,40,45,46]. The results obtained with EPR

* Corresponding authors.

E-mail addresses: pmichor@pk.edu.pl (P. Michorczyk), jhandz@pk.edu.pl (J. Handzlik).

spectroscopy indicate the presence of Cr(III) clusters, isolated Cr(III), and isolated Cr(V) on the silica surface [1,16,18,22,43–45]. Cr(VI) and Cr(III) oxidation states in chromia–silica systems were also observed by XPS [4,22,23]. Although surface Cr(IV) oxide species could be expected as the intermediate oxidation state of chromium during the reduction from Cr(VI)/SiO₂ to Cr(II)/SiO₂ by a two-electron reducing agent, such as CO or H₂, they were not observed in the past. However, it was recently proposed that Cr(IV) oxide species are formed after controlled oxidation of the Cr(II)/SiO₂ system by N₂O [37]. Moreover, in another recently published work [45], it is claimed that the intermediate Cr(IV) species are detected during the reduction of the Phillips catalyst with CO.

The molecular structure of the surface species of the initial oxidized Cr(VI)/SiO₂ catalyst is still the subject of much discussion. Monochromate, dichromate, and polychromate surface Cr(VI) species have been proposed, mainly based on UV–vis DRS studies [1,2,4,6,17–19,24–27,32,35,43,46]. The monochromate/dichromate ratio depends on the chromium loading, the calcination temperature, and the type of silica support. It is often postulated that monomeric species are the dominant or even the only surface Cr(VI) species on silica at low chromium loadings [4,15,16,20,21,28–36]. Recent Raman spectroscopy data indicate the presence of two distinct isolated Cr(VI) species under dehydrated conditions: the major dioxo species and the minor monooxo species [29–32]. Moreover, it was shown that the former is reduced by H₂ faster than the latter [29,31,32]. The presence of four-coordinate dioxo Cr(VI) species on the silica surface has been also confirmed by EXAFS studies [7,36].

As full information about surface metal sites is still not accessible from experimental techniques, their complementary description can be provided by computational chemistry methods. Most theoretical papers on the Cr/SiO₂ system have reported exploration of reaction mechanisms using rather small cluster models of reduced Cr(II) and Cr(III) species supported on silica [47–52]. Such models enable effective computations of many complex reaction pathways [49–54]; however, they cannot fully reproduce the complexity of the surface and the heterogeneity of the metal sites. In some works, large SiO₂ clusters cut from the β-cristobalite framework [8] or having an amorphous structure [55] have been applied to model Cr(II) sites on silica. Modeling of amorphous silica is a challenging task and several attempts have been made to develop realistic models of this material [56–59]. Recently, an advanced periodic model of amorphous silica [58] was adapted to theoretically investigate a variety of possible surface Cr(VI) species under partially hydrated and dehydrated conditions [60,61]. Additionally, large cluster models, based on the amorphous structure of silica, have been used in parallel [61]. It was shown that under dehydrated conditions surface dioxo Cr(VI) species are more stable than the monooxo Cr(VI) species [61], which is consistent with their experimentally estimated ratio [32].

The main aim of this work is to shed light on the reduction of chromia–silica catalysts and the nature of the reduced chromium species by combining the computational (DFT) and experimental approaches. Determining the detailed structure of reduced Cr species, as the active sites or their precursors for many important catalytic reactions, is a good starting point for further computational investigations of reaction mechanisms and is necessary for better understanding of the surface processes. However, for sites composed of a metal atom grafted to an amorphous support, each site is slightly different from the others [62,63]. Therefore, in contrast to other authors [49–52], we use a variety of systematically generated large cluster and periodic models, which enable us to sample the site heterogeneity of the amorphous catalyst surface. First, we model and theoretically characterize variously located monomeric Cr(IV) and Cr(II) oxide species, based on our previously calculated Cr(VI) structures on the dehydrated surface of amorphous silica

[61]. Moreover, several distinct dimeric Cr(VI) species and a variety of their reduced analogues, including mixed oxidation states of chromium, are modeled for the first time and theoretically investigated. We also compare the thermodynamic stability of monomeric and dimeric Cr(VI) species. Having a large number of realistic models of surface chromium sites at various oxidation states, we can further analyze the energetic effects of multistep reduction of monomeric and dimeric Cr(VI) species. It is worth emphasizing that the proposed structures containing chromium in lower oxidation states are not arbitrarily modeled, but can be always obtained from the initial Cr(VI) species by reduction with a two-electron reducing agent, analogously to experimental conditions. We discuss possible differences when CO or H₂ molecules are assumed as the reducing agents, which is mainly connected with the possible role of water, which is a by-product in the second case. Last, using *in situ* UV–vis DRS, we monitor the oxidation state of Cr species reduced with CO or H₂, indicating different redox behavior in each case. In the experimental studies, an ordered mesoporous silica, SBA-1, with cubic structure and large specific surface area was applied as a support for achieving high dispersion of Cr species.

2. Computational models and methods

2.1. Periodic calculations

The periodic models of surface chromium oxide species are based on the amorphous hydroxylated silica structure proposed and verified by Tielens and co-workers [58] and recently successfully employed in computational studies of Cr(VI) [60,61], Mo(VI) [64], V(V) [65], Nb(V) [66], and Au(I) [67] oxide centers on SiO₂. The surface unit cell dimensions are $a = 12.77 \text{ \AA}$, $b = 17.64 \text{ \AA}$, $c = 25.17 \text{ \AA}$, including 15 Å of vacuum. The original hydroxylated surface was partially dehydroxylated to represent the catalyst under dehydrated conditions. More details are given in the previous work [61]. The models of monomeric Cr(IV) and Cr(II) species have been obtained by adequate modification of selected monooxo and dioxo Cr(VI) structures reported previously [61]. Models of dimeric Cr(VI) species have been developed in this work and, on their basis, reduced dimeric Cr species have been modeled as well. The chromium coverage in the models is about 0.4 atoms nm⁻² for monomeric species (one Cr atom per unit cell), which is typical for the Phillips catalysts [3–5,34], and approximately 0.8 atoms nm⁻² for dimeric species (two Cr atoms per unit cell). Although these coverage are higher than that reached in the system characterized experimentally in this work, the models still represent isolated Cr species. The distance between Cr atoms of two neighboring surface species is in the range 8.43–12.77 Å, so the possible lateral interactions between the Cr sites and their periodic images are negligible. The positions of all atoms in the unit cell have been relaxed during geometry optimization.

The calculations have been done with the Vienna Ab Initio Simulation Package (VASP) [68–70]. For the graphic presentation of the structures, Materials Studio 5.5 software is applied [71]. Taking into account the previously reported assessment of various DFT methods for thermochemistry of chromium oxo compounds [72], which was based on experimental reference data, the PW91 exchange–correlation functional [73] has been selected for the present study. For this functional, the determined mean unsigned error and maximum error in enthalpies for gas phase reactions involving chromium compounds are 12 and 22 kJ mol⁻¹, respectively [72], although larger errors are possible for the large systems investigated in this work. The plane-wave basis set and the projector-augmented wave method (PAW) [74] are applied to describe valence electrons and atomic cores, respectively. Standard

PAW atomic parameters are used with a cutoff energy of 400 eV. For chromium, the PAW is built with 12 electrons in the valence. The Γ point is used in the Brillouin-zone integration. To determine harmonic vibrational frequencies, the Hessian matrix has been computed by the finite difference method. Chromium atoms and their neighbors, including at least the second coordination sphere, are considered in the Hessian matrix. The presented vibrational frequencies are scaled by a previously determined scaling factor of 0.9241, obtained through a least-squares approach, based on the experimental Cr=O frequencies for gas phase chromium compounds [61]. The calculations for models of reduced Cr-species are spin-polarized. The ground state for the reduced Cr species has been verified. For monomeric Cr(IV) and Cr(II) species it is triplet and quintet, respectively. High-spin coupled ground states have consistently been found for reduced dimeric Cr systems, similarly to other authors [48].

2.2. Cluster calculations

Most cluster models in this work, containing 33 Si atoms, are based on a previously modified periodic model of the amorphous silica structure [58,61]. Some additional models of the monomeric Cr species, containing 21, 24, and 26 Si atoms (Fig. S2, Supplementary Data), have been derived from another structure of amorphous silica (Materials Studio database [71]), previously applied in investigations of surface chromium and molybdenum species [61,75]. The dangling bonds of the clusters have been saturated with hydrogen atoms, replacing the removed Si atoms. The models of monomeric Cr(IV) and Cr(II) species have been obtained by adequate modification of selected monooxo and dioxo Cr(VI) structures reported previously [61]. Cluster models of dimeric Cr species have been developed on the basis of selected periodic models representing the Cr dimers.

Geometry optimization of the whole system, including the terminated H-atoms, has been carried out using the PW91 functional combined with the split-valence def2-SVP basis set [76]. Vibrational frequencies have been calculated for each structure to confirm the potential energy minimum and to obtain Gibbs energy corrections ($T = 873.15\text{ K}$, if not stated otherwise, $p = 1\text{ atm}$) within the harmonic oscillator and rigid-rotor approximations. The presented vibrational frequencies are scaled by a previously determined scaling factor of 0.9149 [61]. The Gibbs energy corrections are added to PW91 single-point energies calculated with the triple- ζ valence def2-TZVPP basis set [76], in order to obtain a better estimation of Gibbs energies (ΔG_{873}). The reported energies (ΔE) are not ZPE-corrected, to enable comparison with the results obtained with the periodic models. This computational methodology was successfully applied in previous studies of surface chromium species [61,77]. Spin-unrestricted calculations have been performed for the open-shell systems. High-spin ground states for the reduced Cr species have always been found. Excitation energies have been computed using the TD-DFT formalism with the Tamm–Dancoff approximation [78]. The long-range corrected hybrid ω B97X-D functional [79] with the def2-SVP basis set has been applied for the geometries optimized on the PW91/def2-SVP level. All calculations have been done with the Gaussian 09 set of programs [80]. For the graphic presentation of the structures, GaussView 5.0 software has been applied [81].

2.3. Nomenclature

The basic nomenclature of the models is composed of one or two lower case letters (**m**, **d**, **ma**, **mb**, **mc**) or a capital letter (**M**, **D**) and a number (**1–11**). The lower case letters **m** and **d** specify the cluster models of monomeric and dimeric chromium species, respectively. Analogously, the capital letters **M** and **D** describe

periodic models of the monomeric and dimeric species. The remaining symbols (**ma**, **mb**, **mc**) denote the additional cluster models of monomeric Cr species derived from another structure of amorphous silica [61,71]. The number distinguishes between the species of different oxidation states and/or different structures in one series of models. A Roman numeral (**I–III**) denotes different series of models of dimeric species. In the case of some models studied (for example, **m1** and **m1'**), the prime symbol is used to distinguish between different locations of the Cr sites on the surface described by the same silica model. The partially hydrated species are featured with the “hyd” additive. The periodic and cluster models corresponding to each other are always denoted analogously, for instance, **I_D2** and **I_d2**.

3. Experimental

3.1. Preparation of SBA-1 and $\text{CrO}_x/\text{SBA-1}$

Cubic mesoporous siliceous material SBA-1 ($S_{\text{BET}} > 1100\text{ m}^2\text{ g}^{-1}$) was applied as the support. Pure SBA-1 was obtained under acidic conditions using cetyltriethylammonium bromide as a surfactant and tetraethyl orthosilicate as the silica source, as described elsewhere [82]. In a typical synthesis, 10 g of CTEABr, 1157 cm³ of distilled water and 566 cm³ of hydrochloric acid (37%, Chempur) were combined to form a homogeneous solution, which was cooled to 273 K and stirred (400 rpm) for 30 min. Finally, 27.90 cm³ of TEOS (98%, Aldrich) precooled to 273 K was added while vigorous stirring. The molar composition of the reaction mixture was TEOS: CTEABr:HCl:H₂O = 1:0.2:56:700. Stirring was continued for 5 h until the precipitation of the silica–surfactant assemblies was completed. After that precipitant formed at 273 K was aged in the reaction mixture for 1 h at 373 K to improve cross-linking of the silica framework. The resultant precipitate was filtered off and dried (without washing) overnight at 333 K. The dried material was then calcined in air by rising temperature from ambient to 823 K over 9 h and keeping it at 823 K for another 12 h.

The catalyst ($\text{CrO}_x/\text{SBA-1}$) was prepared by impregnating SBA-1 with an aqueous solution of $\text{Cr}(\text{NO}_3)_3$ (99.6% Polish Chemical Reagents, POCH) as a chromium source [18]. Before the impregnation the SBA-1 support was dried for 12 h at 393 K. Typically, 1 g of the mesoporous support was treated with 4.0 cm³ of an aqueous solution containing the desired amount of $\text{Cr}(\text{NO}_3)_3$. The concentration of $\text{Cr}(\text{NO}_3)_3$ in solution was matched so as to obtain about 1 wt.% of total Cr content in the catalyst. The impregnated sample was dried at room temperature overnight and then for 6 h at 333 K, and finally it was calcined for 6 h at 823 K in air.

3.2. *In situ* UV-vis DRS experiments

The oxidation state of chromium species during reduction of the fresh $\text{CrO}_x/\text{SBA-1}$ samples was monitored by UV-vis DRS using an Ocean Optics HR2000 + instrument (integration time 20 ms, 20 scans) equipped with an Ocean Optics DH-2000 BAL halogen-deuterium light source and a high-temperature reflection probe (FCR-7UV400-2-ME-HTX, 7 × 400 μm fibers). The spectra were collected within the wavelength range 225–1100 nm using BaSO_4 as a reflection standard. The spectra are shown in the Kubelka–Munk format ($F(R) = (1 - R)^2/2R$, where R stands for reflectance). The scheme of the UV-vis DRS setup is shown in Fig. S6 (Supplementary Data). The high-temperature probe was attached at the top of the quartz microreactor. The distance between the sample bed and the high-temperature probe tip was 2–3 mm. The sample bed thickness was 4–5 mm. Before the reduction, the $\text{CrO}_x/\text{SBA-1}$ sample was pre-heated in air at 873 K for 30 min and then for another 30 min in a dry He stream. After that, an inert gas (He) was replaced with a

mixture of either CO/He (5/95 vol.%, Air Liquide) or H₂/N₂ (5/95 vol. % Air Liquide), which served as combined carrier and reducing gases at the total flow rate of 40 cm³ min⁻¹.

In selected cases, the oxidation state of the CrO_x/SBA-1 sample was monitored during treatment under oxidative (air) and reducing (mixture of CO/He and H₂/N₂) conditions in the presence and absence of water. In the experiments with wet reducing agents, water ($V_{\text{liq}} = 4 \text{ ml h}^{-1}$) was injected using an infusion pump (Ascort AP14) into the preheating system (heating to 423 K) for evaporation and mixing of water with the reduction mixture. The total flow rate of reduction mixtures and dry air (during reoxidation) was 40 cm³ min⁻¹. Before each set of cyclic experiments, the fresh CrO_x/SBA-1 sample was oxidized/flashed as described above.

4. Results and discussion

4.1. Computational studies

4.1.1. Monomeric Cr species

Periodic and cluster models of monomeric Cr oxide species are presented in Figs. 1 and 2, respectively. Other models of Cr monomers, which are also discussed in this section, can be found in Figs. S1 and S2 (Supplementary Data). Previously reported [61] monooxo and dioxo Cr(VI) structures, which now represent the initial surface centers before reduction, are also included. Whereas the periodic models are directly based on the previously verified structure of amorphous silica [58] and are more convenient for the calculation of the surface metal species, the cluster approach allows us to take into account the effect of temperature when

the relative thermodynamic stabilities and reaction Gibbs energies are considered.

Considering the periodic models, after one oxo ligand is removed from the tetrahedral dioxo species, the intermediate Cr (IV) species has a trigonal configuration. Further reduction gives a typical (≡SiO)₂Cr(II) species, which was calculated in the past using small and/or somewhat arbitrarily built clusters of silica [8,47,49,50,55]. The cluster models of the reduced Cr species (Fig. 2) are generally similar to the corresponding periodic structures (Fig. 1). However, the silica clusters are more flexible than the periodic structure, which allows additional interactions between some chromium species and the surface, mainly neighboring hydroxyl groups. For monooxo Cr(IV) species, formation of a hydrogen bond between a surface silanol group and the oxo ligand (**m2**, **m2_hyd**, **mb2**, **mc2_2**) or an interaction between a silanol group and the chromium atom (**ma2**) is observed (Figs. 2 and S1 and S2, Supplementary Data). The latter interaction is also seen for some Cr(II) species (**m3_hyd**, **ma3**), as was suggested in the literature [46,55].

In the Cr(II) species **m3**, the distance between the chromium atom and a neighboring surface siloxane bridge is very short (2.06 Å). Consequently, the chromium is threefold bonded to the surface. Such a species was proposed in the literature and it can play a role in ethylene polymerization [8,39,41,45,55]. Analogous interactions are also observed for some other Cr(II) species (**m3_hyd**, **ma3**, **mb3**—Figs. S1 and S2, Supplementary Data).

The Cr=O bond length in the Cr(IV) species is almost unchanged after reduction of the Cr(VI) site (Table S1, Supplementary Data). There are no experimental structural data reported for surface Cr (IV) species on silica, but the Cr=O distances for the Cr(VI) models are very close to those obtained with EXAFS for Cr(VI)/SiO₂ systems [7,36]. Moreover, the accuracy of the present computational methodology in predicting geometrical parameters for reference gas-phase chromium compounds was recently proved [61]. A clear relationship is observed between the oxidation state of chromium and the Cr—OSi bond length. The lower the oxidation state of Cr, the greater the average Cr—OSi distance. This is in agreement with earlier suggestions in the literature [3,4,26] and was also confirmed by reported EXAFS data for Cr(II)/SiO₂ [42] and Cr(VI)/SiO₂ [7,36] systems (Table S1, Supplementary Data). The calculated Cr—OSi bond lengths for the Cr(II) species are consistent with the experimental values.

It was postulated that the polymerization activity of the surface Cr sites in the Phillips catalyst depends on the size of the chromasiloxane ring [7,47], which determines the O—Cr—O angle in the monomeric Cr(II) species [4,47]. Our results indicate that the direct relationship between the size of the chromasiloxane ring and the O—Cr—O angle, earlier computationally confirmed using simple catalyst models [47], does not obtain (Table S2, Supplementary Data). This is explained by the interactions between Cr(II) species and surface siloxane bridges or silanols, as well as by the complex structure of amorphous silica. For instance, the O—Cr—O angle varies from 92° to 156° for Cr(II) species that constitute chromasiloxane rings with four silicon atoms. On the other hand, non-interacting Cr(II) sites forming strained rings with two silicon atoms possess the expected pseudo-tetrahedral geometry [4], characterized by the O—Cr—O angle of 111–113°, which can be compared with the angle of 140° predicted for the Cr(OH)₂ molecule and is in agreement with earlier calculations [47]. Hence, our models of the chromia–silica system give insight into the heterogeneity of the surface Cr species and, consequently, enable further investigations of structure–activity relationships [8,32,62]. Goldsmith et al. recently showed how subtle structural variations in Mo sites on amorphous silica can lead to substantial changes in reactivity [62]. Analogously, slightly different Cr sites may much more significantly differ each other in activity.

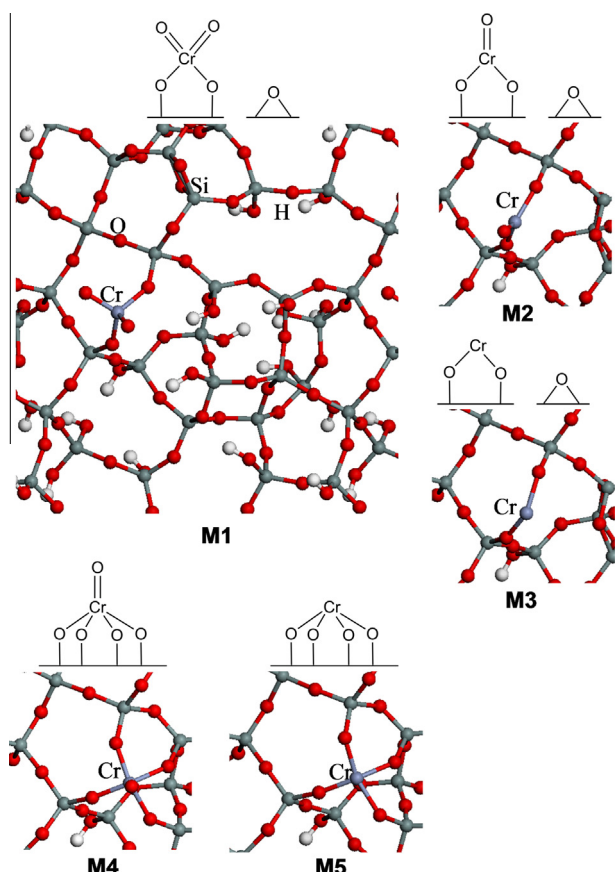


Fig. 1. Optimized structures of the monomeric dioxo (**M1**) and monooxo (**M4**) Cr (VI) species [61] and the corresponding Cr(IV) (**M2**, **M5**) and Cr(II) (**M3**) species on silica (periodic models).

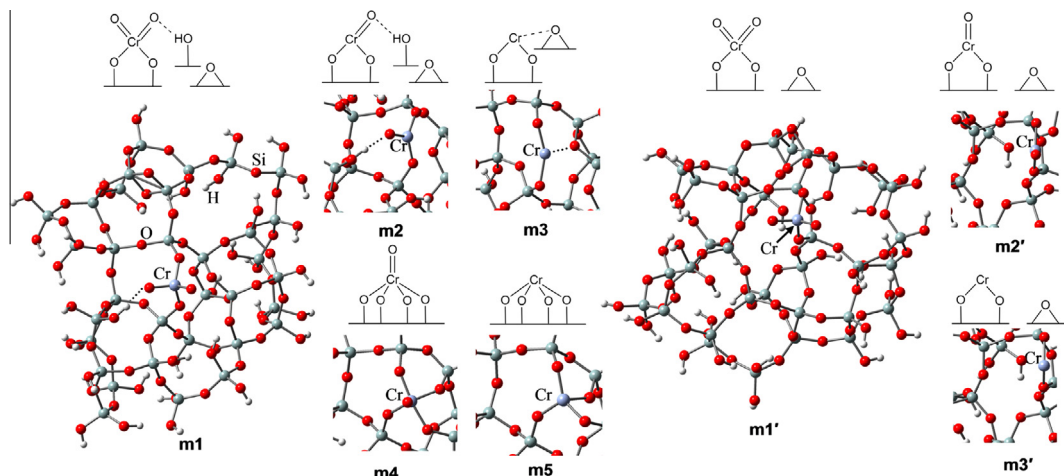


Fig. 2. Optimized structures of the monomeric dioxo (**m1**, **m1'**) and monooxo (**m4**) Cr(VI) species [61] and the corresponding Cr(IV) (**m2**, **m2'**, **m5**) and Cr(II) (**m3**, **m3'**) species on silica (cluster models). For clarity, only a fragment of the silica cluster is shown in most cases.

A two-step reduction scheme of initial dioxo (**m1**, **m1_{hyd}**) and monooxo (**m4**) Cr(VI) species to the Cr(II) species is presented in Fig. 3, together with the reaction Gibbs energy for each step at $T = 873$ K (the temperature used in the experimental part of this work). The CO molecule is assumed as the reducing agent. More detailed calculation data, including both periodic and all cluster models of the surface Cr oxide species, are given in Table S3 (Supplementary Data). Reduction of the initial dioxo and monooxo Cr(VI) species to the corresponding Cr(IV) species is a clearly exothermic and exergonic process. This effect is stronger for the monooxo Cr(VI) species. On the other hand, Lee and Wachs [29] reported that the dioxo Cr(VI) species on silica is reduced faster than the monooxo Cr(VI) species. It should be noted, however, that our calculations are limited to thermodynamics only. It is worth noticing here that reduction of surface monomeric Mo(VI) species on silica to Mo(IV) sites is predicted to be a highly endergonic process [75], in accordance with much worse reducibility of molybdena–silica systems, compared with chromia–silica catalysts. Reduction of

the dioxo Cr(VI) species should rather occur via reaction with the oxo ligand, but for the monooxo Cr(VI) species there is another potential reduction path involving two Cr–O–Si bridges and leading to the formation of the monooxo Cr(IV) species **m2** and the surface siloxane bridge.

The thermodynamic driving force for the Cr(VI) \rightarrow Cr(IV) reduction step is greater than that for Cr(IV) \rightarrow Cr(II) reduction (Fig. 3 and Table S3, Supplementary Data). In the case of the more probable monooxo Cr(IV) species, their reduction is predicted to be an exergonic or endergonic process, depending on the surface model applied (**m2** or **m2_{hyd}**). It is seen that the local structural changes have an impact on reaction energetics in greater than typical DFT error. Hence, taking the local structural heterogeneity into account is crucial in modeling isolated catalyst sites on amorphous supports. Based on the thermodynamic data for $\text{CO}_{(g)}$, $\text{CO}_2_{(g)}$, $\text{H}_2_{(g)}$, and $\text{H}_2\text{O}_{(g)}$ [83], reduction with H_2 must be a more endergonic and endothermic process than reduction with CO, by 7 (ΔG_{873}) and approximately 29 (ΔE) kJ mol⁻¹, respectively. Therefore, it is even more likely that the reduction of Cr(IV) to Cr(II) may be an equilibrium or endergonic process if H_2 is used as the reducing agent, instead of CO.

The reduction of grafted Cr(VI) species, discussed above, is the first phenomenon that takes place upon interaction of silica-supported chromium oxide systems with various probe molecules. Another possibility is hydrolysis of surface Cr–O–Si bonds. The interactions of the supported Cr species with water molecules can transform an anchored Cr species to a nonanchored species [23,25], which might be a precursor for various reduced chromium forms on silica, e.g., clusters of Cr_2O_3 . To take this possibility into account, we have calculated thermodynamic parameters for hydrolysis of Cr–O–Si bonds in the models of Cr oxide species on a partially hydrated silica surface (Table S4, Supplementary Data). The reactions are exothermic; thus they become less favorable at higher temperatures. The predicted Gibbs energies (ΔG_{873}) for hydrolysis of the surface Cr species and for reduction of the partially hydrated Cr(IV) species are comparable (Tables S3 and S4, Supplementary Data). One should note, however, that in these model hydrolysis reactions, formation of gas phase chromium compounds is assumed, whereas the real process is more complex and probably irreversible, leading to phase transitions and Cr_2O_3 clusters. Thus, it is possible that reduction of surface monomeric Cr(VI) oxide species with H_2 mainly leads to Cr_2O_3 rather than to Cr(II), because H_2O formed during the first step of reduction can hydrolyze the Cr–O–Si bonds before Cr(IV) species are reduced.

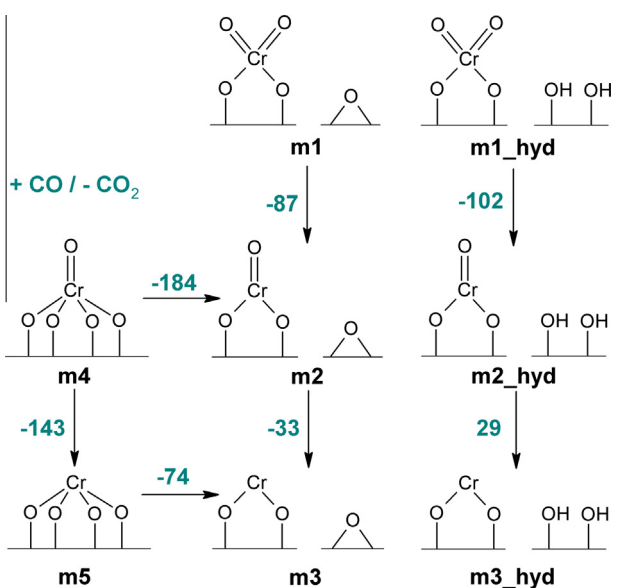


Fig. 3. Gibbs energies at $T = 873$ K (ΔG_{873} , kJ mol⁻¹) for reduction reactions of the monomeric Cr oxide species on silica (cluster models).

This is consistent with reported predominant formation of Cr(III) after reduction of the Cr(VI)/SiO₂ system with H₂ [9,18,32] and with our present experimental results (following).

4.1.2. Dimeric Cr species

As the presence of dimeric Cr oxide species on silica has often been postulated [1,2,4,6,17–19,24–27,32,35,43,46], three different series of their periodic models, containing chromium in various oxidation states, have been developed (Figs. 4–6). Dimeric Cr structures are attached to the silica surface in the same locations as in the case of the monomeric species, to enable better comparison of the results obtained for the monomers and dimers. In order to evaluate the effect of temperature on the relative stability of oxidized and reduced Cr species, a series of cluster models have been also prepared (Fig. S3, Supplementary Data).

The calculated Cr=O, Cr—OSi, and Cr—Si bond lengths are in the same range for monomeric and dimeric structures (compare Tables S1 and S5, Supplementary Data). Analogously to the monomeric Cr species, for the dimers it is also predicted that the lower the oxidation state of the Cr center, the longer the Cr—OSi bond is. The obtained wide range of Cr—Cr distances (2.45–3.30 Å, periodic models) confirms heterogeneity of the surface dimeric Cr species. These values are consistent with recently reported structural parameters for well-defined dinuclear surface Cr sites on silica [84]. Not surprisingly, the Cr—Cr distances are shorter, on the average, than the calculated Mo—Mo distances for surface dimeric Mo oxide species on alumina (2.99–3.95 Å) [85] and titania (2.96–3.77 Å) [86].

The initial Cr(VI) dimeric species can be classified as double-dioxo (**I_D1**, Fig. 4), monooxo-dioxo (**II_D1**, Fig. 5), and double-monoxxo species (**III_D1**, Fig. 6). Their relative energies increase in the order **I_D1** < **II_D1** < **III_D1** (Fig. 7); hence, the dimeric dioxo species are predicted to be more stable than the dimeric monooxo species. What is more important, the initial oxidized dimeric Cr(VI) species are less stable than the monomeric Cr(VI) species, although the calculated energy and Gibbs energy differences are small in the case of the most stable dimeric species **I_D1** (Fig. 7). This is in general agreement with postulated dominance of monomeric surface Cr(VI) species on silica at low chromium loadings [4,15,16,20,21,28–36]. An analogous energetic preference was earlier predicted for surface monomeric Mo(VI) species on the most exposed (110) γ -alumina face [85] and on titania [86].

The calculated energetic effects of possible reduction steps and further hydration and/or rearrangement steps for the initial double-dioxo (**I_D1**), monooxo-dioxo (**II_D1**), and double-monoxxo (**III_D1**) dimeric Cr(VI) species are shown in Figs. 8–10, respectively. If CO is applied as a reducing agent, almost all considered reduction steps are predicted to be exothermic. Starting from the most stable double-dioxo Cr(VI) species (**I_D1**, Fig. 8), the final oxidation state Cr(II)Cr(II) (**I_D6**) can be obtained. This is in accordance with the reported [1,24–27] and present (following) experimental results indicating the preferential formation of Cr(II) species after reduction of the Cr(VI)/SiO₂ system with CO. Double-monoxxo Cr(VI) species (**III_D1**, Fig. 10) can be reduced by CO to dimeric Cr(III)Cr(III) species (**III_D4**), but the subsequent slightly exothermic reduction step leads to two neighboring monomeric Cr(II) species (**III_D6**). Potential rearrangement of a linear **III_D4** structure to a cyclic Cr(III)Cr(III) species (**II_D7**) is highly endothermic, because of formation of a strained surface siloxane bridge. In the case of the monooxo-dioxo Cr(VI) species (**II_D1**, Fig. 9), reduction with CO can lead to mixed Cr(IV)Cr(II) species (**II_D6**). Again, potential transformation to dimeric Cr(III)Cr(III) species (**II_D7**) requires high energy. Possible rearrangement of **II_D6** resulting in two monomeric Cr(III) species of different geometries (**II_D11**) is also highly endothermic.

As mentioned above, reduction with H₂ is less energetically preferable than reduction with CO, by approximately 29 kJ mol^{−1} (ΔE). Double-dioxo Cr(VI) species can finally be reduced to Cr(III)Cr(III) dimeric species (**I_D8**, Fig. 8), although this step is predicted to be slightly endothermic. Further reduction to Cr(II)Cr(II) site (**I_D6**) is possible, but in the presence of water, hydration giving two neighboring hydroxylated Cr(III) monomers (**I_D9**) is an alternative route. Treating the monooxo-dioxo Cr(VI) species (**II_D1**) with hydrogen (Fig. 9) might lead to hydroxylated Cr(III) monomers (**II_D10**), formed by highly exothermic hydration of the mixed Cr(IV)Cr(II) site (**II_D6**). Finally, the double-monoxxo Cr(VI) species (**III_D1**) would be reduced to a Cr(III)Cr(III) dimer (**III_D4**). It can be further reduced to the Cr(II) monomers (**III_D6**) or, in an excess of water, transformed into the hydrated Cr(III) monomers (**III_D5**) (Fig. 10).

To estimate reaction Gibbs energies at high temperature (873 K), a series of cluster models (**I_d**) have been applied (Fig. S5, Supplementary Data). They correspond to the **I_D** series of the periodic models, including the most stable dimeric Cr(VI) structure (**I_D1**). The general picture of the reduction process is

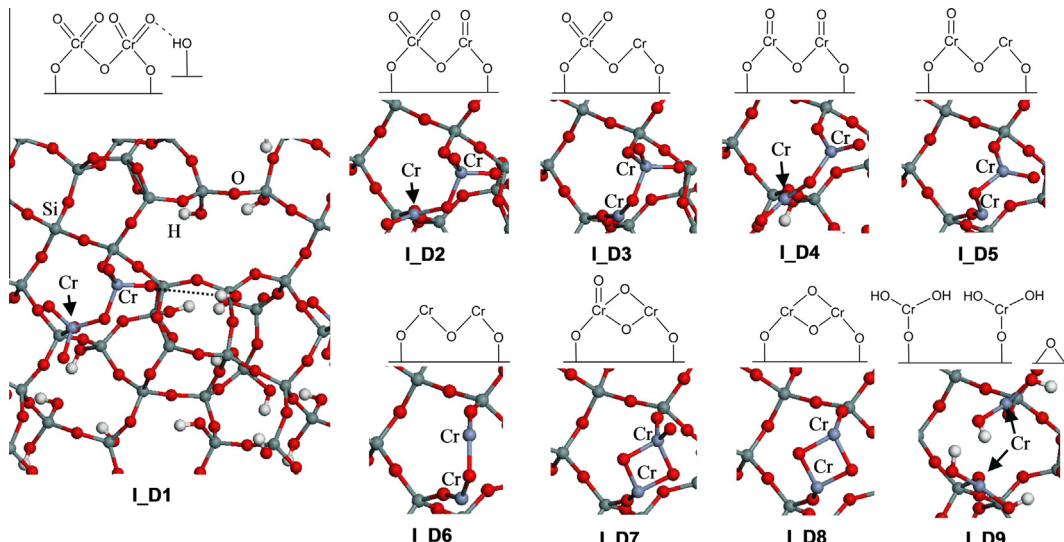


Fig. 4. Optimized structures of the dimeric double-dioxo Cr(VI) species (**I_D1**) and the corresponding reduced species (**I_D2**–**I_D9**) on silica (periodic models).

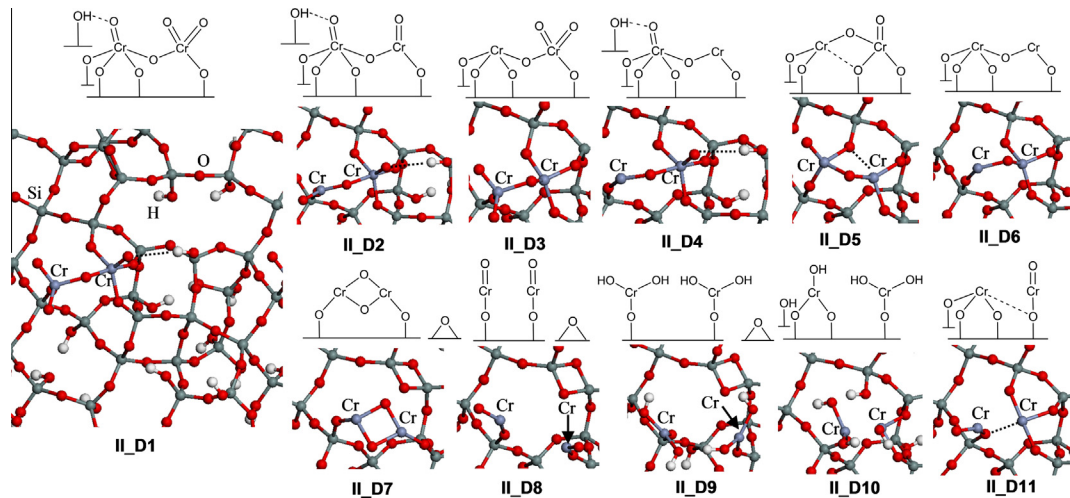


Fig. 5. Optimized structures of the dimeric monooxo-dioxo Cr(VI) species (**II_D1**) and the corresponding reduced species (**II_D2–II_D11**) on silica (periodic models).

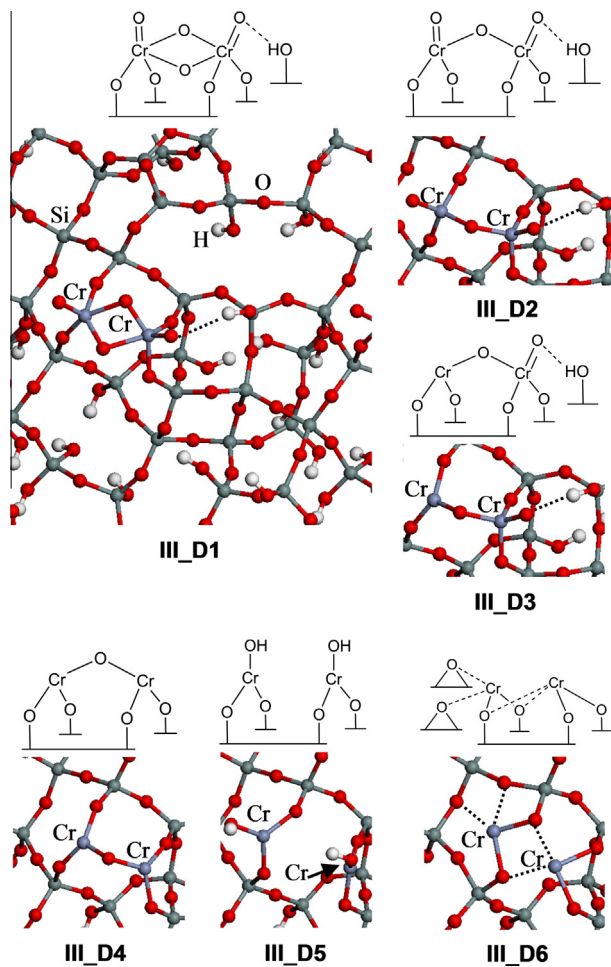


Fig. 6. Optimized structures of the dimeric double-monooxo Cr(VI) species (**III_D1**) and the corresponding reduced species (**III_D2–III_D6**) on silica (periodic models).

similar to that discussed above on the basis of the periodic calculations. Reduction should finally result in formation of dimeric Cr(III)Cr(III) species (**I_d8**) and Cr(II)Cr(II) species (**I_d6**), although the last steps can be close to equilibrium. As expected, exothermic hydration of **I_d8** is not thermodynamically preferred at high temperatures, and we might suppose that the hydrolysis of the

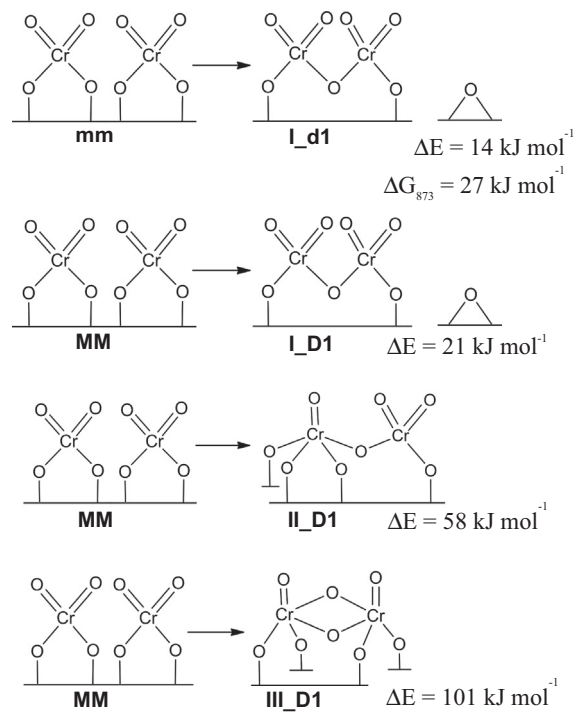


Fig. 7. Relative energies (ΔE) and Gibbs energy at $T = 873\text{ K}$ (ΔG_{873}) for the monomeric and dimeric Cr(VI) oxide species on silica (cluster and periodic models). The reference models of two neighboring monomeric dioxo Cr(VI) species (**mm**, **MM**) are presented in Fig. S4 (Supplementary Data).

Si—O—Cr bonds will be more probable in this case (compare Table S4, Supplementary Data). On the other hand, an excess of water can cause the reoxidation of potentially formed Cr(II)Cr(II) sites (**I_d6**), in accordance with earlier suggestions in the literature [25,46] and the present experimental findings (following).

To conclude, according to the calculation results, reduction of the dimeric Cr(VI) species by CO should mainly lead to Cr(II) dimeric or monomeric species, whereas both Cr(III) and Cr(II) species can be formed in the presence of H₂. In the latter case, water, generated as a by-product during the reduction, can reoxidize surface Cr(II) species and/or hydrolyze the Cr—O—Si or Cr—O—Cr bonds. Therefore, the final Cr(III)/Cr(II) ratio should depend on the partial water pressure, governed by the process conditions,

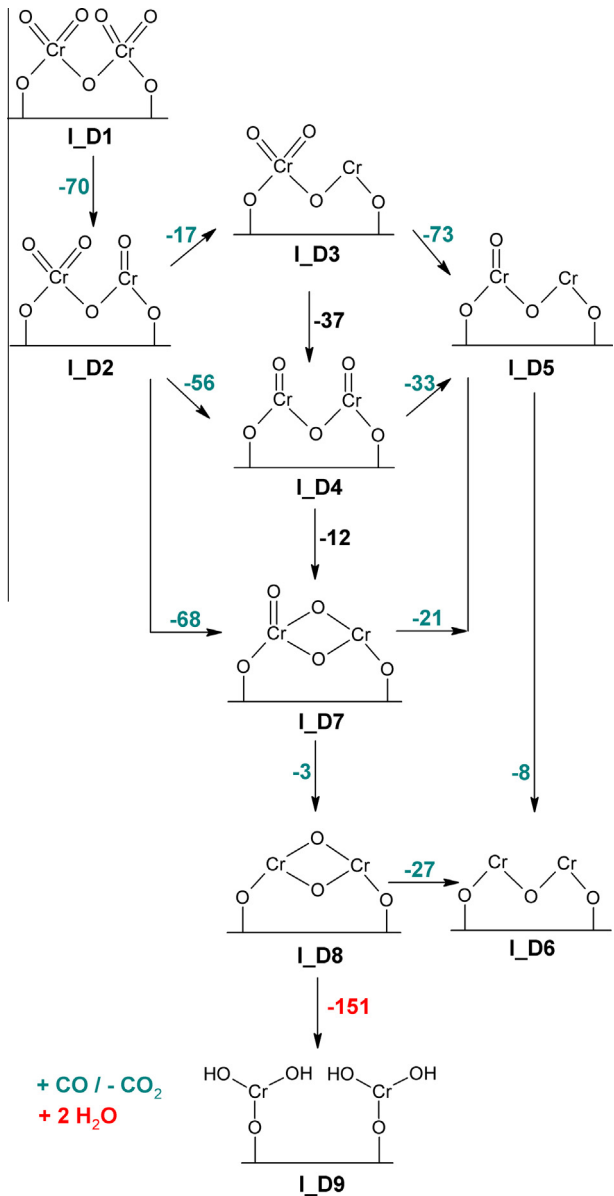


Fig. 8. Energies (ΔE , kJ mol⁻¹) for reduction, rearrangement, and hydration reactions of the dimeric Cr oxide species on silica (periodic models, series I_D).

for instance, the flow velocity [46]. With larger amounts of water, the formation of Cr(III) is facilitated. The latter statement is also true if CO is used as the reducing agent. Although Cr dimers or oligomers are expected to be at most minor species at low Cr loadings, these computational results are in a very good agreement with earlier [46] and present (following) experimental results and additionally explain the reduction behavior of the chromia–silica system.

Finally, it is interesting to note possible disproportionation reactions involving intermediate Cr dimeric species formed during the reduction process. For example, it is predicted that dimeric Cr (IV)Cr(IV) oxide species (I_D4, I_d4) can transform into mixed Cr (V)Cr(III) sites (I_D7, I_d7) (Figs. 8 and S5, Supplementary Data). Such reactions may additionally explain the presence of various oxidation states of chromium, experimentally detected.

4.1.3. Vibrational frequencies

The theoretically determined vibrational frequencies for the monomeric Cr species are collected in Tables 1 and S6 (Supplementary Data). Raman spectroscopy data reported for chromia–silica systems are also included. The calculated vibrational modes are usually coupled with the support vibrations. Vibrational frequencies for the Cr(VI) structures were obtained and discussed in detail previously [61] and now they are provided only for comparison. It is seen that the scaled frequencies are close to the corresponding experimental data, confirming the adequacy of the models.

The predicted Cr=O stretching frequencies for the monooxo Cr (IV) oxide species are above 1000 cm⁻¹ for the models that do not represent any interactions between the Cr center and silanol groups (M2, m2, m2_hyd, mc2_1). Otherwise, the frequencies are significantly redshifted (m2, m2_hyd, ma2, mb2, mc2_2). Groppo and co-workers [37] recently published Raman spectroscopy data that might be attributed to Cr(IV) species on silica generated by controlled oxidation of Cr(II) species with N₂O, although the Cr(IV) oxidation state was not unambiguously determined. They obtained a double peak at 1015 and 1028 cm⁻¹. The first value can be assigned to the well-distinguished Cr=O stretching mode with calculated frequencies in the range 1004–1013 cm⁻¹ (Tables 1 and S6, Supplementary Data). The second value is more problematic to assign. However, our Cr(IV) models, both periodic and cluster, predict another Cr=O stretching mode at 1027–1035 cm⁻¹, hence matching the experimental band at 1028 cm⁻¹. Nevertheless, this assignment should be treated with caution, because the vibration would be rather weak and strongly coupled with the Si—O—Si vibrational modes of the support.

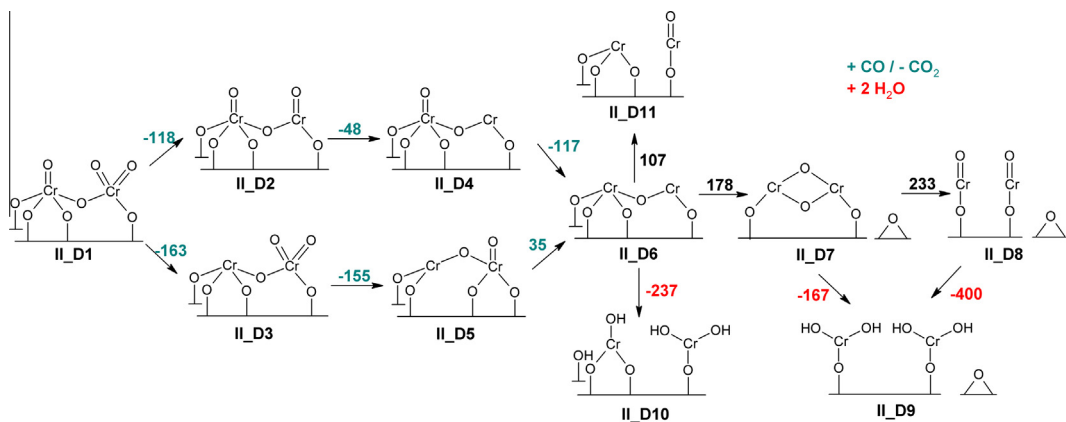


Fig. 9. Energies (ΔE , kJ mol⁻¹) for reduction, rearrangement, and hydration reactions of the dimeric Cr oxide species on silica (periodic models, series II_D).

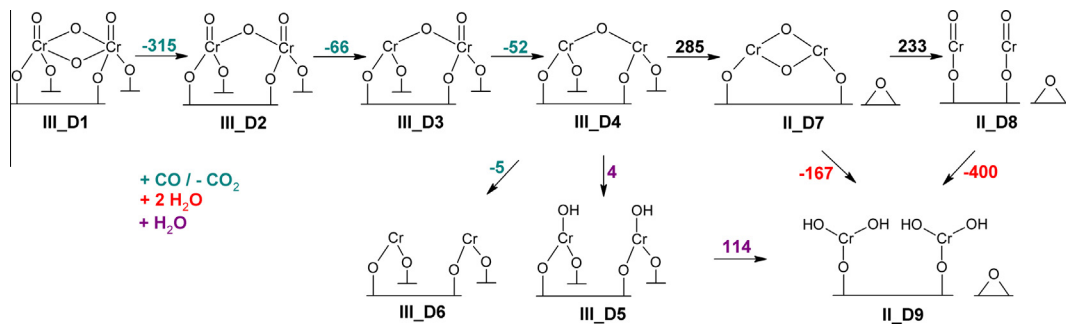


Fig. 10. Energies (ΔE , kJ mol^{-1}) for reduction, rearrangement, and hydration reactions of the dimeric Cr oxide species on silica (periodic models, series **III_D**).

Table 1

Calculated^a and experimental vibrational frequencies (cm^{-1}) for the monomeric Cr oxide species on silica.

Species	Model	$\nu(\text{Cr}=\text{O})$	$\nu_s(\text{O}=\text{Cr}=\text{O})$	$\nu_{as}(\text{O}=\text{Cr}=\text{O})$	$\nu(\text{Cr}-\text{O}-\text{Si})$
Dioxo Cr(VI)	M1	–	977	1007	919
	m1	–	948	994, 1001	896
	m1'	–	975	1004	865
Monooxo Cr(VI)	M4	1005	–	–	914
	m4	1002, 1015	–	–	906–935
Monooxo Cr(IV)	M2	1007, 1027	–	–	964
	m2	956	–	–	867–895
	m2'	1004, 1010, 1033	–	–	878
Fourfold bonded Cr(IV)	m5	–	–	–	856–875
Cr(II)	m3	–	–	–	920
	m3'	–	–	–	889
Exp. Cr(VI)		1011 ^b	980–990 ^c	1004 ^d , 1014 ^e	905–919 ^f
Exp. Cr(IV)		1015 ^g , 1028 ^g			

^a The frequencies are scaled by 0.9241 and 0.9149 for the periodic (**M1**, **M2**, **M4**) and cluster (**m1**–**m5**, **m1'**–**m3'**) calculations, respectively. The results for the Cr(VI) systems are taken from Ref. [61].

^b Refs. [29,30].

^c Refs. [29,30,33,34,36,37].

^d Ref. [33].

^e Ref. [34].

^f Refs. [29,36].

^g Ref. [37].

What is important and a bit surprising, the predicted $\nu(\text{Cr}=\text{O})$ frequencies for the monooxo Cr(IV) species ($1004\text{--}1013\text{ cm}^{-1}$) are exactly in the same range as the calculated $\nu(\text{Cr}=\text{O})$ frequencies for the monooxo Cr(VI) species ($1002\text{--}1015\text{ cm}^{-1}$). Lee and Wachs [29] observed that upon reduction of the Cr(VI)/ SiO_2 system with H_2 , the Raman band at 982 cm^{-1} , assigned to the dioxo Cr(VI) species, decreases in intensity faster than the band at 1011 cm^{-1} , assigned to the monooxo Cr(VI) species. Hence, they showed that these Raman bands indeed originate from two different surface Cr(VI) species and the dioxo species is more reactive toward reduction than the monooxo species [29–32]. However, according to our computational results, the situation may be more complex. The monomeric dioxo Cr(VI) species are reduced to monooxo Cr(IV) species, but subsequent reduction to Cr(II) can be thermodynamically less favored (Fig. 3). Moreover, the monooxo Cr(VI) species might be also reduced to the monooxo Cr(IV) species. Therefore, the monooxo Cr(IV) species, being formed during the reduction process, can be present on the surface and their $\text{Cr}=\text{O}$ stretching vibrations may contribute to the band at 1011 cm^{-1} . Consequently, slower disappearance of this band may be caused partially by formation of intermediate Cr(IV) species. It can be also noted that reduction of the monooxo Cr(VI) species to Cr(IV) species is predicted to be even more thermodynamically preferable than the reduction of the dioxo Cr(VI) species (Fig. 3), although any conclusions about the reduction kinetics cannot be drawn on this basis.

Some authors assigned the band above 1000 cm^{-1} to the asymmetric $\text{O}=\text{Cr}=\text{O}$ mode [33,34] or postulated that this mode overlaps other vibrational modes [36]. Indeed, the typical $\nu_{as}(\text{O}=\text{Cr}=\text{O})$ frequencies predicted for the dehydrated dioxo Cr(VI) species ($1000\text{--}1015\text{ cm}^{-1}$) confirm possible overlapping of this mode with the monooxo $\nu(\text{Cr}=\text{O})$ stretching modes. Thus, even three different surface Cr species, (i) monooxo Cr(VI), (ii) monooxo Cr(IV), and (iii) dioxo Cr(VI), can contribute to the Raman band above 1000 cm^{-1} observed during the reduction of the Cr/ SiO_2 system.

Recently, a sharp Raman band at 988 cm^{-1} , detected for the partially reduced Cr/ SiO_2 system, synthesized in the form of sol-gel monoliths, was assigned to intermediate Cr(IV) oxo species [45]. In a comparison with the spectrum for the initial Cr(VI)/ SiO_2 catalyst, a small blueshift of 6 cm^{-1} was observed. For some of our models of Cr(VI) species interacting with surface hydroxyl groups (**m1**, **mb1**, **mc1**), a blueshift in a similar range is predicted ($1\text{--}8\text{ cm}^{-1}$) after reduction to Cr(IV) (Tables 1 and S6, Supplementary Data). In the case of the Cr(VI) species not interacting with silanols (**M1**, **m1'**, **m1'_hyd**), the calculations show much greater shift in frequencies ($29\text{--}48\text{ cm}^{-1}$). This result can correspond to a reported shoulder on the high-energy side of the experimental peak [45].

Considering the $\text{Cr}-\text{O}-\text{Si}$ stretching vibrations calculated for the monomeric Cr(IV) and Cr(II) species, it is seen that they are in a broad range similar to those predicted for the initial Cr(VI) species (Tables 1 and S6, Supplementary Data). No general relation-

ship between the oxidation state of the chromium site and the vibrational frequency is observed.

Calculated vibrational frequencies for dimeric Cr species supported on silica are summarized in Table S7 (Supplementary Data). For the initial double-monooxo Cr(VI) species (**III_D1**), the Cr=O stretching frequencies are generally predicted to be in a range similar to that for the monomeric monooxo Cr(VI) species, but in the case of the reduced forms these vibrations are redshifted. The same tendency is observed for symmetric and asymmetric O=Cr=O stretching modes. The calculated numbers for the double-dioxo Cr(VI) species (**I_D1**, **I_d1**) are close to those for the monomeric dioxo Cr(VI) models, whereas for the reduced forms (**I_d2**, **I_d3**) these vibrations appear at lower wavenumbers. Some frequencies are clearly decreased because of an interaction between the oxo ligand and a neighboring OH group (**II_D1**, **III_D1**, **I_d1**, **I_d2**, **I_d4**). The Cr—O—Si stretching frequencies predicted for the dimeric Cr species are generally in the same range (849–963 cm⁻¹) as those calculated for the monomeric species (810–964 cm⁻¹).

The only vibrational feature that would enable distinguishing between the chromium monomers and potential dimers (or polymers) on the silica surface is the Cr—O—Cr modes. For most stable dimeric Cr(VI) species (**I_D1**, **I_d1**), the calculated symmetric Cr—O—Cr frequencies (515–536 cm⁻¹) are slightly lower than the observed very weak band at 576 cm⁻¹, assigned to $\nu_s(\text{Cr—O—Cr})$ vibration for the Cr(VI)/SiO₂ system [29]. The asymmetric Cr—O—Cr modes are obtained at 723–731 cm⁻¹. Additionally, coupled $\nu_s(\text{Cr—O—Si})$ and $\nu_{as}(\text{Cr—O—Cr})$ vibrational modes are predicted, between 800 and 900 cm⁻¹ (Table S7, Supplementary Data).

4.1.4. Excitation energies

Electronic transitions have been computed for dehydrated monomeric and selected dimeric Cr species represented by the cluster models and compared with the experimental data (Table 2). In the case of the Cr(VI) species, the calculated charge transfer (CT) excitation energies moderately depend on the model and they are consistent with the experimentally measured values (270 and

360 nm in this work). The interpretation of the third experimental band (445–465 nm) was a subject of much discussion in the literature. This band was assigned either to dimeric/polymeric [87] or to monomeric [29] Cr(VI) species. Our calculations do not reproduce this transition for the dimeric double-dioxo Cr(VI) species, or for the monomeric dioxo Cr(VI) species. The only exception is the model **m1'**, characterized by a weak absorption at 411 nm. However, an intense band in this range (414 nm) is predicted for the monomeric monooxo Cr(VI) species.

Although the considered model of the dimeric double-monooxo Cr(III)Cr(III) species (**I_d8**) cannot represent all possible Cr(III) structures on silica, the theoretically determined transitions at 313 and 625 nm well agree with the experimental data assigned for pseudo-octahedral Cr(III) species [87].

The geometry of the Cr(II) species significantly influences the theoretically predicted band positions, in accordance with the recently reported study of Cr(II)/SiO₂ model system [55]. For the monomeric Cr(II) sites interacting with neighboring surface siloxane bridges and silanol groups (**m3**, **ma3**, **mb3**), electronic transitions at 555–795 nm are obtained, corresponding to the value of 800 nm, proposed for pseudo-octahedral Cr(II) species [87]. In the case of the noninteracting Cr(II) species having pseudo-tetrahedral geometry (**m3'**, **mc3**), the expected transitions close to 1000 nm [87] are reproduced, however, a stronger absorption at about 700 nm is predicted. An additional strong band at 430 nm is computed for potential dimeric Cr(II)Cr(II) species (**I_d6**).

The intermediate Cr(IV) species are rather not observed by UV-vis during the reduction of Cr(VI) to Cr(III)/Cr(II). According to the calculations, the CT bands for the most probable monomeric monooxo Cr(IV) species could overlap with the signals observed for Cr(VI) species (Table 2). However, the predicted absorption in the *d*-*d* transition region (880–1053 nm) is stronger than that for the Cr(II) species at about 1000 nm. This could explain the experimentally observed signal at 1000 nm that appeared after controlled oxidation of Cr(II)/SiO₂ system and might come from surface Cr(IV) species [37].

Table 2
Calculated and experimental UV-vis band maxima for Cr species on the dehydrated silica surface.

Calculated		
Model	Species	Wavelength (nm)
m1 , m1' , ma1 , mb1 , mc1	Monomeric dioxo Cr(VI)	230–265, 309–333, 411 ^a
m4	Monomeric monooxo Cr(VI)	274, 328, 414, 646
I_d1	Dimeric double-dioxo Cr(VI)	243, 327
m2 , m2' , ma2 , mb2 , mc2_1 , mc2_2	Monomeric monooxo Cr(IV)	230–270, 305–334, 398–491, 880–1053
m5	Monomeric four fold bonded Cr(IV)	248, 355, 461, 685
I_d4	Dimeric double-monooxo Cr(IV)Cr(IV)	232, 277, 371, 569, 1237
I_d8	Dimeric Cr(III)Cr(III)	313, 381, 625, 973, 1080
m3 , ma3 , mb3	Monomeric Cr(II)	211–244, 555–795, 1074
m3' , mc3	Monomeric Cr(II)	311–314, 689–699, 1002–1006
I_d6	Dimeric Cr(II)Cr(II)	241, 308, 430, 697, 1170

Experimental		
Assignment		Wavelength (nm)
Cr(VI) ^b		270, 360, 455
Cr(III)/Cr(II) ^b		780
Monomeric Cr(VI) ^c		275, 370
Monomeric Cr(VI) ^d		250, 340, 460
Dimeric Cr(VI) ^c		275, 322, 445
Pseudo-octahedral Cr(III) ^c		295, 465, 625
Pseudo-octahedral Cr(II) ^c		800
Pseudo-tetrahedral Cr(II) ^c		1000

^a Predicted only for the **m1'** model.

^b This work.

^c Ref. [87].

^d Ref. [29].

4.2. In situ UV-vis DRS investigations

Experimentally, the oxidation state of chromium species during reduction with CO or H₂ at 873 K was monitored with UV-vis DRS. Chromium species were dispersed on ordered mesoporous silica support, SBA-1 that possesses cubic 3D pore structure (*Pm3n* space group) and high specific surface area. This unique textural properties and thermal stability make this mesoporous silica very promising for sorption and catalytic application as the support. Detailed physicochemical characterization of pure SBA-1 and CrO_x/SBA-1 samples were reported elsewhere [18]. The total loading of Cr, determined by ICP, was 1.07 wt%. The content of Cr(VI) species in the fresh catalyst, estimated by chemical titration using the Bunsen–Rupp method, was 0.91 wt%. Raman spectra of the catalyst indicated that Cr(VI) species in the hydrated sample existed in the form of mono- and dichromates. EPR showed very weak γ signal indicating the presence of trace amounts of isolated Cr(V) species. XRD, Raman, and EPR show no specific bands/signals characteristic for Cr₂O₃ particles, confirming high dispersion of chromium on SBA-1.

UV-vis DRS spectra recorded during the reduction of CrO_x/SBA-1 sample by H₂ and CO are reported in Fig. 11. The experiments were conducted at the same temperature (873 K) to obtain total reduction of the sample and similar variation of signal-to-noise ratio as well as thermal changes of spectra (e.g., baseline and band drift). The temperature at which the CrO_x/SBA-1 sample is fully reduced using both reducers was estimated based on the temperature-programmed reduction (TPR). The CO TPR and H₂ TPR profiles are reported in Fig. S7 (Supplementary Data). These studies revealed that full reduction of the CrO_x/SBA-1 sample with CO occurs at about 723 K. In contrast, the reduction with H₂ is extended to higher temperatures and the CrO_x/SBA-1 sample is fully reduced above 823 K.

Fig. 11A summarizes the spectra recorded during reduction of the CrO_x/SBA-1 sample with hydrogen. The spectrum of the out-gassed sample (blue line) shows two intense bands characteristic of the O → Cr⁶⁺ charge transfer (CT) transitions, at 270 and 360 nm [1,87]. Additionally, a shoulder at around 455 nm is present. This shoulder band was assigned to the dichromate/polychromate species (with low symmetry) [87] or to the isolated Cr(VI) species [29], the latter assignment being more consistent with our calculation results (Table 2). During reduction with H₂ at 873 K the CT bands characteristic of Cr(VI) species disappear gradually, while at the same time a new broad band located at 780 nm appears (inset to Fig. 11A). The latter band is a superposition of two bands characteristic of *d*-*d* transitions of pseudo-tetrahedral Cr(II)

and pseudo-octahedral Cr(II)/(III) species [87,88]. The presence of the broad maximum indicates clearly that the reduction with H₂ produced both Cr(III) and Cr(II) species. The reduction of CrO_x/SBA-1 with CO also leads to formation of a band in the *d*-*d* region (Fig. 11B). However, the band is more distinct and shifts to higher wavelength (ca. 800 nm), confirming that the formation of Cr(II) is preferred when CO is applied as the reducing agent.

The course of Cr(VI) reduction with CO is in agreement with previous experimental knowledge obtained by various techniques including FTIR, Raman, CO TPR, and UV-vis DRS [1,24,27,37,46,87]. All these investigations indicate that CO reduces Cr(VI) to Cr(II) species. As CO is a two-equivalent reducing agent, the above reduction probably proceeds via Cr(IV) species. The latter species were suggested recently as unstable intermediates in redox processes between Cr(II)/Cr(VI) species over various CrO_x/silica materials [27,37,45]. The DFT calculations reported in this work confirm that reduction of Cr(VI) species with CO can proceed via Cr(IV) species that further are reduced to Cr(II) species. On the other hand, the UV-vis DRS results indicate that reduction of CrO_x/SBA-1 with H₂ leads to a Cr(III) and Cr(II) species mixture. Early studies employed H₂ TPR to determine the oxidation state of chromium in a reduced CrO_x/SiO₂ sample, indicating that reduction degree depends on several factors, such as Cr loading and reduction conditions [12,46]. Hakuli et al. [12] have shown that the concentration of Cr(II) species decreases with the increase of total Cr content. This is also confirmed by previous studies applying H₂ TPR coupled with in situ UV-vis DRS, which showed that with increased Cr loading in CrO_x/SBA-1, the broad *d*-*d* band shifts to lower wavelength, indicating decreased Cr(II) content [18]. Moreover, Kim and Woo [46] have proposed that the oxidation state of the Cr species in a reduced sample depends on a kinetic factor of reduction, such as gas velocity. They have suggested that at a low flow rate of H₂, reduced Cr species could easily be reoxidized with water produced during TPR. As a result, at a low flow rate, the final oxidation state of the sample reduced with H₂ is close to 3+, while at a high flow rate, when the water produced during the reduction is effectively removed, a deep reduction to the 2+ oxidation state is also possible. Taken together all the above pieces, it can be suggested that water produced during reduction with H₂ is probably responsible for the presence of Cr(III) species in the reduced CrO_x/SBA-1 system. This is also consistent with the conclusions based on the DFT calculations, concerning possible hydrolysis and reoxidation reactions involving surface Cr species.

To clarify the effect of water, we investigated CrO_x/SBA-1 behavior during reduction with either H₂ or CO, in the presence and absence of water. In each experiment, the fresh CrO_x/SBA-1

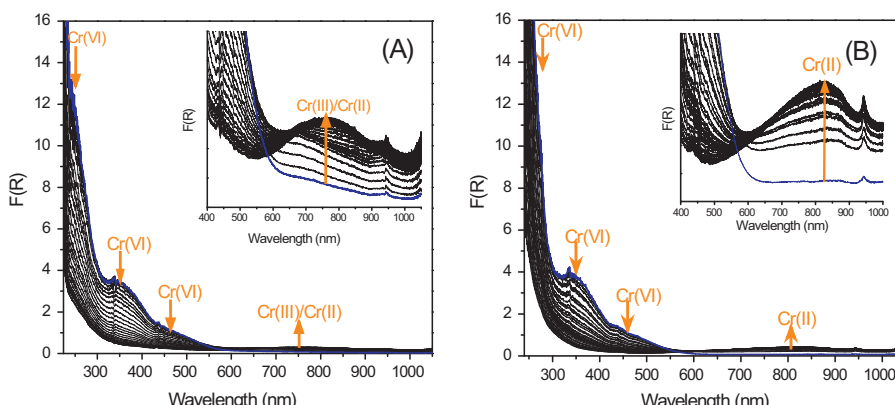


Fig. 11. Isothermal reduction of CrO_x/SBA-1 with H₂/N₂ (A) and CO/He (B) mixture at T = 873 K. Blue line indicates spectrum for outgassed sample (before reduction) and orange arrows indicate the direction of changes during reduction.

sample was first reduced with dry H₂ or CO and then reoxidized with dry air at 873 K. After five standard reduction/oxidation cycles, the next five cycles were carried out with the presence of additional water, which was added during the reduction. The spectra recorded during all the cycles for oxidized and reduced CrO_x/SBA-1, in the absence and presence of water, are summarized in Fig. 12. It is clearly seen that reduction with dry H₂ leads to formation of both Cr(III) and Cr(II) species. In each dry reduction cycle (without additional water), a clear broad *d-d* band appears, indicating formation of Cr(III) and Cr(II) species together. Reoxidation with dry air during the regeneration step restores the CT bands characteristic of Cr(VI) species (270, 360, and 450 nm). However, the intensity of these bands decreases in the consecutive regeneration step, indicating that after oxidation, the Cr(VI) species are only partially regenerated with air. This effect is even clearer after the cycles with injection of additional water during the reduction. Moreover, in the cycles with wet H₂ reduction, a new band at about 620 nm and two others at 290 and 460 nm appear, suggesting that during the reduction, Cr₂O₃ particles are produced together with grafted Cr(III) (pseudo-octahedral) species (Fig. 12B). The Cr₂O₃ particles are probably formed by thermal decomposition of hydrolyzed Cr(VI) species. Such formation of Cr₂O₃ particles, catalyzed by moisture, was previously reported by McDaniel and co-workers [5] for the Phillips catalyst. They found that surface chromate esters are hydrolyzed to free chromic

acid, which is thermally unstable and decomposes to α -Cr₂O₃ particles at high temperatures.

Interestingly, the redox behavior of CrO_x/SBA-1 samples is different in cycles with CO as the reduction agent. In the absence of water, Cr(II) species are formed almost selectively and during the reoxidation step the characteristic CT bands are completely restored (Fig. 12C and D). In contrast, during wet reduction with CO, the band at 810 nm, characteristic of pseudo-octahedral Cr(II) species, shifts to lower wavelength (ca. 720 nm). This shifting, together with the appearance of a new weak band at about 465 nm, confirms that water suppresses deep reduction to Cr(II). In the presence of wet CO, the reduction process leads to Cr(III) species formation, similar to that in the presence of H₂. However, no band characteristic of Cr₂O₃ particles (at 620 nm) is formed during the reduction with wet CO, suggesting that the hydrolysis pathway of Cr₂O₃ particles formation is less preferable in this process. A difference in the final oxidation state of Cr species reduced with H₂ and CO under wet and dry conditions (reduction with H₂ and without extra water) are probably due to competition between reduction and hydrolysis reactions. Fast reduction of Cr(VI) species with CO hampers hydrolysis and final Cr₂O₃ particles formation, while slower reduction with H₂ leads to higher contribution of hydrolysis reaction. As a result, during the CrO_x/SBA-1 reduction by H₂ (with extra water) larger Cr₂O₃ particles are produced, being more resistant to reoxidation.

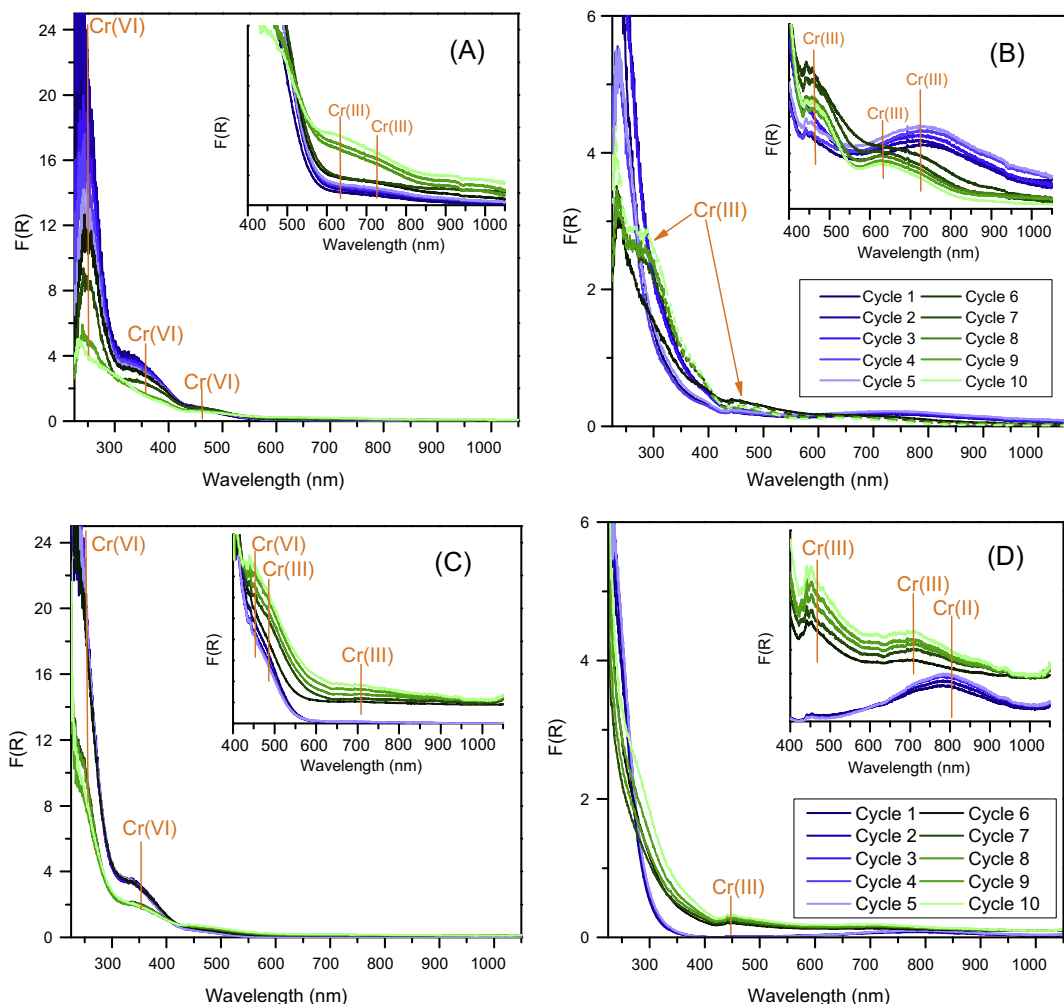


Fig. 12. UV-vis DR spectra of a CrO_x/SBA-1 sample recorded during consecutive reduction/oxidation cycles in the presence (green lines) and absence (blue lines) of water at 873 K. (A) and (C) spectra of the sample oxidized with air; (B) and (D) spectra of the samples reduced with H₂ and CO, respectively.

5. Conclusions

Comprehensive DFT studies combined with *in situ* UV-vis DRS experiments have been performed to give new detailed insights into the reduction process of the chromia–silica system. For the first time, such advanced models of the chromia–silica system, both periodic and cluster, have been applied to deal with the heterogeneity of surface monomeric and dimeric Cr oxide sites at various oxidation states. The obtained variety of Cr structures on amorphous silica can be a good starting point for future studying of the structure–activity relationships. Additionally, the vibrational frequency analysis allow us to propose some new assignments for reported Raman spectroscopy data concerning reduced chromia–silica systems.

It is shown that dimeric Cr(VI) species are less stable than monomeric Cr(VI) sites; hence, the latter are expected to be dominant species at low Cr loadings, in agreement with many experimental works [4,15,16,20,21,28–36]. Reduction of monomeric Cr (VI) species to intermediate Cr(IV) species is predicted to be a clearly exergonic process, whereas the thermodynamic driving force for the further reduction to Cr(II) is weaker. In the case of dimeric Cr(VI) species, multistep reduction involving various oxidation states can finally lead to Cr(III) or Cr(II) species. In the presence of water, some reduced dimeric Cr sites can eventually be hydrated to monomeric Cr(III) species. Water may also reoxidize surface Cr(II) species or hydrolyze the Cr—O—Si bonds.

The redox behavior of the surface Cr species and especially the role of water have been also investigated experimentally. The chromium oxidation state in the $\text{CrO}_x/\text{SBA-1}$ sample has been monitored by *in situ* UV-vis DRS during reduction with CO and H_2 in the presence and absence of water, as well as during the regeneration with dry air. For both reducing agents, the addition of water during reduction has a great impact on the redox behavior of the $\text{CrO}_x/\text{SBA-1}$ system. It is shown that during reduction under dry conditions using CO, the Cr(VI) species are almost selectively converted into Cr(II) species. In contrast, after water addition, Cr(III) species in pseudo-octahedral coordination are formed. The reduction of Cr(VI) species with wet H_2 is more complex, because two effects of water presence can be considered. The first one is similar to that in the case of wet CO reduction: water hampers a deep reduction of Cr(VI) species to Cr(II) sites. The second effect is due to chromate esters hydrolysis, which may further lead to formation of $\alpha\text{-Cr}_2\text{O}_3$ particles. The reoxidation/hydrolysis processes mentioned above also occur during the reduction with dry H_2 , because of water produced in the process. This can explain the observed difference in the final oxidation state of the $\text{CrO}_x/\text{SBA-1}$ system reduced with dry H_2 and CO.

Acknowledgments

This work was supported in part by the National Science Centre, Poland, under Grant DEC-2013/09/B/ST5/03419, and by PL-Grid Infrastructure. Other computing resources from Academic Computer Centre CYFRONET AGH (Grants MNiSW/IBM_BC_HS21/PK/003/2013 and MNiSW/IBM_BC_HS21/PK/037/2014) are acknowledged.

Appendix A. Supplementary material

Supplementary data associated with this article can be found, in the online version, at <http://dx.doi.org/10.1016/j.jcat.2016.04.022>.

References

- [1] B.M. Weckhuysen, I.E. Wachs, R.A. Schoonheydt, *Chem. Rev.* 96 (1996) 3327–3349.
- [2] B.M. Weckhuysen, R.A. Schoonheydt, *Catal. Today* 51 (1999) 215–221.
- [3] E. Groppo, C. Prestipino, F. Cesano, F. Bonino, S. Bordiga, C. Lamberti, P.C. Thüne, J.W. Niemantsverdriet, A. Zecchina, *J. Catal.* 230 (2005) 98–108.
- [4] E. Groppo, C. Lamberti, S. Bordiga, G. Spoto, A. Zecchina, *Chem. Rev.* 105 (2005) 115–183.
- [5] M.P. McDaniel, K.S. Collins, E.A. Benham, T.H. Cymbaluk, *Appl. Catal. A: Gen.* 335 (2008) 252–261.
- [6] V.N. Panchenko, V.A. Zakharov, E.A. Paukshtis, *Appl. Catal. A: Gen.* 313 (2006) 130–136.
- [7] C.A. Demmelmair, R.E. White, J.A. van Bokhoven, S.L. Scott, *J. Catal.* 262 (2009) 44–56.
- [8] L. Zhong, M.-Y. Lee, Z. Liu, Y.-J. Wanglee, B. Liu, S.L. Scott, *J. Catal.* 293 (2012) 1–12.
- [9] A.B. Gaspar, R.L. Martins, M. Schmal, L.C. Dieguez, *J. Mol. Catal. A: Chem.* 169 (2001) 105–112.
- [10] A.B. Gaspar, L.C. Dieguez, *Appl. Catal. A: Gen.* 227 (2002) 241–254.
- [11] A.B. Gaspar, J.L.F. Brito, L.C. Dieguez, *J. Mol. Catal. A: Chem.* 203 (2003) 251–266.
- [12] A. Hakuli, M.E. Harlin, L.B. Backman, A.O.I. Krause, *J. Catal.* 184 (1999) 349–356.
- [13] G.S. Pozan, A. Tavman, I. Boz, *Chem. Eng. J.* 143 (2008) 180–185.
- [14] J.J.H.B. Sattler, J. Ruiz-Martinez, E. Santillan-Jimenez, B.M. Weckhuysen, *Chem. Rev.* 114 (2014) 10613–10653.
- [15] N.C. Ramani, D.L. Sullivan, J.G. Ekerdt, J.-M. Jehng, I.E. Wachs, *J. Catal.* 176 (1998) 143–154.
- [16] M. Cherian, M.S. Rao, A.M. Hirt, I.E. Wachs, G. Deo, *J. Catal.* 211 (2002) 482–495.
- [17] P. Michorczyk, J. Ogonowski, K. Zeńczak, *J. Mol. Catal. A: Chem.* 349 (2011) 1–12.
- [18] P. Michorczyk, P. Pietrzik, J. Ogonowski, *Micropor. Mesopor. Mater.* 161 (2012) 56–66.
- [19] M.A. Botavina, G. Martra, Yu.A. Agafonov, N.A. Gaidai, N.V. Nekrasov, D.V. Trushin, S. Coluccia, A.L. Lapidus, *Appl. Catal. A: Gen.* 347 (2008) 126–132.
- [20] D.S. Kim, I.E. Wachs, *J. Catal.* 142 (1993) 166–171.
- [21] D.S. Kim, J.M. Tatibouet, I.E. Wachs, *J. Catal.* 136 (1992) 209–221.
- [22] L.F. Liotta, A.M. Venezia, G. Pantaleo, G. Deganello, M. Gruttaduria, R. Noto, *Catal. Today* 91–92 (2004) 231–236.
- [23] B. Liu, M. Terano, *J. Mol. Catal. A: Chem.* 172 (2001) 227–240.
- [24] B.M. Weckhuysen, L.M. De Ridder, R.A. Schoonheydt, *J. Phys. Chem.* 97 (1993) 4756–4763.
- [25] B.M. Weckhuysen, A.A. Verberckmoes, A.L. Buttens, R.A. Schoonheydt, *J. Phys. Chem.* 98 (1994) 579–584.
- [26] B.M. Weckhuysen, R.A. Schoonheydt, J.-M. Jehng, I.E. Wachs, S.J. Cho, R. Ryoo, S. Kijlstra, E. Poels, *J. Chem. Soc. Faraday Trans.* 91 (1995) 3245–3253.
- [27] P. Michorczyk, J. Ogonowski, *Chem. Commun.* 48 (2012) 7283–7285.
- [28] M.A. Vuurman, I.E. Wachs, D.J. Stufkens, A. Oskam, *J. Mol. Catal.* 80 (1993) 209–227.
- [29] E.L. Lee, I.E. Wachs, *J. Phys. Chem. C* 111 (2007) 14410–14425.
- [30] E.L. Lee, I.E. Wachs, *J. Phys. Chem. C* 112 (2008) 6487–6498.
- [31] I.E. Wachs, C.A. Roberts, *Chem. Soc. Rev.* 39 (2010) 5002–5017.
- [32] A. Chakrabarti, I.E. Wachs, *Catal. Lett.* 145 (2015) 985–994.
- [33] T.J. Dines, S. Inglis, *Phys. Chem. Chem. Phys.* 5 (2003) 1320–1328.
- [34] E. Groppo, A. Damin, F. Bonino, A. Zecchina, S. Bordiga, C. Lamberti, *Chem. Mater.* 17 (2005) 2019–2027.
- [35] A. Zecchina, E. Groppo, A. Damin, C. Prestipino, *Top. Organomet. Chem.* 16 (2005) 1–35.
- [36] C. Moisii, E.W. Deguns, A. Lita, S.D. Callahan, L.J. van de Burgt, D. Magana, A.E. Stiegman, *Chem. Mater.* 18 (2006) 3965–3975.
- [37] E. Groppo, A. Damin, C.O. Arean, A. Zecchina, *Chem. Eur. J.* 17 (2011) 11110–11114.
- [38] S. Bordiga, E. Groppo, G. Agostini, J.A. van Bokhoven, C. Lamberti, *Chem. Rev.* 113 (2013) 1736–1850.
- [39] E. Groppo, C. Lamberti, G. Spoto, S. Bordiga, G. Magnacca, A. Zecchina, *J. Catal.* 236 (2005) 233–244.
- [40] E. Groppo, C. Lamberti, S. Bordiga, G. Spoto, A. Damin, A. Zecchina, *J. Phys. Chem. B* 109 (2005) 15024–15031.
- [41] E. Groppo, C. Lamberti, F. Cesano, A. Zecchina, *Phys. Chem. Chem. Phys.* 8 (2006) 2453–2456.
- [42] D. Gianolio, E. Groppo, J.G. Vitillo, A. Damin, S. Bordiga, A. Zecchina, C. Lamberti, *Chem. Commun.* 46 (2010) 976–978.
- [43] B.M. Weckhuysen, L.M. De Ridder, P.J. Grobet, R.A. Schoonheydt, *J. Phys. Chem.* 99 (1995) 320–326.
- [44] B.M. Weckhuysen, R.A. Schoonheydt, F.E. Mabbs, D. Collison, *J. Chem. Soc. Faraday Trans.* 92 (1996) 2431–2436.
- [45] C. Brown, J. Krzystek, R. Achey, A. Lita, R. Fu, R.W. Meulenberg, M. Polinski, N. Peek, Y. Wang, L.J. van de Burgt, S. Profeta Jr., A.E. Stiegman, S.L. Scott, *ACS Catal.* 5 (2015) 5574–5583.
- [46] C.S. Kim, S.I. Woo, *J. Mol. Catal.* 73 (1992) 249–263.
- [47] Ø. Espelid, K.J. Børve, *J. Catal.* 195 (2000) 125–139.
- [48] Ø. Espelid, K.J. Børve, *J. Catal.* 206 (2002) 331–338.
- [49] Z. Liu, R. Cheng, X. He, X. Wu, B. Liu, *J. Phys. Chem. A* 116 (2012) 7538–7549.
- [50] A. Fong, Y. Yuan, S.L. Ivry, S.L. Scott, B. Peters, *ACS Catal.* 5 (2015) 3360–3374.
- [51] M.P. Conley, M.F. Delley, F. Núñez-Zarur, A. Comas-Vives, C. Copéret, *Inorg. Chem.* 54 (2015) 5065–5078.

- [52] M.F. Delley, F. Núñez-Zarur, M.P. Conley, A. Comas-Vives, G. Siddiqi, S. Norsic, V. Monteil, O.V. Safonova, C. Copéret, Proc. Natl. Acad. Sci. U.S.A. 111 (2014) 11624–11629 (Proc. Natl. Acad. Sci. USA 112 (2015) E4505).
- [53] B. Peters, S.L. Scott, A. Fong, Y. Wang, A.E. Stiegman, Proc. Natl. Acad. Sci. U.S.A. 112 (2015) E4160–E4161.
- [54] M.F. Delley, F. Núñez-Zarur, M.P. Conley, A. Comas-Vives, G. Siddiqi, S. Norsic, V. Monteil, O.V. Safonova, C. Copéret, Proc. Natl. Acad. Sci. U.S.A. 112 (2015) E4162–E4163.
- [55] A. Budnyk, A. Damin, E. Groppo, A. Zecchina, S. Bordiga, J. Catal. 324 (2015) 79–87.
- [56] C. Schumacher, J. Gonzales, P.A. Wright, N.A. Seaton, J. Phys. Chem. B 110 (2006) 319–333.
- [57] P. Ugliengo, M. Sodupe, F. Musso, I.J. Bush, R. Orlando, R. Dovesi, Adv. Mater. 20 (2008) 4579–4583.
- [58] F. Tielens, C. Gervais, J.F. Lambert, F. Mauri, D. Costa, Chem. Mater. 20 (2008) 3336–3344.
- [59] C.S. Ewing, S. Bhavsar, G. Veser, J.J. McCarthy, J.K. Johnson, Langmuir 30 (2014) 5133–5141.
- [60] H. Guesmi, F. Tielens, J. Phys. Chem. C 116 (2012) 994–1001.
- [61] J. Handzlik, R. Grybos, F. Tielens, J. Phys. Chem. C 117 (2013) 8138–8149.
- [62] B.R. Goldsmith, E.D. Sanderson, D. Bean, B. Peters, J. Chem. Phys. 138 (2013) 204105-1–204105-11.
- [63] B. Peters, S.L. Scott, Chem. Phys. 142 (2015) 104708-1–104708-5.
- [64] H. Guesmi, R. Grybos, J. Handzlik, F. Tielens, Phys. Chem. Chem. Phys. 16 (2014) 18253–18260.
- [65] M.M. Islam, D. Costa, M. Calatayud, F. Tielens, J. Phys. Chem. C 113 (2009) 10740–10746.
- [66] D. Tranca, A. Wojtaszek-Gurdak, M. Ziolek, F. Tielens, Phys. Chem. Chem. Phys. 17 (2015) 22402–22411.
- [67] A. Wojtaszek, I. Sobczak, M. Ziolek, F. Tielens, J. Phys. Chem. C 113 (2009) 13855–13859.
- [68] G. Kresse, J. Hafner, Phys. Rev. B 47 (1993) 558–561.
- [69] G. Kresse, J. Furthmüller, Comput. Mater. Sci. 6 (1996) 15–50.
- [70] G. Kresse, J. Furthmüller, Phys. Rev. B 54 (1996) 11169–11186.
- [71] Materials Studio v. 5.5, Accelrys Software Inc., San Diego, CA, 2010.
- [72] J. Handzlik, K. Kurleto, Chem. Phys. Lett. 561–562 (2013) 87–91.
- [73] J.P. Perdew, J.A. Chevary, S.H. Vosko, K.A. Jackson, M.R. Pederson, D.J. Singh, C. Fiolhais, Phys. Rev. B 46 (1992) 6671–6687.
- [74] G. Kresse, D. Joubert, Phys. Rev. B 59 (1999) 1758–1775.
- [75] J. Handzlik, J. Ogonowski, J. Phys. Chem. C 116 (2012) 5571–5584.
- [76] F. Weigend, R. Ahlrichs, Phys. Chem. Chem. Phys. 7 (2005) 3297–3305.
- [77] J. Gao, Y. Zheng, Y. Tang, J.-M. Jehng, R. Grybos, J. Handzlik, I.E. Wachs, S.G. Podkolzin, ACS Catal. 5 (2015) 3078–3092.
- [78] S. Hirata, M. Head-Gordon, Chem. Phys. Lett. 314 (1999) 291–299.
- [79] J.-D. Chai, M. Head-Gordon, Phys. Chem. Chem. Phys. 10 (2008) 6615–6620.
- [80] M.J. Frisch, G.W. Trucks, H.B. Schlegel, G.E. Scuseria, M.A. Robb, J.R. Cheeseman, G. Scalmani, V. Barone, B. Mennucci, G.A. Petersson, H. Nakatsuji, M. Caricato, X. Li, H.P. Hratchian, A.F. Izmaylov, J. Bloino, G. Zheng, J.L. Sonnenberg, M. Hada, M. Ehara, K. Toyota, R. Fukuda, J. Hasegawa, M. Ishida, T. Nakajima, Y. Honda, O. Kitao, H. Nakai, T. Vreven, J.A. Montgomery Jr., J.E. Peralta, F. Ogliaro, M. Bearpark, J.J. Heyd, E. Brothers, K.N. Kudin, V.N. Staroverov, R. Kobayashi, J. Normand, K. Raghavachari, A. Rendell, J.C. Burant, S.S. Iyengar, J. Tomasi, M. Cossi, N. Rega, J.M. Millam, M. Klene, J.E. Knox, J.B. Cross, V. Bakken, C. Adamo, J. Jaramillo, R. Gomperts, R.E. Stratmann, O. Yazev, A.J. Austin, R. Cammi, C. Pomelli, J.W. Ochterski, R.L. Martin, K. Morokuma, V.G. Zakrzewski, G.A. Voth, P. Salvador, J.J. Dannenberg, S. Dapprich, A.D. Daniels, Ö. Farkas, J.B. Foresman, J.V. Ortiz, J. Cioslowski, D.J. Fox, Gaussian 09, Revision D. 01, Gaussian Inc., Wallingford, CT, 2013.
- [81] R. Dennington, T. Keith, J. Millam, GaussView, Version 5, Semichem Inc., Shawnee Mission, KS, 2009.
- [82] P. Michorczyk, J. Ogonowski, M. Niemczyk, Appl. Catal. A: Gen. 374 (2010) 142–149.
- [83] M.W. Chase Jr., NIST-JANAF Thermochemical Tables, J. Phys. Chem. Ref. Data, fourth ed., Monograph 9, 1998, pp. 1–1951.
- [84] M.P. Conley, M.F. Delley, G. Siddiqi, G. Lapadula, S. Norsic, V. Monteil, O.V. Safonova, C. Copéret, Angew. Chem. Int. Ed. 53 (2014) 1872–1876.
- [85] J. Handzlik, P. Sautet, J. Phys. Chem. C 114 (2010) 19406–19414.
- [86] K. Hamraoui, S. Cristol, E. Payen, J.-F. Paul, J. Mol. Struct. THEOCHEM 903 (2009) 73–82.
- [87] B.M. Weckhuysen, A.A. Verberckmoes, A.R. De Baets, R.A. Schoonheydt, J. Catal. 166 (1997) 160–171.
- [88] B.M. Weckhuysen, A.A. Verberckmoes, J. Debaere, K. Ooms, I. Langhans, R.A. Schoonheydt, J. Mol. Catal. A: Chem. 151 (2000) 115–131.

Artykuł D3

Operando Molecular Spectroscopy During Ethylene Polymerization by Supported CrO_x/SiO_2 Catalysts: Active Sites, Reaction Intermediates, and Structure-Activity Relationship

Anisha Chakrabarti, **Maciej Gierada**, Jarosław Handzlik, Israel E. Wachs✉

Top. Catal. 59 (2016) 725-739

Operando Molecular Spectroscopy During Ethylene Polymerization by Supported $\text{CrO}_x/\text{SiO}_2$ Catalysts: Active Sites, Reaction Intermediates, and Structure-Activity Relationship

Anisha Chakrabarti¹ · Maciej Gierada² · Jaroslaw Handzlik² · Israel E. Wachs¹

Published online: 21 March 2016
© Springer Science+Business Media New York 2016

Abstract Time-resolved operando molecular spectroscopy was applied during ethylene polymerization by supported $\text{CrO}_x/\text{SiO}_2$ catalysts to investigate the structure-activity relationships for this important industrial catalytic reaction. A combination of spectroscopic techniques (Raman, UV–Vis, XAS, DRIFTS and TPSR) during ethylene polymerization allows for the *first time* to monitor the molecular events taking place during activation of supported $\text{CrO}_x/\text{SiO}_2$ catalysts by ethylene and establishment of the structure-activity relationships for this reaction. Based on complementary DFT computational studies, a new initiation mechanism for ethylene polymerization is proposed. During reaction, the initial surface Cr^{+6}O_x sites reduce to Cr^{+3} sites to form $\text{Cr}-(\text{CH}_2)_2\text{CH}=\text{CH}_2$ and $\text{Cr}-\text{CH}=\text{CH}_2$ reaction intermediates with the latter representing the catalytic active site.

Keywords Polymerization · Ethylene · Cr · Spectroscopy · Operando · DFT

Electronic supplementary material The online version of this article (doi:[10.1007/s11244-016-0546-6](https://doi.org/10.1007/s11244-016-0546-6)) contains supplementary material, which is available to authorized users.

✉ Israel E. Wachs
iew0@lehigh.edu

¹ Operando Molecular Spectroscopy and Catalysis Laboratory, Department of Chemical and Biomolecular Engineering, Lehigh University, Bethlehem, PA 18015, USA

² Faculty of Chemical Engineering and Technology, Cracow University of Technology, ul. Warszawska 24, 31-155 Kraków, Poland

1 Introduction

In the early 1950s, Hogan and Banks of Phillips Petroleum Company made the discovery that ethylene can be converted to polyethylene by a chromium oxide-silica-alumina catalyst [1] that was subsequently commercialized. The original catalyst system has since been fine-tuned and ethylene polymerization by silica-supported CrO_x catalysts is now responsible for ~40 to 50 % of all high-density polyethylene produced [2]. In spite of the extensive research studies that have been performed about the supported $\text{CrO}_x/\text{SiO}_2$ catalyst system over the past six decades, many of the same fundamental structural and mechanistic questions are still being debated [1–4].

There has been much confusion on studies about the initial chromia structures in the initial dehydrated catalyst, particularly due to interpretations of UV–Vis results. Many early studies concluded that the initial dehydrated catalyst consists of only surface chromia dimers (Cr_2O_7) [5–9]. Groppo et al. however, pointed out that there are many limitations to applying UV–Vis to identify the surface chromate species due to their very broad and overlapping bands [10, 11]. Additionally, the presence of Cr_2O_3 nanoparticles has also further complicated analysis [8, 9, 12]. Employing *in situ* UV–Vis and Raman spectroscopy, Lee et al. determined the molecular structures of the dehydrated CrO_x sites on SiO_2 , and showed there are two distinct surface sites—dioxo ($\text{O}=\text{)}_2\text{Cr}(-\text{O}-\text{Si})_2$ and mono-oxo $\text{O}=\text{Cr}(-\text{O}-\text{Si})_4$ [13]. However, there has been little appreciation in the literature for the presence of these two distinct isolated surface chromia sites on silica for ethylene polymerization catalysts. A recent review compared the nature of the surface chromia catalytic sites on silica in the most investigated environments (ambient, O_2 , CO , H_2 , and C_2H_4) [11] and indicated that reducing in different

environments produces different chromia oxidation states (e.g., Cr⁺² in CO and Cr⁺³ in H₂). In industry, activation of the supported CrO_x/SiO₂ catalyst is performed with the ethylene reactant, but activation studies with C₂H₄ are limited due to complications associated with the presence of multiple hydrocarbons and possibly the H₂O reaction product that can interact with the surface CrO_x sites on silica [11].

The development of modern spectroscopy methods for catalysis research has allowed for studies in the past decade to examine the initiation, propagation, and termination mechanisms of ethylene polymerization [14–23]. Despite these new studies, researchers have yet to come to a consensus concerning the structure(s) of the initial active sites and the ethylene polymerization initiation mechanism as indicated by the summary of the findings in Table 1 below [14–18, 20–25].

Most literature research studies begin the ethylene polymerization reaction with a catalyst that contains the Cr⁺² oxidation state because the supported CrO₃/SiO₂ catalysts have been activated by reduction with CO at elevated temperatures [14–18, 23]. This activation procedure, however, eliminates the induction period and is atypical for the industrial reaction conditions that employ the ethylene reactant as the reducing agent [26]. Furthermore, the CO activation also results in a lower Cr oxidation state than when activated with ethylene that forms Cr⁺³ sites [11]. Thus, it is important to be conscious of the specific activation procedure employed in a given study since the initiation mechanisms appear to be dependent on the activation procedure.

Multiple reaction intermediates have been proposed for ethylene polymerization for CO-reduced supported chromia/silica catalysts and are summarized in Table 1: vinyl Cr-hydride formed by C–H activation of ethylene [27], carbene Cr=CH₂ created by breaking the C=C bond of ethylene [27], Cr-vinyl produced by C–H activation of ethylene over an O–H bond in the catalyst to make a Cr–C bond [20–22, 24, 25], Cr=CH–CH₃ Cr-alkylidene [28–31], and Cr-metallacycles formed from the addition or two or three ethylene molecules [14–18] [21].

Only a limited number of studies investigated the structure(s) and oxidation state(s) of the surface Cr sites of supported chromia/silica catalysts activated with CO at elevated temperatures. The oxidation state of the Cr after CO activation at 350 °C was found to be Cr⁺² from in situ UV–Vis, XANES and HF-EPR spectroscopy [23]. It was concluded that the Cr⁺² site reacts with ethylene to form a organo-Cr⁺³ intermediate, but the molecular structure of the organo-Cr⁺³ complex was not discussed. It was also proposed from computational modeling and EXAFS [32] analysis that two surface Cr⁺²O_x structures (x = 3 with trigonal pyramidal coordination and x = 4 square

pyramidal coordination) are formed with the former more dominant and active than the latter.

Model organometallic catalysts have also been investigated in an effort to elucidate the initiation mechanism [20–22, 24, 25]. Using a variety of spectroscopy techniques (IR, UV–Vis, EPR, XAS) as well as DFT, it was concluded that the formation of the first Cr–C bond occurs via the heterolytic C–H activation of ethylene on a surface Cr–O bond. Poisoning with CO revealed that two different surface Cr⁺³ sites were present. The model catalysts were prepared by grafting Cr⁺³ onto silica that was partially dehydroxylated at 700 °C and an impregnated CrO_x/SiO₂ catalyst that was activated with CO was also investigated for comparison, and they were found to give rise to the same IR bands at 3692 and 3643 cm⁻¹ assigned to silanols interacting with the polymer, and at 3605 cm⁻¹ which was due to the C–H overtone of the PE chain.

The aim of the present study is to elucidate the roles of the two initial surface chromia sites on silica for the ethylene polymerization reaction through application of in situ and operando molecular spectroscopy before and during the initial stages of ethylene polymerization by supported CrO_x/SiO₂ catalysts. Using a combination of spectroscopic techniques (Raman, UV–Vis, XAS, DRIFTS and TPSR) during ethylene polymerization allows for the *first time* to monitor the molecular events taking place during activation of supported CrO_x/SiO₂ catalysts by ethylene and establishment of the structure-activity relationships for this reaction. Based on complementary DFT computational studies, a new initiation mechanism for ethylene polymerization is proposed.

2 Experimental Methods

2.1 Catalyst Synthesis

The silica support material used was amorphous SiO₂ (Cabot, Cab-O-Sil fumed silica EH-5, S.A. = 332 m²/g). Following previous methods [13], the Cab-O-Sil was found to be more easily handled by an initial water pretreatment without changing material properties. The highly dispersed silica-supported metal oxide catalyst was prepared under ambient conditions via the incipient wetness impregnation method of an aqueous solution of the chromium (III) nitrate precursor (Cr(NO₃)₃·9H₂O, Alfa Aesar, 98.5 %). The samples were then dried overnight. In a programmable furnace (Thermolyne, Model 48000), the samples were dried in a second step in air by holding the samples at 120 °C for 2 h, and the final step was calcination of the catalyst by ramping the temperature at 1 °C/min under flowing air (Airgas, Zero grade) to 500 °C and holding for 6 h. The final synthesized catalyst was then denoted as 3 %CrO₃/SiO₂.

Table 1 Summary of the proposed active sites and surface reaction intermediates reported in literature for catalysts activated with CO with the exception of studies reported in references 20–22 that employed model organometallic compounds

Research group	Experimental conditions	Band positions	Assignments	Active sites	Ref
Zielinski et al.	In vacuo IR	1446 cm ⁻¹ 1472 cm ⁻¹ 2850, 2920 cm ⁻¹	$\delta(=CH_2)$ of adsorbed ethylene $\delta(-CH_2-)$ of PE + $\delta(=CH_2)$ of adsorbed ethylene $v_s(CH_2), v_{as}(CH_2)$	Carbene Cr=CH ₂ or Cr vinyl hydride H–Cr–HC=CH ₂	[27]
Zecchina et al.	In vacuo IR	3700 cm ⁻¹ 2750 cm ⁻¹ 2855, 2926 cm ⁻¹	Silica hydroxy groups weakly interacting with polymer chains methylene Bulk PE	Alkylidene Cr=CH–CH ₃	[29, 30]
Szymura et al.	In vacuo IR	2997, 1548, 1448 cm ⁻¹ 3016 cm ⁻¹ 2855, 2927 cm ⁻¹ 2960 cm ⁻¹	$v_s(CH_2), v(C=C), \delta(CH_2)$ of ethylene π -adsorbed on Cr ⁺² sites $v(CH)$ of =CH– $v_s(CH_2), v_{as}(CH_2)$ methyl CH ₃	Alkylidene Cr=CH–CH ₃	[28]
Zecchina et al.	In situ IR ~100 K—RT	3004, 3084, 3104 cm ⁻¹ 2750 cm ⁻¹ 3650 cm ⁻¹ 2861, 2893, 2915, 2931, 2965 cm ⁻¹ 2850, 2920	Cr ⁺² ...(C_2H_4) _n π -bonded complexes ethylene molecules interacting with the silanol groups Perturbed silanol groups “anomalous bands” (metallacycle structure) $v_s(CH_2), v_{as}(CH_2)$	Metallacycle (ring structure)	[14–18]
Copéret et al.	In situ IR 70 °C	3692, 3643 3605 cm ⁻¹	Silanols interacting with PE C–H overtone of the PE chain	Cr-vinyl formed by C–H activation over O–H band	[20–22, 24, 25]
Scott et al.	In situ EXAFS Computational modeling	Curve fitting of spectra NA		Trigonal pyramidal and four-coordinate square pyramidal	[32]
Scott et al.	In situ UV-Vis C_2H_4 80 °C In situ EPR C_2H_4 80 °C In situ XANES C_2H_4 80 °C	463 and 676 nm $g = \sim 2$ T Cr^{+3}	Cr^{+3}	organo-Cr ⁺³	[23]

2.2 In Situ Raman Spectroscopy

Raman spectra of the silica-supported catalyst were taken with a high-resolution, dispersive Raman spectrometer system (Horiba-Hobin Yvon LabRam HR), which is equipped with three lasers (532, 442, and 325 nm). The laser employed in these studies was the visible laser at 442 nm (blue), generated by a He–Cd laser (Kimmon, model IK5751I-G; 441.6 nm output power of 110 mW). The lasers were focused on the samples with a confocal microscope equipped with a $\times 50$ long working distance objective (Olympus BX-30-LWD) for the visible laser. The LabRam HR spectrometer was optimized for the best spectra resolution by using a 900 grooves/mm grating (Horiba-Jobin Yvon 51093140HR); the resolution of the

grating is ~ 2 cm⁻¹. Wavenumber calibration was achieved using a silica standard, where the peak is at 520.7 cm⁻¹. Spectra shown were taken using a 200 μ m size hole. Raman vibrations from the SiO₂ support were used as internal standards to normalize signal intensities of the spectra.

Catalyst sample was loaded as loose powder (~ 20 mg) into an in situ cell (Harrick, HVC-DR2 with a CaF₂ window). The protocol for obtaining the in situ Raman spectra was as follows. The sample was initially heated at 10 °C/min from room temperature to 500 °C, held for 1 h, and then cooled to 100 °C at a rate of 10 °C/min, all under flowing 10 %O₂/Ar at 25 mL/min (Airgas, certified, 9.926 %O₂/Ar balance). After the sample cell was flushed with Ar (Airgas, UHP), 1 %C₂H₄/Ar (Praxair, certified,

1.00 %C₂H₄/Ar balance) was flowed at 25 mL/min for ~3 h, during which the catalyst was monitored through the collection of Raman spectra.

2.3 In Situ Ultra Violet–Visible (UV–Vis) Spectroscopy

UV–Vis spectra were obtained with a Varian Cary 5E UV–Vis–NIR spectrophotometer employing the integration sphere diffuse reflectance attachment (Harrick Praying Mantis Attachment, DRA-2). The catalyst sample was loaded as loose powder (~20 mg) into an in situ cell (Harrick, HVC-DR2 with a CaF₂ window). Each spectrum was taken for ~10 min from 200 to 800 nm. A MgO sample was used as a standard for the background absorbance. A Microsoft Excel Macro spreadsheet was used to calculate the edge energies, E_g.

The protocol for obtaining the in situ UV–Vis spectra was as follows. The sample was initially heated at 10 °C/min from room temperature to 500 °C, held for 1 h, and then cooled to 100 °C at a rate of 10 °C/min, all under flowing 10 %O₂/Ar at 25 mL/min (Airgas, certified, 9.926 %O₂/Ar balance). The sample cell was then flushed with Ar (Airgas, UHP) for 30 min. Dehydrated spectra were taken before and after the 30 min period. Then, 1 %C₂H₄/Ar (Praxair, certified, 1.00 %C₂H₄/Ar balance) was flowed at 25 mL/min for ~3 h, during which the catalyst was monitored through the collection of UV–Vis spectra.

2.4 In Situ X-ray Absorption Spectroscopy: X-ray Absorption Near-Edge Spectroscopy (XANES) and Extended X-ray Absorption Fine Structure (EXAFS)

Cr K-edge XAS experiments were carried out at Brookhaven National Lab at the X19A beamline. The catalyst was first pressed into a thin pellet, and then loaded into a Nashner–Adler cell to allow for in situ treatment of the catalyst.

The protocol for obtaining in situ XAS spectra was as follows. The sample was initially heated to 500 °C, held for ~30 min, and cooled to 100 °C, all under flowing 20 %O₂/He at 25 mL/min. After the cell was flushed with UHP He, the dehydrated spectrum was obtained under He at 100 °C.

2.5 In Situ and Operando Diffuse Reflectance Infrared Spectroscopy (DRIFTS)

IR spectra were obtained with a Thermo Scientific Nicolet 8700 spectrometer equipped with a Harrick Praying Mantis attachment (model DRA-2). Flow rates were monitored

with Brooks flow controllers. The catalyst sample was loaded as loose powder (~20 mg) into an in situ cell (Harrick HVC-DR2). Spectra were collected using an MCT detector (cooled with liquid N₂) with a resolution of 4 cm⁻¹ and an accumulation of 72 scans (total of ~1 min per spectrum) in the range of 600–4000 cm⁻¹. IR vibrations from the bulk of the SiO₂ support were used as internal standards to normalize signal intensities of the spectra.

The procedure to obtain the in situ and operando FTIR spectra was as follows. The sample was initially heated at 10 °C/min from room temperature to 500 °C, held for 1 h, and then cooled to 100 °C at a rate of 10 °C/min, all under flowing 10 %O₂/Ar at 25 mL/min (Airgas, certified, 9.926 %O₂/Ar balance). The sample cell was then flushed with Ar (Airgas, UHP) for 30 min. Then, 1 %C₂H₄/Ar (Praxair, certified, 1.00 %C₂H₄/Ar balance) was flowed for ~3 h at 25 mL/min. The appearance of surface species was monitored through the collection of IR spectra at this time.

2.6 C₂H₄-TPSR Spectroscopy

The temperature programmed surface reaction (TPSR) experiment was performed with an AMI-200 equipped with a Dycor ProLine Process Mass Spectrometer (MS). The catalyst sample was loaded as loose powder (~20 mg) into a U-shaped reactor packed with quartz wool.

The protocol for obtaining the C₂H₄-TPSR data was as follows. The catalyst bed was initially heated to 500 °C at 10 °C/min, held for 1 h, and then cooled to 100 °C, all under flowing 10 %O₂/Ar at 25 mL/min (Airgas, certified, 9.926 %O₂/Ar balance). The catalyst bed was then flushed with Ar (Airgas, UHP) for ~30 min. Then, under flowing 1 %C₂H₄/Ar (Praxair, certified 1.00 %C₂H₄/Ar balance) at 25 mL/min, the temperature was ramped to 800 °C at 10 °C/min. An online mass spectrometer (AMI 200) turned on before the C₂H₄ flow was started and was used to monitor gaseous products.

2.7 Computational Models and Methods

Cluster models of Cr⁺³ surface species have been developed based on the β-cristobalite structure [33, 34], often used to represent amorphous silica [32, 34–39]. They contain 9 or 7 Si atoms and are larger or comparable to other proposed models of the supported CrO_x/SiO₂ catalyst, that have been applied in theoretical studies of the ethylene polymerization mechanism [22, 31, 40–44]. The dangling bonds have been saturated with hydrogen atoms replacing the removed Si atoms. The structures have been fully relaxed to allow for the amorphous nature of the support.

The geometry optimization has been performed using the PBE0 functional [45] combined with the def2-SVP

basis set [46]. In order to confirm the potential energy minimum for each intermediate or the transition state, and to compute Gibbs energy corrections, the harmonic vibrational frequencies have been calculated. The transition state structures have been additionally verified by the IRC analysis [47, 48]. Single point energy calculations have been performed for each optimized structure using the PBE0 functional and the def2-TZVPP basis set [46]. The reaction pathways are discussed in terms of Gibbs energies estimated by adding the Gibbs energy corrections and DFT-D3(BJ) dispersion corrections [49, 50] to the PBE0/def2-TZVPP single point energies. Spin-unrestricted calculations for the Cr⁺³ species have been performed. In each case, the verified ground state is quartet.

All calculations have been done with the Gaussian 09 package [51]. For the graphic presentation of the models, the GaussView 5.0 program [52] has been used.

3 Results

3.1 In Situ XANES/EXAFS of Oxidized Supported CrO_x/SiO₂ Catalyst

The normalized in situ XANES of the reference compounds CrO₃ (consisting of poorly ordered polymeric Cr⁺⁶O₄ units due to its low temperature synthesis), Cr₂O₃ (containing linked Cr⁺³O₆ units in the bulk lattice), and dehydrated supported 3 %CrO₃/SiO₂ catalyst are presented in Fig. 1. The XANES spectrum for Cr₂O₃ does not give

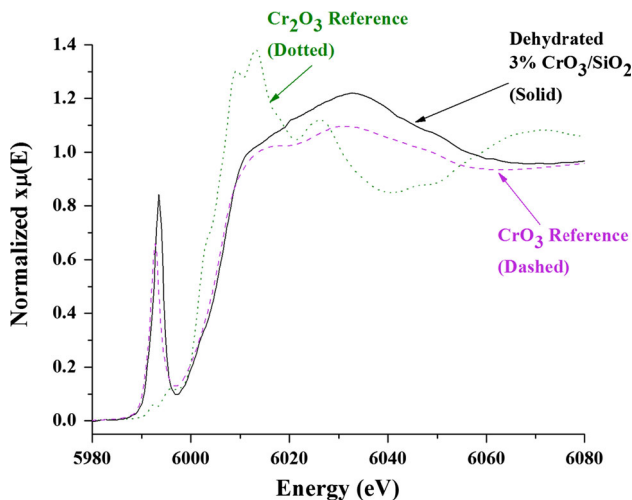


Fig. 1 In situ normalized XANES of dehydrated supported 3 %CrO₃/SiO₂. The XANES spectrum of the dehydrated catalyst was taken at 100 °C in flowing He (solid black), and the reference compounds CrO₃ (Cr⁺⁶) (dashed purple) and Cr₂O₃ (Cr⁺³) (dotted green) were collected under ambient conditions

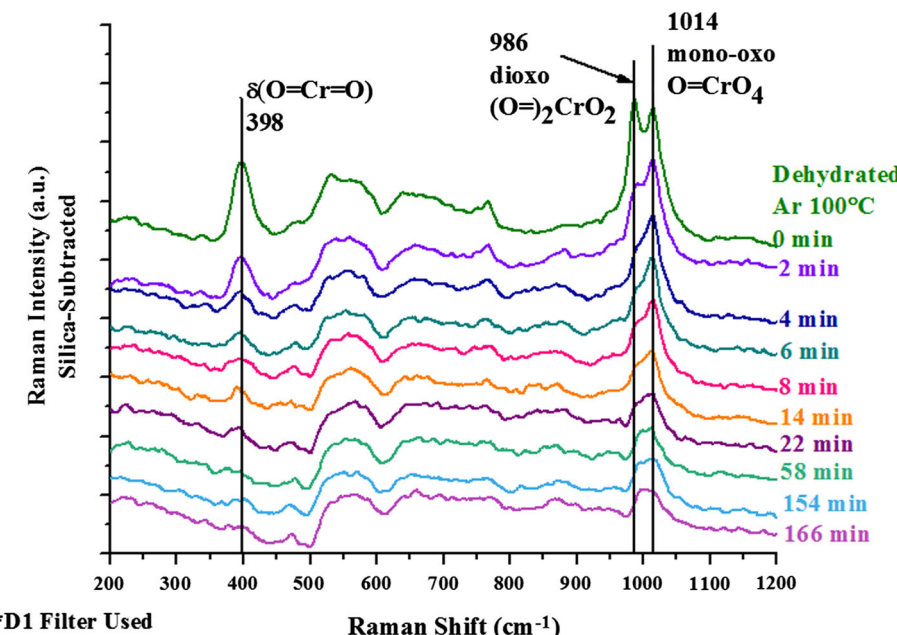
rise to a pre-edge feature because this transition is not allowed for structures with inverse symmetry such as CrO₆. [9, 12] In contrast, the XANES spectrum of CrO₃ exhibits a strong pre-edge feature (~5994 eV) because it is composed of Cr⁺⁶O₄ site that do not possess inverse symmetry [9, 12]. The similar leading edge energy from ~6000 to 6010 eV for the supported 3%CrO_x/SiO₂ catalyst and CrO₃, Cr⁺⁶ reference, indicates that the surface CrO_x sites are present as Cr⁺⁶. The strong pre-edge feature at ~5994 eV in the XANES spectrum of the dehydrated 3 %CrO₃/SiO₂ catalyst shows that CrO₄ coordinated sites are dominant in this catalyst. The slightly stronger XANES pre-edge for the supported 3 %CrO₃/SiO₂ catalyst than CrO₃ reflects the greater symmetry of the Cr⁺⁶O₄ sites in the catalyst.

The corresponding in situ k^2 -weighted, phase-uncorrected Fourier Transform (FT) EXAFS provides information about the radial distribution of the atoms surrounding Cr and is presented in Fig. S1. The phase-uncorrected EXAFS of the dehydrated catalyst shows a strong peak at ~1.2 Å from Cr=O and a weak peak at ~1.8 Å from longer Cr–O. The absence of a peak at ~3 Å for Cr–Cr [9, 12] is consistent with the presence of isolated chromia sites on the silica support.

3.2 In Situ Raman Spectroscopy During Ethylene Polymerization

The time-resolved in situ Raman spectra of the supported CrO₃/SiO₂ catalyst during ethylene polymerization are reported in Fig. 2. The spectrum of the silica support was subtracted from each Raman spectrum to emphasize observation of the chromia sites. Prior to ethylene activation and polymerization, strong bands are present at ~986 and ~1014 cm⁻¹ from the symmetric stretching vibrations of surface dioxo $\nu_s((O=)_2CrO_2)$ and mono-oxo $\nu_s(O=CrO_4)$ sites, respectively [13]. The corresponding bending mode for both surface chromia sites appears at ~398 cm⁻¹. The absence of Raman bands in the 200–300 cm⁻¹ demonstrates that bridging Cr–O–Cr bonds are not present and that the surface CrO_x sites are isolated on the silica support [13]. The Raman spectrum also indicates that crystalline Cr₂O₃ NPs (~550 cm⁻¹) [13] are not present in the initial dehydrated catalyst. During ethylene polymerization, the intensity of the Raman bands from the surface CrO_x sites decreases, with the band for the dioxo sites (~986 cm⁻¹) decreasing more rapidly than the band from the mono-oxo sites (~1014 cm⁻¹). This demonstrates that the dioxo surface chromia sites are easier to activate with ethylene than the mono-oxo surface chromia sites. The mono-oxo surface chromia sites are not fully reduced after 166 min since a residual Raman band is still present above 1000 cm⁻¹.

Fig. 2 Time-resolved in situ Raman spectra (442 nm) of supported 3 %CrO₃/SiO₂ catalyst in flowing 1 %C₂H₄/Ar at T = 100 °C



3.3 C₂H₄-TPSR Spectroscopy

C₂H₄-TPSR spectroscopy was performed to determine the relative concentrations of the initial surface dioxo and mono-oxo CrO_x sites as shown in Fig. 3. The formation of CO₂ during C₂H₄-TPSR demonstrates that ethylene is reducing the initial surface Cr⁺⁶ sites to lower chromia oxidation states. The CO₂ was the only oxidation product detected, and H₂O was not detected since the line from the reactor to the MS was not heated causing condensation. The easier reduction of the surface dioxo chromia sites than that of the surface mono-oxo chromia sites, as shown above with Raman spectroscopy, suggests that the CO₂ peak at

~280 °C corresponds to reduction of the dioxo sites, and the CO₂ peak at ~410 °C is from the mono-oxo site. The ratio of CO₂(280 °C)/CO₂(410 °C)~1.7 indicates that the surface dioxo chromia sites represent ~63 %, and the surface mono-oxo sites represent ~37 % of the total supported chromia on the silica. This demonstrates that the mono-oxo surface O=CrO₄ site is present in significant concentrations and cannot be neglected in analysis of the supported CrO₃/SiO₂ catalysts.

The CO₂/C₂H₄-TPSR spectrum also allows for calculation of the ethylene reduction kinetics of the two surface chromia sites. Application of the Redhead equation [53] yields the first-order kinetic constants of k_{dioxo} = 92 s⁻¹ and k_{mono} = 0.48 s⁻¹ for the activation of the dioxo and mono-oxo sites, respectively. The ratio of k_{dioxo}/k_{mono} is ~400 indicating that the surface dioxo chromia sites are significantly easier to activate with ethylene than the surface mono-oxo chromia sites.

3.4 In Situ UV–Vis Spectroscopy During Ethylene Polymerization

The time-resolved in situ UV–Vis spectra of the dehydrated supported 3 %CrO₃/SiO₂ catalyst are presented in Fig. 4. Multiple ligand-to-metal charge transfer (LMCT) bands are present at ~250, ~340, and ~460 nm in Fig. 4 a that are characteristic of surface Cr⁺⁶O_x sites on silica [54]. The surface CrO_x Eg value is ~2.4 eV, corresponding to isolated surface chromia sites [13]. The intensity of the Cr⁺⁶O_x LMCT bands is minimally decreased under these reaction conditions suggesting minimal reduction (see Fig. S2). The difference curves in Fig. 4b were obtained by subtracting

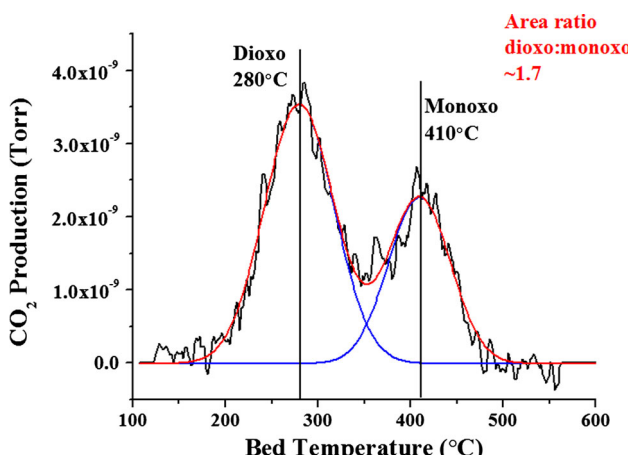


Fig. 3 The CO₂/C₂H₄-TPSR spectrum of supported 3 %CrO₃/SiO₂—the temperature was ramped from 100 to 800 °C (heating rate of 10 °C/min in flowing 1 %C₂H₄/Ar)

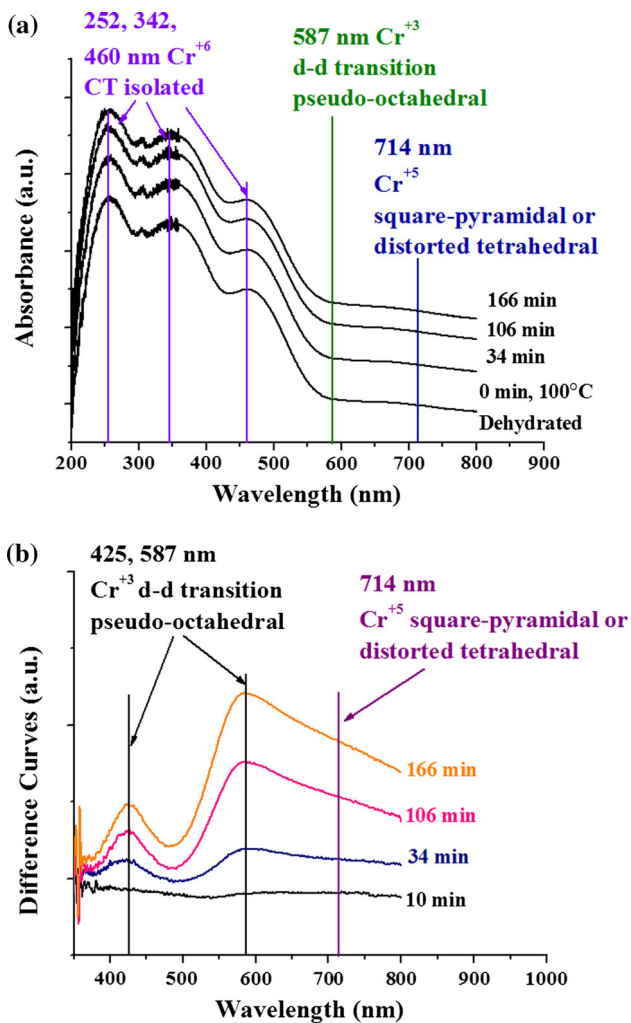


Fig. 4 Time-resolved in situ UV-Vis spectra of supported 3 %CrO₃/SiO₂ in flowing 1 %C₂H₄/Ar at T=100 °C. **a** Entire spectra showing CT region; **b** Difference curves magnified to show d-d transition bands

the UV-Vis spectrum of the initial dehydrated catalyst from each UV-Vis spectrum taken during ethylene polymerization and allowed for improved observation of the weak d-d transition bands at 425 and 587 nm that have been assigned to pseudo-octahedral Cr⁺³O₆ sites [54]. A UV-Vis d-d band from surface Cr⁺⁵ sites is not apparent, and a small amount may be also present under the broad d-d band from the surface Cr⁺³ site at 587 nm.

3.5 In Situ and Operando IR Spectroscopy During Ethylene Polymerization

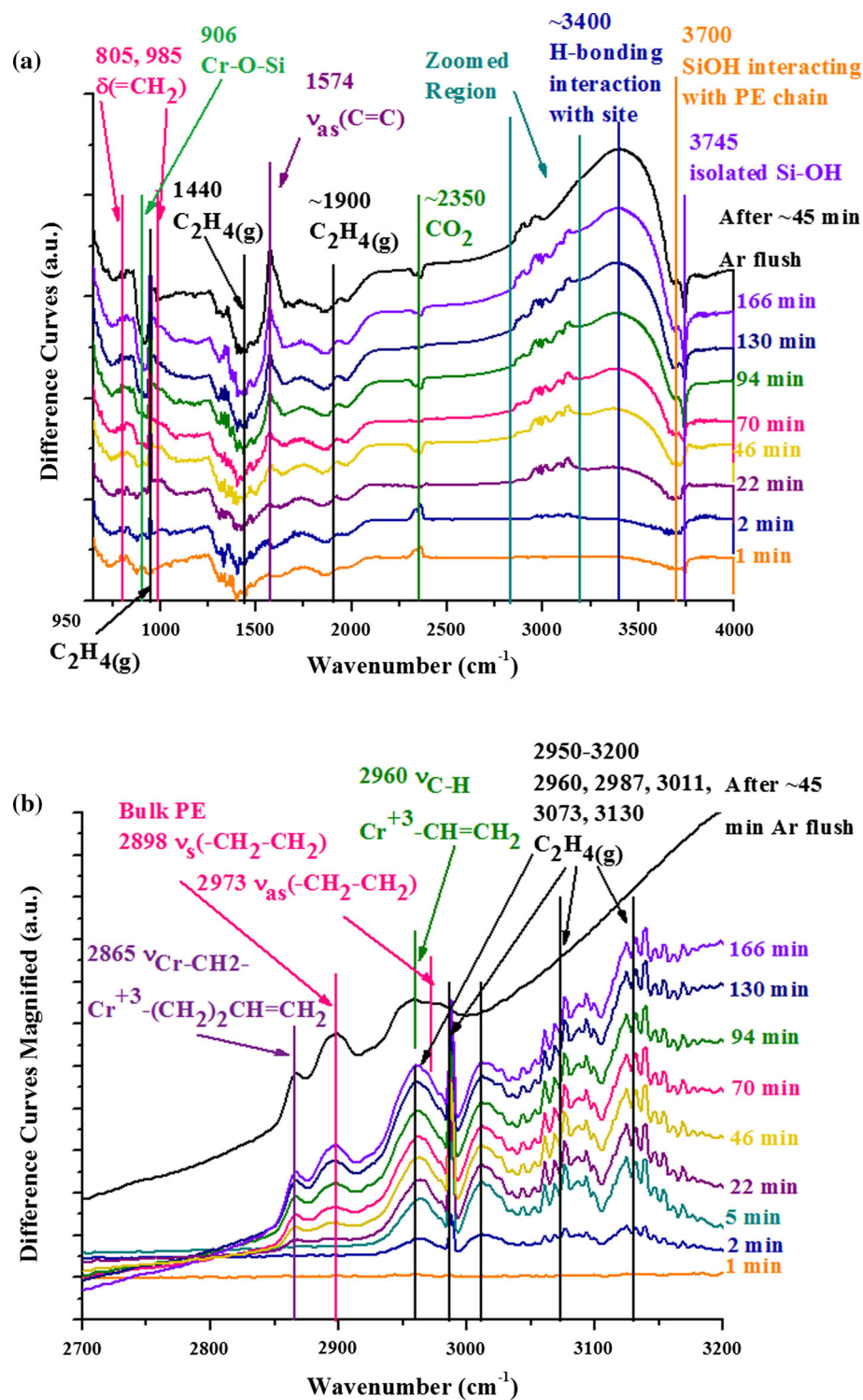
The time-resolved in situ IR spectra during ethylene polymerization are presented in Fig. 5. The IR difference spectra were obtained by subtracting the IR spectrum of the initial dehydrated catalyst from each IR spectrum taken during ethylene polymerization, after normalizing against the SiO₂

vibration at 1350 cm⁻¹. The entire range (650–4000 cm⁻¹) is presented in Fig. 5a, and the zoomed region (2700–3200 cm⁻¹) is given in Fig. 5b. Positive IR bands represent bands being formed while negative IR bands represent bands being consumed. Gas phase ethylene gives rise to bands at ~950, ~1450, ~1900, and 2950–3200 cm⁻¹ in Fig. 5a [55]. The band at 3745 cm⁻¹ for isolated silanols [15–18, 56] decreases with reaction time, and the bands at 3700 and 3400 cm⁻¹ increase with reaction time because the isolated silanols interact with the PE chain [18, 26]. In the bending region, the increasing IR bands at ~805 and 985 cm⁻¹ are assigned to $\delta(\text{=CH}_2)$ modes of PE [26, 57]. The band at 1574 cm⁻¹ also increases with reaction time and is assigned to $\nu_{\text{as}}(\text{C}=\text{C})$ of the PE chain [26, 57]. The 906 cm⁻¹ band from bridging Cr-O-Si decreases in intensity with time reflecting the interaction of the surface intermediates and PE with this bond.

The area in Fig. 5a labeled as “Zoomed Region” is replotted in Fig. 5b to allow better observation of the relevant IR bands. This region contains significant IR bands that increase with reaction time and are assigned to the surface intermediates, PE product, and also gas phase ethylene vibrations (2950–3200 cm⁻¹) [55]. The band at 2898 cm⁻¹ is assigned to the $\nu_s(-\text{CH}_2-\text{CH}_2)$ vibration of the bulk PE chain since it is expected to vibrate in the 2850–3000 cm⁻¹ range, and the band at 2865 cm⁻¹ is assigned to $\nu_s(\text{Cr}-\text{CH}_2-)$ of the PE forming close to the Cr site; it would be expected to vibrate with lower energy than the bulk PE since it is closer to the Cr center [26, 57]. The bulk PE bands in the literature are seen at ~2850 cm⁻¹ for $\nu_s(-\text{CH}_2-\text{CH}_2)$ and ~2920 cm⁻¹ for $\nu_{\text{as}}(-\text{CH}_2-\text{CH}_2)$. The ~Δ50 cm⁻¹ red shift previously reported could be related to the higher temperature used for the current measurements (room temperature vs. 100 °C) that are more aligned with industrial reaction conditions (85–150 °C) [2–4].

An Ar flush was performed at the end of the experiment to detect any additional bands that may have been obscured by the gas-phase ethylene reactant. After the Ar flush, two new IR bands are also present at 2973 cm⁻¹ from the $\nu_{\text{as}}(-\text{CH}_2-\text{CH}_2)$ of the bulk PE chain, which is ~70 cm⁻¹ higher than the $\nu_s(-\text{CH}_2-\text{CH}_2)$ of the bulk PE, a typical difference in wavenumber between asymmetric and symmetric vibrations, and a second band at 2960 cm⁻¹ that is assigned to the $\nu(\text{C}-\text{H})$ of the vinyl reaction intermediate Cr⁺³-CH=CH₂ [26, 57]. In general, the C-H stretch vibrations for a vinyl group fall in the range of 2980–3110 cm⁻¹, and specifically for σ-bonded olefinic metal compounds, the CH₂ and CH stretches fall in the 2900–3100 cm⁻¹ range. In the case of a vinyl active reaction intermediate bonded to the Cr metal center, this vibration would shift to lower wavenumbers because of the bond to the metal center and the reduced symmetry of the coordinated ethylene molecule.

Fig. 5 In situ IR spectra of supported 3 %CrO₃/SiO₂ in flowing 1 %C₂H₄/Ar at 100 °C as a function of time with an Ar flush after 3 h. **a** Difference curves of the entire spectrum (650–4000 cm⁻¹); **b** Difference curves magnified to show growing surface species and polyethylene product (2700–3200 cm⁻¹)



3.6 Kinetics of Formation of PE Product and Surface Cr⁺³ Sites

The evolution of the IR bands for formation of PE product, surface Cr⁺³–(CH₂)₂CH=CH₂, and surface Cr⁺³–CH=CH₂ sites during the ethylene polymerization reaction is plotted

as a function of reaction time in Fig. 6. The initial positive slope for IR band of the formation of the surface Cr⁺³–(CH₂)₂CH=CH₂ reveals that this is one of the initial reaction intermediates during ethylene polymerization by surface CrO_x on silica. At slightly longer times, the IR band for the surface Cr⁺³–(CH₂)₂CH=CH₂ reaction intermediates

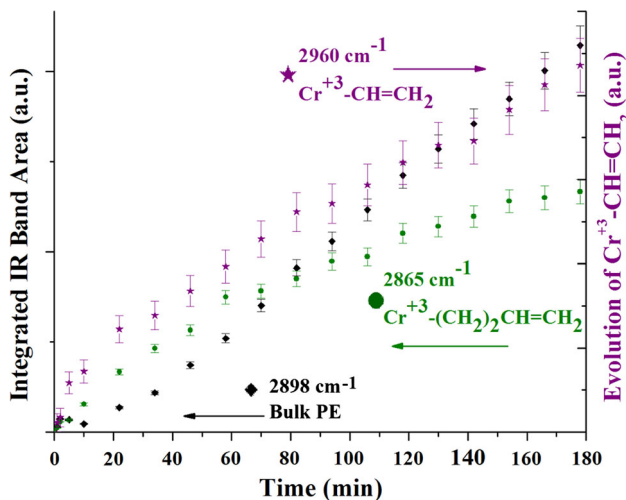


Fig. 6 Evolution of IR bands from PE product, surface $\text{Cr}^{+3}\text{-CH=CH}_2$, and surface $\text{Cr}^{+3}\text{-(CH}_2\text{)}_2\text{CH=CH}_2$ as a function of reaction time

appears to saturate. The formation of the PE product, however, initially exhibits a zero slope indicating that it is a secondary product during ethylene polymerization by supported $\text{CrO}_x/\text{SiO}_2$ and is formed by reaction of ethylene with surface reaction intermediates. At longer reaction times (>20 min), the slope for PE formation linearly increases and is greater than the decreasing slope for formation of the surface $\text{Cr}^{+3}\text{-(CH}_2\text{)}_2\text{CH=CH}_2$ reaction intermediates. The continued modest increase in the area of the IR band for the surface $\text{Cr}^{+3}\text{-(CH}_2\text{)}_2\text{CH=CH}_2$ intermediates even at 180 min suggests that not all of the surface chromia sites have been activated at this point in time under these experimental conditions. The IR band area for the surface $\text{Cr}^{+3}\text{-CH=CH}_2$ intermediate at 2960 cm^{-1} could not be directly monitored because of overlap with the IR bands of gas phase ethylene. The gas phase contribution of ethylene, however, could be determined by subtracting the IR spectrum collected after 178 min in flowing Ar with the spectrum collected at 178 min in flowing ethylene. This difference was then subtracted from the time-resolved spectra at 2960 cm^{-1} . The resulting plot for the intensity of surface $\text{Cr}^{+3}\text{-CH=CH}_2$ intermediates seems to track the evolution of the PE reaction product.

The evolution of the UV–Vis bands for the two distinct surface Cr^{+3} sites as a function of reaction time of ethylene polymerization by the supported $\text{CrO}_x/\text{SiO}_2$ catalyst is presented in Fig. 7. Both UV–Vis Cr^{+3} bands initially increase linearly with reaction time and their lines go through the origin suggesting that they are initial reaction intermediates during ethylene polymerization. At longer reaction times (>20 min), the slope for the 587 nm band remains constant while the slope of the 425 nm band decreases and appears to approach saturation. Comparison

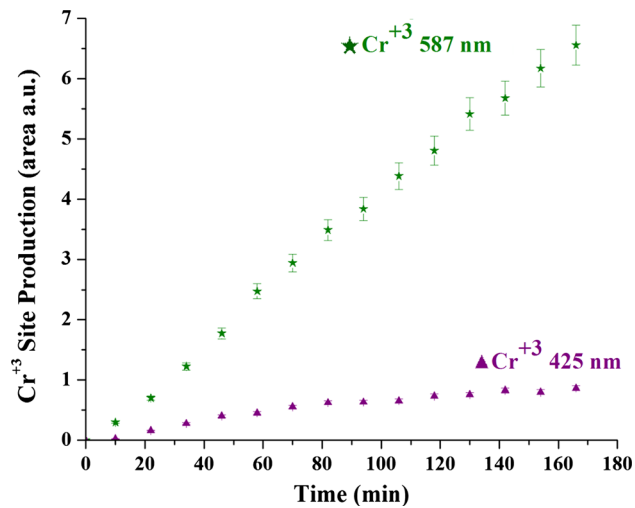


Fig. 7 The production of UV–Vis detectable surface Cr^{+3} sites as a function of ethylene polymerization reaction time by supported $\text{CrO}_x/\text{SiO}_2$ catalysts at $100\text{ }^\circ\text{C}$ (1 % $\text{C}_2\text{H}_4/\text{Ar}$)

of evolution of the UV–Vis and IR bands suggests that the UV–Vis bands at 425 and 587 nm follow the time dependent trends observed for the IR bands for the surface $\text{Cr}^{+3}\text{-(CH}_2\text{)}_2\text{CH=CH}_2$ and $\text{Cr}^{+3}\text{-CH=CH}_2$ reaction intermediates, respectively (see Fig. 8). The non-zero slopes of both UV–Vis Cr^{+3} bands at ~ 170 min indicates that not all the surface chromia sites have been activated at this initial stage of the ethylene polymerization reaction under the current reaction conditions.

3.7 Density Functional Theory (DFT)

Two proposed models of surface Cr^{+3} oxide sites are shown in Fig. 9. Proposed models of isolated surface Cr^{+3} oxide sites: (A) $(\equiv \text{SiO})_2\text{Cr}^{+3}\text{-OH}$ and (B) $(\equiv \text{SiO})_3\text{Cr}^{+3}$ Fig. 9. The surface $(\equiv \text{SiO})_3\text{Cr}^{+3}$ site (B) was recently postulated in the literature [22, 43, 44]; however, the existence of hydroxylated surface $(\equiv \text{SiO})_2\text{Cr}^{+3}\text{-OH}$ sites (A) cannot be excluded. We have calculated initiation mechanisms for ethylene polymerization, considering both of these potential surface Cr^{+3} sites on silica as the precursors of the active site complexes.

The Gibbs energy profile at $T = 373\text{ K}$ for the initiation mechanism for surface site A is presented in Fig. 10. The coordination of an ethylene molecule to chromium, resulting in π -complex A1, is predicted to be an equilibrium process ($\Delta G \approx 0\text{ kJ mol}^{-1}$), allowing both A and A1 structures to exist on the surface of the reduced catalyst in the presence of gaseous ethylene.

After A1 formation, the subsequent hydrogen transfer from the π -coordinated ethylene to the hydroxyl group can take place. It directly leads to the vinyl $\text{Cr}^{+3}\text{-CH=CH}_2$ active site (A2), which is experimentally confirmed in this

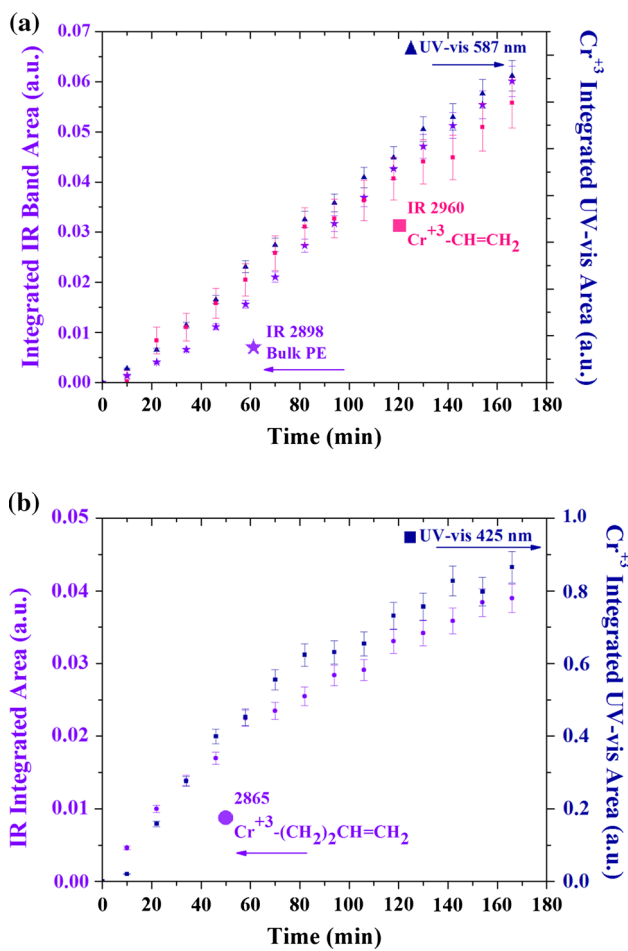


Fig. 9 Proposed models of isolated surface Cr^{+3} oxide sites: **a** $(\equiv \text{SiO})_2\text{Cr}^{+3}-\text{OH}$ and **b** $(\equiv \text{SiO})_3\text{Cr}^{+3}$

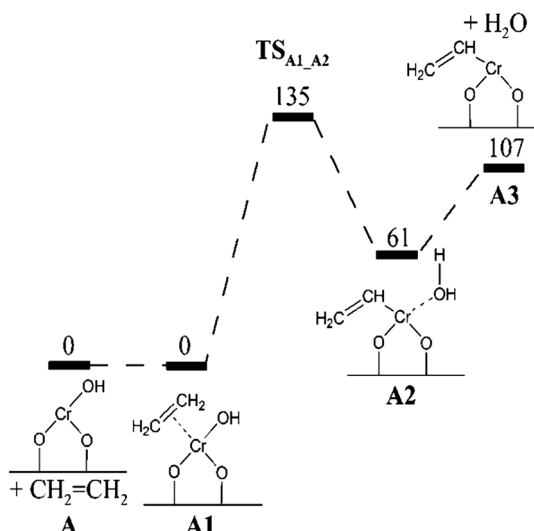
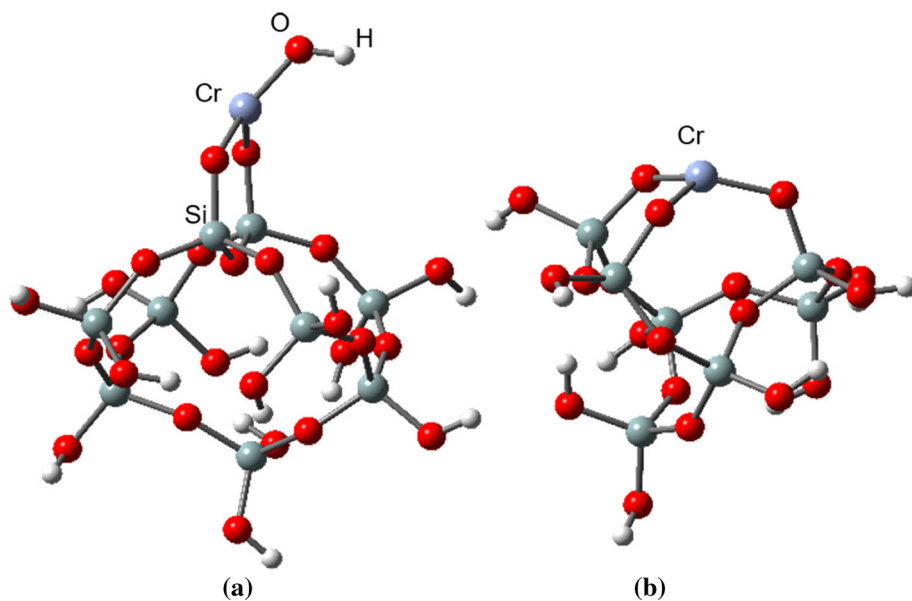


Fig. 10 The Gibbs energy profile (kJ mol^{-1}) at $T = 373 \text{ K}$ for the initiation stage of ethylene polymerization over surface $(\equiv \text{SiO})_2\text{Cr}^{+3}-\text{OH}$ site (A)

work. This elementary step is endergonic (61 kJ mol^{-1}) and proceeds with a rather high predicted activation barrier ($\Delta G = 135 \text{ kJ mol}^{-1}$), but recently calculated activation Gibbs energies for other initiation mechanisms of ethylene polymerization are comparable [22, 43, 44].

Desorption of the by-product water molecule is calculated to be a moderately endergonic process (46 kJ mol^{-1}) under water vapour pressure of 1 atm (Fig. 10). Under more dehydrated conditions, expected during the catalytic process, the desorption step will be less endergonic, for instance 32 and 10 kJ mol⁻¹ for water vapor pressures of

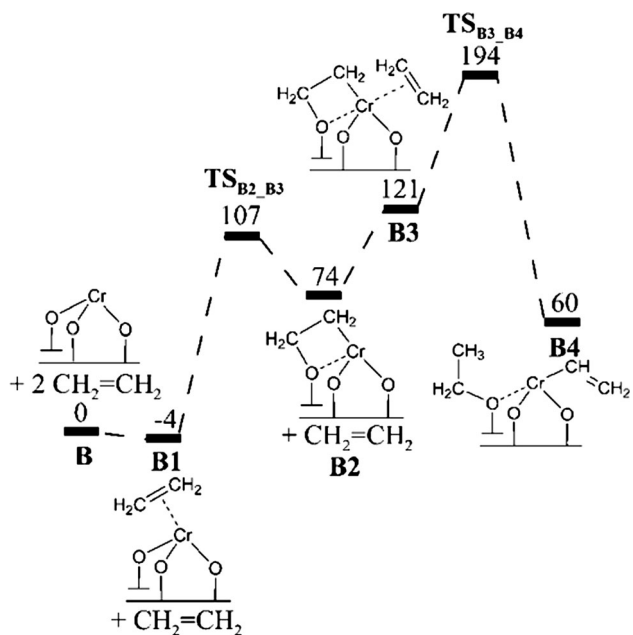


Fig. 11 The Gibbs energy profile (kJ mol^{-1}) at $T = 373 \text{ K}$ for the initiation stage of ethylene polymerization over surface $(\equiv \text{SiO}_2)_3\text{Cr}^{3+}$ site (**B**)

0.01 and 10^{-5} atm, respectively. Thus, the water molecule can easily desorb to leave a bare surface $(\equiv \text{SiO}_2)_2\text{Cr}^{3+}-\text{CH}=\text{CH}_2$ site (**A3**) for ethylene adsorption during the propagation stage.

The initiation mechanism for surface $(\equiv \text{SiO}_2)_3\text{Cr}^{3+}$ site (**B**) as the precursor of the active site (Fig. 11) is different than that calculated for the surface site **A**. The coordination of ethylene leading to the π -complex **B1** is predicted to be a slightly more exergonic process (-4 kJ mol^{-1}) than the **A** \rightarrow **A1** step (Fig. 10), but it can still be regarded as an equilibrium step. The subsequent ethylene insertion into the Cr–O σ -bond, resulting in an oxachromacycle site **B2**, is endergonic (78 kJ mol^{-1}) and proceeds with an activation barrier of 111 kJ mol^{-1} . The Cr–O distance is only moderately increased during the formation of **B2**, from 1.77 to 2.06 Å, indicating that the threefold coordination of the chromium atom to the surface is still preserved. The coordination of another ethylene molecule to **B2** is an endergonic step (47 kJ mol^{-1}), therefore the complex **B3** is thermodynamically unstable. Instead of considering the insertion of ethylene into the oxachromacycle, like Peters et al. [44] did in the case of surface Cr^{+2} sites, we propose another activation mechanism, in which the active site having a vinyl substituent is formed (**B4**) by the subsequent hydrogen transfer from π -bounded ethylene to the oxachromacycle moiety. The formation of surface ethoxy group during this transformation effectively prevents proton transfer to the growing chain and the termination step is avoided. On the other hand, the overall predicted activation

Gibbs energy for this initiation route is very high (198 kJ mol^{-1}) suggesting that such mechanism is rather unlikely.

4 Discussion

4.1 Initial Surface CrO_x Sites on SiO_2

The initial surface CrO_x sites on the SiO_2 support are fully oxidized as indicated by Cr^{+6} UV–Vis bands at 252, 342, and 460 nm [54] and XANES leading edge energy (see Fig. 1). The isolated nature of the initial surface Cr^{+6}O_x sites is demonstrated by *in situ* Raman (absence of $\sim 230 \text{ cm}^{-1}$ band for bridging Cr–O–Cr bands) [13] and UV–Vis (high E_g value of 2.4 eV). There is no experimental evidence supporting the presence of dimeric surface Cr_2O_x sites.

There are, however, two distinct isolated surface CrO_x sites on silica in the initial oxidized catalyst: dioxo $v_s((\text{O})_2\text{CrO}_2)$ (Raman band at $\sim 986 \text{ cm}^{-1}$) and mono-oxo $v_s(\text{O}=\text{CrO}_4)$ (Raman band at $\sim 1014 \text{ cm}^{-1}$) [58]. The ratio of the dioxo/mono-oxo sites is ~ 1.7 in the initial oxidized catalyst. The higher concentration of dioxo surface CrO_4 sites is also indicated by the strong XANES pre-edge of the initial oxidized catalyst.

As indicated in the introduction, most researchers do not appreciate that two distinct surface CrO_x sites are present for the initial oxidized supported $\text{CrO}_x/\text{SiO}_2$ catalyst [1, 5, 14, 18, 23, 27–30, 32, 44]. The presence of surface dioxo CrO_4 and mono-oxo CrO_5 sites can only be detected with molecular spectroscopies such as Raman spectroscopy with laser excitation of 442 nm or greater energies ($< 442 \text{ nm}$) and previously missed detection with lower energy excitations ($> 442 \text{ nm}$) [23]. Characterization methods that are not molecular in nature (e.g., XANES, EXAFS, XPS, etc.) only yield a signal that is an ensemble average of multiple sites if more than one site is present, and cannot provide molecular level information. Consequently, surface CrO_x molecular structures on silica derived from such ensemble averaging spectroscopic techniques are suspect since more than one surface chromia site is always present.

The presence of dimeric Cr_2O_x sites on SiO_2 was first proposed by Hogan based on titration of silica surface hydroxyls [5]. The Cr/OH stoichiometry, however, was assumed to be 1:2 for isolated dioxo $(\text{O})_2\text{Cr}(-\text{O}-\text{Si})_2$ sites and 1:1 for dimeric dioxo $\text{Si}-\text{O}-\text{Cr}=(\text{O})_2-\text{O}-(\text{O})_2\text{Cr}-\text{O}-\text{Si}$ sites. The titration calculations assume a molecular structure and anchoring stoichiometry without direct evidence of the actual molecular structures and anchoring sites. Thus, titration cannot provide proof of a dimeric surface Cr_2O_x site on silica.

4.2 Catalyst Activation

The surface Cr^{+6}O_x dioxo and mono-oxo sites are activated by reduction with ethylene in the present study. The *in situ* UV–Vis spectroscopic measurements indicate that only a small number of surface Cr^{+6}O_x sites become reduced (see Fig. 4) while the *in situ* Raman spectra suggest extensive reduction of the surface Cr^{+6}O_x sites (see Fig. 2). The reason for this discrepancy is that the laser may be heating the catalyst during the Raman analysis and also inducing the reduction of the surface chromia sites by ethylene. Consequently, the actual extent of reduction of the surface chromia sites is better reflected by the UV–Vis spectra that do not stimulate the reduction of the surface chromia sites. Nevertheless, the Raman results, as well as the C_2H_4 -TPSR spectra (see Fig. 3), indicate that the dioxo surface CrO_4 sites reduce much more readily than the mono-oxo surface CrO_5 sites during ethylene polymerization. The extent of reduction under the present experimental conditions (1 % C_2H_4 /Ar and 100 °C) is minimal since the UV–Vis Cr^{+6} band is barely reduced and indicates that the reaction conditions are representative of the initiation stage of the ethylene polymerization reaction.

The reduction during ethylene polymerization at 100 °C yields two distinct pseudo-octahedral surface Cr^{+3} sites exhibiting UV–Vis at bands at 425 and 587 nm (see Fig. 4b). The different time-resolved evolution trajectories of the two bands confirms that they arise from two independent Cr^{+3} sites (see Fig. 7). Given the sluggish activation of the surface mono-oxo CrO_5 sites on silica (see Fig. 3), it is most likely that these two reduced Cr^{+3} sites derive from the surface dioxo CrO_4 sites during ethylene polymerization. Supported $\text{CrO}_x/\text{SiO}_2$ catalysts activated with CO, and then exposed to ethylene exhibit UV–Vis bands at 463 and 676 nm, which are different than those found in the present study with ethylene activation (425 and 587 nm). This suggests that the activated chromia sites may not be the same when initially activated with CO or C_2H_4 [23].

Formaldehyde (HCHO) has been proposed to be the major oxygenated product during catalyst activation of supported $\text{CrO}_x/\text{SiO}_2$ catalysts with ethylene and thought to be responsible for the slow catalyst activation because it acts as a poison that bonds to the activated chromia sites and blocks ethylene coordination [2, 3, 59, 60]. The current measurements, however, did not detect HCHO as an initial reaction product and only combustion of ethylene was initially observed.

Hydrolysis of the bridging Cr–O–Si bonds has been proposed to be responsible for the agglomeration of surface chromia on silica to form crystalline Cr_2O_3 NPs during ethylene polymerization, but direct evidence was not provided [2, 61, 62]. The present *in situ* and *operando*

spectroscopy measurements during ethylene polymerization demonstrate that the bridging Cr–O–Si bond is indeed perturbed by the reaction environment (see Fig. 5 a), but this does not lead to formation of Cr_2O_3 NPs that would give a strong Raman band at $\sim 550 \text{ cm}^{-1}$ (see Fig. 2).

4.3 Surface Reaction Intermediates and Initiation Mechanism

Many initiation mechanisms have been proposed for ethylene polymerization by supported $\text{CrO}_x/\text{SiO}_2$ catalysts. Most of the studies did not even have IR bands for the proposed reaction intermediates and this has led to much speculation and ambiguity in the literature. The current *operando* IR spectroscopy measurements reveal that both surface $\text{Cr}-(\text{CH}_2)_2\text{CH}=\text{CH}_2$ and $\text{Cr}-\text{CH}=\text{CH}_2$ reaction intermediates are present during the initiation stage of the ethylene polymerization reaction (see Figs. 6, 8) with the concentration of the former saturating, and the concentration of the latter linearly increasing with reaction time.

The surface Cr-vinyl hydride ($\text{H}-\text{Cr}-\text{CH}=\text{CH}_2$) and Cr-carbene ($\text{Cr}=\text{CH}_2$) reaction intermediates [27] were proposed from *in vacuo* IR studies of a CO-reduced catalyst, but the IR bands for these intermediates were not observed, with only the bands for the PE product and adsorbed ethylene detected. The proposed initiation mechanism was based on the assumption that ethylene dissociation is the first step. It was proposed that surface $\text{Cr}=\text{CH}_2$ carbene is the most likely reaction intermediate since it was detected earlier with adsorption of propylene and 1-hexene. This study, however, does not provide any direct evidence for any reaction intermediates and was performed under vacuum.

A surface Cr-alkylidene ($\text{Cr}=\text{CH}-\text{CH}_3$) reaction intermediate [29, 30] has also been proposed from *in vacuo* IR studies of a CO-activated catalyst. In this case, a few bands were seen for the intermediate in addition to the bands for the PE product. An IR band at 3700 cm^{-1} was detected from the weak interaction of silica hydroxyl groups with polymer chains, and a second band was present at 2750 cm^{-1} that was assigned to methylene. Similar to the study proposing the Cr-vinyl hydride or Cr-carbene structures, this study was performed under vacuum. Furthermore, the IR band at 2750 cm^{-1} overlaps with many other possible structures and typically two bands are seen for a methyl group.

The surface metallacycle reaction intermediate was previously proposed from *in situ* IR studies of a CO-reduced $\text{CrO}_x/\text{SiO}_2$ [14–18]. When the temperature was increased from $\sim 100 \text{ K}$ to room temperature, bands for polyethylene were seen. Right before PE is detected, IR bands are observed at 2915 and 2893 cm^{-1} , and at short polymerization times, bands were present at 2931, 2861,

and 2965 cm^{-1} . These five “anomalous” IR bands are overshadowed by the growing polyethylene bands at increasing times, and disappear when the cell is evacuated. This reversible phenomenon led the authors to conclude it is more likely that the reaction intermediate is cyclic rather than containing a methyl group (the ethylene molecules would not need to transfer H making it more easily reversible) [14–18]. Two of the IR bands were also observed at 2865 and 2960 cm^{-1} in the present study during ethylene polymerization and after flushing with Ar, indicating that they are both from strongly bound surface reaction intermediates. In the present study, the band at 2865 cm^{-1} is assigned to the $\nu_s(\text{Cr}-\text{CH}_2-)$ of the surface $\text{Cr}^{+3}-(\text{CH}_2)_2\text{CH}=\text{CH}_2$ or the PE forming close to the Cr metal center, while the band at 2960 cm^{-1} is assigned to the $\nu(\text{C}-\text{H})$ of the surface $\text{Cr}^{+3}-\text{CH}=\text{CH}_2$ vinyl reaction intermediate.

An organo-Cr $^{+3}$ reaction intermediate has also been proposed [23] on the basis of previous EXAFS analysis and computational modeling [32]. In vacuo IR of CO adsorption on the CO-reduced catalyst showed the possibility of two Cr $^{+2}$ structures. Using EXAFS analysis and computational modeling, it was also proposed that these two surface Cr $^{+2}$ structures are likely three-coordinated with trigonal pyramidal coordination and four-coordinated with square pyramidal coordination, with the former more dominant and active than the latter. Given the EXAFS is an ensemble averaging spectroscopy, it is not possible to deconvolute and curve fit a system simultaneously containing two sites. In the study of the redox processes of ethylene polymerization, a general organo-Cr $^{+3}$ site was proposed as the active site, but the primary focus was on the oxidation state. On the basis of the earlier study, it was concluded that the two structures are likely for the CO-reduced catalyst. Concerning the structure of the active site proposed, it was only said that it would be in a higher coordination since the UV-Vis bands shifted to lower wavelengths. Although these studies included discussion of the catalyst structure, only the structure of the CO-reduced Cr $^{+2}$ catalyst was discussed at length, and it was remarked that this structure is affected by the bonding with CO. Of the different initiation mechanisms proposed in literature, the IR spectra presented in the current study provide direct evidence for a surface Cr $^{+3}-\text{CH}=\text{CH}_2$ vinyl reaction intermediate during ethylene polymerization by the supported $\text{CrO}_x/\text{SiO}_2$ catalyst. Additional insights about formation of the surface Cr-vinyl reaction intermediate come from the DFT calculations.

4.4 DFT

In the recent proposals of mechanisms for ethylene polymerization, based on computational studies [22, 42–

44], there are two main obstacles. The first one is the high activation barrier for formation of the active sites. The second one is that the termination reaction can be more preferred than the propagation steps, so shorter oligomers of ethylene would be expected instead of the polyethylene product. Copéret et al. [22, 43] and Peters et al. [44] recently studied initiation mechanisms, in which monoalkylchromium(+2) or (+3) sites are formed by the proton transfer from ethylene to the surface Si-O-Cr bridging oxygen, resulting in a surface Si(OH)Cr-vinyl site. They found that the initiation occurs with a high activation barrier, in contrast to the propagation reaction. The termination step, however, can compete with the propagation step or can even be more kinetically preferred because the proton transfer from Si(OH)Cr-alkyl site to the growing chain can occur more easily than the insertion of another ethylene molecule into the Cr-alkyl σ -bond [44, 63].

Based on the presently proposed mechanism (Fig. 10), the predicted overall Gibbs energy barrier for the initiation reaction (135 kJ mol^{-1}) is reasonable and it is in a similar range as the barriers calculated for the formation of surface Si(OH)Cr $^{+2}$ -vinyl site [44] and Si(OH)Cr $^{+3}$ -vinyl site [22, 43, 44]. It should be noted, however, that different models and computational methodologies were used in those works. After slow initiation, according to the proposed mechanism (Fig. 10), further chain growing reaction is expected to easily occur via the standard Cossee-type mechanism, i.e., insertion of ethylene into the Cr-C σ -bond [44].

What is worth noting, the advantage of our new proposal of the initiation mechanism (Fig. 10) is that the too fast termination reaction is no longer a drawback. After water desorption, there is no reactive hydrogen in the vicinity of the active Cr site, hence, the premature termination step will not take place and the formation of oligomers, instead of the polyethylene product, should not be facilitated.

4.5 Structure-Activity Relationships

Prior to ethylene polymerization, the oxidized supported $\text{CrO}_x/\text{SiO}_2$ catalyst consists of two distinct isolated surface chromia sites: dioxo CrO_4 and mono-oxo CrO_5 . The dioxo surface CrO_4 site is preferentially activated by ethylene by reducing to two surface Cr $^{+3}$ sites: $\text{Cr}-\text{CH}=\text{CH}_2$ and $\text{Cr}-(\text{CH}_2)_2\text{CH}=\text{CH}_2$ reaction intermediates. The time-resolved evolution of the surface Cr $^{+3}-\text{CH}=\text{CH}_2$ reaction intermediate appears to track the formation of the PE product, which implicates it as the active reaction intermediate. The time-resolved evolution of the surface $\text{Cr}^{+3}-(\text{CH}_2)_2\text{CH}=\text{CH}_2$ reaction intermediate seems to saturate in the early stages of the ethylene polymerization reaction possibly implicating it as a spectator species.

5 Conclusions

This is the first study to monitor the evolution of the supported $\text{CrO}_x/\text{SiO}_2$ catalyst during activation with ethylene and the ethylene polymerization reaction. The initial oxidized supported $\text{CrO}_3/\text{SiO}_2$ catalyst consists of two distinct and isolated surface chromia species in a Cr^{+6} oxidation state: the dioxo $(\text{O})_2\text{CrO}_2$ in tetrahedral coordination and the mono-oxo $\text{O}=\text{CrO}_4$ in a distorted square pyramidal coordination (dioxo:mono-oxo ratio $\sim 2:1$). The dioxo CrO_4 site is ~ 400 times easier to activate with ethylene than the mono-oxo CrO_5 site. Two distinct surface Cr^{+3} reaction intermediates were found upon activation: $\text{Cr}^{+3}-(\text{CH}_2)_2\text{CH}=\text{CH}_2$ (PE oligomers forming nearer to the metal center) and the $\text{Cr}^{+3}-\text{CH}=\text{CH}_2$. The concentration of the surface $\text{Cr}^{+3}-(\text{CH}_2)_2\text{CH}=\text{CH}_2$ structure saturates in the early stages of ethylene polymerization and may represent a spectator intermediate. The evolution of the surface $\text{Cr}^{+3}-\text{CH}=\text{CH}_2$ reaction intermediate tracks the formation of the PE product after the early induction period, which implicates it as the active reaction intermediate during ethylene polymerization by supported $\text{CrO}_x/\text{SiO}_2$ catalysts.

The computational results indicate the possibility of formation of Cr^{+3} active sites on SiO_2 for ethylene polymerization and are in agreement with the experimental findings presented in this work. Further calculations are in progress to establish the mechanism of Cr^{+6} reduction with ethylene and to better understand the overall process of ethylene polymerization over the supported $\text{CrO}_x/\text{SiO}_2$ catalyst.

Acknowledgments A. Chakrabarti and I. E. Wachs would like to acknowledge Professor A. I. Frenkel and Y. Li (Department of Physics, Yeshiva University) for assistance with the XAS collection and analysis. They acknowledge the facilities support provided at the National Synchrotron Light Source at Brookhaven National Laboratory (U. S. DOE BES, Contract No. DE-SC1112704) and the Synchrotron Catalysis Consortium (U. S. DOE BES, Grant No. DE-SC0012335). They would also like to acknowledge Dr. Christopher Ketarakis for the use of his XAS data of the reference compounds. The computational research was supported in part by PL-Grid Infrastructure. Other computing resources from Academic Computer Centre CYFRONET AGH (grants MNiSW/IBM_BC_HS21/PK/003/2013 and MNiSW/IBM_BC_HS21/PK/037/2014) are acknowledged.

References

- Hogan JP (1983) In: Leach BE (ed) Applied industrial catalysis, 1st edn. Academic Press Inc, New York
- McDaniel M (2010) In: Gates BC, Jentoft FC, Knozinger H (eds) Advances in Catalysis, 1st edn. Elsevier Inc, Amsterdam
- Groppi E, Lamberti C, Bordiga S, Spoto G, Zecchina Z (2005) Chem Rev 105:115–183
- Hogan JP, Banks RL (1958) US Patent 2825721
- Hogan JP (1970) J Polym Sci Part A 8:2637–2652
- Zecchina A, Garrone E, Ghiotti G, Morterra C, Borello E (1975) J Phys Chem 79:966–972
- Fubini B, Ghiotti G, Stradella L, Garrone E, Morterra C (1980) J Catal 66:200–213
- Weckhuysen BM, De Ridder LM, Schoonheydt RA (1993) J Phys Chem 97:4756–4763
- Weckhuysen BM, Schoonheydt RA, Jehng JM, Wachs IE, Cho SJ, Ryoo R, Klijstra S, Poels E (1995) J Chem Soc Far Trans 91:3245–3253
- Groppi E, Damin A, Bonino F, Zecchina A, Bordiga S, Lamberti C (2005) Chem Mater 17:2019–2027
- Chakrabarti A, Wachs IE (2015) Catal Lett 145:985–994
- Groppi E, Prestipino C, Cesano F, Bonino F, Bordiga S, Lamberti C, Thune PC, Niemantsverdriet JW, Zecchina A (2005) J Catal 230:98–108
- Lee EL, Wachs IE (2007) J Phys Chem C 111:14410–14425
- Bordiga S, Bertarione S, Damin A, Prestipino C, Spoto G, Lamberti C, Zecchina A (2003) J Mol Catal A 204–205:527–534
- Groppi E, Lamberti C, Bordiga S, Spoto G, Damin A, Zecchina A (2005) J Phys Chem B 109:15024–15031
- Groppi E, Lamberti C, Bordiga S, Spoto G, Zecchina A (2006) J Catal 240:172–181
- Groppi E, Estephane J, Lamberti C, Spoto G, Zecchina A (2007) Catal Today 126:228–234
- Barzan C, Groppi E, Quadrelli EA, Monteil V, Bordiga S (2012) Phys Chem Chem Phys 14:2239–2245
- McGuinness DS, Davies NW, Horne J, Ivanov I (2010) Organometallics 29:6111–6116
- Conley MP, Delley MF, Siddiqi G, Lapadula G, Norsic S, Monteil V, Safanova OV, Coperet C (2014) Angew Chem Int Ed 53:1872–1876
- Delley MF, Conley MP, Coperet C (2014) Catal Lett 144:805–808
- Delley MF, Nunez-Zarur F, Conley MP, Comas-Vives A, Siddiqi G, Norsic S, Monteil V, Safanova OV, Coperet C (2014) PNAS 111:11624–11629
- Brown C, Krzystek J, Achey R, Lita A, Fu R, Meullenberg RW, Polinski M, Peek N, Wang Y, van de Burgt LJ, Profeta JS, Stiegman AE, Scott SL (2015) ACS Catal 5:5574–5583
- Conley MP, Delley MF, Siddiqi G, Lapadula G, Norsic S, Monteil V, Safanova OV, Coperet C (2015) Angew Chem Int Ed 53:6657–6671
- Delley MF, Nunez-Zarur F, Conley MP, Comas-Vives A, Siddiqi G, Coperet C (2015) PNAS 112:E4505
- Davydov A (2003) Molecular spectroscopy of oxide catalyst surfaces. Wiley, England
- Zielinski P, Dalla Lana IG (1992) J Catal 137:368–376
- Kantcheva M, Dalla Lana IG, Szymbura JA (1995) J Catal 154:329–334
- Ghiotti G, Garrone E, Zecchina A (1988) J Mol Catal 46:61–77
- Ghiotti G, Garrone E, Coluccia S, Morterra C, Zecchina A (1979) J Chem Soc Chem Comm 22:1032–1033
- Espelid O, Borve KJ (2002) J Catal 205:366–374
- Zhong L, Lee MY, Liu Z, Wang Lee YJ, Liu B, Scott SL (2012) J Catal 293:1–12
- Wright AF, Leadbetter AJ (1975) Philos Mag 31:1391–1401
- Handzlik J (2007) J Phys Chem C 111:9337–9348
- Mortensen JJ, Parrinello M (2000) J Phys Chem B 104:2901–2907
- Solans-Monfort X, Filhol JS, Copéret C, Eisenstein O (2006) New J Chem 30:842–850
- Mian SA, Saha LC, Jang J, Wang L, Gao X, Nagase S (2010) J Phys Chem C 114:20793–20800
- Handzlik J (2009) Chem Phys Lett 469:140–144
- Handzlik J, Kurleto K (2013) Chem Phys Lett 561–562:87–91
- Espelid O, Borve KJ (2000) J Catal 195:125–139

41. Espelid O, Borve KJ (2002) *J Catal* 206:331–338
42. Zhong L, Liu Z, Cheng R, Tang S, Qiu P, He X, Terano M, Liu B (2012) *ChemCatChem* 4:872–881
43. Conley MP, Delley MF, Núñez-Zarur F, Comas-Vives A, Copéret C (2015) *Inorg Chem* 54:5065–5078
44. Fong A, Yuan Y, Ivry SL, Scott SL, Peters B (2015) *ACS Catal* 5:3360–3374
45. Adamo C, Barone VJ (1999) *J Chem Phys* 110:6158–6170
46. Weigand F, Ahlrichs R (2005) *Phys Chem Chem Phys* 7:3297–3305
47. Gonzalez C, Schlegel HB (1989) *J Chem Phys* 90:2154–2161
48. Gonzalez C, Schlegel HB (1990) *J Phys Chem* 94:5523–5527
49. Grimme S, Antony J, Ehrlich S, Krieg H (2010) *J Chem Phys* 132:154104/1–154104/19
50. Grimme S, Ehrlich S, Goerigk L (2011) *J Comput Chem* 32:1456–1465
51. Frisch MJ, Trucks GW, Schlegel HB, Scuseria GE, Robb MA, Cheeseman JR, Scalmani G, Barone V, Mennucci B, Petersson GA, Nakatsuji H, Caricato M, Li X, Hratchian HP, Izmaylov AF, Bloino J, Zheng G, Sonnenberg JL, Hada M, Ehara M, Toyota K, Fukuda R, Hasegawa J, Ishida M, Nakajima T, Honda Y, Kitao O, Nakai H, Vreven T, Montgomery Jr JA, Peralta JE, Ogliaro F, Bearpark M, Heyd JJ, Brothers E, Kudin KN, Staroverov VN, Kobayashi R, Normand J, Raghavachari K, Rendell A, Burant JC, Iyengar SS, Tomasi J, Cossi M, Rega N, Millam JM, Klene M, Knox JE, Cross JB, Bakken V, Adamo C, Jaramillo J, Gomperts R, Stratmann RE, Yazyev O, Austin AJ, Cammi R, Pomelli C, Ochterski JW, Martin RL, Morokuma K, Zakrzewski VG, Voth GA, Salvador P, Dannenberg JJ, Dapprich S, Daniels AD, Farkas O, Foresman JB, Ortiz JV, Cioslowski J, Fox DJ (2013) Gaussian 09, Revision D. 01; Gaussian, Inc.: Wallingford
52. Dennington R, Keith T, Millam JM (2009) GaussView, Version 5. Semichem Inc, Shawnee Mission
53. Redhead PA (1962) *Vacuum* 12:203–211
54. Weckhuysen BM, Wachs IE, Schoonheydt RA (1996) *Chem Commun* 96:3327–3349
55. NIST Chemistry WebBook (2011) National Institute of Standards and Technology <http://webbook.nist.gov/chemistry/>
56. Vuurman M, Wachs IE, Stukens DJ, Oskam A (1993) *J Mol Catal* 80:209–227
57. Socrates G (2001) Infrared and Raman characteristic group frequencies: tables and charts. Wiley, England
58. Handzlik J, Grybos R, Tielens F (2013) *J Phys Chem C* 117:8138–8149
59. Baker LM, Carrick WL (1968) *J Org Chem* 33:616–618
60. Liu B, Nakatani H, Terano M (2002) *J Mol Catal A* 184:387–398
61. McDaniel MP, Collins KS, Benham EA, Cymbaluk TH (2008) *Appl Catal A* 335:252–261
62. McDaniel MP, Collins KS, Benham EA, Cymbaluk TH (2008) *Appl Catal A* 335:180–186
63. Peters B, Scott SL, Fong A, Wang Y, Stiegman AE (2015) *PNAS* 112:E4160–E4161

Artykuł D4

Active sites formation and their transformations during ethylene polymerization by the Phillips CrO_x/SiO₂ catalyst

Maciej Gierada, Jarosław Handzlik✉

J. Catal. 352 (2017) 314-328



Active sites formation and their transformations during ethylene polymerization by the Phillips CrO_x/SiO₂ catalyst

Maciej Gierada, Jarosław Handzlik *

Faculty of Chemical Engineering and Technology, Cracow University of Technology, ul. Warszawska 24, 31-155 Kraków, Poland



ARTICLE INFO

Article history:

Received 25 February 2017

Revised 5 May 2017

Accepted 30 May 2017

Keywords:

Phillips catalyst

Chromium oxide

Silica

Surface

Ethylene polymerization

Active site

Defect site

Mechanism

DFT

Cluster model

ABSTRACT

The nature of the active sites and the mechanism of ethylene polymerization over the Phillips CrO_x/SiO₂ catalyst are still under debate. In this work, a number of potential initiation, propagation and termination mechanisms for ethylene polymerization are investigated using density functional theory and cluster models. Cr(II), Cr(III), Cr(III)-OH and Cr(V) oxide species are considered as the active site precursors. It is predicted that the oxachromacycle ring expansion mechanism is more probable than the routes involving $\equiv\text{Si}(\text{OH})\text{Cr}(\text{II})\text{-vinyl}$ or $\equiv\text{Si}(\text{OH})\text{Cr}(\text{III})\text{-vinyl}$ sites. We also show that the hydroxylated Cr(III)-OH species, further transforming into the active Cr(III) vinyl sites, can be effective for ethylene polymerization. Additionally, we propose that defect sites in the amorphous silica framework can play a role in low-temperature transformation of the Cr(II) species into the active Cr(III) sites. A potential polymerization mechanism involving minor Cr(V) oxide species is also calculated.

© 2017 Elsevier Inc. All rights reserved.

1. Introduction

The famous Phillips (CrO_x/SiO₂) catalyst is one of the simplest and the oldest heterogeneous catalysts for ethylene polymerization [1–9]. This system was discovered in 1950s [10], however, it is still successfully employed for the industrial production of polyethylene. It is estimated that 40–50% of the total world production of high-density polyethylene (HDPE) is directly associated with this catalyst [11]. Its widespread use is mainly related to the fact that, in contrast to other catalysts exhibiting activity in ethylene polymerization (Ziegler-Natta and metallocene catalysts), no cocatalyst is necessary in this case. Sole ethylene leads to the formation of the active sites [1,4–9], which makes this system unique among all known olefin polymerization catalysts. Moreover, the synthesis procedure for the CrO_x/SiO₂ catalyst is simple [1,5,8].

A lot of effort has been made to determine the structure of the active sites and their precursors, as well as the mechanism of ethylene polymerization. Despite many years of extensive investigations, these issues still remain unsolved. Experimental and theoretical studies showed that Cr(VI) dominates on the surface after catalyst preparation [1,2,5,12–23]. The major surface forms

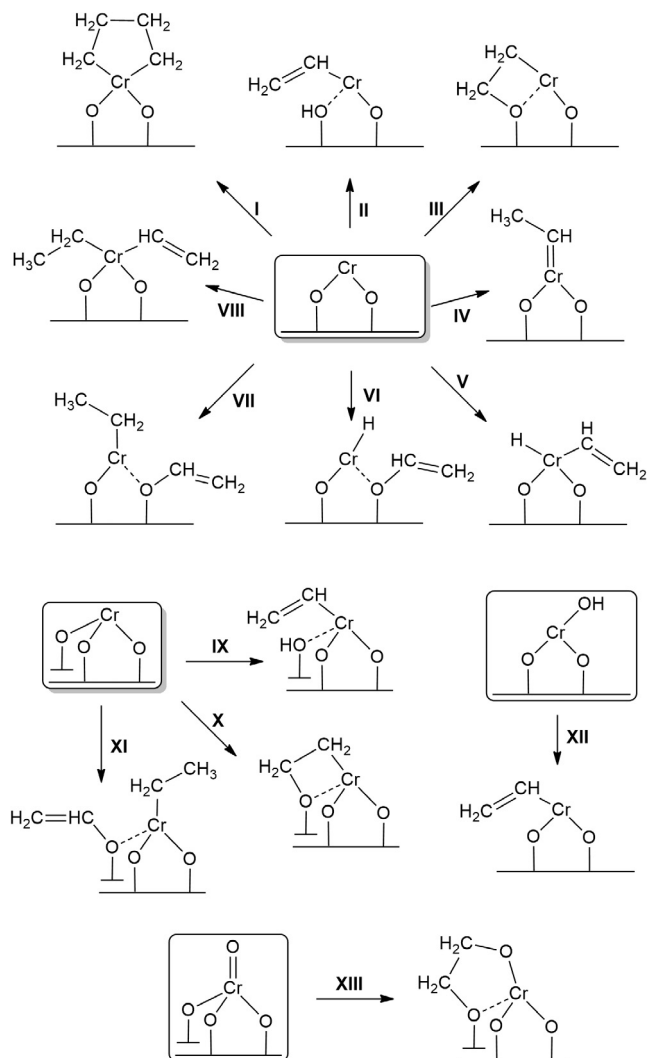
at low Cr loadings are monomeric dioxo Cr(VI) species [1,5,14,18–23], but monomeric monooxo Cr(VI) sites [18–22,24] cannot be excluded as well. Dimeric and polymeric surface Cr(VI) species have also been proposed, mainly based on the UV-Vis DRS studies [1,3,5,17,25–28], however, recent computational results predict that they are less stable than the monomeric dioxo Cr(VI) species [29].

Based on the observation that the pre-reduction of the CrO_x/SiO₂ system by CO produces the catalyst which polymerizes ethylene very effectively, it is believed that reduced Cr oxide species are directly involved into the polymerization mechanism. Because Cr (II) oxide species dominates on the catalyst surface after reduction [1,2,5,9,11,25,30], such form was frequently postulated to be the precursor of the active sites [5,31–43]. Starting from Cr(II), several initiation species were proposed, leading to acyclic [5,33,37,38,42,43] (in some cases carbene [5,32–37,42]) or cyclic [5,31,37,39–42] active species, usually organo-Cr(IV) intermediates. Initiation mechanisms involving dimeric Cr(II) species [39] or two monomeric Cr sites [33] were also considered, but such propositions seem to be less likely, taking into account the reported high activity of the system with very low Cr loadings [44].

A great attention has been paid to oxidative coupling of two ethylene molecules over the Cr(II) species resulting in chromacyclopentane formation (metallacycle mechanism, Scheme 1 I). This

* Corresponding author.

E-mail address: jhandz@pk.edu.pl (J. Handzlik).



Scheme 1. Potential pathways for the active site formation from Cr(II), Cr(III), Cr(III)-OH and Cr(V) oxide precursors upon the contact with ethylene, considered in this work.

mechanism has been proposed mainly based on experimental studies [5,31,40]. Theoretical works showed [37,41,42] that activation barrier calculated for chromacyclopentane formation is low, however, the rate of insertion of another ethylene molecule to the metallacycle ring (propagation step) is very slow. For the chromacycloheptane site, the termination route is more likely than propagation [37,42], thus, such a mechanism can explain the formation of side-products, such as 1-hexene, observed experimentally [45,46].

Fong et al. [42] performed DFT calculations for initiation mechanism involving active $\equiv\text{Si}(\text{OH})\text{Cr}(\text{II})$ -vinyl species, which are formed through proton transfer from ethylene to silanolate oxygen of Cr(II) species (Scheme 1 II). However, the calculated initiation barrier is rather high (152 kJ mol^{-1}) and the predicted rate of termination is faster than that for propagation. Hence, again such a mechanism does not seem to be suitable for ethylene polymerization and the authors conclude that only short oligomers would be formed. They also examined another possible mechanism preserving Cr⁺² oxidation state, which can proceed through oxachromacycle ring expansion (Scheme 1 III), but the predicted activation barrier for the initiation stage is too high (165 kJ mol^{-1}) [42].

After reduction of the $\text{CrO}_x/\text{SiO}_2$ system, Cr(III) oxide species are also detected, especially when H_2 or C_2H_4 is used as the reducing

agent [1,2,5,12–14,16,17,20,29,47–50]. Hence, it has been postulated that Cr(III) might be the precursor of the polymerization active sites [51–59]. Copéret and co-workers [53–56] proposed that $\equiv\text{Si}(\text{OH})\text{Cr}(\text{III})$ -vinyl species can be generated through the proton transfer from ethylene to silanolate oxygen of the Cr(III) oxide precursor (Scheme 1 IX). Comparative cluster studies [42] suggest that this C–H bond activation mechanism is more likely for the Cr(II) site than for the Cr(III) one. Moreover, in the latter case the termination is also predicted to be faster than the propagation [42], in contrast to the conclusions of Copéret and co-workers, also based on cluster calculations [55,56]. Very recently, it was shown that termination by proton-transfer step becomes more demanding when more realistic periodic model of the amorphous silica surface is used, hence, for Cr(III) sites termination is most probably not competing with propagation [59]. It was postulated that both C–H bond activation and oxachromacycle formation (Scheme 1 X), the latter being proposed and investigated by us using cluster models [58], can give the active Cr(III) sites for ethylene polymerization and the reaction rate depends on their strain [59]. As we previously suggested, Cr(III) might also exist on the silica surface as hydroxylated species [29,58]. Such a structure can be formed as a result of hydration of threefold-bounded Cr (III) (*vide infra*) or reduction and further hydration of dimeric Cr oxide species [29]. Its further transformation into catalytically active sites is also possible [58] (Scheme 1 XII).

Recently, Fong et al. [43] postulated two step initiation route, according to Kissin and Brandolini mechanism [60]. In the first step, oxidative addition of ethylene to Cr(II) gives organo-Cr(IV) species. Then, Cr–C bond homolysis leads to the formation of the active Cr(III) vinyl site and alkyl radical. Although the calculated overall activation barriers are high, the computational results suggest that they might be reduced provided that the silica surface is flexible enough to enable subsequent decoordination and coordination of siloxanes to the Cr site during the first and second initiation step, respectively. However, the limitations of the cluster models used did not allow to prove this proposal directly.

So far, none of the proposed overall mechanisms of ethylene polymerization over the Phillips catalyst is widely accepted [5,42,43]. The main problem is to explain the initiation stage giving the active species with alkyl/vinyl or another organic ligand attached to Cr [37–39,41–43,56,59]. Hence, the structure of the active sites, as well as the route leading to their formation is still not unambiguously determined and contradictory conclusions are sometimes drawn [42,43,55,56,59,61,62].

Experimental studies also do not provide clear information about the polymerization mechanism, although recent works [53–58] indicate Cr(III) species as the active sites. The biggest challenge in the experimental investigations of the mechanism is the high rate of polymerization, especially when experiments are done with the pre-reduced catalysts [5,11]. Additionally, it is estimated that only a fraction (approximately 10%) of Cr sites are active [5,11], so, the catalyst characterization with spectroscopic techniques can concern mainly inactive Cr species.

In this work, we theoretically investigate reactivity of the $\text{CrO}_x/\text{SiO}_2$ catalyst toward ethylene using DFT approach. We propose several new initiation mechanisms (Scheme 1 VI, VII, X–XIII) leading to the active site formation and compare them with the recently published ones (Scheme 1 I–V, VIII–X). In our studies various structures and oxidation states of the Cr sites are taken into account, in particular, Cr(II), Cr(III), Cr(III)-OH and Cr(V) oxide species (Fig. 1) are considered as the potential precursors of the active sites. A number of polymerization mechanisms involving Cr(II) have been proposed in the literature and we confront them with our results. We show that the initial stages of the chromacycle and oxachromacycle ring expansion mechanisms [42] can be kinetically undistinguishable (Scheme 1 I, III). Moreover, for the latter, a

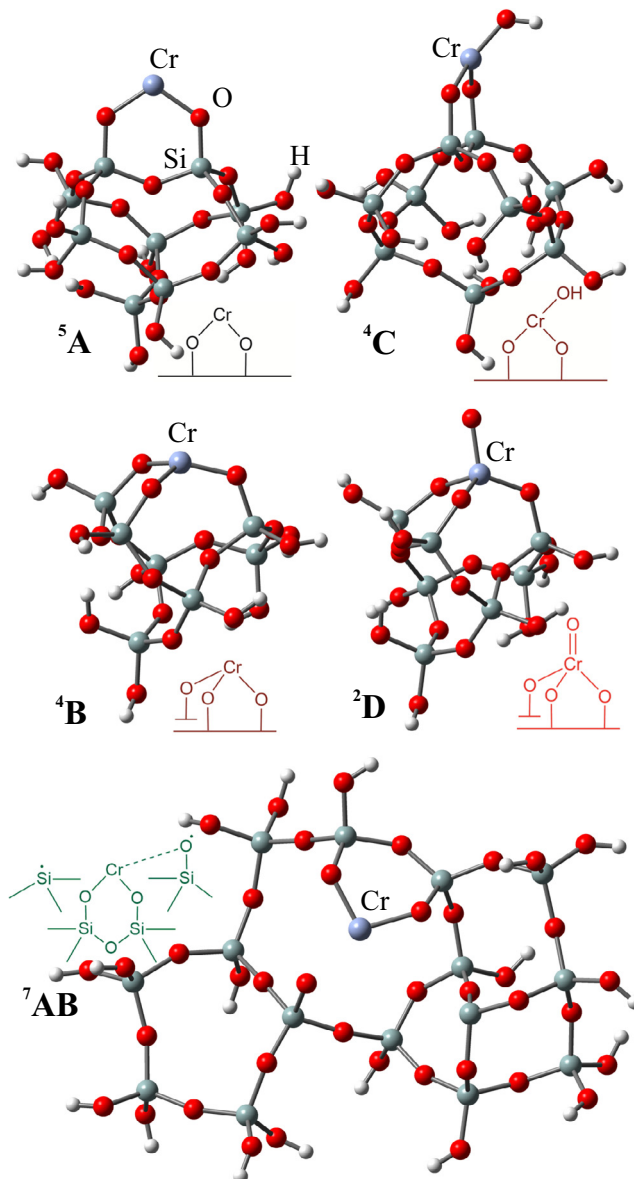


Fig. 1. Optimized models of isolated surface Cr sites: ⁵A – Cr(II), ⁴B – Cr(III), ⁴C – Cr(III)-OH, ²D – Cr(V) and ⁷AB – Cr(II) with adjacent surface defects.

high rate of termination is avoided, in contrast to the chromacycle mechanism, making the oxachromacycle ring expansion mechanism an interesting alternative.

As Cr(III) recently starts to gain more and more attention in ethylene polymerization, new possible initiation routes involving Cr(III) species are considered. We show that the active sites can be formed from hydroxylated Cr(III) oxide precursors (**Scheme 1 XII**), being the alternative for dehydroxylated Cr(III) species (**Scheme 1 IX, X**). Additionally, we propose that defects in amorphous silica framework, likely to be formed during the high-temperature pretreatment of the catalyst, can play a role in low-temperature transformation of the Cr(II) species into the active Cr(III) sites. Alongside the postulated role of the increased surface strain [59], caused by dehydroxylation [63], this may also explain why higher calcination temperature enhances the catalytic activity [5,11].

Finally, Cr(V) is theoretically examined for the first time as the potential active species and a new mechanism of ethylene polymerization involving these sites is proposed (**Scheme 1 XIII**).

Although the idea that Cr(V) might be active in ethylene polymerization [64,65] has mostly been abandoned many years ago [11,66], EPR [17,48,49,66–68] and XPS [69] data indicate that Cr(V) oxide species exist in minority on the surface of the CrO_x/SiO₂ catalyst.

2. Computational models and methods

The reaction pathways of ethylene polymerization over the CrO_x/SiO₂ catalyst were studied using cluster models of the Cr surface sites. The structures considered as the precursors of the active sites are shown in **Fig. 1**. Most of the models (⁵A, ⁴B, ⁴C, ²D) were developed based on the initial β-cristobalite structure [70] which was frequently used to represent amorphous silica [9,24,58,71–76]. These models, containing 9 or 7 Si atoms, are larger or comparable to other proposed cluster models of the supported CrO_x/SiO₂ catalyst that were applied in theoretical studies of the ethylene polymerization mechanism [37–39,41–43,55,56]. To describe interactions between surface defects and Cr oxide species we also built a bigger model of Cr surface sites, containing 15 Si atoms (⁷AB). This cluster model was obtained from previously reported periodic models of Cr surface species [18,29], based on the amorphous silica framework developed by Tielens et al. [77]. In all cases, the dangling bonds were saturated with hydrogen atoms replacing the removed Si atoms. The structure ⁷AB and the derivate models were optimized with the fixed positions of the terminating H atoms, whereas all other systems were fully relaxed to allow for their amorphization.

The hybrid PBE0 functional [78], which was shown to perform well in predicting geometries of transition metal complexes [79–81], was applied for geometry optimization of the systems, in combination with the def2-SVP basis set [82]. Confirmations of the local minimum for each intermediate and the 1st order saddle point for each transition state structure were done by calculating harmonic vibrational frequencies. This also enables determination of Gibbs energy corrections for $T = 373$ K (typical temperature of the process) and $p = 1$ atm (if not stated otherwise). The IRC method [83,84] was used to verify the transition states. Single point energy calculations were performed for each optimized structure employing the PBE0 functional and the def2-TZVPP basis set. [82] The reaction pathways are discussed in terms of Gibbs energies (if not stated otherwise) estimated by adding the Gibbs energy corrections and DFT-D3(BJ) dispersion corrections [85,86] to the PBE0/def2-TZVPP single point energies. Test calculations for selected reactions energies, barrier heights and vibrational frequencies have been also performed to validate the methods and models on the basis of theoretical and experimental reference data (**Tables S1–S5, Supplementary Data**).

To localize the minimum energy crossing points (MECP), the methodology developed by Harvey and co-workers [87] was applied. Spin-unrestricted calculations were performed for the open-shell systems. The ground state for each structure was verified. High-spin ground states for the reduced Cr species have always been found.

All the calculations were done with the Gaussian 09 set of programs [88]. For the graphic presentation of the structures, the GaussView 5.0 software [89] was applied.

3. Results and discussion

3.1. Nomenclature

The nomenclature of the models used in this work is based on the capital letters, numbers and numbers in superscript. Capital letters (**A, B, C, D**) are used to distinguish between different series

of the models, representing Cr(II), Cr(III), Cr(III)—OH and Cr(V) oxide species on silica, respectively (Fig. 1), and their derivatives. **AB** describes series of models reproducing surface defects. Numbers (**1–35**) after each letter denote different species belonging to each series. The superscript numeral (^{2–5}) before the letter shows the spin state. In the figures presenting Gibbs energy profiles for the mechanisms studied red, blue, brown, black and green colours are used to distinguish between doublet, triplet, quartet, quintet and septet reaction pathways, respectively.

3.2. Ethylene transformations over Cr(II)/SiO₂ species (⁵**A**)

3.2.1. Ethylene coordination to Cr(II) species

Ethylene coordination to the bare Cr(II) oxide species (⁵**A**) results in complex ⁵**A1** (Fig. 2). The Gibbs energy of its formation is -22 kJ mol^{-1} , close to the corresponding value calculated by Fong et al. (-24 kJ mol^{-1}) [42] using different methodologies. The C=C double bond in ⁵**A1** is hardly elongated (1.35 Å), compared to free ethylene (1.33 Å). The average Cr—C distance (2.40 Å) is in a perfect agreement with the reported result of Fong et al. [42], whereas a slightly higher value was predicted by Zhong et al. (2.47 Å) [41]. Coordination of the second ethylene molecule to ⁵**A1** is thermodynamically preferred ($\Delta G = -12 \text{ kJ mol}^{-1}$), but less exergonic than binding the first C₂H₄ ligand. Not surprisingly, the average Cr—C distance in bis(ethylene) complex ⁵**A2** is slightly longer (2.46 Å) than that in ⁵**A1**. These findings are consistent with other computational studies [38,42]. Stationary points of complexes with three and more ethylene molecules coordinated to Cr(II) have not been located. For all Cr(II) structures the ground state is quintet.

3.2.2. Initiation reactions involving one ethylene coordinated to Cr(II)

Starting from Cr(II) mono(ethylene) site (⁵**A1**), various initiation reactions can be considered. Among different initiation mechanisms proposed in the literature [5,31–43,90–92], only few [90–

92] address polymerization activity to Cr hydride species. It was proposed [91,92] that surface silanols play a role in the formation of such species. As highly dehydroxylated catalysts show very good catalytic properties, participating of silanols in active sites formation is doubtful, making these mechanisms rather unlikely. On the other hand, Cr—H bond might be formed during reaction of Cr(II) and ethylene (Fig. 3). Proton transfer from π -bonded ethylene (⁵**A1**) can lead to Cr hydride (⁵**A9**) and a surface —OCH=CH₂ ligand. A short distance between oxygen atom of that ligand and Cr (2.11 Å) indicates that a strong interaction is still present. However, the ⁵**A9** formation is endergonic (178 kJ mol⁻¹) with an extremely high activation barrier (301 kJ mol⁻¹), so, this mechanism is very unlikely.

Another possible proton transfer reaction can generate Cr(IV) vinyl hydride site ³**A10** (Fig. 3). Such a structure was proposed in the literature as an active intermediate [33,37]. Geometry analysis suggests that the carbon atoms in ³**A1** have sp³ hybridization rather than sp², in contrast to the π -complex ⁵**A1**. An average Cr—C bond distance in ³**A1** is much shorter (2.03 Å) than in ⁵**A1** (2.40 Å), whereas the carbon–carbon bond in the former is longer (1.42 Å) than in the latter (1.35 Å). The predicted Gibbs energy barrier for the proton transfer leading to ³**A10** is very high (192 kJ mol⁻¹, relatively to ⁵**A**, or, 214 kJ mol⁻¹, relatively to ⁵**A1**).

Much lower activation barrier (143 kJ mol⁻¹) is predicted when proton transfer from ethylene generates $\equiv\text{Si(OH)}\text{Cr(II)}$ -vinyl site ⁵**A3** (Fig. 2). The oxygen atom of the OH moiety is 3-fold bonded and the Cr—(OH)(—Si≡) distance in ⁵**A3** is longer (2.05 Å) than the average Cr—O bond length in ⁵**A1** (1.84 Å).

The Green-Rooney mechanism, involving chromium carbene intermediate species, was also considered for the initiation stage of ethylene polymerization [5,32–37,42]. The calculated high activation Gibbs energy for a direct 1,2-hydrogen transfer resulting in Cr(IV) ethyldiene site ³**A11** (Fig. 3) is in a general agreement with other computational results [42]. Moreover, it can be expected that chain growth steps over ³**A11** also proceed with very high barriers [37,42].

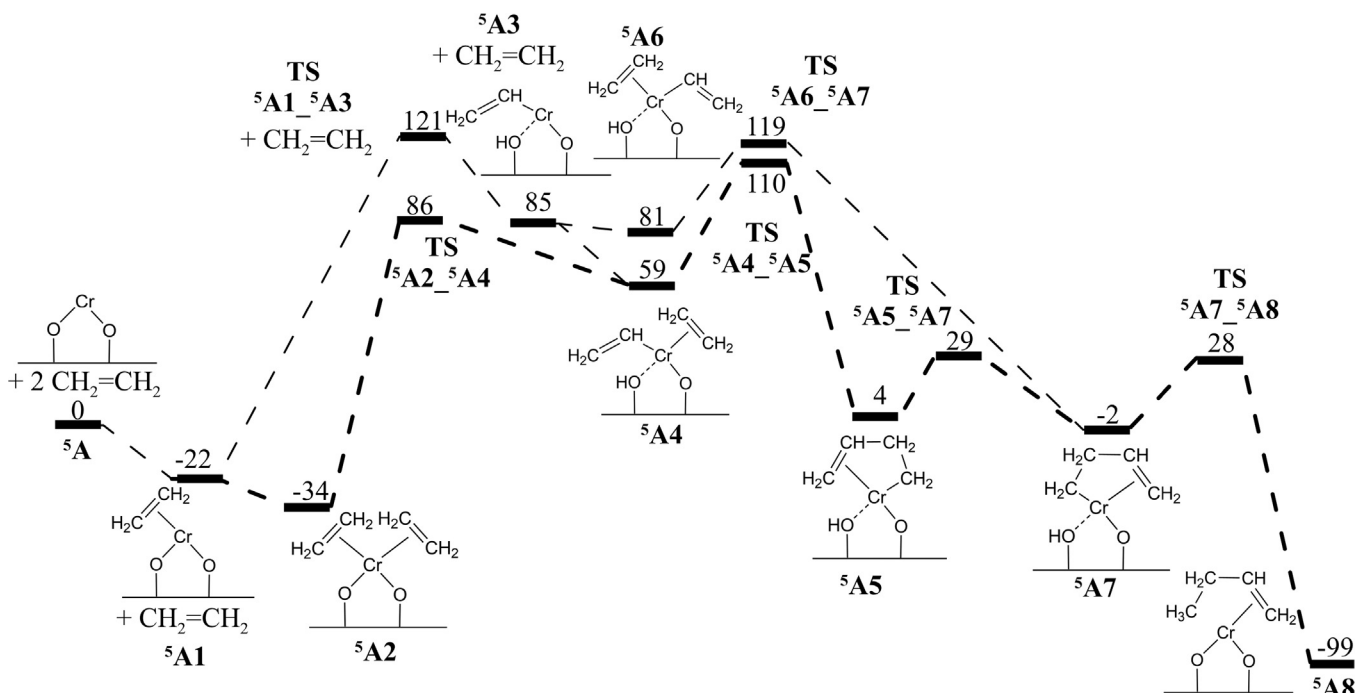


Fig. 2. Gibbs energy profile (kJ mol⁻¹) at T = 373 K for the initiation mechanism involving $\equiv\text{Si(OH)}\text{Cr(II)}$ -vinyl site formation through a proton transfer from Cr(II) mono and bis(ethylene) species (quintet reaction pathway). The thicker line represents the preferred route.

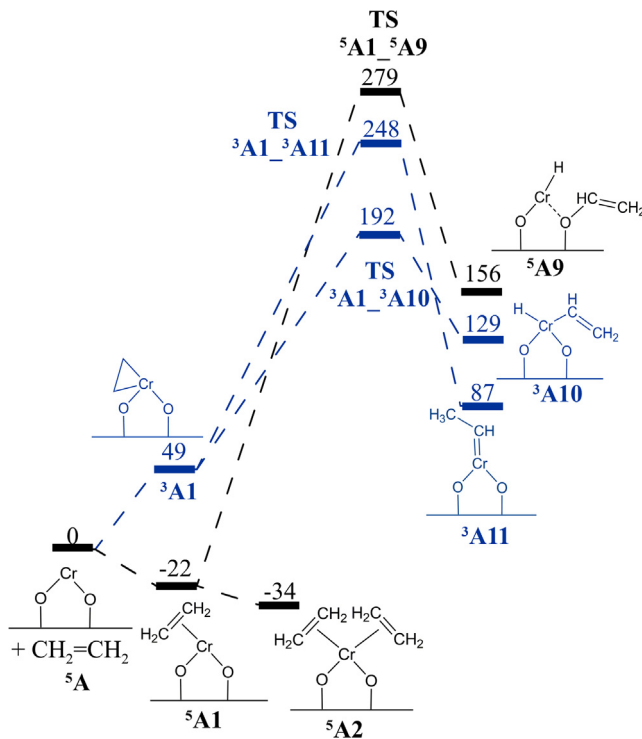


Fig. 3. Gibbs energy profiles (kJ mol^{-1}) at $T = 373 \text{ K}$ for Cr(II) hydride, Cr(IV) vinyl hydride and Cr(IV) carbene site formation. Blue and black colours denote triplet and quintet reaction pathways, respectively.

Thus, it can be concluded that the rearrangement of a single ethylene molecule over Cr(II) site would most probably result in formation of $\equiv\text{Si(OH)}\text{Cr(II)}$ -vinyl intermediate (⁵A3).

3.2.3. Mechanism involving $\equiv\text{Si(OH)}\text{Cr(II)}$ -vinyl site

The $\equiv\text{Si(OH)}\text{Cr(II)}$ -vinyl site ⁵A3 can easily bind another ethylene molecule (Fig. 2). Depending on which side of ⁵A3 ethylene is coordinated, two structures are possible, ⁵A4 and ⁵A6, the former being more thermodynamically favorable. Additionally, ⁵A4 can be also directly formed from Cr(II) bis(ethylene) complex ⁵A2. This ethylene-assisted proton transfer is kinetically preferred over the corresponding transformation of the mono(ethylene) complex ⁵A1, by 35 kJ mol⁻¹. Further chain growth reaction over ⁵A4 and ⁵A6 can proceed via the Cossee-Arlman-type mechanism suited for the Ziegler-Natta catalysts [93], resulting in ⁵A5 and ⁵A7, respectively. Although in the first case the activation barrier for the insertion step is higher (51 kJ mol⁻¹) than in the second case (38 kJ mol⁻¹), the formation of ⁵A5 is kinetically more favored. The calculated overall activation Gibbs energy for this route is 144 kJ mol⁻¹, relatively to the bis(ethylene) complex ⁵A2. On the other hand, TS ⁵A1-⁵A3 is the rate-determining transition state for the pathway leading to ⁵A7, hence, the overall activation barrier here is 155 kJ mol⁻¹, relatively to the lowest-energy structure ⁵A2. However, ⁵A5 can easily convert to ⁵A7 (Fig. 2) and for the latter the termination step leading to 1-butene coordinated to Cr(II) (⁵A8) is geometrically facilitated. Similar results were reported by Fong et al. [42], who considered an analog of ⁵A7.

For the potential further chain propagation reaction over ⁵A5, butenyl ligand must first decoordinate to generate labile vacant site able to coordinate next ethylene (Fig. 4). Again, two different complexes are possible (⁵A12, ⁵A17), depending on which side ⁵A5 is attacked by ethylene. The kinetically and thermodynamically preferred pathway for ethylene insertion into Cr-C bond starts from the slightly less stable conformer (⁵A12), probably

because of a lower steric hindrance, compared to ⁵A17. However, the predicted propagation barrier (74 kJ mol⁻¹) is much higher than that for the competitive termination pathway ($\Delta G^\ddagger = 30 \text{ kJ mol}^{-1}$, Fig. 2). Moreover, in the insertion product ⁵A13, the distance between the hydrogen of the OH moiety and the C_α atom is short (2.51 Å), so, again the termination proton transfer reaction can easily occur. A stable Cr(II) species with π-bonded 1-hexene (⁵A16) is formed with the activation barrier of 27 kJ mol⁻¹. The alternative chain propagation step, resulting in Cr(II) species ⁵A15, requires over three times higher Gibbs activation energy (91 kJ mol⁻¹). Thus, the mechanism involving $\equiv\text{Si(OH)}\text{Cr(II)}$ -vinyl sites cannot account for ethylene polymerization, but might explain formation of low-molecular-weight products, in agreement with the conclusions of Fong et al. [42].

3.2.4. Chromacycle ring expansion mechanism over Cr(II) species

Ethylene activation over Cr(II) oxide species can also involve formation of metallacycle sites and their further transformations. In the past, Ghiotti et al. [32] proposed the chromacycle mechanism, based on the lack of evidence indicating the presence of $-\text{CH}=\text{CH}_2$ or $-\text{CH}_3$ groups during the first stages of ethylene polymerization. In this proposal it is assumed that two ethylene molecules react with bare Cr(II) oxide species to give chromacyclopentane. Further propagation reaction occurs through ethylene insertion into Cr-C σ-bond, hence, both ends of growing polymer chain are attached to the Cr(II) site. Groppo et al. [40] assigned observed IR bands during ethylene polymerization to $-\text{CH}_2-$ groups of chromacycle Cr species, which might support the chromacycle mechanism. On the other hand, theoretical studies [37,38,41,42,94] did not confirm this initiation route. Although the predicted activation barrier of chromacyclopentane formation is quite low, the ring expansion is expected to occur very slowly. Therefore, we consider the chromacycle mechanism only for comparison with the oxachromacycle mechanism and other initiation routes investigated in this work.

The chromacycle expansion mechanism (Fig. 5) requires two ethylene molecules in the coordination sphere of Cr(II). The ground states for the Cr(II) bis(ethylene) and Cr(IV) chromacyclopentane complexes are quintet (⁵A2) and triplet (³A19), respectively. Hence, the spin change occurs during the oxidative coupling step. The localized MECP (Fig. S1, Supplementary Data) indicates that the relevant transition state is TS ³A2-³A19, so the predicted activation Gibbs energy for the formation of the chromacyclopentane species is 83 kJ mol⁻¹, in agreement with the recent studies of Fong et al. (81 kJ mol⁻¹) [43]. Higher activation barriers for this transformation were reported by Zhong et al. ($\Delta G^\ddagger = 99 \text{ kJ mol}^{-1}$) [41] and Ma et al. ($\Delta G^\ddagger = 93 \text{ kJ mol}^{-1}$) [94]. Our calculated activation energy for the triplet pathway (14 kJ mol⁻¹, Fig. S1) is close to the corresponding value determined by Espelid and Børve (9 kJ mol⁻¹) [37].

Further ethylene insertion into Cr-C σ-bond in ³A19, leading to chromacycloheptane species ³A21, is an exergonic process (-69 kJ mol^{-1}) with the activation Gibbs energy of 129 kJ mol⁻¹ ($\Delta E^\ddagger = 61 \text{ kJ mol}^{-1}$). Higher activation barriers for the ring expansion step were reported by Espelid and Børve ($\Delta E^\ddagger = 119 \text{ kJ mol}^{-1}$) [37], Fong et al. ($\Delta G^\ddagger = 149 \text{ kJ mol}^{-1}$, $\Delta E^\ddagger = 89 \text{ kJ mol}^{-1}$) [42] and Zhong et al. ($\Delta G^\ddagger = 138 \text{ kJ mol}^{-1}$) [41]. Interestingly, the Cr-C σ-bond distance in TS ³A20-³A21 increases from 1.99 Å to 2.31 Å to join incoming ethylene, which is in accordance with the results of Espelid and Børve (2.21 Å) [37], but in contrary with the much longer distances reported by Zhong et al. (3.01 Å) [41] and Fong et al. (2.99 Å) [42]. Nevertheless, there is no clear relationship between this bond distance and the predicted value of the activation energy. It should be noted that different methodologies were used in those works. Another possible transformation of the chromacyclopentane species ³A19 might be an intramolecular β-H transfer (Fig. S2, Supplementary Data) resulting in formation of

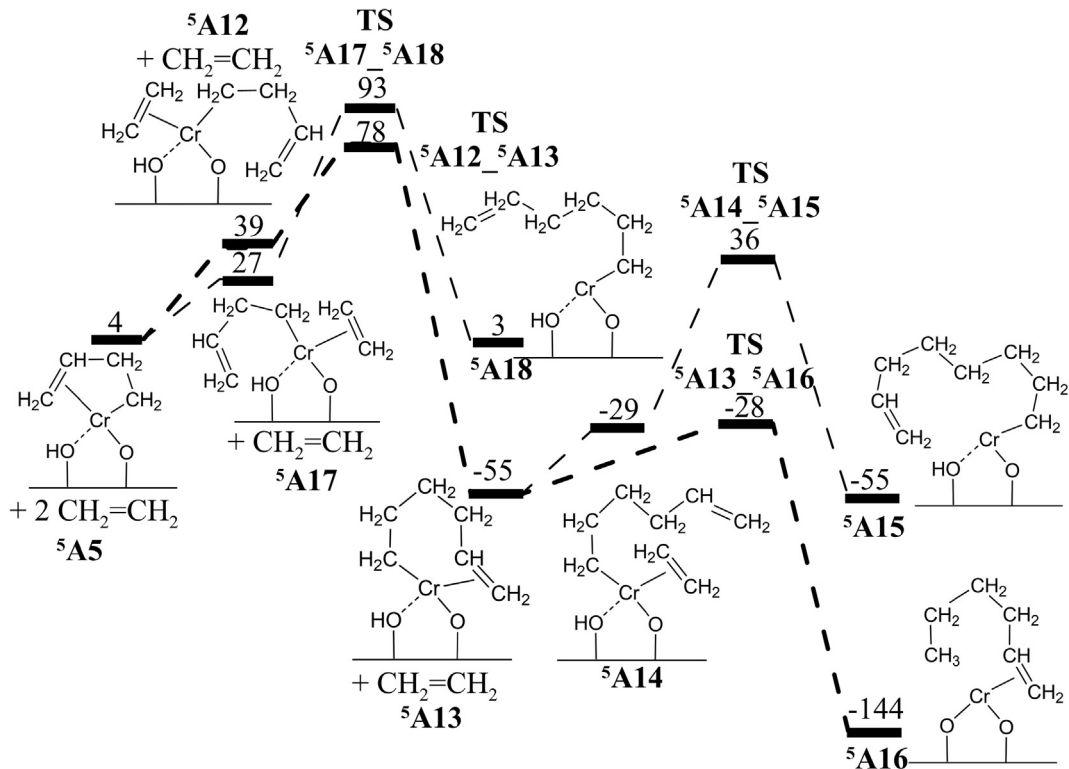


Fig. 4. Gibbs energy profile (kJ mol⁻¹) at T = 373 K for the propagation and termination routes following the initiation stage involving $\equiv\text{Si}(\text{OH})\text{Cr}(\text{II})\text{-vinyl}$ site formation through a proton transfer from Cr(II) bis(ethylene) species (quintet reaction pathway). The energy values are related to ${}^5\text{A}$. The thicker line represents the preferred route.

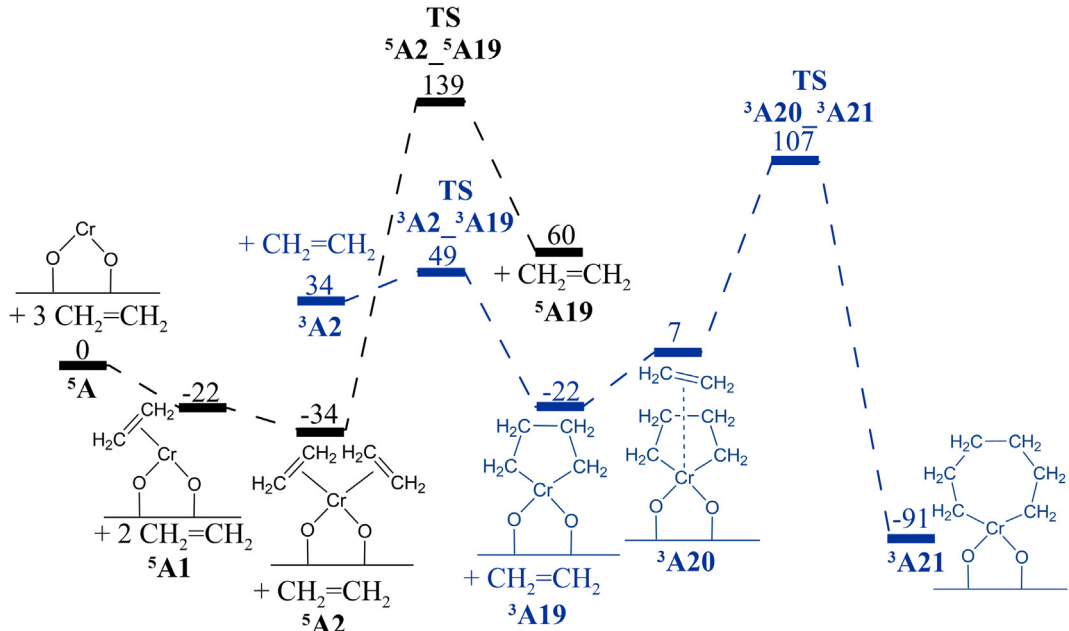


Fig. 5. Gibbs energy profile (kJ mol⁻¹) at T = 373 K for the chromacycle ring expansion mechanism starting from Cr(II) oxide species. Blue and black colours denote triplet and quintet reaction pathways, respectively.

1-butene as a by-product. However, the activation barrier calculated for this step is very high ($\Delta G^\ddagger = 186 \text{ kJ mol}^{-1}$, $\Delta E^\ddagger = 190 \text{ kJ mol}^{-1}$), in agreement with Espelid and Børve ($\Delta E^\ddagger = 192 \text{ kJ mol}^{-1}$) [37].

The predicted overall activation Gibbs energy for the formation of the chromacycloheptane ${}^3\text{A}21$ (Fig. 5) is not very high

(141 kJ mol⁻¹, relatively to ${}^5\text{A}2$), but the termination reaction giving 1-hexene was shown to be kinetically preferred over the next insertion step [37,42]. On this basis, it was claimed that the chromacycle mechanism might explain side-products formation, i.e., experimentally observed 1-hexene [45,46]. An alternative mechanism leading to low-molecular-weight products might involve

$\equiv\text{Si}(\text{OH})\text{Cr}(\text{II})$ -vinyl site transformation (Figs. 2 and 4), as the predicted overall activation barriers are similar for both routes ($\Delta G^\ddagger = 141$ and 144 kJ mol^{-1} , respectively).

3.2.5. Oxachromacycle ring expansion mechanism over Cr(II) species

The mechanism involving oxachromacycle intermediates, derived from the studies of homogenous polymerization catalysts [95], was recently computationally investigated by Fong et al. [42]. They predicted a preclusive, very low effective rate constant for this initiation route, but suggested that the results may depend on the local geometry of the support. In the present work we examine this mechanism with larger cluster models, considering more propagation steps and including the termination paths.

Ethylene insertion into the Cr—O bond can start from the Cr(II) mono(ethylene) complex (⁵A1), resulting in the endergonic formation of oxachromacyclobutane species ⁵A22 with the Gibbs activation energy of 99 kJ mol^{-1} (Fig. 6). The Cr—O($-\text{CH}_2-$) $(-\text{Si}\equiv)$ bond in ⁵A22 is preserved, but elongated (1.99 Å), compared to the average Cr—O bond distance in ⁵A1 (1.84 Å). Another ethylene molecule can be easily bounded to ⁵A22 giving ⁵A23. However, the latter species can be also obtained with the lower activation barrier (83 kJ mol^{-1}) directly from the Cr(II) bis(ethylene) complex ⁵A2. It can be noted that the same Gibbs activation energy is calculated for the chromacyclopentane (³A19) formation (Fig. 5).

Ethylene insertion into the Cr—C bond in ⁵A23 gives oxachromacyclohexane species ⁵A24 with the activation barrier of 78 kJ mol^{-1} (Fig. 6). This value is much lower than that predicted for ethylene insertion into the chromacyclopentane ³A19 (129 kJ mol^{-1}) and significantly lower than the corresponding value reported by Fong et al. (97 kJ mol^{-1}) [42]. Interestingly, the overall activation Gibbs energies for the formation of chromacycloheptane ³A21 and oxachromacyclohexane ⁵A24 are almost identical (141 and 140 kJ mol^{-1} , respectively), suggesting that these pathways might compete each other. However, the oxachromacycle mechanism does not require spin-crossing, in contrast to the chromacycle one.

An alternative route starting from ⁵A23 is a formation of Cr vinyl site together with a surface ethoxy ligand (⁵A29), as a result of proton transfer from ethylene (Fig. 6). Additionally, the ethoxy group would effectively prevent proton transfer to the growing chain, hence, the termination step would be avoided. However,

the overall Gibbs activation energy for this transformation is very high (188 kJ mol^{-1} , relatively to ⁵A2), excluding such a mechanism.

Insertion of the next ethylene molecule to ⁵A24 (Fig. 6) proceeds with the quite low activation barrier (52 kJ mol^{-1}) and gives oxachromacyclooctane species ⁵A26. Alternatively, 1-butene might be eliminated from ⁵A24 via β -H transfer, leading finally to Cr(II) alkene complex ⁵A28. However, the Gibbs activation energy for this transformation is very high (198 kJ mol^{-1} , relatively to ⁵A24). Ethylene insertion to ⁵A26 also proceeds with lower activation barrier than the corresponding intramolecular β -H transfer (48 and 86 kJ mol^{-1} , respectively – see Fig. S3, Supplementary Data). It is worth noting that the predicted rate of the propagation increases with increasing size of the oxachromacycle moiety, corresponding to the less strained ring. On the other hand, the termination reaction is also faster for the larger ring, but still slower than the propagation step.

Therefore, the oxachromacycle ring expansion mechanism cannot be excluded as the potential route for ethylene polymerization or higher oligomeric products formation, taking into account that the calculated overall activation barrier for the initial stage is not very high (140 kJ mol^{-1}) and the following propagation steps are much faster and clearly kinetically preferred over the termination paths.

3.2.6. Formation of $\equiv\text{Si}(\text{O}-\text{CHCH}_2)\text{Cr}(\text{II})$ -alkyl and Cr(IV)(-alkyl)(-vinyl) sites

Cr-alkyl species were frequently proposed as the active sites for ethylene polymerization [5,11,37,38,42,43,90,94], however, the mechanism of their formation is not determined. Such a pathway might start from the Cr(II) bis(ethylene) complex (⁵A2) and proceed through the unstable radical-type intermediate ⁵A33, finally leading to $\equiv\text{Si}(\text{O}-\text{CHCH}_2)\text{Cr}(\text{II})$ -alkyl site ⁵A34 (Fig. 7). The Cr—O($-\text{CHCH}_2$) $(-\text{Si}\equiv)$ distance in ⁵A34 (2.11 Å) is moderately elongated compared to the average Cr—O bond length in ⁵A (1.81 Å), indicating that 2-fold coordination of the chromium atom to the surface is still preserved. However, the predicted activation barrier for the endergonic reaction is extremely high (316 kJ mol^{-1}), precluding this route. Even higher barrier (325 kJ mol^{-1}) is computed, if ⁵A34 is formed directly from ⁵A2 (Fig. S4, Supplementary Data).

Cr(II) bis(ethylene) complex ⁵A2 can also undergo transformation to Cr(IV)(-alkyl)(-vinyl) species ³A35, as a result of hydrogen

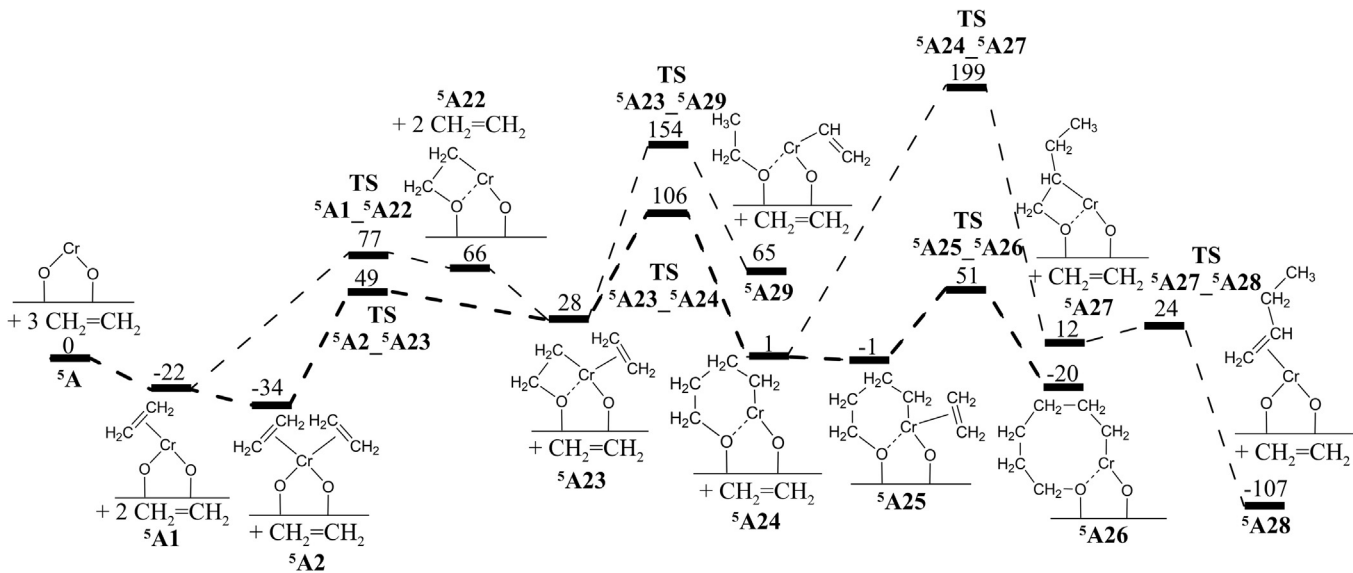


Fig. 6. Gibbs energy profile (kJ mol^{-1}) at $T = 373 \text{ K}$ for the oxachromacycle ring expansion mechanism over Cr(II) oxide species (quintet reaction pathway). The thicker line represents the preferred route.

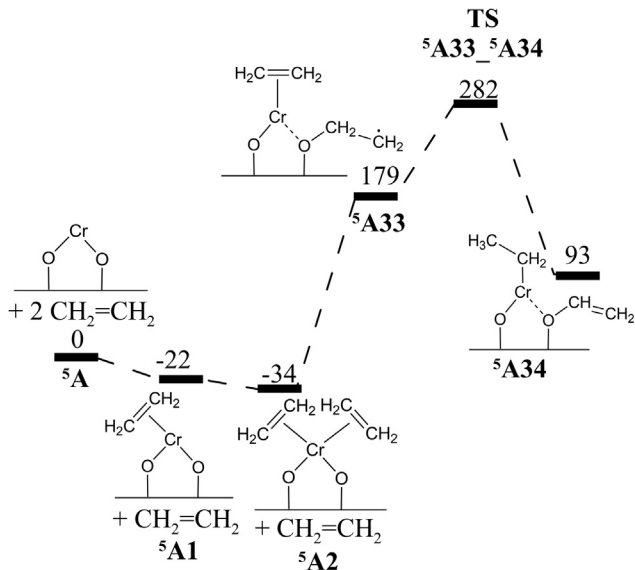


Fig. 7. Gibbs energy profile (kJ mol^{-1}) at $T = 373 \text{ K}$ for two-step $\equiv\text{Si}(\text{O}-\text{CHCH}_2)\text{Cr}(\text{II})$ -alkyl site formation (quintet reaction pathway).

transfer from one ethylene ligand to another (Fig. 8). Further propagation steps could proceed through ethylene insertion into either Cr-alkyl or Cr-vinyl bond. The calculated activation Gibbs energy for this pathway (150 kJ mol^{-1}), being very close to the value recently reported by Fong et al. (151 kJ mol^{-1}) [43], is higher than the barriers determined for other initiation mechanisms starting from ${}^5\text{A}2$ (Figs. 2 and 4–6). Moreover, spin-crossing occurs in this case (the MECP has been localized, see Fig. S5, Supplementary

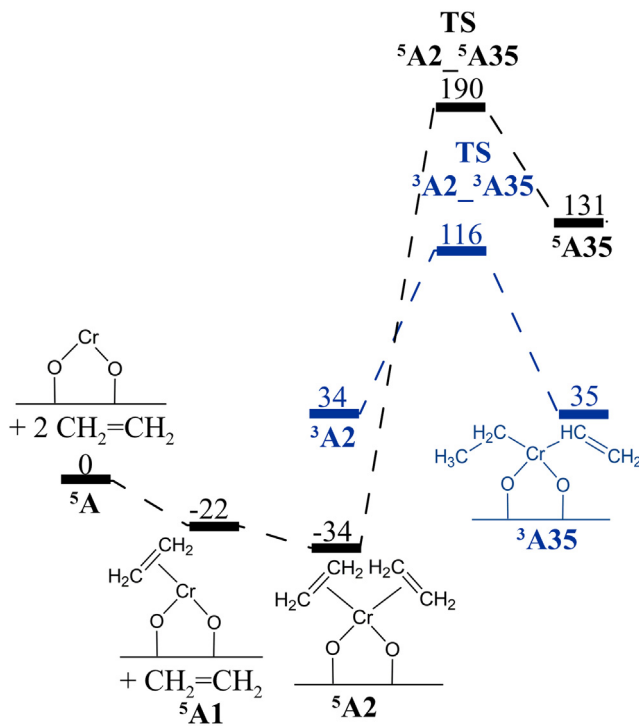


Fig. 8. Gibbs energy profile (kJ mol^{-1}) at $T = 373 \text{ K}$ for $\text{Cr}(\text{IV})(-\text{alkyl})(-\text{vinyl})$ site formation. Blue and black colours denote triplet and quintet reaction pathways, respectively.

Data). For these reasons we have not considered this route anymore.

3.3. Formation of $\text{Cr}(\text{III})/\text{SiO}_2$ and $\text{Cr}(\text{III})$ -vinyl/ SiO_2 site from $\text{Cr}(\text{II})/\text{SiO}_2$ species and a surface defect

$\text{Cr}(\text{III})$ oxide species 3-fold bonded to the surface (model ${}^4\text{B}$, Fig. 1) was recently considered as the potential active site precursor for ethylene polymerization [42,55,56,59]. While minor $\text{Cr}(\text{III})$ species might be present after the high-temperature calcination of the Phillips catalyst [5,11], it is difficult to explain how isolated $\text{Cr}(\text{III})$ sites could be formed from the initial monomeric $\text{Cr}(\text{VI})$ species via reduction with two-electron reducing agents, such as CO , H_2 or C_2H_4 . On the other hand, it is well known that various defect sites are present on the silica surface, especially after high-temperature treatment [21,96–102]. As only $0.2\text{--}0.4 \text{ Cr atoms per nm}^2$ are typically present in the Phillips catalyst [4–6,11] and the percentage of the active sites is probably not higher than 10% of the Cr atoms introduced [5,11], the participation of the surface defects in the generation of the active sites or their precursors cannot be excluded. Moreover, it was experimentally shown that higher calcination temperature increases the catalytic activity [5,11], which might correspond to a higher number of the surface defect sites.

Here, we propose a mechanism based on the assumption that there is a surface defect $\equiv\text{Si}=\text{O}\cdot$ in the vicinity of the monomeric $\text{Cr}(\text{II})$ site (Fig. 9). The presence of radical defect sites on both crystalline and amorphous silica, mainly $\equiv\text{Si}=\text{O}\cdot$ (nonbridging oxygen, NBO) and $\equiv\text{Si}\cdot$ (E' center), is supported by experimental evidences [96,98,99,102–104]. The NBO and E' centers were also detected on

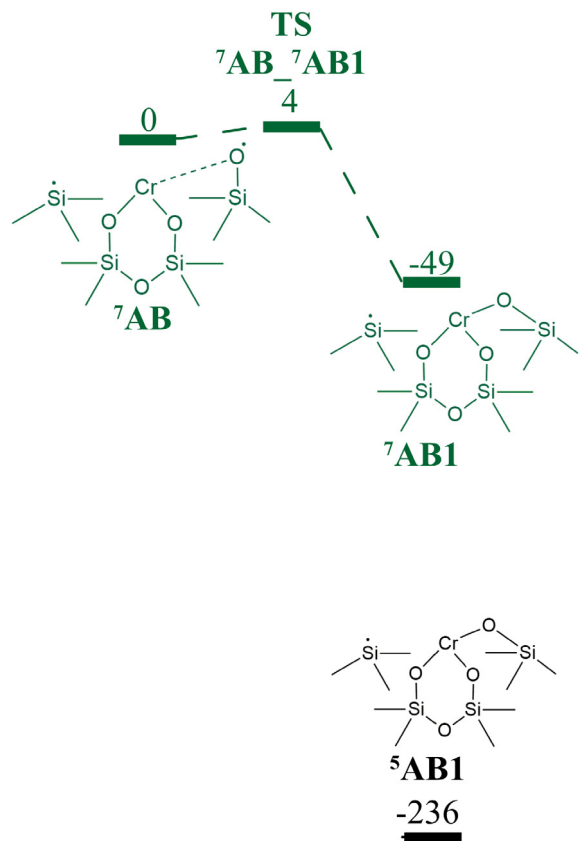


Fig. 9. Gibbs energy profile (kJ mol^{-1}) at $T = 373 \text{ K}$ for $\text{Cr}(\text{III})$ site formation from $\text{Cr}(\text{II})$ species and a neighboring silica defect site. Black and green colours denote systems in quintet and septet states, respectively.

high surface area silica materials and proposed to be the active sites for olefin photometathesis [98]. It is postulated that these radical species can be generated by dehydroxylation of silica surface at high temperatures [98,102–104]. The model **7AB** (Fig. 1), representing both types of defect sites, $\equiv\text{Si}-\text{O}\cdot$ and $\equiv\text{Si}'$, is not arbitrarily built. It is derived from the corresponding periodic model of Cr(VI) species, which was obtained from a non-defect strained initial structure during the geometry optimization [18]. The quintet counterpart of **7AB** has not been localized. It is shown that the exergonic addition of the $\equiv\text{Si}-\text{O}\cdot$ radical to the Cr(II) species has a negligible activation barrier (4 kJ mol^{-1}) and results in formation of Cr(III) site with the $\equiv\text{Si}'$ defect in the neighborhood (**7AB1**). The ground state of the latter system is quintet (**5AB1**), being 187 kJ mol^{-1} more stable than the septet state (**7AB1**), so, the overall reaction Gibbs energy for this transformation is -236 kJ mol^{-1} . Thus, Cr(III) sites on silica can be easily and irreversibly formed from Cr(II) species and neighboring surface defects.

Dissociative adsorption of ethylene over monomeric Cr(II) site and a neighboring $\equiv\text{Si}-\text{O}\cdot$ radical site is another reaction mechanism where surface defects may play a role (Fig. 10). H transfer reaction from π -bonded ethylene to $\equiv\text{Si}-\text{O}\cdot$ (**7AB2**) produces Cr(III) vinyl site and a new silanol (**5AB3**) with the relatively low overall activation Gibbs energy (111 kJ mol^{-1}). The hydroxyl group formed within this step would rather still interact with Cr, as evidenced by the short Cr—OH distance (2.41 \AA). Cr(III) vinyl site was proposed to be active in ethylene polymerization [53–56,59], however, it was postulated that it is formed by ethylene transformation over Cr(III) oxide species (*vide infra*). Hence, the mechanism shown in Fig. 10 represents an alternative route of $\equiv\text{Si}(\text{OH})\text{Cr}(\text{III})$ -vinyl site formation.

3.4. Ethylene transformations over Cr(III)/ SiO_2 species (**4B**)

3.4.1. Ethylene coordination to Cr(III) species

Coordination of the first ethylene molecule to the bare Cr(III) oxide species (**4B**) is a less exergonic process ($\Delta G = -4 \text{ kJ mol}^{-1}$, Fig. 11) than in the case of the Cr(II) site **5A** ($\Delta G = -22 \text{ kJ mol}^{-1}$, Fig. 2) and the average Cr—C distance in the Cr(III) mono(ethylene) complex **4B1** (2.57 \AA) is longer, compared to the corresponding Cr(II) species **5A1** (2.40 \AA). Hence, as expected, the C_2H_4 ligand is weaker bonded to Cr(III) than to Cr(II). Coordination of another ethylene molecule is predicted to be endergonic ($\Delta G = 26 \text{ kJ mol}^{-1}$), suggesting that the Cr(III) bis(ethylene) complex **4B2** is thermodynamically unstable, in qualitative agreement with some reported cluster [42] and periodic [59] calculations, but in contrast to other cluster results [55,56]. Not surprisingly, the average Cr—C distance in **4B2** is elongated (2.68 \AA) compared to **4B1**.

3.4.2. $\equiv\text{Si}(\text{OH})\text{Cr}(\text{III})$ -vinyl site formation

The idea of this mechanism is derived from the results of Copéret and co-workers [53–56,59] and it was also studied elsewhere [42]. Therefore, we have only considered the first stage of this mechanism to compare it with other reaction pathways presented in this work.

The proton transfer from one of the two ethylene ligands in **4B2** to a bridge oxygen atom can give the active $\equiv\text{Si}(\text{OH})\text{Cr}(\text{III})$ -vinyl site **4B3** (Fig. 11). The calculated overall activation barrier for this initiation route (161 kJ mol^{-1}) is between the corresponding values reported by Copéret and co-workers (153 kJ mol^{-1}) [55,56] and Fong et al. (163 kJ mol^{-1}) [42], being higher than the activation barriers obtained for some other initiation mechanisms in this work. However, the activation energy of such a transformation can be significantly decreased (to 132 kJ mol^{-1}) using the more

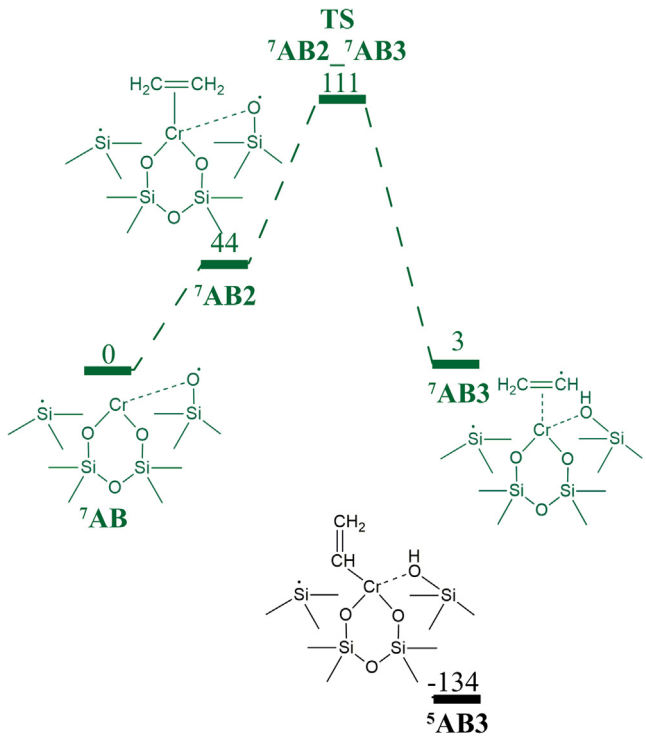


Fig. 10. Gibbs energy profile (kJ mol^{-1}) at $T = 373 \text{ K}$ for Cr(III) vinyl site formation as a result of dissociative adsorption of ethylene over Cr(II) species and a neighboring silica defect site. Black and green colours denote systems in quintet and septet states, respectively.

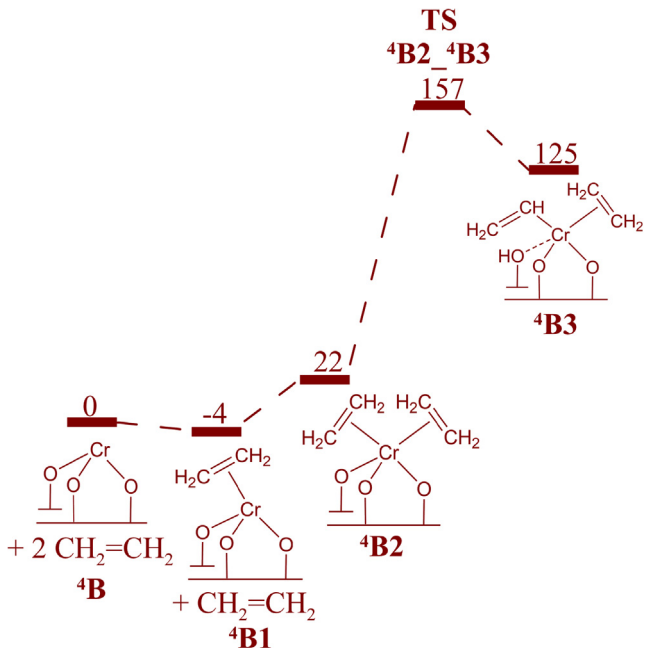


Fig. 11. Gibbs energy profile (kJ mol^{-1}) at $T = 373 \text{ K}$ for $\equiv\text{Si}(\text{OH})\text{Cr}(\text{III})$ -vinyl site formation as a result of dissociative adsorption of ethylene over Cr(III) species (quartet reaction pathway).

advanced amorphous silica model (Fig. 12). A similar effect was very recently reported for periodic models of Cr(III)/ SiO_2 system, compared to a simple cluster model [59]. The Cr(III) site **5AB1** can be easily formed from the Cr(II) species and the neighboring silica defect site (Fig. 9). As mentioned earlier, the $\equiv\text{Si}(\text{OH})\text{Cr}$

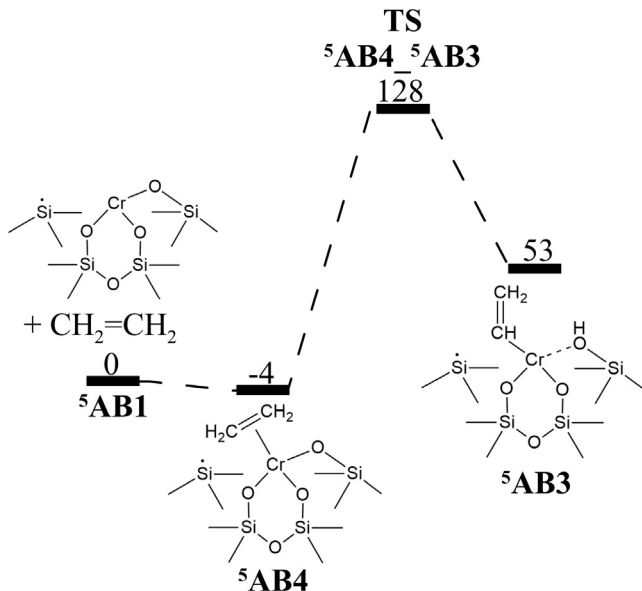


Fig. 12. Gibbs energy profile (kJ mol^{-1}) at $T = 373 \text{ K}$ for Cr(III) vinyl site formation as a result of dissociative adsorption of ethylene over Cr(III) species generated from Cr(II) species and a neighboring silica defect site (quintet reaction pathway).

(III)-vinyl site ⁵AB3 might be also directly generated by a dissociative ethylene adsorption on Cr(II) site and the silica defect site (Fig. 10), which is an interesting alternative to the mechanism proposed by Copéret and co-workers [55,56,59].

It was concluded, based on cluster calculations, that $\equiv\text{Si(OH)}\text{Cr(III)}$ -vinyl species cannot be the active sites for ethylene polymerization, because the termination is predicted to be faster than propagation [42], in contrast to other computational studies using cluster models [55,56]. The very recent computational work applying periodic models of well-defined Cr(III) sites on amorphous silica [59] indicates that this is not the case at least for highly strained Cr(III) species. They are also predicted to be more active for ethylene polymerization than the less strained sites. The formation of the strained Cr(III) species is explained by the high-temperature treatment of the support [59,63] and was also suggested by the EXAFS data for the well-defined Cr(III)/ SiO_2 system [55]. One should note, however, that after the calcination of the conventional Phillips $\text{CrO}_x/\text{SiO}_2$ catalyst, dioxo Cr(VI) species 2-fold bonded to the surface are mostly present on silica [1,5,14,18–23]. Their reduction and possible generation of the Cr(III) sites take place at lower temperatures. Silica defect sites, favored by the earlier high-temperature calcination, can participate in this process, enabling formation of 3-fold bonded Cr(III) oxide species (Fig. 9) or organo-Cr(III) sites (Fig. 10).

3.4.3. $\equiv\text{Si(OCHCH}_2\text{)}\text{Cr(III)}$ -alkyl site formation

Proton transfer reaction similar to the mechanism presented in Fig. 7 might also proceed over Cr(III) oxide species (Fig. 13). Consequently, Cr(III)-alkyl site is formed together with the surface ligand $-\text{O}-\text{CH}=\text{CH}_2$ (⁴B5). The transformation involves the unstable intermediate radical species ⁴B4. The calculated overall activation Gibbs energy (247 kJ mol^{-1}) is much too high to further consider this mechanism.

3.4.4. Oxachromacycle ring expansion mechanism over Cr(III) oxide species

As the oxachromacycle mechanism seems to be most kinetically preferred among the considered initiation routes involving Cr(II) species (Fig. 6), we have also examined this possibility for Cr(III) sites (Fig. 14). Some preliminary computational results on this

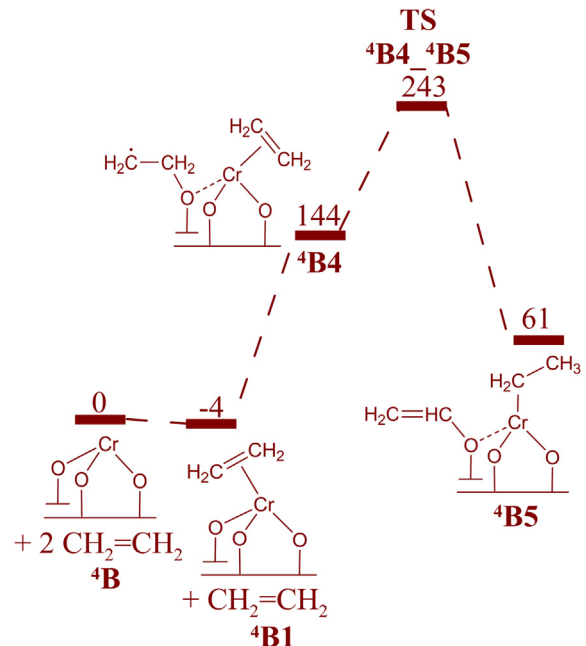


Fig. 13. Gibbs energy profile (kJ mol^{-1}) at $T = 373 \text{ K}$ for $\equiv\text{Si(OCHCH}_2\text{)}\text{Cr(II)}$ -alkyl site formation (quartet reaction pathway).

mechanism were reported by us elsewhere [58] and it was the first time when such a route was investigated. During the final preparation of the present paper, periodic calculation results for the oxachromacycle mechanism over Cr(III) species were also published [59].

Ethylene insertion into Cr—O bond of the Cr(III) mono(ethylene) complex ⁴B1 produces the unstable oxachromacyclobutane intermediate ⁴B6 (Fig. 14). The Cr—O($-\text{CH}_2-$)($-\text{Si}\equiv$) distance in ⁴B6 (2.06 Å) is slightly longer than that in the corresponding Cr(II) structure ⁵A22 (1.99 Å). Endergonic coordination of another ethylene molecule to ⁴B6 results in ⁴B7, which can be also formed directly from the Cr(III) bis(ethylene) complex ⁴B2. Although this ethylene-assisted insertion proceeds with a lower activation barrier (94 kJ mol^{-1}), compared to the competitive pathway leading to ⁴B6 (111 kJ mol^{-1}), the overall activation Gibbs energy for the former reaction is higher (120 kJ mol^{-1} , relatively to ⁴B1). Further ring expansion to oxachromacyclohexane species ⁴B8 is an exergonic step proceeding with a quite low activation barrier (45 kJ mol^{-1} , relatively to ⁴B7). However, the overall activation Gibbs energy is much higher (149 kJ mol^{-1}), indicating that the reaction might be slower over Cr(III) sites than over Cr(II) sites ($\Delta G^\ddagger = 140 \text{ kJ mol}^{-1}$, Fig. 6). The initiation route is also preferred for the Cr(II) oxide precursors, compared to the Cr(III) species ($\Delta G^\ddagger = 83$ and 111 kJ mol^{-1} , respectively). On the other hand, the activation barriers can be lower for more strained Cr(III) sites [59].

The ethylene ligand in ⁴B7 may also undergo a proton transfer reaction with the formation of Cr(III) vinyl site (⁴B9) together with the surface ethoxy group (Fig. 14), similar to the corresponding side-mechanism involving the Cr(II) sites (Fig. 6). The presence of Cr(III) vinyl species during ethylene polymerization on the Phillips catalyst was recently experimentally confirmed [58]. However, the predicted overall activation barrier for this mechanism is too high (198 kJ mol^{-1}).

3.5. Ethylene polymerization over surface Cr(III)—OH species

Besides Cr(III) oxide species such as ⁴B (Fig. 1), other monomeric Cr(III) structures on silica are also possible. We theoretically showed [29] that reduction and further hydration of dimeric Cr

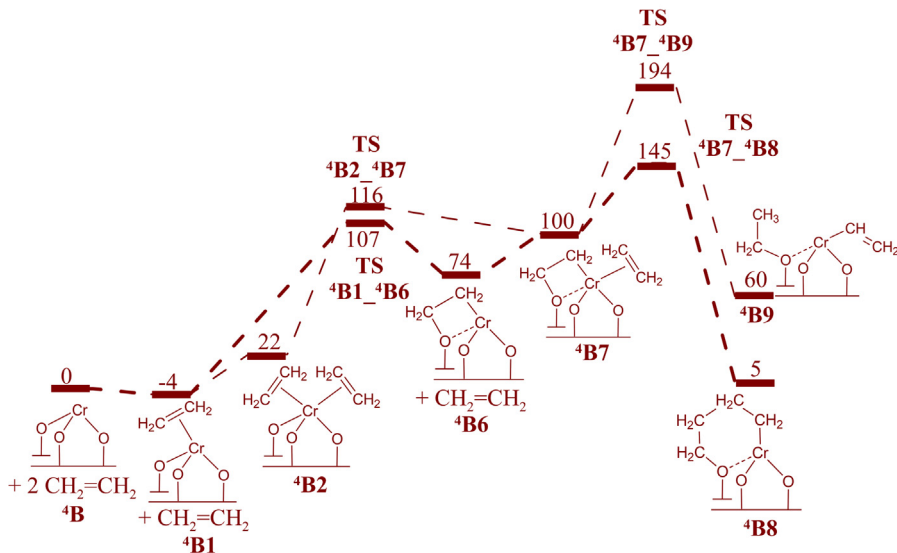


Fig. 14. Gibbs energy profile (kJ mol⁻¹) at T = 373 K for the oxachromacycle ring expansion mechanism over Cr(III) oxide species (quartet reaction pathway). The thicker line represents the preferred route.

oxide species might result in formation of hydroxylated monomeric Cr(III) species (⁴C, Fig. 1). Likewise, hydration of ⁴B leads to ⁴C analog (⁴B11, Fig. 15). Assuming a very low water vapor pressure (10⁻⁵ atm) and a typical temperature of ethylene polymerization (373 K), this transformation is predicted to be slightly endergonic with the activation Gibbs energy of only 64 kJ mol⁻¹. Water can be formed during the induction period of the polymerization process. Indeed, water and carbon dioxide were recently detected as the products of the reduction of the Cr(VI) oxide species with ethylene [46,58]. An alternative mechanism generating hydroxylated monomeric Cr(III) species might involve dissociative adsorption of H₂O molecule over Cr(II) and an adjacent surface defect (⁷AB, Fig. 1). Hydrated Cr(III) species could be also formed from the intermediate structure ⁴B6 (Fig. S6, Supplementary Data), however, the latter is thermodynamically unstable (Fig. 14) and, consequently, the overall activation barrier for this process is quite high (156 kJ mol⁻¹).

Therefore, we have examined surface Cr(III)-OH species, represented by the model ⁴C (Fig. 1), as the potential precursor of the active site for ethylene polymerization. Some preliminary results were reported previously [58] and here we present the complete

pathways for the initiation, propagation and termination mechanisms (Fig. 16).

Coordination of ethylene molecule to ⁴C is an equilibrium process, giving ⁴C1 with the average Cr-C bond distance of 2.55 Å. As a result of hydrogen transfer from the ethylene ligand to the hydroxyl group, Cr(III) vinyl site ⁴C2 is formed, together with a coordinated H₂O molecule. The predicted activation Gibbs energy for this step is moderate (135 kJ mol⁻¹). Water desorption from ⁴C2 is not thermodynamically preferred at p(H₂O) = 1 atm ($\Delta G = 46$ kJ mol⁻¹), however, at much lower water vapor pressure (10⁻⁵ atm) it becomes more probable ($\Delta G = 10$ kJ mol⁻¹). Releasing H₂O molecule leaves vacant site, where another C₂H₄ monomer can coordinate to give ⁴C4.

At this point it should be noted that the desorbed water can hydrate another surface Cr(III) species to give HO-Cr(III)/SiO₂ site (Fig. 15). Hence, the number of such hydroxylated sites may increase during the catalytic process and the initial amount of water in the system may be very low. On the other hand, too high water vapor pressure would probably cause the catalyst deactivation, by, for instance, hydrolysis of the Cr-O-Si bonds [29].

Alternatively, ⁴C4 can be also formed by a rearrangement of Cr(III)-OH bis(ethylene) complex (⁴C5), although the latter is less stable than its mono(ethylene) analog (Fig. 16). The ethylene-assisted proton transfer, resulting in ⁴C6, proceeds with lower activation barrier, compared to the corresponding pathway leading to ⁴C2 (108 and 135 kJ mol⁻¹, respectively). However, the overall activation energies for both routes are similar (137 and 135 kJ mol⁻¹, respectively).

The first ethylene insertion into Cr-C bond in ⁴C4 occurs with a very low activation barrier (34 kJ mol⁻¹), but the overall activation Gibbs energy (138 kJ mol⁻¹) is close to that for the initiation stage (Fig. 16). However, assuming low water vapor pressure (10⁻⁵ atm), this energy barrier is decreased by 36 kJ mol⁻¹ (water desorption, see above), so the initiation (TS ⁴C1-⁴C2) is still the rate determining step ($\Delta G^\ddagger = 135$ kJ mol⁻¹). The insertion product ⁴C7 can coordinate another ethylene molecule (⁴C8) and undergo further propagation reaction, giving Cr(III) hexenyl complex ⁴C9. The predicted activation barrier for this step (78 kJ mol⁻¹) is very close to the corresponding value calculated by Fong et al. [42] for Cr(III) alkyl species (80 kJ mol⁻¹). The possible termination reaction via β-H transfer from the monomer to the butenyl ligand, recovering

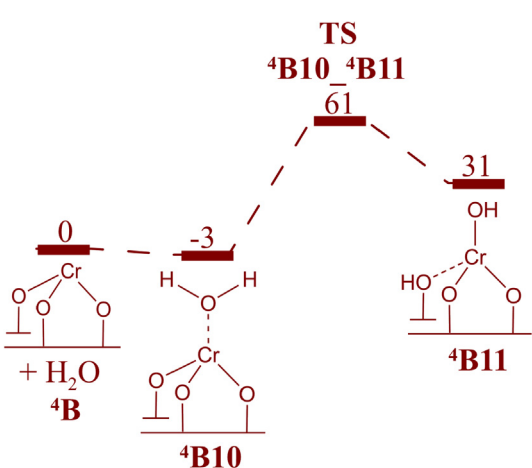


Fig. 15. Gibbs energy profile (kJ mol⁻¹) at T = 373 K and p(H₂O) = 10⁻⁵ atm for hydration of ⁴B (quartet reaction pathway).

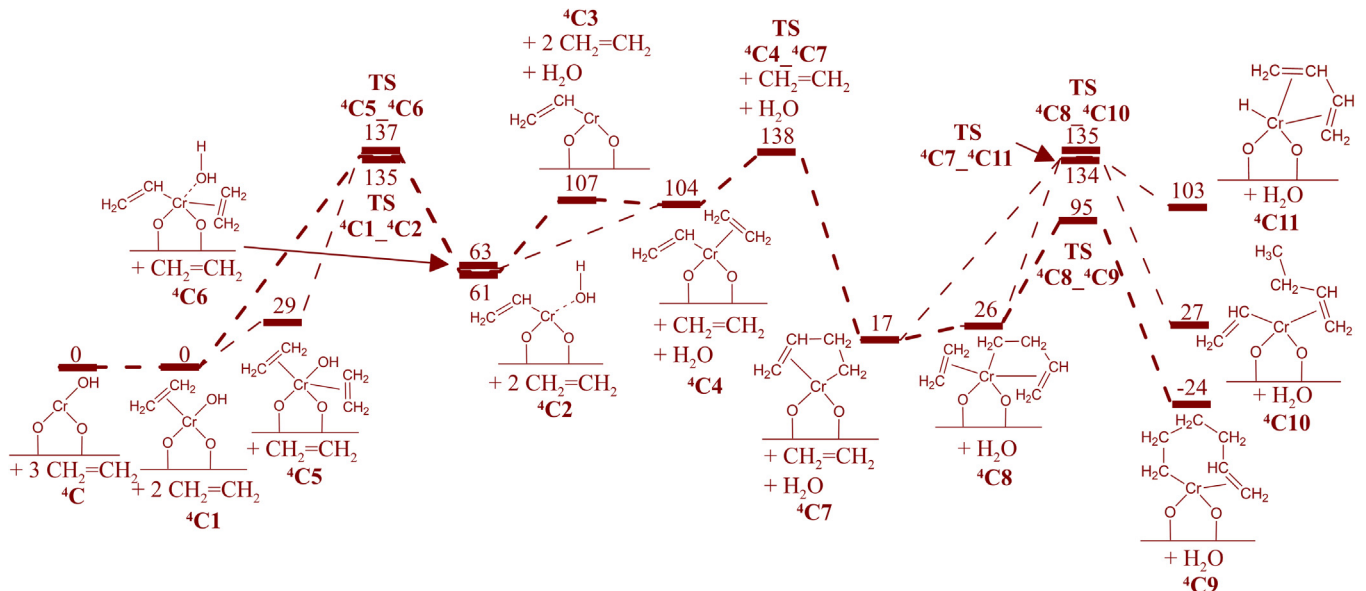


Fig. 16. Gibbs energy profile (kJ mol^{-1}) at $T = 373 \text{ K}$ for the mechanism of ethylene polymerization over Cr(III)-OH species (quartet reaction pathway). The thicker line represents the preferred route.

the active vinyl site ($^4\text{C10}$), is clearly less kinetically preferred ($\Delta G^\ddagger = 118 \text{ kJ mol}^{-1}$) than the propagation step. β -H elimination resulting in Cr(III) hydride intermediate with butadiene ligand ($^4\text{C11}$) is also less probable than the propagation pathway ($\Delta G^\ddagger = 117 \text{ kJ mol}^{-1}$). Another potential chain termination route is β -H transfer to the monomer (Fig. S7, Supplementary Data) resulting in Cr alkyl site with an agostic hydride and butadiene coordinated ($^4\text{C12}$). However, this mechanism is least kinetically feasible ($\Delta G^\ddagger = 127 \text{ kJ mol}^{-1}$). These predictions are in contrast to the reported computational results for Cr(III) alkyl sites, which show comparable barriers for the propagation step and the most kinetically preferred termination step (β -H elimination to metal hydride species) [42]. Hence, Cr(III) vinyl species seems to be more suitable than Cr(III) alkyl species as the active site for ethylene polymerization, in agreement with the recent experimental results [58].

Thus, the new proposed mechanism involving the initial Cr(III)-OH/SiO₂ species and the propagating Cr(III) vinyl sites appears to be reasonable for explaining the polymerization activity of the Phillips catalyst. Although the predicted Gibbs energy barrier (135 kJ mol^{-1}) for the initiation stage is higher than the value estimated from experimental kinetic data for the corresponding reaction conditions (120 kJ mol^{-1}) [43], the difference is still within the typical error of the DFT methods. Moreover, the initial vinyl Cr(III) sites might be also generated from Cr(II) species (Fig. 10), which are most likely formed during the reduction of the calcinated catalyst with 2-electron reducing agents, such as C₂H₄ or CO [1,2,5,9,11,25,30]. Very recently, another potential route leading to Cr(III) vinyl site and alkyl radical, i.e., oxidative addition of ethylene to Cr(II), followed by Cr-C bond homolysis, was proposed [43]. The authors indicate that subsequent decoordination and coordination of siloxanes to the Cr site are necessary to lower the activation barriers, but further computational study with more advanced surface models is required to confirm definitively that proposal.

3.6. Ethylene polymerization over Cr(V)/SiO₂ species

Another initiation mechanism which can generate Cr(III) vinyl intermediate involves transformations of Cr(V) oxide species ^2D (Fig. 17). The idea that Cr(V) species might be active in ethylene

polymerization is not new and some reaction mechanisms involving this rather minor species were proposed in the past [64,65]. Cr(V) was detected by EPR studies of CrO_x/SiO₂ system [17,48,49,66–68], however, to the best of our knowledge, the activity of Cr(V) oxide species in ethylene polymerization has never been theoretically examined.

The proposed route (Fig. 17) starts from ethylene attack on the oxo ligand of ^2D giving radical species $^2\text{D2}$ with a moderate activation barrier of 98 kJ mol^{-1} . The doublet ($^2\text{D2}$) and quartet ($^4\text{D2}$) states of the obtained complex are energetically comparable. Then, it reacts through the terminal C atom with silanolate oxygen to form dioxachromacyclopentane complex $^4\text{D3}$ ($\Delta G^\ddagger = 50 \text{ kJ mol}^{-1}$). Spin-crossing occurs during this step and the MECP has been successfully found (Fig. S8, Supplementary Data). Although the Cr—O($-\text{CH}_2-$)($-\text{Si}\equiv$) bond length in $^4\text{D3}$ (2.12 Å) is significantly elongated, compared to the average Cr—OSi≡ distance in ^2D (1.74 Å), the Cr atom is still 3-fold bonded to the surface.

After next ethylene coordination ($^4\text{D4}$), proton transfer from the ethylene ligand can occur, resulting in formation of Cr(III) vinyl site and surface $-\text{OCH}_2\text{CH}_2\text{OH}$ ligand ($^4\text{D5}$). The overall activation barrier for this transformation is 139 kJ mol^{-1} . The $-\text{OCH}_2\text{CH}_2\text{OH}$ ligand remains in the coordination sphere of Cr, as evidenced by Cr—O($-\text{CH}_2-$)($-\text{Si}\equiv$) (2.15 Å) and Cr—OH— (2.16 Å) distances.

Another ethylene molecule can be bonded to $^4\text{D5}$, resulting in two conformers, $^4\text{D6}$ or $^4\text{D10}$, which differs each other in the orientation of the hydroxyl group. Further C₂H₄ insertion into the Cr—C bond is kinetically and thermodynamically preferred for the more stable conformer $^4\text{D6}$, leading to Cr(III) butenyl complex $^4\text{D7}$ ($\Delta G^\ddagger = 56 \text{ kJ mol}^{-1}$). To allow for coordination of a next ethylene molecule, the $-\text{OCH}_2\text{CH}_2\text{OH}$ ligand has to decoordinate ($^4\text{D8}$) and then the subsequent insertion product ($^4\text{D9}$) is formed ($\Delta G^\ddagger = 43 \text{ kJ mol}^{-1}$). The predicted overall activation Gibbs energy for this pathway is 147 kJ mol^{-1} , as determined by the transition state $\text{TS } ^4\text{D6-}^4\text{D7}$, relatively to $^4\text{D3}$. Hence, it would be slower than the pathway starting from the hydroxylated Cr(III) site ^4C (Fig. 16).

A direct termination reaction via the reverse proton transfer in $^4\text{D9}$ is rather inhibited by the long distance between the C_α atom of the growing chain and the —OH moiety (7.14 Å), as well as by the steric hindrance. On the other hand, the less preferred pathway of ethylene addition to $^4\text{D5}$ leads to the alternative Cr(III) butenyl complex $^4\text{D11}$ (Fig. 17), for which the reverse proton transfer pro-

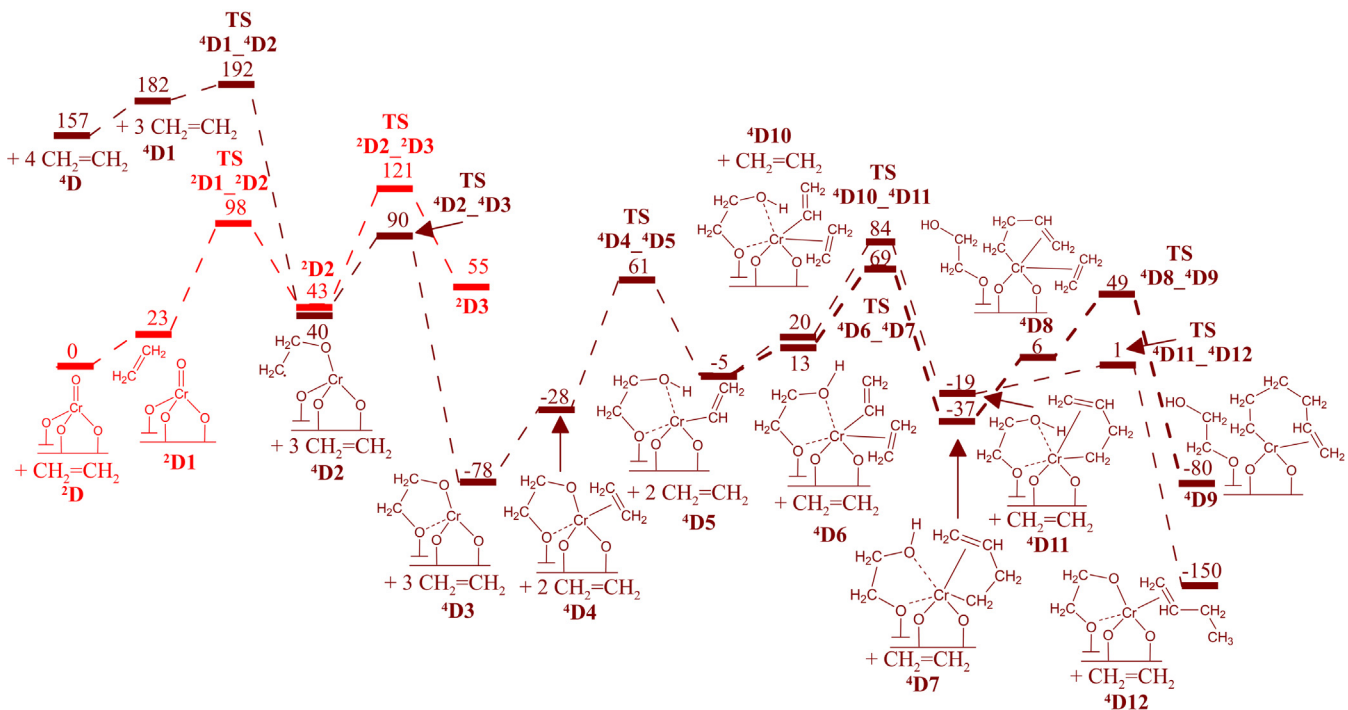


Fig. 17. Gibbs energy profile (kJ mol^{-1}) at $T = 373 \text{ K}$ for the mechanism involving Cr(V) oxide species as the precursor of the active site. Red and brown colours denote doublet and quartet reaction pathways, respectively. The thicker line represents the preferred route.

ceeds easily ($\Delta G^\ddagger = 20 \text{ kJ mol}^{-1}$), because the hydroxyl group is pointing toward the growing chain, which is not a case for $^4\text{D7}$. However, a rearrangement of $^4\text{D7}$ to $^4\text{D11}$ by the $-\text{OH}$ group rotation is also possible, so the termination step might be preferred even for the former.

4. Conclusions

Various potential mechanisms for the initiation, propagation and termination stages of ethylene polymerization over the Phillips $\text{CrO}_x/\text{SiO}_2$ catalyst have been computationally studied using the cluster approximation. We have considered surface Cr(II), Cr(III), Cr(III)-OH and Cr(V) oxide species as the precursors of the active sites.

In the case of the pathways calculated for the Cr(II) species, the initial steps giving the oxachromacyclobutane and chromacyclopentane sites can compete to each other, however the latter requires spin-crossing to occur. The alternative formation of $\equiv\text{Si}(\text{OH})\text{Cr(II)}$ -vinyl site is less kinetically and thermodynamically favored. Including the propagation steps, the calculated overall activation Gibbs energies are comparable for all these mechanisms, but only in the case of the oxachromacycle mechanism the propagation steps are predicted to be kinetically preferred over the termination paths.

The mechanisms involving $\equiv\text{Si}(\text{OH})\text{Cr(III)}$ -vinyl and Cr(III) oxachromacycle species are predicted to be less kinetically accessible than the corresponding routes for the Cr(II) sites, based on our standard models. On the other hand, the calculated activation barriers for the Cr(III) species 3-fold bonded to the surface can be lower if more advanced models of amorphous silica are used (Fig. 12) and more strained Cr(III) sites are taken into account [59].

As the reduction of the isolated Cr(VI) oxide species in the calcined $\text{CrO}_3/\text{SiO}_2$ catalyst by two-electron reducing agents leads to the Cr(II) species, we propose that some of them can transform into the monomeric Cr(III) sites with the participation of the neighboring defect sites on the silica surface (Figs. 9 and 10). Dissociation

of water adsorption may lead to the hydroxylated Cr(III)-OH species, which appears to be a promising candidate for the precursor of the active site. The calculated activation Gibbs energy for the initiation stage is reasonable (135 kJ mol^{-1}) and further propagation steps starting from the generated Cr(III) vinyl site are predicted to be rapid and kinetically preferred over the potential termination pathways. Moreover, after the decoordination of the polymer chain, a new active site is formed. Our proposal is in agreement with the recent operando spectroscopy studies [58] indicating Cr(III) vinyl species as the reactive intermediate during ethylene polymerization over $\text{CrO}_x/\text{SiO}_2$ catalyst.

Finally, a potential polymerization mechanism involving the minor Cr(V) oxide species on silica has been calculated for the first time. Although less kinetically preferred than that starting from the Cr(III)-OH site, this mechanism also predicts formation of a new active site after the decoordination of the growing chain.

One cannot exclude that there are more than one type of the active sites that are responsible for ethylene polymerization over the $\text{CrO}_x/\text{SiO}_2$ catalyst. Thus, unambiguous determination of the polymerization mechanism might be a challenging task. Further computational studies are in progress to uncover other mysteries of the Phillips $\text{CrO}_x/\text{SiO}_2$ catalyst, i.e., its reactivity toward ethylene during the induction period, including the reduction mechanism.

Acknowledgments

This work was supported by the National Science Centre, Poland, Project No. 2015/19/N/ST4/00007, and by the PL-Grid Infrastructure.

Appendix A. Supplementary material

Supplementary data associated with this article can be found, in the online version, at <http://dx.doi.org/10.1016/j.jcat.2017.05.025>.

References

- [1] B.M. Weckhuysen, I.E. Wachs, R.A. Schoonheydt, *Chem. Rev.* 96 (1996) 3327–3350.
- [2] A.B. Gaspar, J.L.F. Brito, L.C. Dieguez, *J. Mol. Catal. A: Chem.* 203 (2003) 251–266.
- [3] V.N. Panchenko, V.A. Zakharov, E.A. Paukshtis, *Appl. Catal. A Gen.* 313 (2006) 130–136.
- [4] E. Groppo, C. Prestipino, F. Cesano, F. Bonino, S. Bordiga, C. Lamberti, P. Thune, J. Niemantsverdriet, A. Zecchina, *J. Catal.* 230 (2005) 98–108.
- [5] E. Groppo, C. Lamberti, S. Bordiga, G. Spoto, A. Zecchina, *Chem. Rev.* 105 (2005) 115–183.
- [6] M.P. McDaniel, K.S. Collins, E.A. Benham, T.H. Cymbaluk, *Appl. Catal. A Gen.* 335 (2008) 252–261.
- [7] C.A. Demmelmair, R.E. White, J.A. van Bokhoven, S.L. Scott, *J. Catal.* 262 (2009) 44–56.
- [8] A. Zecchina, S. Bordiga, E. Groppo, *Selective Nanocatalysts and Nanoscience: Concepts for Heterogeneous and Homogeneous Catalysis*, Wiley-VCH, 2011.
- [9] L. Zhong, M.-Y. Lee, Z. Liu, Y.-J. Wang, B. Liu, S.L. Scott, *J. Catal.* 293 (2012) 1–12.
- [10] J.P. Hogan, R.L. Banks, *Polymers and Production Thereof*, US Patent 2 825 721, 1958.
- [11] M.P. McDaniel, in: *Adv. Catal.*, vol. 53, 2010, pp. 123–606.
- [12] A. Hakuli, M.E. Harlin, L.B. Backman, A.O.I. Krause, *J. Catal.* 184 (1999) 349–356.
- [13] G.S. Pozan, A. Tavman, I. Boz, *Chem. Eng. J.* 143 (2008) 180–185.
- [14] J.J.H.B. Sattler, J. Ruiz-Martinez, E. Santillan-Jimenez, B.M. Weckhuysen, *Chem. Rev.* 114 (2014) 10613–10653.
- [15] N.C. Ramani, D.L. Sullivan, J.G. Ekerdt, J. Jehng, I.E. Wachs, *J. Catal.* 176 (1998) 143–154.
- [16] M. Cherian, M.S. Rao, A.M. Hirt, I.E. Wachs, G. Deo, *J. Catal.* 211 (2002) 482–495.
- [17] P. Michorczyk, P. Pietrzak, J. Ogonowski, *Micropor. Mesopor. Mater.* 161 (2012) 56–66.
- [18] J. Handzlik, R. Gryboś, F. Tielens, *J. Phys. Chem. C* 117 (2013) 8138–8149.
- [19] H. Guessmi, F. Tielens, *J. Phys. Chem. C* 116 (2012) 994–1001.
- [20] A. Chakrabarti, I.E. Wachs, *Catal. Lett.* 145 (2015) 985–994.
- [21] E.L. Lee, I.E. Wachs, *J. Phys. Chem. C* 111 (2007) 14410–14425.
- [22] E.L. Lee, I.E. Wachs, *J. Phys. Chem. C* 112 (2008) 6487–6498.
- [23] C. Moisni, E.W. Deguns, A. Lita, S.D. Callahan, L.J. van der Burgt, D. Magana, A.E. Stiegman, *Chem. Mater.* 18 (2006) 3965–3975.
- [24] J. Handzlik, K. Kurleto, *Chem. Phys. Lett.* 561–562 (2013) 87–91.
- [25] B.M. Weckhuysen, L.M. De Ridder, R.A. Schoonheydt, *J. Phys. Chem.* 97 (1993) 4756–4763.
- [26] B.M. Weckhuysen, A.A. Verberckmoes, A.L. Buttines, R.A. Schoonheydt, *J. Phys. Chem.* 98 (1994) 579–584.
- [27] B.M. Weckhuysen, R.A. Schoonheydt, J.-M. Jehng, I.E. Wachs, S.J. Cho, R. Ryoo, S. Kijlstra, E. Poels, *J. Chem. Soc. Faraday Trans.* 91 (1995) 3245–3253.
- [28] A. Zecchina, E. Groppo, A. Damin, C. Prestipino, *Top. Organomet. Chem.* 16 (2005) 1–35.
- [29] M. Gierada, P. Michorczyk, F. Tielens, J. Handzlik, *J. Catal.* 340 (2016) 122–135.
- [30] A.B. Gaspar, L.C. Dieguez, *Appl. Catal. A Gen.* 227 (2002) 241–254.
- [31] B. Rebenstorf, R. Larsson, *J. Mol. Catal.* 11 (1981) 247–256.
- [32] G. Ghiotti, E. Garrone, A. Zecchina, *J. Mol. Catal.* 46 (1988) 61–77.
- [33] P. Zielinski, I.G. Dalla Lana, *J. Catal.* 137 (1992) 368–376.
- [34] M. Kantcheva, I.G. Dalla Lana, J.A. Szymbura, *J. Catal.* 154 (1995) 329–334.
- [35] S.L. Scott, J. Amor Nait Ajjou, *Chem. Eng. Sci.* 56 (2001) 4155–4168.
- [36] J. Amor, Nait Ajjou, S.L. Scott, *J. Am. Chem. Soc.* 122 (2000) 8968–8976.
- [37] Ø. Espelid, K.J. Børve, *J. Catal.* 195 (2000) 125–139.
- [38] Ø. Espelid, K.J. Børve, *J. Catal.* 205 (2002) 366–374.
- [39] Ø. Espelid, K.J. Børve, *J. Catal.* 206 (2002) 331–338.
- [40] E. Groppo, C. Lamberti, S. Bordiga, G. Spoto, A. Zecchina, *J. Catal.* 240 (2006) 172–181.
- [41] L. Zhong, Z. Liu, R. Cheng, S. Tang, P. Qiu, X. He, M. Terano, B. Liu, *ChemCatChem* 4 (2012) 872–881.
- [42] A. Fong, Y. Yuan, S.L. Ivry, S.L. Scott, B. Peters, *ACS Catal.* 5 (2015) 3360–3374.
- [43] A. Fong, B. Peters, S.L. Scott, *ACS Catal.* 6 (2016) 6073–6085.
- [44] A. Budnyk, A. Damin, C. Barzan, E. Groppo, C. Lamberti, S. Bordiga, A. Zecchina, *J. Catal.* 308 (2013) 319–327.
- [45] D. Cicmil, I.K. van Ravenhorst, J. Meeuwissen, A. Vantomme, B.M. Weckhuysen, *Catal. Sci. Technol.* 6 (2016) 731–743.
- [46] K.C. Potter, C.W. Beckerle, F.C. Jentoft, E. Schwerdtfeger, M.P. McDaniel, *J. Catal.* 344 (2016) 657–668.
- [47] P. Michorczyk, J. Ogonowski, K. Zeńczak, *J. Mol. Catal. A: Chem.* 349 (2011) 1–12.
- [48] L.F. Liotta, A.M. Venezia, G. Pantaleo, G. Deganello, M. Gruttaduria, R. Noto, *Catal. Today* 91–92 (2004) 231–236.
- [49] B.M. Weckhuysen, L.M. De Ridder, P.J. Grobet, R.A. Schoonheydt, *J. Phys. Chem.* 99 (1995) 320–326.
- [50] D. Cicmil, J. Meeuwissen, A. Vantomme, J. Wang, I.K. Ravenhorst, H.E. van der Bij, A. Muñoz-Murillo, B.M. Weckhuysen, *Angew. Chemie* 127 (2015) 13265–13271.
- [51] D.L. Myers, J.H. Lunsford, *J. Catal.* 92 (1985) 260–271.
- [52] D.L. Myers, J.H. Lunsford, *J. Catal.* 99 (1986) 140–148.
- [53] M.P. Conley, M.F. Delley, G. Siddiqi, G. Lapadula, S. Norsic, V. Monteil, O.V. Safonova, C. Copéret, *Angew. Chem. Int. Ed.* 53 (2014) 1872–1876.
- [54] M.F. Delley, M.P. Conley, C. Copéret, *Catal. Lett.* 144 (2014) 805–808.
- [55] M.F. Delley, F. Nuñez-Zarur, M.P. Conley, A. Comas-Vives, G. Siddiqi, S. Norsic, V. Monteil, O.V. Safonova, C. Copéret, *Proc. Natl. Acad. Sci. USA* 111 (2014) 11624–11629.
- [56] M.P. Conley, M.F. Delley, F. Nuñez-Zarur, A. Comas-Vives, C. Copéret, *Inorg. Chem.* 54 (2015) 5065–5078.
- [57] C. Brown, J. Krzystek, R. Achey, A. Lita, R. Fu, R.W. Meulenberg, M. Polinski, N. Peek, Y. Wang, L.J. van der Burgt, S. Profeta, A.E. Stiegman, S.L. Scott, *ACS Catal.* 5 (2015) 5574–5583.
- [58] A. Chakrabarti, M. Gierada, J. Handzlik, I.E. Wachs, *Top. Catal.* 59 (2016) 725–739.
- [59] L. Floryan, A.P. Borosy, F. Nuñez-Zarur, A. Comas-Vives, C. Copéret, *J. Catal.* 346 (2017) 50–56.
- [60] Y.V. Kissin, A.J. Brandolini, *J. Polym. Sci. Part A Polym. Chem.* 46 (2008) 5330–5347.
- [61] B. Peters, S.L. Scott, A. Fong, Y. Wang, A.E. Stiegman, *Proc. Natl. Acad. Sci. USA* 112 (2015) E4160–E4161.
- [62] M.F. Delley, F. Nuñez-Zarur, M.P. Conley, A. Comas-Vives, G. Siddiqi, S. Norsic, V. Monteil, O.V. Safonova, C. Copéret, *Proc. Natl. Acad. Sci. USA* 112 (2015) E4162–E4163.
- [63] A. Comas-Vives, *Phys. Chem. Chem. Phys.* 18 (2016) 7475–7482.
- [64] L.L. van Reijen, P. Cossee, *Discuss. Faraday Soc.* 41 (1966) 277–289.
- [65] V.B. Kazanski, J. Turkevich, *J. Catal.* 8 (1967) 231–239.
- [66] D.D. Beck, J.H. Lunsford, *J. Catal.* 68 (1981) 121–131.
- [67] A. Cimino, D. Cordischi, S. Febbraro, D. Gazzoli, V. Indovina, M. Occhipuzzi, M. Valigi, F. Bocuzzi, A. Chiorino, G. Ghiotti, *J. Mol. Catal.* 55 (1989) 23–33.
- [68] P.B. Aycough, C. Eden, H. Steiner, *J. Catal.* 4 (1965) 278–290.
- [69] B. Liu, P. Šindelář, Y. Fang, K. Hasebe, M. Terano, *J. Mol. Catal. A: Chem.* 238 (2005) 142–150.
- [70] A.F. Wright, A.J. Leadbetter, *Philos. Mag.* 31 (1975) 1391–1401.
- [71] J. Handzlik, J. Ogonowski, *J. Phys. Chem. C* 116 (2012) 5571–5584.
- [72] J.J. Mortensen, M. Parrinello, *J. Phys. Chem. B* 104 (2000) 2901–2907.
- [73] D. Ceresoli, M. Bernasconi, S. Iarlori, M. Parrinello, E. Tosatti, *Phys. Rev. Lett.* 84 (2000) 3887–3890.
- [74] X. Solans-Monfort, J.-S. Filhol, C. Copéret, O. Eisenstein, *New J. Chem.* 30 (2006) 842–850.
- [75] S.A. Mian, L.C. Saha, J. Jang, L. Wang, X. Gao, S. Nagase, *J. Phys. Chem. C* 114 (2010) 20793–20800.
- [76] J. Handzlik, *Chem. Phys. Lett.* 469 (2009) 140–144.
- [77] F. Tielens, C. Gervais, J.F. Lambert, F. Mauri, D. Costa, *Chem. Mater.* 20 (2008) 3336–3344.
- [78] C. Adamo, V. Barone, *J. Chem. Phys.* 110 (1999) 6158–6170.
- [79] M. Bühl, C. Reimann, D.A. Pantazis, T. Bredow, F. Neese, *J. Chem. Theory Comput.* 4 (2008) 1449–1459.
- [80] P. Śliwa, J. Handzlik, *Chem. Phys. Lett.* 493 (2010) 273–278.
- [81] R. Kang, H. Chen, S. Shaik, J. Yao, *J. Chem. Theory Comput.* 7 (2011) 4002–4011.
- [82] F. Weigend, R. Ahlrichs, *Phys. Chem. Chem. Phys.* 7 (2005) 3297–3305.
- [83] C. Gonzalez, H.B. Schlegel, *J. Chem. Phys.* 90 (1989) 2154–2161.
- [84] C. Gonzalez, H.B. Schlegel, *J. Phys. Chem.* 94 (1990) 5523–5527.
- [85] S. Grimme, J. Antony, S. Ehrlich, H. Krieg, *J. Chem. Phys.* 132 (2010) 154104–154123.
- [86] S. Grimme, S. Ehrlich, L. Goerigk, *J. Comput. Chem.* 32 (2011) 1456–1465.
- [87] J.N. Harvey, M. Aschi, H. Schwarz, W. Koch, *Theor. Chem. Acc.* 99 (1998) 95–99.
- [88] M.J. Frisch, G.W. Trucks, H.B. Schlegel, G.E. Scuseria, M.A. Robb, J.R. Cheeseman, G. Scalmani, V. Barone, B. Mennucci, G.A. Petersson, H. Nakatsuji, M. Caricato, X. Li, H.P. Hratchian, A.F. Izmaylov, J. Bloino, G. Zheng, J.L. Sonnenberg, M. Hada, M. Ehara, K. Toyota, R. Fukuda, J. Hasegawa, M. Ishida, T. Nakajima, Y. Honda, O. Kitao, H. Nakai, T. Vreven, J.A.J. Montgomery, J.E. Peralta, F. Ogliaro, M. Bearpark, J.J. Heyd, E. Brothers, K.N. Kudin, V.N. Staroverov, R. Kobayashi, J. Normand, K. Raghuvarachari, A. Rendell, J.C. Burant, S.S. Iyengar, J. Tomasi, M. Cossi, N. Rega, J.M. Millam, M. Klene, J.E. Knox, J.B. Cross, V. Bakken, C. Adamo, J. Jaramillo, R. Gomperts, R.E. Stratmann, O. Yazyev, A.J. Austin, R. Cammi, C. Pomelli, J.W. Ochterski, R.L. Martin, K. Morokuma, V.G. Zakrzewski, G.A. Voth, P. Salvador, J.J. Dannenberg, S. Dapprich, A.D. Daniels, Ö. Farkas, J.B. Foresman, J. V. Ortiz, J. Cioslowski, D.J. Fox, *Gaussian 09, Revision D.01, Gaussian Inc., Wallingford CT*, 2013.
- [89] R. Dennington, T. Keith, J. Millam, *GaussView, Version 5, Semichem Inc., Shawnee Mission, KS*, 2009.
- [90] J.P. Hogan, *J. Polym. Sci. A-1 Polym. Chem.* 8 (1970) 2637–2652.
- [91] C. Groeneveld, P.P.M.M. Wittgen, H.P.M. Swinnen, A. Wernsen, G.C.A. Schuit, *J. Catal.* 83 (1983) 346–361.
- [92] W.K. Jozwiak, I.G. Dalla Lana, R. Fiedorow, *J. Catal.* 121 (1990) 183–195.
- [93] E. Ariman, P. Cossee, *J. Catal.* 3 (1964) 99–104.
- [94] Y. Ma, L. Wang, Z. Liu, R. Cheng, L. Zhong, Y. Yang, X. He, Y. Fang, M. Terano, B. Liu, *J. Mol. Catal. A: Chem.* 401 (2015) 1–12.
- [95] L.M. Baker, W.L. Carrick, *J. Org. Chem.* 35 (1970) 774–776.
- [96] A. Rimola, D. Costa, M. Sodipe, J.F. Lambert, P. Ugliengo, *Chem. Rev.* 113 (2013) 4216–4313.
- [97] X. Gao, S.R. Bare, J.L.G. Fierro, M.A. Banares, I.E. Wachs, *J. Phys. Chem. B* 102 (1998) 5653–5666.
- [98] Y. Inaki, H. Yoshida, T. Yoshida, T. Hattori, *J. Phys. Chem. B* 106 (2002) 9098–9106.

- [99] J.M. Antonietti, M. Michalski, U. Heiz, H. Jones, K.H. Lim, N. Rösch, A. Del Vitto, G. Pacchioni, Phys. Rev. Lett. 94 (2005) 213402.
- [100] L. Giordano, P.V. Sushko, G. Pacchioni, A.L. Shluger, Phys. Rev. Lett. 99 (2007) 136801.
- [101] F. Musso, P. Ugliengo, X. Solans-Monfort, M. Sodupe, J. Phys. Chem. C 114 (2010) 16430–16438.
- [102] V. Zeleňák, A. Zeleňáková, J. Kováč, Colloids Surf. A 357 (2010) 97–104.
- [103] Yu.D. Glinka, C.P. Jaroniec, M. Jaroniec, J. Colloid Interface Sci. 201 (1998) 210–219.
- [104] Yu.D. Glinka, S.-H. Lin, L.-P. Hwang, Y.-T. Chen, J. Phys. Chem. B 104 (2000) 8652–8663.

Artykuł **D5**

Computational insights into reduction of the Phillips CrO_x/SiO₂ catalyst by ethylene and CO

Maciej Gierada, Jarosław Handzlik✉

J. Catal. 359 (2018) 261-271



Computational insights into reduction of the Phillips CrO_x/SiO₂ catalyst by ethylene and CO

Maciej Gierada, Jarosław Handzlik *

Faculty of Chemical Engineering and Technology, Cracow University of Technology, ul. Warszawska 24, 31-155 Kraków, Poland



ARTICLE INFO

Article history:

Received 8 October 2017

Revised 5 January 2018

Accepted 14 January 2018

Keywords:

Phillips catalyst

Chromium oxide

Silica

Reduction

Ethylene

Induction period

Carbon monoxide

Mechanism

DFT

Vibrational frequency

ABSTRACT

The mechanism of the reduction of the Phillips CrO_x/SiO₂ catalyst with ethylene is still not determined. In this work, full reaction pathways for this process, including further transformations of the oxygenated products, are calculated. The mechanism of the CrO_x/SiO₂ reduction with CO is also studied. It is predicted that the most kinetically favored reduction mechanism involves the reaction between ethylene and both oxo ligands of the surface dioxo Cr(VI) species, leading to formation of Cr(II) site and two formaldehyde molecules. We show that formaldehyde oxidation to carbon oxides and water over the dioxo Cr(VI) sites can be kinetically more accessible than conversion to methyl formate over Cr(II) sites. Formaldehyde can also easily generate various surface intermediates. The calculated activation barrier for the reduction of the CrO_x/SiO₂ system with CO is higher than in the case of the reduction with ethylene.

© 2018 Elsevier Inc. All rights reserved.

1. Introduction

The Phillips catalyst, composed of Cr oxide species supported on silica, is still one of the most important catalytic systems that is successfully used in the industrial production of high-density polyethylene [1–9]. Despite many years since the discovery [10] of its unique activity in ethylene polymerization, several questions about its nature are still being discussed. Among others, there is no clear picture how ethylene reacts with Cr(VI) surface oxide species to produce reduced Cr sites which are able to initiate ethylene polymerization.

Typical experimental procedure of the Phillips catalyst preparation leads to a system with a surface covered by well-dispersed Cr(VI) oxide species [2,4,9,11–16]. Different structures of such a species were proposed, i.e., monomeric, dimeric and polymeric [2,4,5,11–14,17–32]. However, it is often claimed that monomeric Cr(VI) sites dominates on the silica surface at low chromium loadings [4,12–15,21,23,25,26,28–32]. Our previous computational studies [27] also indicate thermodynamic preference for the monomeric Cr(VI) structures over their dimeric counterparts. Monomeric dioxo Cr(VI) species are commonly postulated

[4,12–15,25–27], although some authors also proposed minor monooxo Cr(VI) species [12–14,24–27]. The previous DFT calculations [25] showed that the dioxo Cr(VI) species is thermodynamically much more stable than the monooxo one. *In situ* and *operando* Raman spectroscopy studies suggested that the former species are easier to reduce/activate than the latter [12,14,26].

When the calcinated Phillips catalyst is contacting with ethylene, usually at about 373 K, an induction period of the polymerization process is observed. Cr(VI) species are reduced to Cr(II) and/or Cr(III) [1,2,4,14,32–35]. Several authors postulate formation of various by-products, i.e., formaldehyde [33,34,36], esters [37–39], aldehydes/ketones [37] and oligomers of ethylene [33,34,37] at the initial stage of the reaction. In the past, Baker and Carrick [36] reported formation of carbonyl compounds together with Cr(II) sites when Cr(VI) reacts with various olefins. They also proposed a concerted mechanism of these transformations, involving formation of dioxachromacyclopentane intermediate. Liu et al. [33,34], based on XPS and TPD data, demonstrated that formaldehyde can be formed, together with unsaturated hydrocarbons, mainly propylene and butylene, when the calcinated Phillips catalyst is contacted with ethylene. They postulated that formaldehyde-coordinated Cr(IV) ethyldene site, possibly generated via 1,2-hydrogen transfer of π-bonded ethylene, is responsible for propylene and butylene formation through alkene metathesis

* Corresponding author.

E-mail address: jhandz@pk.edu.pl (J. Handzlik).

type mechanism [34]. On the other hand, our recent computational studies on ethylene polymerization over the Phillips catalyst suggest that direct 1,2-hydrogen shift resulting in Cr(IV) ethylidene species is a very unlikely process, at least in the absence of formaldehyde [40], in accordance with other works [41–43]. Zhong et al. [43] theoretically found that bare Cr(II) oxide species strongly interacts with formaldehyde, suggesting that the latter acts as a mild poisoning agent. Such a role of ethylene-oxidized by-products was also postulated elsewhere [1,4,44,45]. Zhong et al. [43] concluded that no reaction can start over Cr(II) site with two formaldehyde ligands coordinated, in contrast to bare Cr(II) site and Cr(II) with one formaldehyde molecule adsorbed. Barzan et al. [38,39] recently proposed that aldehydes react with the reduced Cr sites giving ester species, which would remain in the coordination sphere of Cr and can influence the activity towards ethylene polymerization. Other experimental results suggest that partially oxidized products, formed during the reduction of the $\text{CrO}_x/\text{SiO}_2$ system with ethylene, can be converted to CO_2 and H_2O at temperatures much higher than those typical of ethylene polymerization [26,37].

Pre-reduction of the Phillips catalyst with CO results mainly in Cr(II) formation [1,2,4,8,9,16,17,46]. The reduced catalyst shows activity in ethylene polymerization even at room temperature practically without the induction period and the oxygenated by-products are not formed. Hence, many authors investigate ethylene polymerization over the Phillips catalyst starting from the reduced system [3,4,35,41–43,47–53]. However, in the case of the industrial process, the reduction step using CO is usually not carried out [1,4,9].

From the information given above it is seen that the mechanistic aspects of ethylene transformations over Cr(VI) oxide species on silica are not established, despite their particular importance. Reduction from Cr(VI) to Cr(II) and consecutive reactions involving oxygenated by-products can account for most of the induction period. As the polymerization process might start rapidly after formation of reduced Cr species, experimental discrimination between the reduction of the Cr(VI) species and ethylene polymerization is a challenging task. Additionally, unambiguous determination of partially oxidized products is difficult, because of coinciding signals coming from different organic species [37].

In this computational work, for the first time full reaction pathways of the Phillips catalyst reduction with ethylene are investigated. We propose several reduction mechanisms involving the most commonly postulated dioxo Cr(VI) species. In particular, the path proposed by Baker and Carrick [36] is studied in detail. Additionally, we investigate reduction of the monooxo Cr(VI) species with ethylene. This enables us to explain different behavior of the monooxo and dioxo Cr(VI) species towards ethylene, recently observed experimentally [26]. Moreover, we also consider further transformations of oxygenated by-products. Among others, possible oxidation of formaldehyde to CO/CO_2 and H_2O , as well as, ester formation, are studied in detail. Additionally, calculated vibrational frequencies for the adsorbed oxygenated organic species are discussed. A mechanism of reduction of the Cr(VI) species by CO is also investigated. To the best of our knowledge, such comprehensive theoretical studies on the reduction of the Phillips $\text{CrO}_x/\text{SiO}_2$ catalyst and other related transformations involving the oxygenated by-products have never been reported before.

2. Computational models and methods

Cluster models of the chromium surface species used in this work were developed based on the β -cristobalite framework [54] and they were fully relaxed to allow for the amorphous nature of the support. Fig. 1 presents the optimized structures of the dioxo (¹A) and monooxo (¹B) Cr(VI) oxide species. The models, containing

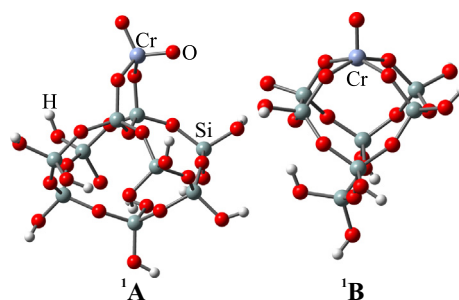


Fig. 1. Models of isolated surface Cr(VI) species: ¹A – dioxo, ¹B – monooxo.

9 and 7 Si atoms, respectively, are larger or comparable to other proposed cluster models of the supported $\text{CrO}_x/\text{SiO}_2$ catalyst [41–43,49,50,52,55]. Analogous models were previously successfully applied in the studies of the mechanism of ethylene polymerization over the Phillips catalyst [26,40] and olefin metathesis catalyzed by molybdena-silica system [56,57]. Additionally, to account for possible interactions between Cr(II) site and surface groups, another cluster model was also developed (Fig. S1, Supplementary Data).

Geometry optimization was carried out using the hybrid PBE0 functional [58], known to be accurate in predicting geometries of transition metal complexes [59–61], combined with the def2-SVP basis set [62]. Harmonic vibrational frequencies were calculated to confirm local minima or first-order saddle points, and, to determine Gibbs energy corrections at $T = 373$ K (typical catalyst operation temperature) and $p = 1$ atm (if not stated otherwise). The transition states were additionally verified applying the IRC method [63,64]. The presented $\nu(\text{CH})$, $\nu(\text{CO})$ and $\delta(\text{CH})$ frequencies are scaled by 0.9569, 0.9274 and 0.9835, respectively. The scaling factors were obtained through a least-square approach, based on the experimental and theoretical frequencies for methyl formate and formaldehyde in gas phase. Although a common practice is to use a generic scaling factor for a given theory level, the ratios of the observed frequencies to the calculated harmonic frequencies are not constant for different vibrational modes [65,66].

In order to obtain better estimation of energy, further single point calculations were performed for each optimized structure using the PBE0 functional and the def2-TZVPP basis set [62]. The reaction pathways are discussed in terms of Gibbs energies (if not stated otherwise) estimated by adding the Gibbs energy corrections and the DFT-D3(BJ) dispersion corrections [67,68] to the PBE0/def2-TZVPP single point energies. The computational methodology is the same as in our previous papers on the Phillips catalyst [26,40]. By performing test calculations, we have recently shown [40] that this methodology is adequate for studying the properties and reactivity of the $\text{CrO}_x/\text{SiO}_2$ system.

The minimum energy crossing points (MECP) between two potential energy surfaces of different spin states were localized using the method developed by Harvey and co-workers [69]. Spin-unrestricted calculations were performed for the open-shell systems. The ground state for each structure was verified. High-spin ground states for the reduced Cr species were always found, whereas for the Cr(VI) species the ground state is singlet.

Gaussian 09 package [70] was used to perform all calculations. GaussView 5.0 software [71] was applied for the graphic presentation of the structures.

3. Results and discussion

3.1. Nomenclature

The nomenclature of the models studied in this work is based on the capital letters, numbers and numbers in superscript. Capital

letters (**A**, **B**) are used to distinguish between the models representing the initial dioxo and monooxo Cr(VI) species, respectively (Fig. 1), and their derivatives. Numbers (1–27) after each letter denote different structures belonging to a given series of models (**A** or **B**). The superscript numeral before the letter indicates the spin state. The prime symbol is used for models with an additional ethylene ligand. The star symbol (*) denotes the models which represent Cr(II) species interacting with siloxane and/or silanol groups (Figs. S1 and S8, Supplementary Data). Black, blue and orange colour is used for the Gibbs energy profiles to distinguish between singlet, triplet and quintet reaction pathways, respectively.

3.2. Reduction of dioxo Cr(VI) oxide species by ethylene

3.2.1. Mechanism involving two oxo ligands

Fig. 2 presents the Gibbs energy profile for the mechanism originally proposed by Baker and Carrick [36], where two oxo ligands of dioxo Cr(VI) species (**1A**) react with ethylene molecule. In its preferential coordination mode at the initial stage of the reaction, ethylene is oriented symmetrically and parallelly to the oxo ligands (**1A1**), in qualitative agreement with the results of Liu et al. [72] based on the paired interacting orbitals (PIO) method. In the triplet counterpart **3A1**, which is slightly less stable in terms of Gibbs energy, ethylene is bound to the former oxo ligand. The subsequent reaction of **3A1**, involving the terminal $-\text{CH}_2\cdot$ moiety and another oxo ligand, proceeds thorough the low-lying transition state **3A1–3A2** to generate Cr(IV) dioxachromacyclopentane intermediate **3A2**. The overall Gibbs activation energy for **3A2** formation along the triplet pathway (63 kJ mol^{-1}) is significantly lower than that for its singlet counterpart (140 kJ mol^{-1}). Hence, the concerted mechanism for this reductive coupling reaction, proposed by Baker and Carrick [36], is less likely.

Further reductive decomposition of the cyclic Cr(IV) intermediate **3A2** produces two formaldehyde molecules coordinated to Cr (II) (**5A3**). Because the ground state of the latter is quintet, spin crossing should occur. The calculated MECP (Fig. S2, Supplementary Data) suggests that the quintet transition state **TS 5A2–5A3** is decisive for the effective Gibbs activation barrier for this transformation (127 kJ mol^{-1}), which is the rate-determining step. Interestingly, the calculated barrier is slightly lower than the activation barriers recently predicted for the potential initiation mechanisms of ethylene polymerization [40].

Formaldehyde is strongly bound to the Cr(II) site (Table 1), which is in a qualitative agreement with the computational data reported by Zhong et al. [43]. The predicted short distance between the chromium atom and the oxygen atom of formaldehyde (2.09 and 2.11 Å for one and two formaldehyde molecules adsorbed on the Cr(II) site, respectively) confirms this interaction. Additional bonding of one or two ethylene ligands to **5A3**, resulting in 5-fold or 6-fold coordinated Cr(II) site is not preferred in terms of Gibbs energy (Table 1). Obviously, at very low HCHO partial pressure, expected under the conditions of the working catalyst, formaldehyde adsorption is less favored. For instance, at $p(\text{HCHO}) = 10^{-5}$ and 10^{-7} atm , the predicted adsorption Gibbs energy is only -46 kJ mol^{-1} and -34 kJ mol^{-1} , respectively (two aldehyde ligands coordinated by the Cr(II) site). These numbers are comparable with the Gibbs energy of adsorption of two ethylene molecules on the bare Cr(II) site at $p(\text{C}_2\text{H}_4) = 1 \text{ atm}$ (-34 kJ mol^{-1} , Table 1) [40]. Hence, the substitution of formaldehyde by ethylene can occur under the strong excess of the latter.

3.2.2. Mechanism involving one oxo ligand

A coordination mode where ethylene approaches the dioxo Cr (VI) species from the Cr-O-Si side (**1A5**) favors the subsequent transition state leading to the Cr(VI) oxachromacyclobutane species

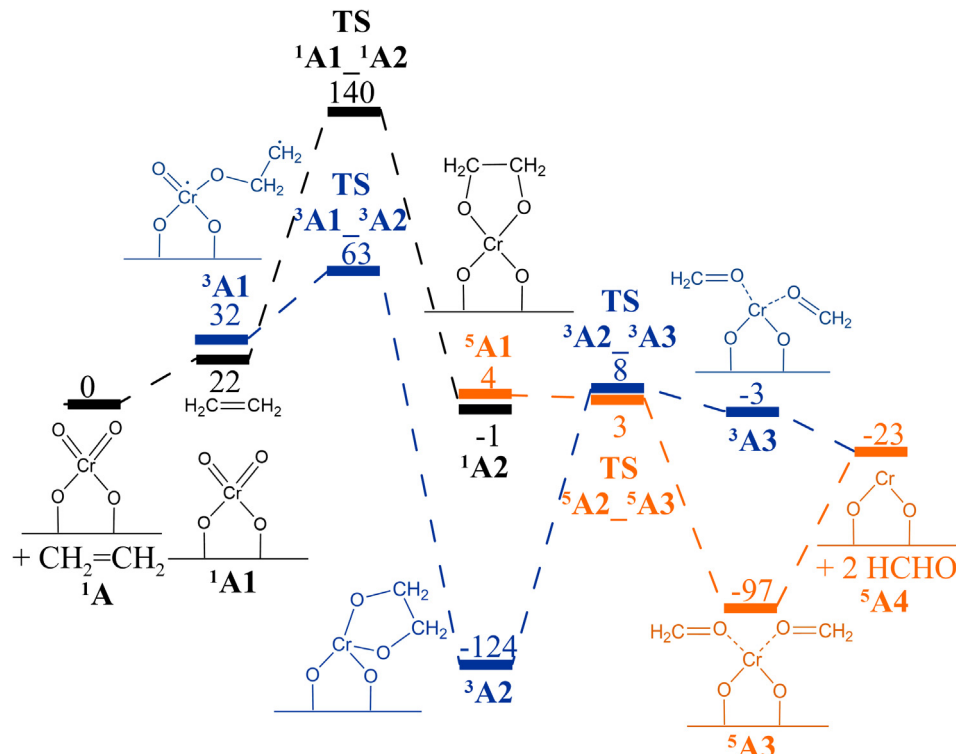


Fig. 2. Gibbs energy profile (kJ mol^{-1}) at $T = 373 \text{ K}$ for the reduction of the dioxo Cr(VI) species with ethylene to Cr(II) species and formaldehyde. Black, blue and orange colours denote singlet, triplet and quintet reaction pathways, respectively.

Table 1

Calculated energies (ΔE , kJ mol^{-1}) and Gibbs energies at $T = 373 \text{ K}$ and $p = 1 \text{ atm}$ (ΔG , kJ mol^{-1}) for adsorption of various molecules on the silica-supported bare Cr(II) species, and the distances between the Cr atom and the nearest O or C atom of the coordinated molecule ($d(\text{Cr-X})$, Å).

Surface species	ΔE	ΔG	$d(\text{Cr-X})$
	-127	-34	2.09
	-236	-74	2.11
	-271	-60	2.11 3.07–3.19 ^a
	-300	-43	2.11 3.12–3.33 ^a
	-101	-22	2.40
	-179	-34	2.46
	-129	-38	2.07
	-210	-56	2.10 2.42 ^a
	-246	-40	2.11 2.41–3.12 ^a
	-91	-9	2.14
	-35	38	2.27
	-63	-2	2.19

^a Cr-C distance for ethylene ligands.

1A6 (Fig. 3). Its triplet counterpart **3A6**, being more stable by 40 kJ mol^{-1} (ΔG), is a radical type complex with the Cr-C distance (3.11 Å) significantly elongated, compared to **1A6** (2.08 Å). The localized MECP (Fig. S3, Supplementary Data) has the geometry similar to **1A6** (Cr-C σ -bond length of 2.19 Å). Subsequent rearrangement of **3A6** to the Cr(IV) intermediate **3A7** can occur easily, whereas the corresponding transformation of **1A6** along the singlet pathway would require a much higher activation energy. Finally, after decoordination of ethylene oxide, the monooxo Cr(IV) species **3A8** might be formed. Such species were recently postulated on the basis of experimental [35,73] and computational [27] evidences.

An alternative transformation of **3A6** might result in the Cr(IV) site and acetaldehyde (Fig. 4). This direct 1,2-hydrogen transfer is predicted to be kinetically more accessible than the formation of ethylene oxide (Fig. 3). The calculated energies for adsorption of ethylene oxide ($\Delta E = -125 \text{ kJ mol}^{-1}$, $\Delta G = -44 \text{ kJ mol}^{-1}$) and acetaldehyde ($\Delta E = -122 \text{ kJ mol}^{-1}$, $\Delta G = -34 \text{ kJ mol}^{-1}$) on the monooxo Cr(IV) species are comparable with the corresponding quantities for formaldehyde adsorption on the Cr(II) site (Table 1). The predicted strong interactions are in accordance with the reported stability of acetaldehyde-coordinated CrOCl_2 moiety [74]. Nevertheless, the overall activation Gibbs energy for the mechanisms presented in Figs. 3 and 4 (about 160 kJ mol^{-1}) is clearly higher than the rate-limiting barrier predicted for the

reduction pathway leading to the Cr(II) species and formaldehyde (127 kJ mol^{-1} , Fig. 2).

Oxachromacyclobutane **1A6** can also undergo the so-called pseudo-Wittig mechanism (Fig. 5). As a result, Cr(VI) alkylidene complex would be formed (**1A11**). It was proposed that such a mechanism might explain the active site formation in supported Mo [75,76], Re [77] and W [78] olefin metathesis catalysts. According to our calculations, the generation of the Cr(VI) alkylidene complex together with a formaldehyde molecule would proceed with a very high Gibbs activation energy (234 kJ mol^{-1}), precluding this pathway as kinetically accessible.

To sum up, the most kinetically preferred mechanism for the reduction of the dioxo Cr(VI) oxide species with ethylene involves both oxo ligands (Fig. 2). Consequently, the Cr(II) sites and formaldehyde are most likely to be formed. Our calculations indicate that HCHO strongly interacts with the Cr(II) site, but its desorption under an excess of ethylene is possible. Formaldehyde formation after contacting of $\text{CrO}_x/\text{SiO}_2$ system with ethylene was indeed reported by some authors [33,34] and very recently suggested by Barzan et al., on the basis of their comprehensive spectroscopic studies [39]. On the other hand, CO_2 and H_2O was observed as the gas phase products of ethylene oxidation over the $\text{CrO}_x/\text{SiO}_2$ catalyst at higher temperatures [26,37]. As we show in Section 3.4, HCHO can further react with the surface Cr sites to produce other by-products, eventually leading to CO/CO_2 and H_2O .

3.3. Reduction of monooxo Cr(VI) oxide species by ethylene

It was proposed that the minor monooxo Cr(VI) oxide species can be present on the surface of the calcinated chromia-silica system [12–14,24–26]. This square-pyramidal coordinated Cr(VI) species (**1B**, Fig. 1) might be also reduced/activated after a contact with ethylene. A one-step ethylene attack on the oxo ligand and silanolate oxygen would result in **1B3** formation (Fig. 6), but the ground state of the product is triplet (**3B3**). The overall Gibbs activation energy for the two-step triplet reaction pathway is higher (112 kJ mol^{-1}) than that for the singlet pathway (94 kJ mol^{-1}), but spin crossing occurs before the **3B2** intermediate is formed (Fig. S4, Supplementary Data). Hence, the effective Gibbs energy barrier for **3B3** formation would be between 35 and 94 kJ mol^{-1} , suggesting that this process is kinetically accessible under the reaction conditions. The reduction of the monooxo Cr(VI) species **1B** with ethylene to the Cr(IV) species **3B3** (Fig. 6) is predicted to be more exergonic than the reduction of the dioxo Cr(VI) species **1A** to **3A2** (Fig. 2). This is in agreement with our previous thermodynamic calculations [27] where more advanced periodic and cluster models of the chromia-silica system were used.

The Cr-O(silanolate) bond in the cyclic **3B3** complex is significantly elongated (2.20 Å), compared to the monooxo Cr(VI) species **1B** (1.77 Å) and **3B** (1.78 Å), but the oxygen atom still remains in the coordination sphere of Cr, being 3-fold bonded. Further reaction of **3B3** with ethylene might result in formation of Cr(IV) vinyl site **3B5** (Fig. 6). Cr(II) and Cr(III) vinyl species were recently considered as the active sites in ethylene polymerization [26,40,42,52,53,55,79–82]. However, the very high activation barrier calculated ($\Delta G^\ddagger = 240 \text{ kJ mol}^{-1}$) precludes generation of the Cr(IV) vinyl site according to this mechanism. A similar transformation involving monooxo Cr(V) species was recently predicted to be more kinetically accessible [40].

Competitive pathways starting from **3B3** can lead to 4-fold bonded Cr(IV) species without the oxo ligand (**3B7**), which was recently studied by us [27], and ethylene oxide (Fig. S5, Supplementary Data) or acetaldehyde (Fig. S6). However, these routes are also highly improbable ($\Delta G^\ddagger = 293$ and 228 kJ mol^{-1} , respectively).

Although the first step of the reaction between ethylene and the monooxo Cr(VI) species might occur relatively easily, it produces

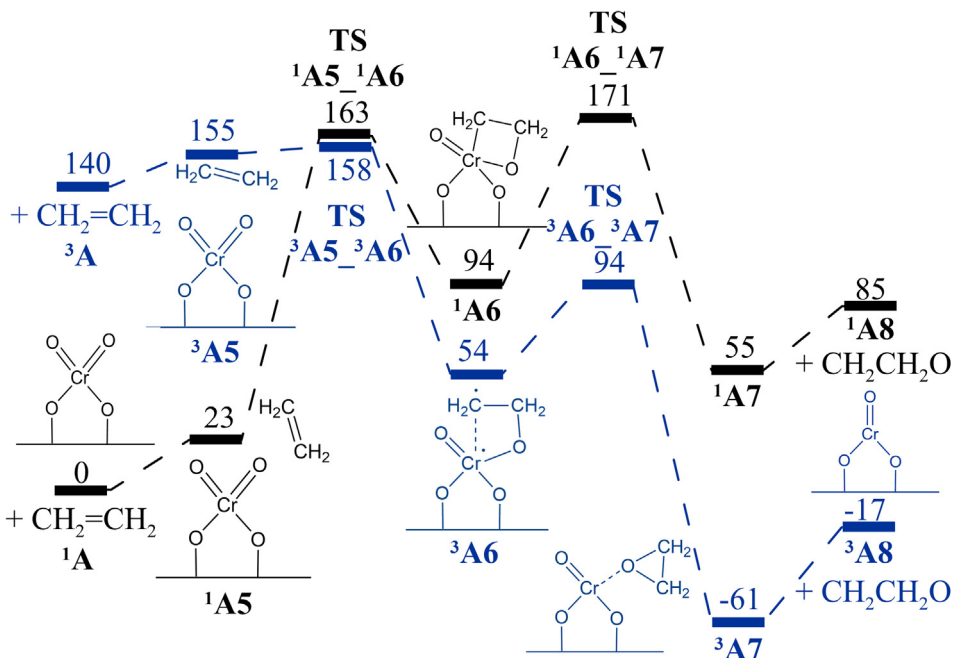


Fig. 3. Gibbs energy profile (kJ mol⁻¹) at T = 373 K for the reduction of the dioxo Cr(VI) species with ethylene to monooxo Cr(IV) species and ethylene oxide. Black and blue colours denote singlet and triplet reaction pathways, respectively.

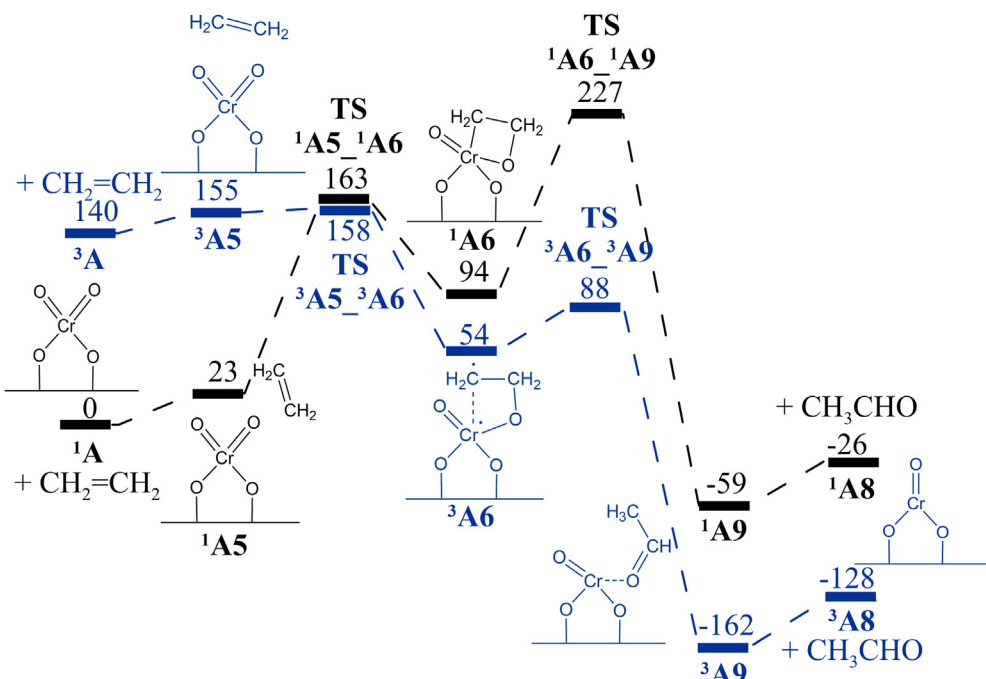


Fig. 4. Gibbs energy profile (kJ mol⁻¹) at T = 373 K for the reduction of the dioxo Cr(VI) species with ethylene to monooxo Cr(IV) species and acetaldehyde. Black and blue colours denote singlet and triplet reaction pathways, respectively.

the very stable Cr(IV) intermediate ³B3 that is hardly to be activated/reduced. Hence, ³B3 would rather act as a spectator species. On the other hand, the reduction of the major dioxo Cr(VI) species finally results in formation of the Cr(II) species which can be the precursor of the polymerization active site [4,39,41–43,49–52]. This predicted different reactivity of the dioxo and monooxo Cr(VI) species towards ethylene is in agreement with the reported experimental studies [26] suggesting much faster reduction and activation of the dioxo Cr(VI) species.

3.4. Formaldehyde transformations over CrO_x/SiO₂ catalyst

3.4.1. Oxidation of formaldehyde over dioxo Cr(VI) species

Formaldehyde, formed during reduction of the Cr(VI) species by ethylene, might undergo subsequent oxidation reactions, finally leading to CO₂ and H₂O. A possible route of formaldehyde decomposition can involve its oxidation over the dioxo Cr(VI) species (Fig. 7). In the first step, a hydrogen transfer from formaldehyde to one of the oxo ligands generates Cr(IV) formate species (³A13,

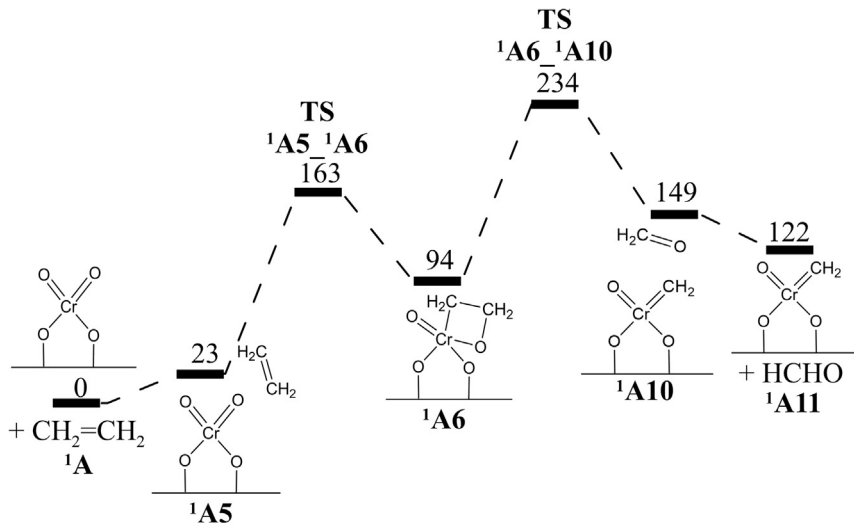


Fig. 5. Gibbs energy profile (kJ mol^{-1}) at $T = 373 \text{ K}$ for the pseudo-Wittig-type transformation of the dioxo Cr(VI) species to Cr(VI) methylidene species (singlet reaction pathway).

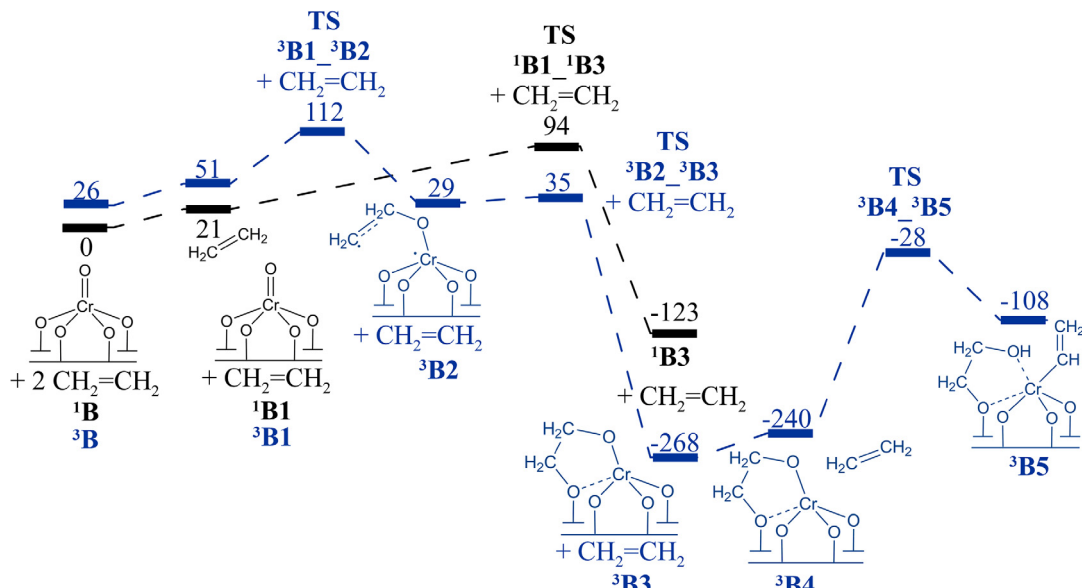


Fig. 6. Gibbs energy profile (kJ mol^{-1}) at $T = 373 \text{ K}$ for the reduction of the monooxo Cr(VI) species with ethylene and further activation to Cr(IV) vinyl site. Black and blue colours denote singlet and triplet reaction pathways, respectively.

³A14). The effective Gibbs energy barrier for ³A13 formation (111 kJ mol^{-1}) is determined by the triplet transition state TS ³A12-³A13.

In the second step, intramolecular hydrogen transfer gives water-coordinated monooxo Cr(IV) species ³A15 ($\Delta G^\ddagger = 148 \text{ kJ mol}^{-1}$). According to the calculations, the CO molecule does not stay in the coordination sphere of chromium. A potential transition state for a direct transformation of ³A14 to CO₂ and H₂O has not been localized. Water decoordination from ³A15 is an endergonic reaction at $p(\text{H}_2\text{O}) = 1 \text{ atm}$ ($\Delta G = 31 \text{ kJ mol}^{-1}$), however, at much lower water vapour pressure it becomes thermodynamically preferred (for instance, $\Delta G = -5 \text{ kJ mol}^{-1}$ at $p(\text{H}_2\text{O}) = 10^{-5} \text{ atm}$). The released CO can be further oxidized to CO₂ over the Cr(VI) or Cr(IV) sites (see Section 3.6). Evolution of CO₂ was experimentally observed at higher temperatures, after treating of

the CrO_x/SiO₂ system with ethylene [26,37]. Hence, this phenomenon might be explained, at least partially, by formaldehyde formation and consecutive oxidation reactions involving the surface Cr species.

3.4.2. Ester formation

Barzan et al. [38,39] recently proposed that aldehyde by-products, most likely formed during the reduction of the Cr(VI)/SiO₂ system by olefins, are rapidly converted to adsorbed ester species. These oxygenated by-products were thought to strongly interact with the surface Cr(II) species, affecting ethylene polymerization. Hence, if formaldehyde is formed as the product of ethylene oxidation, it might then subsequently react to methyl formate via Tishchenko disproportionation [38,39,83,84]. This pro-

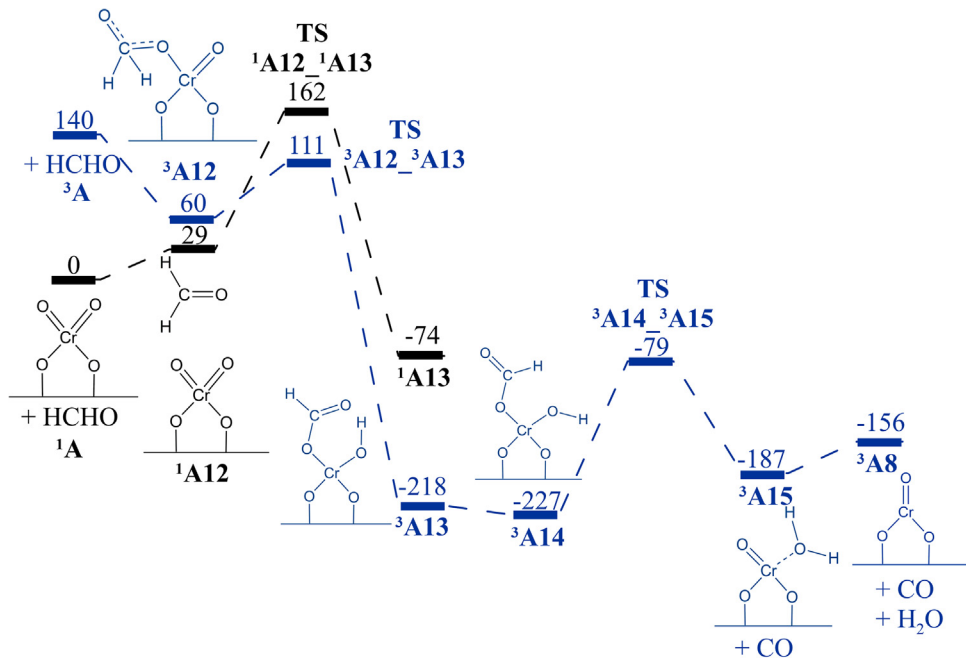


Fig. 7. Gibbs energy profile (kJ mol^{-1}) at $T = 373 \text{ K}$ for formaldehyde oxidation over the dioxo Cr(VI) species. Black and blue colours denote singlet and triplet reaction pathways, respectively.

posal tempted us to investigate theoretically possible transformations of formaldehyde to ester over the Cr(II) oxide species.

The calculated Gibbs energy profile for a three-step reaction pathway leading to methyl formate is presented in Fig. 8. Cr(IV) complex **3A17** is a key-intermediate in the mechanism proposed, being formed by oxidative coupling of two formaldehyde molecules over the Cr(II) oxide species (**5A3**). The localized MECP (Fig. S7, Supplementary Data) indicates that the quintet transition state **TS^{5A16-5A17}** is decisive for the activation barrier ($\Delta G^\ddagger = 123 \text{ kJ mol}^{-1}$). Subsequent rearrangement of **3A17** proceeds with a much higher activation energy ($\Delta G^\ddagger = 181 \text{ kJ mol}^{-1}$) and leads to Cr(IV) hydride complex **3A18**. Then, **3A18** can effortlessly decompose ($\Delta G^\ddagger = 49 \text{ kJ mol}^{-1}$) to ester-coordinated Cr(II) oxide species **5A19**, restoring the spin multiplicity to quintet again (the MECP is computed, see Fig. S7). The predicted distance between the chromium atom and oxygen atom of the ester ligand in **5A19** (2.07 \AA) is the shortest one among the corresponding Cr-X ($X = \text{C}, \text{O}$) bond lengths calculated for the coordinated Cr(II) complexes considered in this work (Table 1). The comparison of the respective adsorption energies (Table 1) confirms that methyl formate is slightly stronger bonded to Cr(II) than formaldehyde ligand. These results are in agreement with the experimental studies of Barzan et al. [38,39] suggesting that ester by-products strongly interact with the reduced Cr(II) species and, consequently, stay in their coordination sphere.

Recently, a 6-fold coordinated Cr(II) species was proposed, with one methyl formate ligand and two ethylene ligands [39]. The present theoretical results indicate, however, that a mono(ethylene) counterpart of **5A19** is more stable in terms of Gibbs energy ($T = 373 \text{ K}, p = 1 \text{ atm}$) than its bis(ethylene) analogue (Table 1). Under the considered conditions, desorption of methyl formate to give Cr(II) mono or bis(ethylene) species is not favored thermodynamically (Table 1), but this tendency changes if low ester pressure is assumed. For instance, regarding the most stable Cr(II) site with one ethylene ligand and one methyl formate ligand, the substitution of the ester ligand by another ethylene ligand is an almost equilibrium process at $p(\text{HCOOCH}_3) = 10^{-3} \text{ atm}$ and it is exergonic by 14 kJ mol^{-1} at $p(\text{HCOOCH}_3) = 10^{-5} \text{ atm}$.

On the other hand, according to our calculations, the total oxidation of formaldehyde over the $\text{CrO}_x/\text{SiO}_2$ catalyst (Fig. 7) is much more kinetically preferred ($\Delta G^\ddagger = 148 \text{ kJ mol}^{-1}$) than its coupling to methyl formate ($\Delta G^\ddagger = 237 \text{ kJ mol}^{-1}$, Fig. 8). This preference is still shown if one considers only the first step of each mechanism ($\Delta G^\ddagger = 111$ and 123 kJ mol^{-1} , respectively). Looking for more kinetically accessible pathway for the transformation of formaldehyde to methyl formate, we have also examined a possible one-step mechanism (Fig. 9). Here, the proton transfer and C–O bond formation occurs simultaneously. This reaction still proceeds through a high-energy transition state, but the activation barrier ($\Delta G^\ddagger = 213 \text{ kJ mol}^{-1}$) is slightly lower than that predicted for the mechanism presented in Fig. 8. Moreover, quintet spin state is conserved along the pathway, which additionally favors the proposed one-step route for the ester formation.

It was proposed that surface siloxane groups can interact with reduced Cr sites affecting their activity in ethylene polymerization [4,7,8,23,35,39,52,73,85,86]. Hence, we were curious whether such interaction could lower the activation barrier of ester formation, following the one-step mechanism. To this end, a model of Cr(II) site coordinating a siloxane ligand was developed (**5A4***, Fig. S1, Supplementary Data). Because of the limitations of this cluster model, silanol groups can also interact with the Cr(II) site. Nevertheless, the calculated mechanism of ester formation over **5A4*** site (Fig. S8, Supplementary Data) is analogous to that involving the Cr(II) species not interacting with the surface groups (Fig. 9) and the predicted activation Gibbs energy is only slightly lowered ($\Delta G^\ddagger = 200 \text{ kJ mol}^{-1}$). Hence, our present calculations are not able to explain the formation of methyl formate, recently postulated on the basis of experimental results [39].

One more potential pathway for formaldehyde coupling over the Cr(II) site is shown in Fig. 10. Insertion of two formaldehyde molecules into the Cr–O bond results in cyclic product **5A23**. It is known that surface dioxymethylene species are formed on various oxides after formaldehyde adsorption [37,83]. The silanolate oxygen in **5A23** is threefold bonded, as indicated by only moderately elongated Cr–O distance (from 1.81 \AA in **5A4** to 2.07 \AA in **5A23**). Taking into account the relatively low activation barrier

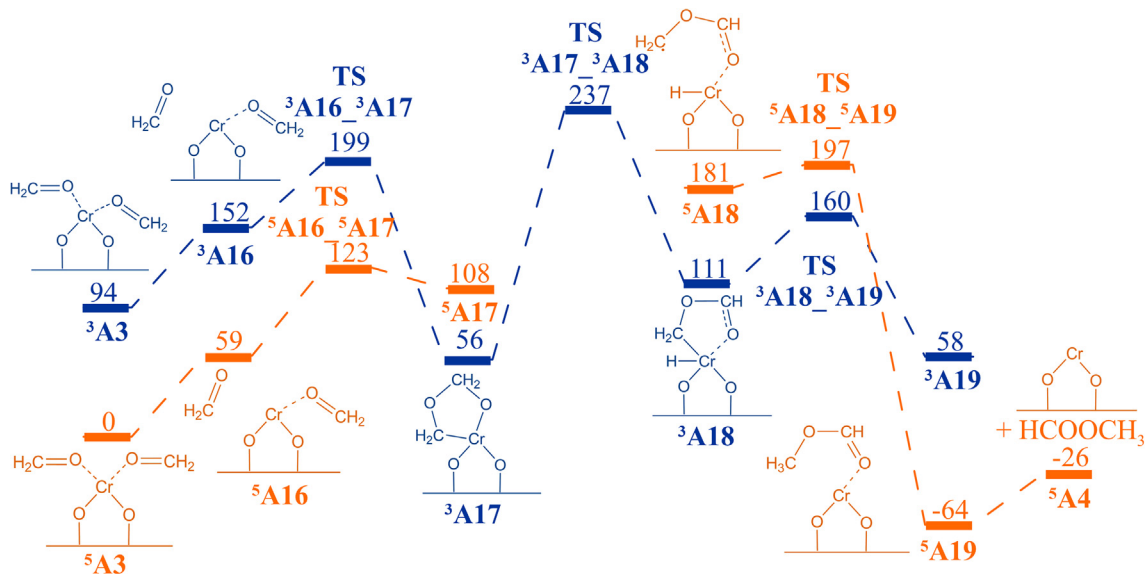


Fig. 8. Gibbs energy profile (kJ mol^{-1}) at $T = 373 \text{ K}$ for the three-step transformation of formaldehyde to methyl formate. Blue and orange colours denote triplet and quintet reaction pathways.

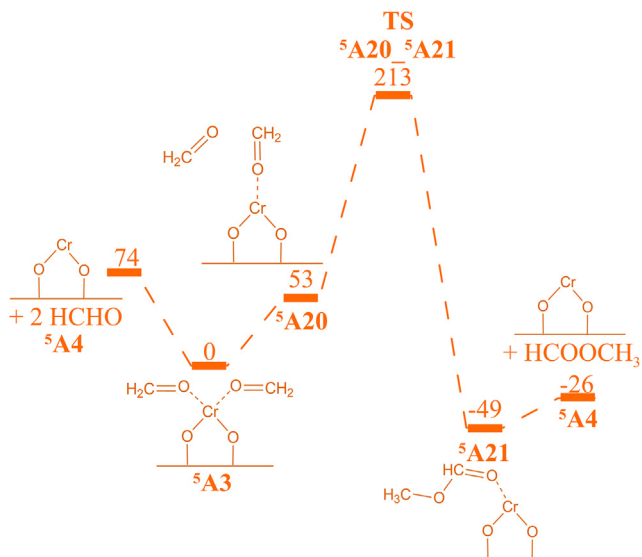


Fig. 9. Gibbs energy profile (kJ mol^{-1}) at $T = 373 \text{ K}$ for the one-step transformation of formaldehyde to methyl formate (quintet reaction pathway).

($\Delta G^\ddagger = 73 \text{ kJ mol}^{-1}$) for this equilibrium reaction ($\Delta G = 10 \text{ kJ mol}^{-1}$), both coordinated Cr(II) species can be present on the catalyst surface. Moreover, ethylene adsorption on ⁵A23 is exergonic by 20 kJ mol^{-1} ($T = 373 \text{ K}$, $p = 1 \text{ atm}$), just increasing the stability of the Cr(II) di(oxymethylene) site under ethylene excess.

To summarize, formaldehyde or intermediate products of its transformations might remain in the coordination sphere of the reduced chromium sites, which is in general agreement with the recent experimental studies [37–39]. Full oxidation of formaldehyde to CO/CO_2 and H_2O is also possible over the $\text{CrO}_x/\text{SiO}_2$ system and, actually, it is predicted to be more kinetically accessible than formaldehyde conversion to methyl formate. These computational results are consistent with the recent temperature programmed surface reaction (TPSR) experiment, where only CO_2 was detected as ethylene oxidation product during the reduction of the surface Cr(VI) species on silica at higher temperatures [26].

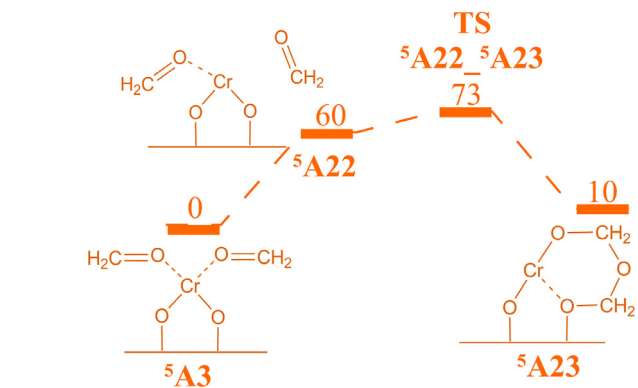


Fig. 10. Gibbs energy profile (kJ mol^{-1}) at $T = 373 \text{ K}$ for formaldehyde coupling resulting in cyclic Cr(II) species (quintet reaction pathway).

3.5. Vibrational frequencies for surface oxygenated products

Selected calculated vibrational frequencies for several stable surface Cr species with organic ligands, localized on the computed pathways, are collected in Table 2. The cyclic Cr(IV) species ³A2 is the intermediate formed during the reduction of the dioxo Cr(VI) species with ethylene (Fig. 2), leading to formaldehyde adsorbed on Cr(II) ⁵A3. The Cr(IV) formate species ³A14 is a possible very stable product of formaldehyde oxidation over the dioxo Cr(VI) species (Fig. 7). The model ⁵A19' represents Cr(II) mono(ethylene) site with methyl formate ligand. Finally, the Cr(II) di(oxymethylene) mono(ethylene) species ⁵A23' can be easily formed by formaldehyde coupling over the Cr(II) site (Fig. 10). Additionally, the positions of the experimental IR absorption bands attributed to ethylene oxidation products in interaction with ethylene-reduced $\text{CrO}_x/\text{SiO}_2$ system, very recently reported by Barzan et al. [39], are also listed in Table 2. The authors assigned them not to adsorbed formaldehyde, but rather to oxygenated products of its disproportionation on the Cr(II) sites, in particular, methyl formate.

It is seen from Table 2 that different species may contribute in the same vibrational region. For instance, $\nu_s(\text{CH}_2)$ modes for the cyclic species ³A2 and ⁵A23' can overlap. The predicted $\nu(\text{CH})$ frequency for the Cr(IV) formate species ³A14 and $\nu_s(\text{CH}_2)$ frequency

Table 2

Calculated vibrational frequencies^a (cm^{-1}) for possible surface Cr species formed after reduction of the $\text{CrO}_x/\text{SiO}_2$ catalyst with ethylene. Vibrational modes for ethylene ligands are omitted. Reported experimental frequencies attributed to adsorbed ethylene oxidation products [39] are listed in the last row of the table.

Surface species	$v_{\text{as}}(\text{CH}_n)$ ^b	$v(\text{CH})$	$v_s(\text{CH}_n)$ ^b	$v_{\text{as}}(\text{OCO})$	$\delta(\text{CH}_n)$ ^b	$\delta(\text{CH})$	$v_s(\text{OCO})$
	2986 2972		2920 2908		1456–1208 ^c		
	3008 3006		2877 2877	1668 ^d 1662 ^d	1449–1207		
		2876		1758 ^e		1376	
	3091 3044	2996	2934	1676 ^f	1466–1431	1398	1362 ^g
	3012 2894		2909 2802		1494–1300		1341 ^h
Exp. [39]	2955 ⁱ (s)	2865 (s)	2892 ^j (s)	1617 (vs) 1573 (vs)	1455 ^k (m)	1383 (s)	1369 (vs)

^a PBE0/def2-SVP calculations. Harmonic frequencies are scaled by 0.9569, 0.9274 and 0.9835 for $v(\text{CH})$, $v(\text{CO})$ and $\delta(\text{CH})$ vibrations, respectively.

^b $n = 2$ or 3.

^c Some vibrational modes include $v(\text{CC})$.

^d $v(\text{CO}) + \delta(\text{CH}_2)$.

^e $v_{\text{as}}(\text{OCO}) + \delta(\text{CH})$.

^f $v_{\text{as}}(\text{OCO}) + \delta(\text{CH}) + \delta(\text{CH}_3)$.

^g $v_s(\text{OCO}) + \delta(\text{CH}_3)$.

^h $v_s(\text{COC}) + v_{\text{as}}(\text{OCO}) + \delta(\text{CH}_2)$.

ⁱ Assigned to $v_{\text{as}}(\text{OCO}) + \delta(\text{CH})$ or $v_{\text{as}}(\text{CH}_3)$ in Ref. [39].

^j Assigned to $v_s(\text{CH}_3)$ in Ref. [39].

^k Assigned to $\delta(\text{CH}_3)$ in Ref. [39].

for formaldehyde coordinated to the Cr(II) site (**5A3**) are almost identical. The stretching modes of the carbonyl groups for formaldehyde and methyl formate adsorbed on the Cr(II) sites would be also observed in the same region, according to our calculations. Hence, any correlation of the theoretical frequencies with the experimental results should be done carefully. It cannot be excluded that various surface species might contribute to the IR bands observed, which is quite reasonable, taking into account the complexity of the reduction process and potential further transformations involved.

3.6. Reduction of the $\text{CrO}_x/\text{SiO}_2$ catalyst by CO

In experimental studies, the $\text{CrO}_x/\text{SiO}_2$ system is commonly pre-reduced by CO to obtain a catalyst showing high activity in ethylene polymerization [1,3,4,35,51,53]. Such a procedure allows to shorten significantly the induction period [9]. However, to the best of our knowledge, the kinetics of the reduction of the Cr(VI) species with CO has never been theoretically studied.

In Figs. 11 and S9 (Supplementary Data), a two-step mechanism for the reduction of the dioxo Cr(VI) species (**1A**) by CO is presented. In the first step, CO attacks one oxo ligand of **1A** to form CO_2 -coordinated monooxo Cr(IV) species **3A25**. The calculated Gibbs energy barrier (164 kJ mol^{-1}) is higher than in the case of the reduction with ethylene (Fig. 2). This is reasonable, since thermal reduction of the $\text{CrO}_x/\text{SiO}_2$ system with CO is usually carried out at much higher temperatures (about 623 K) [4] than the ethylene polymerization process (about 373 K). It is also worth noting that reduction of **1A** by CO (Fig. 11) is less kinetically accessible than reduction of **1A** by formaldehyde (Fig. 7). Decoordination of CO_2 from **3A25** is an exergonic process ($\Delta G = -39 \text{ kJ mol}^{-1}$).

The obtained monooxo Cr(IV) species **3A8** can undergo subsequent reduction with CO, eventually leading to the Cr(II) species **5A4**. Spin-crossing from triplet to quintet takes place and the MECP has been localized (Fig. S9, Supplementary Data). The predicted overall Gibbs energy barrier is rather moderate (143 kJ mol^{-1}).

Potential monooxo Cr(VI) species can be also reduced by CO to give Cr(IV) species **3B7**, 4-fold bonded to the surface (Fig. 12). Although the predicted Gibbs activation barrier for this transformation (150 kJ mol^{-1}) is lower than in the case of the reduction of the dioxo Cr(VI) species (Fig. 11), further reactivity of **3B7** is limited due to the lack of the reactive oxo ligand. We have not found any pathway of **3B7** reduction by CO, considering potential reactions with the bridge oxygen atoms.

4. Conclusions

Detailed DFT studies on the reduction of the Phillips $\text{CrO}_x/\text{SiO}_2$ catalyst with ethylene have been performed for the first time to shed light on the unknown mechanisms of the possible transformations. We have found that the most kinetically favored reduction pathway involves the reaction between ethylene and both oxo ligands of the major dioxo Cr(VI) surface species (Fig. 2). Consequently, the Cr(II) site should be formed together with two formaldehyde molecules.

Although the minor monooxo Cr(VI) species on silica was also proposed by some authors [12–14,26], the idea that it might play a role in ethylene polymerization has not been considered so far in theoretical studies. According to our calculations, initial ethylene reactivity towards the dioxo and monooxo Cr(VI) species can be comparable. However, in the latter case, a very stable cyclic Cr(IV) complex is formed (Fig. 6), being rather a spectator species

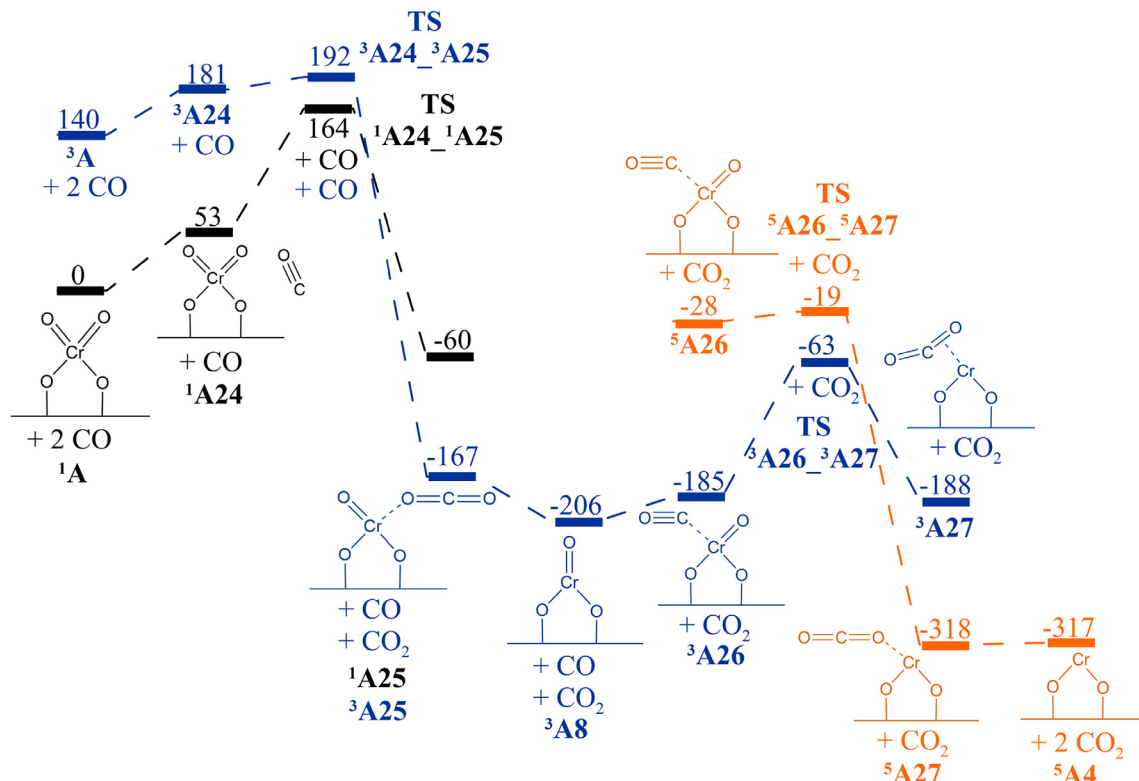


Fig. 11. Gibbs energy profile (kJ mol^{-1}) at $T = 373 \text{ K}$ for the two-step reduction of the dioxo Cr(VI) oxide species with CO. Black, blue and orange colours denote singlet, triplet and quintet reaction pathways, respectively.

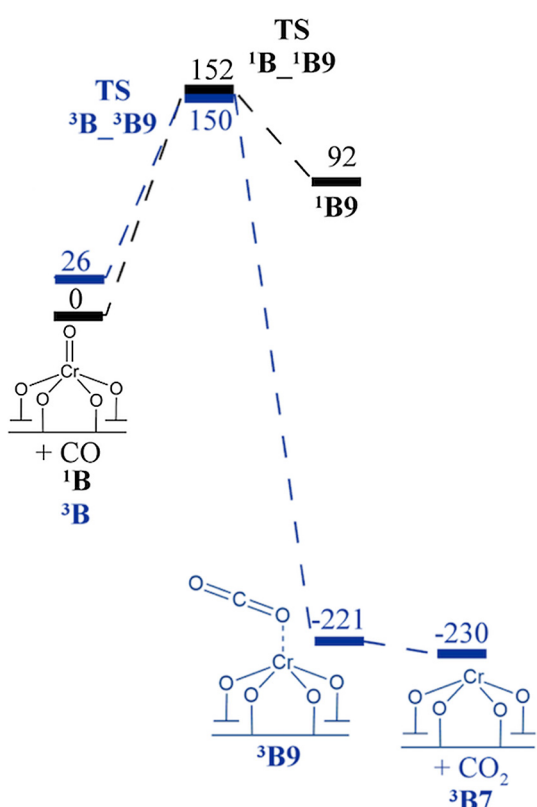


Fig. 12. Gibbs energy profile (kJ mol^{-1}) at $T = 373 \text{ K}$ for the reduction of the monooxo Cr(VI) oxide species with CO. Black and blue colours denote singlet and triplet reaction pathways, respectively.

than a reactive intermediate. This suggests that the participation of the monooxo Cr(VI) species in the catalytic process would be negligible, if any, in accordance with the recent experimental data [26].

Based on the calculated pathways, the mechanism for further formaldehyde oxidation to carbon oxides and water over the dioxo Cr(VI) sites is proposed (Figs. 7 and 11). It might explain, at least to some extent, the reported experimental data indicating CO_2 as the gas phase product of ethylene oxidation over the Cr(VI)/ SiO_2 system at higher temperatures [26]. Formaldehyde to ester conversion over reduced Cr(II) sites, as recently postulated by Barzan et al. [39], has been also considered (Figs. 8 and 9), however, the obtained routes appear to be less kinetically accessible. Transformations of formaldehyde to various surface intermediates (Figs. 7, 8 and 10) are predicted to occur with the barrier heights similar or even lower than those for its formation from ethylene and dioxo Cr (VI) species (Fig. 2). This may explain why formaldehyde is usually not experimentally detected in gas phase during the induction period of ethylene polymerization.

Pathways for the reduction of the $\text{CrO}_x/\text{SiO}_2$ catalyst with CO were also calculated for the first time. This reaction is predicted to be less kinetically favored than reduction using ethylene. The major dioxo Cr(VI) species can be finally reduced to Cr(II), whereas reduction of the potential minor monooxo Cr(VI) species would lead to the Cr(IV) species 4-fold bonded to the surface.

Acknowledgments

This work was supported by the National Science Centre, Poland, Project No. 2015/19/N/ST4/00007, and by the PL-Grid Infrastructure.

Appendix A. Supplementary material

Supplementary data associated with this article can be found, in the online version, at <https://doi.org/10.1016/j.jcat.2018.01.014>.

References

- [1] M.P. McDaniel, in: *Adv. Catal.*, vol. 53, 2010, pp. 123–606.
- [2] B.M. Weckhuysen, I.E. Wachs, R.A. Schoonheydt, *Chem. Rev.* 96 (1996) 3327–3349.
- [3] E. Groppo, C. Prestipino, F. Cesano, F. Bonino, S. Bordiga, C. Lamberti, P. Thune, J. W. Niemantsverdriet, A. Zecchina, *J. Catal.* 230 (2005) 98–108.
- [4] E. Groppo, C. Lamberti, S. Bordiga, G. Spoto, A. Zecchina, *Chem. Rev.* 105 (2005) 115–183.
- [5] M.P. McDaniel, K.S. Collins, E.A. Benham, T.H. Cymbaluk, *Appl. Catal. A Gen.* 335 (2008) 252–261.
- [6] C.A. Demmelmair, R.E. White, J.A. van Bokhoven, S.L. Scott, *J. Catal.* 262 (2009) 44–56.
- [7] A. Zecchina, S. Bordiga, E. Groppo, *Selective Nanocatalysts and Nanoscience: Concepts for Heterogeneous and Homogeneous Catalysis*, Wiley-VCH, 2011.
- [8] L. Zhong, M.-Y. Lee, Z. Liu, Y.-J. Wanglee, B. Liu, S.L. Scott, *J. Catal.* 293 (2012) 1–12.
- [9] M.P. McDaniel, *Appl. Catal. A Gen.* 542 (2017) 392–410.
- [10] J.P. Hogan, R.L. Banks, Polymers and Production Thereof, US Patent 2 825 721, 1958.
- [11] P. Michorczyk, P. Pietrzyk, J. Ogonowski, *Micropor. Mesopor. Mater.* 161 (2012) 56–66.
- [12] E.L. Lee, I.E. Wachs, *J. Phys. Chem. C* 111 (2007) 14410–14425.
- [13] E.L. Lee, I.E. Wachs, *J. Phys. Chem. C* 112 (2008) 6487–6498.
- [14] A. Chakrabarti, I.E. Wachs, *Catal. Lett.* 145 (2015) 985–994.
- [15] C. Moisii, E.W. Deguns, A. Lita, S.D. Callahan, L.J. van de Burgt, D. Magana, A.E. Stiegman, *Chem. Mater.* 18 (2006) 3965–3975.
- [16] J.J.H.B. Sattler, J. Ruiz-Martinez, E. Santillan-Jimenez, B.M. Weckhuysen, *Chem. Rev.* 114 (2014) 10613–10653.
- [17] B.M. Weckhuysen, L.M. De Ridder, R.A. Schoonheydt, *J. Phys. Chem.* 97 (1993) 4756–4763.
- [18] B.M. Weckhuysen, A.A. Verberckmoes, A.L. Buttiens, R.A. Schoonheydt, *J. Phys. Chem.* 98 (1994) 579–584.
- [19] B.M. Weckhuysen, R.A. Schoonheydt, J.-M. Jehng, I.E. Wachs, S.J. Cho, R. Ryoo, S. Kijlstra, E. Poels, *J. Chem. Soc. Faraday Trans.* 91 (1995) 3245–3253.
- [20] B.M. Weckhuysen, R.A. Schoonheydt, *Catal. Today* 49 (1999) 441–451.
- [21] T.J. Dines, S. Inglis, *Phys. Chem. Chem. Phys.* 5 (2003) 1320–1328.
- [22] V.N. Panchenko, V.A. Zakharov, E.A. Paukshtis, *Appl. Catal. A Gen.* 313 (2006) 130–136.
- [23] A. Zecchina, E. Groppo, A. Damin, C. Prestipino, *Top. Organomet. Chem.* 16 (2005) 1–35.
- [24] H. Guesmi, F. Tielens, *J. Phys. Chem. C* 116 (2012) 994–1001.
- [25] J. Handzlik, R. Grybos, F. Tielens, *J. Phys. Chem. C* 117 (2013) 8138–8149.
- [26] A. Chakrabarti, M. Gierada, J. Handzlik, I.E. Wachs, *Top. Catal.* 59 (2016) 725–739.
- [27] M. Gierada, P. Michorczyk, F. Tielens, J. Handzlik, *J. Catal.* 340 (2016) 122–135.
- [28] D.S. Kim, I.E. Wachs, *J. Catal.* 142 (1993) 166–171.
- [29] D.S. Kim, J.-M. Tatibouet, I.E. Wachs, *J. Catal.* 136 (1992) 209–221.
- [30] M.A. Vuurman, I.E. Wachs, D.J. Stufkens, A. Oskam, *J. Mol. Catal.* 80 (1993) 209–227.
- [31] I.E. Wachs, C.A. Roberts, *Chem. Soc. Rev.* 39 (2010) 5002–5017.
- [32] E. Groppo, A. Damin, F. Bonino, A. Zecchina, S. Bordiga, C. Lamberti, *Chem. Mater.* 17 (2005) 2019–2027.
- [33] B. Liu, H. Nakatani, M. Terano, *J. Mol. Catal. A Chem.* 184 (2002) 387–398.
- [34] B. Liu, H. Nakatani, M. Terano, *J. Mol. Catal. A Chem.* 201 (2003) 189–197.
- [35] C. Brown, J. Krzystek, R. Achey, A. Lita, R. Fu, R.W. Meulenbergh, M. Polinski, N. Peek, Y. Wang, L.J. van de Burgt, S. Profeta Jr., A.E. Stiegman, S.L. Scott, *ACS Catal.* 5 (2015) 5574–5583.
- [36] L.M. Baker, W.L. Carrick, *J. Org. Chem.* 33 (1968) 616–618.
- [37] K.C. Potter, C.W. Beckerle, F.C. Jentoft, E. Schwerdtfeger, M.P. McDaniel, *J. Catal.* 344 (2016) 657–668.
- [38] C. Barzan, A.A. Damin, A. Budnyk, A. Zecchina, S. Bordiga, E. Groppo, *J. Catal.* 337 (2016) 45–51.
- [39] C. Barzan, A. Piovano, L. Braglia, G.A. Martino, C. Lamberti, S. Bordiga, E. Groppo, *J. Am. Chem. Soc.* 139 (2017) 17064–17073.
- [40] M. Gierada, J. Handzlik, *J. Catal.* 352 (2017) 314–328.
- [41] Ø. Espelid, K.J. Børve, *J. Catal.* 195 (2000) 125–139.
- [42] A. Fong, Y. Yuan, S.L. Ivry, S.L. Scott, B. Peters, *ACS Catal.* 5 (2015) 3360–3374.
- [43] L. Zhong, Z. Liu, R. Cheng, S. Tang, P. Qiu, X. He, M. Terano, B. Liu, *ChemCatChem* 4 (2012) 872–881.
- [44] K.Y. Choi, S. Tang, *J. Appl. Polym. Sci.* 91 (2004) 2923–2927.
- [45] K.Y. Choi, S. Tang, W.J. Yoon, *Macromol. Theory Simul.* 13 (2004) 169–177.
- [46] A.B. Gaspar, L.C. Dieguez, *Appl. Catal. A Gen.* 227 (2002) 241–254.
- [47] S.L. Scott, J. Amor Nait Ajjou, *Chem. Eng. Sci.* 56 (2001) 4155–4168.
- [48] J. Amor Nait Ajjou, S.L. Scott, *J. Am. Chem. Soc.* 122 (2000) 8968–8976.
- [49] Ø. Espelid, K.J. Børve, *J. Catal.* 205 (2002) 366–374.
- [50] Ø. Espelid, K.J. Børve, *J. Catal.* 206 (2002) 331–338.
- [51] E. Groppo, C. Lamberti, S. Bordiga, G. Spoto, A. Zecchina, *J. Catal.* 240 (2006) 172–181.
- [52] A. Fong, B. Peters, S.L. Scott, *ACS Catal.* 6 (2016) 6073–6085.
- [53] M.F. Delley, M.P. Conley, C. Copéret, *Catal. Lett.* 144 (2014) 805–808.
- [54] A.F. Wright, A.J. Leadbetter, *Philos. Mag.* 31 (1975) 1391–1401.
- [55] M.P. Conley, M.F. Delley, F. Núñez-Zarur, A. Comas-Vives, C. Copéret, *Inorg. Chem.* 54 (2015) 5065–5078.
- [56] J. Handzlik, *J. Phys. Chem. C* 111 (2007) 9337–9348.
- [57] J. Handzlik, M. Czernecki, A. Shiga, P. Śliwa, *Comput. Theor. Chem.* 991 (2012) 174–181.
- [58] C. Adamo, V. Barone, *J. Chem. Phys.* 110 (1999) 6158–6170.
- [59] M. Bühl, C. Reimann, D.A. Pantazis, T. Bredow, F. Neese, *J. Chem. Theory Comput.* 4 (2008) 1449–1459.
- [60] P. Śliwa, J. Handzlik, *Chem. Phys. Lett.* 493 (2010) 273–278.
- [61] R. Kang, H. Chen, S. Shaik, J. Yao, *J. Chem. Theory Comput.* 7 (2011) 4002–4011.
- [62] F. Weigend, R. Ahlrichs, *Phys. Chem. Chem. Phys.* 7 (2005) 3297–3305.
- [63] C. Gonzalez, H.B. Schlegel, *J. Chem. Phys.* 90 (1989) 2154–2161.
- [64] C. Gonzalez, H.B. Schlegel, *J. Phys. Chem.* 94 (1990) 5523–5527.
- [65] S. Kudoh, M. Takayanagi, M. Nakata, *Chem. Phys. Lett.* 322 (2000) 363–370.
- [66] H. Yoshida, A. Ehara, H. Matsuura, *Chem. Phys. Lett.* 325 (2000) 477–483.
- [67] S. Grimme, J. Antony, S. Ehrlich, H. Krieg, *J. Chem. Phys.* 132 (2010) 154104.
- [68] S. Grimme, S. Ehrlich, L. Goerigk, *J. Comput. Chem.* 32 (2011) 1456–1465.
- [69] J.N. Harvey, M. Aschi, H. Schwarz, W. Koch, *Theor. Chem. Acc.* 99 (1998) 95–99.
- [70] M.J. Frisch, G.W. Trucks, H.B. Schlegel, G.E. Scuseria, M.A. Robb, J.R. Cheeseman, G. Scalmani, V. Barone, B. Mennucci, G.A. Petersson, H. Nakatsuji, M. Caricato, X. Li, H.P. Hratchian, A.F. Izmaylov, J. Bloino, G. Zheng, J.L. Sonnenberg, M. Hada, M. Ehara, K. Toyota, R. Fukuda, J. Hasegawa, M. Ishida, T. Nakajima, Y. Honda, O. Kitao, H. Nakai, T. Vreven, J.A. Montgomery, Jr., J.E. Peralta, F. Ogliaro, M. Bearpark, J.J. Heyd, E. Brothers, K.N. Kudin, V.N. Staroverov, R. Kobayashi, J. Normand, K. Ragahavachari, A. Rendell, J.C. Burant, S.S. Iyengar, J. Tomasi, M. Cossi, N. Rega, J.M. Millam, M. Klene, J.E. Knox, J.B. Cross, V. Bakken, C. Adamo, J. Jaramillo, R. Gomperts, R.E. Stratmann, O. Yazyev, A.J. Austin, R. Cammi, C. Pomelli, J.W. Ochterski, R.L. Martin, K. Morokuma, V.G. Zakrzewski, G.A. Voth, P. Salvador, J.J. Dannenberg, S. Dapprich, A.D. Daniels, O. Farkas, J.B. Foresman, J.V. Ortiz, J. Cioslowski, D.J. Fox, *Gaussian 09, Revision D.01*, Gaussian Inc., Wallingford CT, 2013.
- [71] R. Dennington, T.A. Keith, J.M. Millam, *GaussView, Version 5*, Semichem Inc., Shawnee Mission, KS, 2009.
- [72] B. Liu, Y. Fang, M. Terano, *Mol. Simul.* 30 (2004) 963–971.
- [73] E. Groppo, A. Damin, C. Otero Arean, A. Zecchina, *Chem. Eur. J.* 17 (2011) 11110–11114.
- [74] C. Limberg, R. Köppé, H. Schnöckel, *Angew. Chem. Int. Ed.* 37 (1998) 496–499.
- [75] J. Guan, G. Yang, D. Zhou, W. Zhang, X. Liu, X. Han, X. Bao, *Catal. Commun.* 9 (2008) 2213–2216.
- [76] X. Li, J. Guan, A. Zheng, D. Zhou, X. Han, W. Zhang, X. Bao, *J. Mol. Catal. A Chem.* 330 (2010) 99–106.
- [77] A. Salameh, C. Copéret, J.M. Basset, V.P.W. Böhm, M. Röper, *Adv. Synth. Catal.* 349 (2007) 238–242.
- [78] T. Maihom, M. Probst, J. Limtrakul, *ChemPhysChem* 16 (2015) 3334–3339.
- [79] M.P. Conley, M.F. Delley, G. Siddiqi, G. Lapadula, S. Norsic, V. Monteil, O.V. Safonova, C. Copéret, *Angew. Chem. Int. Ed.* 53 (2014) 1872–1876.
- [80] M.F. Delley, F. Nuñez-Zarur, M.P. Conley, A. Comas-Vives, G. Siddiqi, S. Norsic, V. Monteil, O.V. Safonova, C. Copéret, *Proc. Natl. Acad. Sci. USA* 111 (2014) 11624–11629.
- [81] L. Floryan, A.P. Borosy, F. Núñez-Zarur, A. Comas-Vives, C. Copéret, *J. Catal.* 346 (2017) 50–56.
- [82] M.F. Delley, C.S. Praveen, A.P. Borosy, F. Núñez-Zarur, A. Comas-Vives, C. Copéret, *J. Catal.* 354 (2017) 223–230.
- [83] G. Busca, J. Lamotte, J.-C. Lavallee, V. Lorenzelli, *J. Am. Chem. Soc.* 109 (1987) 5197–5202.
- [84] Y. Hoshimoto, M. Ohashi, S. Ogoshi, *J. Am. Chem. Soc.* 133 (2011) 4668–4671.
- [85] D. Gianolio, E. Groppo, J.G. Vitillo, A. Damin, S. Bordiga, A. Zecchina, C. Lamberti, *Chem. Commun.* 46 (2010) 976–978.
- [86] A. Budnyk, A. Damin, E. Groppo, A. Zecchina, S. Bordiga, *J. Catal.* 324 (2015) 79–87.

10. Deklaracje współautorów

Kraków, 28 V 2018

Oświadczenie o udziale w publikacji

Oświadczam, że udział w pracy opublikowanej wspólnie z mgr inż. Maciejem Gieradą jest zgodny z opisem poniżej:

Artykuł:

Maciej Gierada, Jarosław Handzlik
Zastosowanie oraz struktura form powierzchniowych układów katalitycznych Cr/SiO_2
Przem. Chem. 94(6) (2015) 900-905

Udział:

- **mgr inż. Maciej Gierada**

opracowanie koncepcji artykułu, przegląd literaturowy, opracowanie tekstu i przygotowanie do druku, korespondencja z edytorem, przygotowanie odpowiedzi na recenzje.

- **dr hab. inż. Jarosław Handzlik, prof. PK**

konsultacja naukowa, współludział w opracowaniu tekstu, współludział w odpowiedzi na recenzje.


Maciej Gierada


Jarosław Handzlik

Cracow, 28 V 2018

Authorship statement

I declare that my personal scientific contribution to the paper written in collaboration with mgr. inż. Maciej Gierada is according to the description below:

Publication:

Maciej Gierada, Piotr Michorczyk,✉ Frederik Tielens, Jarosław Handzlik✉
Reduction of chromia-silica catalyst: A molecular picture
J. Catal. 340 (2016) 122-135

Contribution:

- **mgr inż. Maciej Gierada**

literature survey, participation in preparing general concept of the manuscript, modelling most of the surface species, performing all QM calculations excluding TD-DFT, participation in data analysis, preparing the first version of the manuscript, proposition of conclusions, participation in responding to referees.

- **dr hab. inż. Piotr Michorczyk, prof. PK**

participation in preparing general concept of the manuscript, performing the experiments, participation in data analysis, preparing experimental part of the manuscript, scientific discussion, participation in responding to referees.

- **dr hab. inż. Jarosław Handzlik, prof. PK**

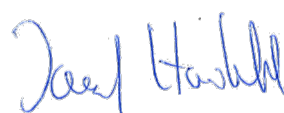
participation in literature survey, general concept of the manuscript, preparing models of monomeric Cr(VI) oxide species, scientific discussion, performing TD-DFT calculations, participation in data analysis, correction of the first version of the manuscript, correspondence with editor, participation in responses to referees.

- **prof. Frederik Tielens**

participation in model development, scientific discussion, proof-reading.

 
Maciej Gierada Piotr Michorczyk


Frederik Tielens


Jarosław Handzlik

Cracow, 28 V 2018

Authorship statement

I declare that my personal scientific contribution to the paper written in collaboration with mgr. inż. Maciej Gierada is according to the description below:

Publication:

Anisha Chakrabarti, **Maciej Gierada**, Jarosław Handzlik, Israel E. Wachs✉
Operando Molecular Spectroscopy During Ethylene Polymerization by Supported CrO_x/SiO_2 Catalysts: Active Sites, Reaction Intermediates, and Structure-Activity Relationship
Top. Catal. 59 (2016) 725-739

Contribution:

- **Dr. Anisha Chakrabarti**

literature survey, participation in preparing general concept of the manuscript, conducting all experiments, data analysis, proposition of conclusions, preparing the first version of the manuscript, participation in responding to referees.

- **mgr inż. Maciej Gierada**

participation in literature survey, modelling all surface species, performing all *QM* calculations, participation in data analysis, preparing computational part of the paper, proposition of conclusions from the computational part of the paper, participation in responding to referees.

- **dr hab. inż. Jarosław Handzlik, prof. PK**

correction of the computational part of the paper, scientific discussion, participation in responding to referees.

- **prof. Israel E. Wachs**

general concept of manuscript, scientific discussion, participation in data analysis, correction of the final version of the manuscript, correspondence with editor, responding to referees.



Anisha Chakrabarti Maciej Gierada Jarosław Handzlik Israel E. Wachs
Anisha Chakrabarti Maciej Gierada Jarosław Handzlik Israel E. Wachs

Kraków, 28 V 2018

Oświadczenie o udziale w publikacji

Oświadczam, że udział w pracy opublikowanej wspólnie z mgr inż. Maciejem Gieradą jest zgodny z opisem poniżej:

Artykuł:

Maciej Gierada, Jarosław Handzlik✉

Active sites formation and their transformations during ethylene polymerization by the Phillips CrO_x/SiO_2 catalyst

J. Catal. 352 (2017) 314-328

Udział:

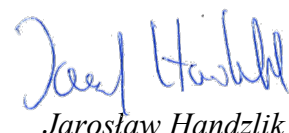
- **mgr inż. Maciej Gierada**

opracowanie koncepcji artykułu, przegląd literaturowy, przygotowanie modeli, wykonanie wszystkich obliczeń, opracowanie wyników, zaproponowanie wniosków, przygotowanie pierwszej wersji manuskryptu, udział w przygotowaniu odpowiedzi na recenzje.

- **dr hab. inż. Jarosław Handzlik, prof. PK**

współdziałał w przygotowaniu koncepcji artykułu, dyskusja naukowa, współdziałał w opracowaniu tekstu i jego korekty, współdziałał w analizie wyników, korespondencja z edytorem, przygotowanie odpowiedzi na recenzje.


Maciej Gierada


Jarosław Handzlik

Kraków, 28 V 2018

Oświadczenie o udziale w publikacji

Oświadczam, że udział w pracy opublikowanej wspólnie z mgr inż. Maciejem Gieradą jest zgodny z opisem poniżej:

Artykuł:

Maciej Gierada, Jarosław Handzlik✉

Computational insights into reduction of the Phillips CrO_x/SiO_2 catalyst by ethylene and CO
J. Catal. 359 (2018) 261-271

Udział:

- **mgr inż. Maciej Gierada**

opracowanie koncepcji artykułu, przegląd literaturowy, przygotowanie modeli, wykonanie wszystkich obliczeń, opracowanie wyników, zaproponowanie wniosków, przygotowanie pierwszej wersji manuskryptu, udział w przygotowaniu odpowiedzi na recenzje.

- **dr hab. inż. Jarosław Handzlik, prof. PK**

współdziałał w przygotowaniu koncepcji artykułu, dyskusja naukowa współdziałał w opracowaniu tekstu i jego korekty, współdziałał w analizie wyników, korespondencja z edytorem, przygotowanie odpowiedzi na recenzje.


Maciej Gierada


Jarosław Handzlik

11. Wykaz dorobku naukowego

Doświadczenie naukowe i zawodowe:

IV 2018	UPMC Sorbonne Université Wizyta naukowa, Paryż, Francja.
I – IV 2018	Vrije Universiteit Brussel, Staż naukowy, Bruksela, Belgia.
XI – XII 2015	Laboratoire de Chimie de la Matière Condensée de Paris, UPMC, Collège de France , Staż naukowy, Paryż, Francja.
X 2013 - II 2015	Centrum Pedagogiki i Psychologii Politechniki Krakowskiej, Kurs Pedagogiczny, Kraków, Polska
X - XII 2014	XI Liceum Ogólnokształcące im. Marii Dąbrowskiej w Krakowie, Praktyka Pedagogiczna, Kraków, Polska
IX 2013	Московский государственный университет , Staż naukowy, Moskwa, Rosja.

Projekty badawcze:

3. **Kierownik projektu NCN PRELUDIUM 10** nr **UMO-2015/19/N/ST4/00007** „*Od prekursora tlenkowego do centrum aktywnego – teoretyczne badania mechanizmu polimeryzacji etylenu na katalizatorze Phillipsa*” (18 VII 2016 – 17 VII 2018).
2. **Wykonawca projektu NCN OPUS 10** nr **UMO-2015/19/B/ST4/01836** „*Nowe uporządkowane nanoporowate katalizatory dla procesu metatezy olefin - struktura form powierzchniowych oraz mechanizm reakcji w ujęciu eksperymentalnym i teoretycznym*” (22 VII 2016 – 21 VII 2019).
1. **Kierownik tematu C-2/294/2016/DS-M** „*Badanie mechanizmu redukcji katalizatora Phillipsa*” (21 IV – 8 XII 2016).

Publikacje (inne niż wymienione w rozdziale 5)

4. **M. Gierada,✉** I. Petit, J. Handzlik, F. Tielens,✉ *Hydration in silica based mesoporous materials: a DFT model* **Phys. Chem. Chem. Phys.** 18 (2016) 32962-32972, <http://dx.doi.org/10.1039/c6cp05460a> (IF = 4.449)
3. P.J. Jodłowski,✉ R.J. Jędrzejczyk, D.K. Chlebda, **M. Gierada**, J. Łojewska, *In situ spectroscopic studies of methane catalytic combustion over Co, Ce, and Pd mixed oxides deposited on a steel surface*, **J. Catal.** 350 (2017) 1-12, <http://dx.doi.org/10.1016/j.jcat.2017.03.022> (IF = 7.354)

2. **M. Gierada**,✉ I. Czeluśniak, J. Handzlik,✉ *Terminal-Alkyne-Induced Decomposition of a Phosphine-Free Ruthenium Alkylidene Catalyst*, **ChemCatChem** 9 (2017) 2284-2291
<http://dx.doi.org/10.1002/cctc.201601647> (IF = 4.724)
1. I. Czeluśniak,✉ J. Handzlik, **M. Gierada**, T. Szymańska-Buzar *Catalytic transformation of phenylacetylene mediated by phosphine-free ruthenium alkylidene complexes*
J. Organom. Chem. 786 (2015) 31-39
<http://dx.doi.org/10.1016/j.jorganchem.2015.03.025> (IF = 2.173)

Autorstwo rozdziałów w opracowaniach zbiorowych:

4. **M. Gierada**,✉ Teoretyczne badania układów chemiczny – metody *ab initio* w chemii kwantowej; Fizyczne, chemiczne i biologiczne aspekty nauki, **Wydawnictwo Naukowe TYGIEL sp. z o. o.**, ISBN: 978-83-65598-20-2; s. 243-258, Lublin, 2016.
3. **M. Gierada**,✉ *Monoterpeny – co o nich wiemy?*; Rośliny: fizjologia, uprawa i ich interdyscyplinarne wykorzystanie, **Fundacja na rzecz promocji nauki i rozwoju TYGIEL**, ISBN: 978-83-65272-12-6; s. 246-260, Lublin, 2015.
2. **M. Gierada**,✉ R. Rachwalik, *Rola reakcji ubocznych w procesie izomeryzacji α -pinenu*; Biotechnologia w analizie, ochronie środowiska, medycynie i przemyśle, **Fundacja na rzecz promocji nauki i rozwoju TYGIEL**, ISBN: 978-83-65272-06-5; s. 221-230, Lublin, 2015.
1. **M. Gierada**,✉ „*Costs of knowledge*”, Экономический вектор, Международной научно-практической студенческой конференции "Экономика и менеджмент"; s. 261-263, Sankt Petersburg, 2016

Nagrody i stypendia:

9. Nagroda Zespołowa Rektora Politechniki Krakowskiej za Osiągnięcia Naukowe, 15 XII 2017, Kraków, Polska.
8. Stypendium Ministra Nauki i Szkolnictwa Wyższego RP dla Doktorantów za Wybitne Osiągnięcia przyznane na rok akademicki 2017/18, 13 XII 2017, Warszawa, Polska.
7. Theoretical Chemistry and Computational Modelling (TCCM) Doctorate Program Prize for Young Scientist, 8 VII 2017, Barcelona, Hiszpania
6. Density Functional Theory 2017 (DFT 2017) Prize for Young Scientist, 21-25 VIII 2017, Tällberg, Szwecja

5. Nagroda Rektora Politechniki Krakowskiej dla najmłodszego pierwszego autora publikacji naukowej w czasopiśmie zagranicznym wskazanym w części A, aktualnego wykazu MNiSW sporządzonego dla potrzeb oceny parametrycznej jednostek naukowych, 12 V 2017, Kraków, Polska
4. Stypendium Rektora PK dla Najlepszych Doktorantów – rok akad. 2014/15; 2015/16, 2016/17; 2017/18
3. Zwiększenie Stypendium Doktoranckiego z Dotacji Projakościowej – rok akad. 2014/15; 2015/16; 2016/17; 2017/18
2. Stypendium Doktoranckie – rok akad. 2017/18
1. Stypendium Doktorskie – IV 2016 – IX 2017

Działalność organizacyjna

4. Członek Doktoranckiej Komisji Stypendialnej WIiTCh PK – kadencja 2014/15 oraz 2015/16
3. Członek Komisji Rekrutacyjnej na Studia III stopnia WIiTCh PK – kadencja 2015/16
2. Członek Samorządu Doktorantów WIiTCh PK – kandencja 2014/15
1. Przedstawiciel Doktorantów WIiTCh PK w Komisji ds. Dydaktyki i Rozwoju Naukowego – kadencja 2014/15

Udział w konferencjach naukowych (18 osobistych komunikatów ustnych w języku obcym na konferencjach międzynarodowych):

45. M. Gierada, F. Tielens, I. Petit, J. Handzlik, **Komunikat ustny (przyjęty):** “Modelling of $\text{CrO}_x/\text{SiO}_2$ and WO_x/SiO_2 catalysts - formation of active sites for ethylene polymerization and propene metathesis”, International Conference on Theoretical Aspects of Catalysis (ICTAC 17), 24-28 VI 2018, Los Angeles, CA, USA.
44. J. Handzlik, K. Kurleto, M. Gierada **Poster:** “Formation of metathesis active sites in $\text{MoO}_x/\text{SiO}_2$ and WO_x/SiO_2 systems from theoretical perspective”, International Conference on Catalysis and Surface Chemistry 2018/50th Ogólnopolskie Kolokwium Katalityczne (50th Polish Annual Conference on Catalysis), 18-23 III 2018, Kraków, Polska.
43. M. Gierada, J. Handzlik, **Poster:** “Reduction of the Phillips $\text{CrO}_x/\text{SiO}_2$ catalyst by ethylene”, International Conference on Catalysis and Surface Chemistry 2018/50th Ogólnopolskie Kolokwium Katalityczne (50th Polish Annual Conference on Catalysis), 18-23 III 2018, Kraków, Polska.

42. M. Gierada, Kamil Kurleto, J. Handzlik, **Komunikat ustny:** “Mechanistic aspects of alkene metathesis over WO_x/SiO_2 system - an initiation stage”, International Conference on Catalysis and Surface Chemistry 2018/50th Ogólnopolskie Kolokwium Katalityczne (50th Polish Annual Conference on Catalysis), 18-23 III 2018, Kraków, Polska.
41. F. Tielens, M. Gierada, I. Petit, J. Handzlik, **Komunikat ustny:** “Silica Based Mesoporous Materials Investigated by DFT”, 34th GFZ Congress - Groupe Français des Zéolithes, 26-29 III 2018, Cabourg, Francja.
40. M. Gierada, I. Petit, J. Handzlik, F. Tielens **Komunikat ustny:** “Modelling of mesoporous amorphous silica – the case of the MCM-41”, 6th TCCM workshop, 8 IX 2017, Barcelona, Hiszpania.
39. M. Gierada, J. Handzlik, **Research Telegram + Poster:** “Computational insights into reactivity of the Phillips $\text{CrO}_x/\text{SiO}_2$ catalyst – role of amorphous silica model”, 11th European Conferences on Theoretical and Computational Chemistry, 4-7 IX 2017, Barcelona, Hiszpania.
38. J. Handzlik, M. Gierada, **Poster:** “Assessment of DFT methods for studying olefin metathesis catalysed by molybdenum and tungsten system”, 11th European Conferences on Theoretical and Computational Chemistry, 4-7 IX 2017, Barcelona, Hiszpania.
37. P.J. Jodłowski, R.J. Jędrzejczyk, D.K. Chlebda, M. Gierada, J. Łojewska, **Komunikat ustny:** “In situ spectroscopic studies of methane catalytic combustion over Co, Ce, and Pd mixed oxides deposited on a steel surface”, 14th International Conference of Molecular Spectroscopy “From Molecules to Functional Materials”, 3-7 IX 2017, Białka Tarzańska, Polska.
36. J. Handzlik, K. Kurleto, M. Gierada, **Poster:** “Computational insight into initiation mechanisms for olefin metathesis over $\text{MoO}_x/\text{SiO}_2$ and WO_x/SiO_2 catalysts”, 13th European Congress on Catalysis EUROPACAT 2017, 27-31 VIII 2017, Florencja, Włochy.
35. M. Gierada, J. Handzlik, **Poster:** “Computational insights into induction period of ethylene polymerization by the $\text{CrO}_x/\text{SiO}_2$ (Phillips) catalyst”, 11th Triennial Congress of the World Association of Theoretical and Computational Chemists (WATOC 2017), 27 VIII - 1 IX 2017 Monachium, Niemcy.
34. M. Gierada, J. Handzlik, **Komunikat ustny:** “Computational insights into reactivity of the supported $\text{CrO}_x/\text{SiO}_2$ (Phillips) catalyst towards ethylene”, 17th International Conference on Density Functional Theory and its Applications, 21-25 VIII 2017, Tällberg, Szwecja.
33. M. Gierada, I. Petit, J. Handzlik, F. Tielens, **Poster:** „Representative and calculable DFT models of the mesoporous silicas”, Current and Future Perspectives of Chemical Modelling in Astrophysics, 17-19 VII 2017, Hamburg, Niemcy.
32. M. Gierada, J. Handzlik, **Poster:** “Mechanism of ethylene polymerization catalysed by the $\text{CrO}_x/\text{SiO}_2$ Phillips catalyst – DFT studies”, Gaussian 16 Workshop “Expanding the limits of computational chemistry” 10-14 VII 2017, Santiago de Compostela, Hiszpania.

31. M. Gierada, J. Handzlik, **Poster:** „Terminal alkynes induced decomposition of phosphine-free ruthenium alkylidene catalyst”, XLIX Ogólnopolskie Kolokwium Katalityczne (XLIX Polish Annual Conference on Catalysis), 15-17 III 2017, Kraków, Polska.
30. P. Jodłowski, R.J. Jędrzejczyk, D. Chlebda, M. Gierada, J. Łojewska, **Flash Oral + Poster:** „In situ spectroscopic studies of methane catalytic combustion over Co, Ce, and Pd mixed oxides deposited on a steel surface”, XLIX Ogólnopolskie Kolokwium Katalityczne (XLIX Polish Annual Conference on Catalysis), 15-17 III 2017, Kraków, Polska.
29. M. Gierada, J. Handzlik, **Flash Oral + Poster:** „Towards better understanding of ethylene polymerization over the Phillips $\text{CrO}_x/\text{SiO}_2$ catalyst”, XLIX Ogólnopolskie Kolokwium Katalityczne (XLIX Polish Annual Conference on Catalysis), 15-17 III 2017, Kraków, Polska.
28. M. Gierada, I. Petit, J. Handzlik, F. Tielens, **Komunikat ustny:** „Realistic and calculable DFT models of the MCM-41 mesoporous silica”, Konferencja Użytkowników Komputerów Dużej Mocy 2017 (KU KDM’17), 8-10 III 2017, Zakopane, Polska.
27. M. Gierada, I. Petit, J. Handzlik, F. Tielens, **Komunikat ustny:** „Towards realistic DFT model of the MCM-41 mesoporous silica”, XXI Zeolite Forum, 7-11 II 2017, Boszkowo, Polska.
26. M. Gierada, J. Handzlik, **Poster:** “Struktura i właściwości redox monomerycznych i dimerycznych form tlenkowych układu $\text{CrO}_x/\text{SiO}_2$ – Badania DFT”, III Ogólnopolskie Forum Chemii Nieorganicznej, 7-9 XII 2016, Kraków, Polska.
25. M. Gierada, J. Handzlik, **Komunikat ustny:** “Theoretical aspects of ethylene polymerization by the supported ($\text{CrO}_x/\text{SiO}_2$) Phillips catalyst”, CGW ’16 Workshop 24-26 X 2016, Kraków, Polska.
24. M. Gierada, J. Handzlik, **Poster:** “Computational insights into mechanism of ethylene polymerization over the Phillips $\text{CrO}_x/\text{SiO}_2$ catalyst”, International Workshop on Functional Nanoporous Materials “FuNaM” 13-14 X 2016, Kraków, Polska.
23. J. Handzlik, P. Śliwa, M. Gierada, **Wykład na zaproszenie** “Teoretyczne aspekty przemian winylosilanów oraz terminalnych alkinów w obecności katalizatorów rutenowych typu Grubbsa”, 59 Zjazd Naukowy PTChem 19-23 IX 2016, Poznań, Polska.
22. M. Gierada, J. Handzlik, **Komunikat ustny:** “Theoretical studies on reaction mechanism of ethylene polymerization over the Phillips $\text{CrO}_x/\text{SiO}_2$ catalyst”, 59 Zjazd Naukowy PTChem 19-23 IX 2016, Poznań, Polska.
21. M. Gierada, J. Handzlik, **Poster:** “Non-metathesis transformations of phenylacetylene mediated by the 3rd generation ruthenium alkylidene catalyst”, 59 Zjazd Naukowy 2016 19-23 IX 2016, Poznań, Polska.

20. M. Gierada, J. Handzlik, **Poster:** “*Insights into mechanism of ethylene polymerization by the supported $\text{CrO}_x/\text{SiO}_2$ catalyst*”, Current Trends in Theoretical Chemistry VII – CTTC VII, 4-8 IX 2016, Kraków, Polska
19. M. Gierada, J. Handzlik, **Poster:** “*New insights into mechanism of ethylene polymerization over the $\text{CrO}_x/\text{SiO}_2$ catalyst*”, The 16th International Congress on Catalysis – ICC-16, 3-8 VII 2016, Pekin, Chiny.
18. M. Gierada, J. Handzlik, **Poster:** „*Active sites formation and theirs transformation in ethylene polymerization over the $\text{CrO}_x/\text{SiO}_2$ catalyst*”, 16th International Conference on Theoretical Aspects of Catalysis – ICTAC-16, 19-23 VI 2016, Zakopane, Polska.
17. M. Gierada, **Wykład na zaproszenie:** „*Costs of knowledge*”, Экономический вектор, Международной научно-практической студенческой конференции "Экономика и менеджмент", 14-16 IV 2016, Sankt Petersburg, Rosja.
16. M. Gierada, J. Handzlik, **Komunikat ustny:** „*Structure and redox properties of the monomeric and dimeric $\text{CrO}_x/\text{SiO}_2$ surface species – DFT studies*”, XLVIII Ogólnopolskie Kolokwium Katalityczne (XLVIII Polish Annual Conference on Catalysis), 16-18 III 2016, Kraków, Polska.
15. M. Gierada, J. Handzlik, **Poster:** „*Transformations of terminal alkynes catalysed by the 3rd generation Grubbs' catalyst*”, XLVIII Ogólnopolskie Kolokwium Katalityczne (XLVIII Polish Annual Conference on Catalysis), 16-18 III 2016, Kraków, Polska.
14. M. Gierada, **Komunikat Ustny:** „*Modelowanie molekularne jako wszechstronne narzędzie w rękach chemików*”, VIII Interdyscyplinarna Konferencja Naukowa TYGIEL 2016 „*Interdyscyplinarność kluczem do rozwoju*”, 12-13 III 2016, Lublin, Polska.
13. M. Gierada, J. Handzlik, **Poster:** „*Monomeric and dimeric chromium oxide species on silica surface*” 58 Zjazd Naukowy PTChem Gdańsk 2015 „*Polska Chemia w Mieście Wolności*”, 21-25 IX 2015, Gdańsk, Polska.
12. M. Gierada, J. Handzlik, I. Czeluśniak, **Komunikat ustny:** „*Dimerization and cyclotrimerization of phenylacetylene mediated by 3rd generation Grubbs' catalyst*” 58 Zjazd Naukowy PTChem Gdańsk 2015 „*Polska Chemia w Mieście Wolności*”, 21-25 IX 2015, Gdańsk, Polska.
11. M. Gierada, J. Handzlik, **Komunikat ustny:** „*DFT study of ethylene polymerization over the Phillips Cr/SiO_2 catalyst – reduction and initiation steps*” 14th Central European Symposium on Theoretical Chemistry, 6-9 IX 2015, Banská Bystrica, Słowacja.
10. A. Chakrabarti, M. Gierada, J. Handzlik, I.E. Wachs, **Komunikat ustny:** „*A combined *in situ* molecular spectroscopic and DFT study of ethylene polymerization by supported CrOx/SiO_2 Catalysts*” 250th American Chemical Society National Meeting & Exposition „*Innovation From Discovery To Application*”, 16-20 VIII 2015, Boston, MA, USA.

9. I. Czeluśniak, A.M. Trzeciak, J. Handzlik, M. Gierada, **Poster:** „Non-metathesis transformations of acetylenes mediated by second generation ruthenium alkylidene complexes” 3rd EuCheMS Inorganic Chemistry Conference, 28 VI – 1 VII 2015, Wrocław, Polska.
8. M. Gierada, J. Handzlik, **Komunikat ustny:** „Monomeric and dimeric chromium oxide species on silica surface – cluster and periodic DFT calculations” V научно-техническая конференция НЕДЕЛЯ НАУКИ, 25-27 III 2015, Sankt Petersburg, Rosja.
7. M. Gierada, **Komunikat ustny:** „Monoterpeny – co o nich wiemy”, VII Interdyscyplinarna Konferencja Naukowa TYGIEL 2015 „Interdyscyplinarność kluczem do rozwoju”, 21-22 III 2015 Lublin, Polska.
6. M. Gierada, J. Handzlik, I. Czeluśniak, **Poster:** „Phosphine-free ruthenium alkylidene complexes mediated dimerization of phenylacetylene” Ogólnopolskie Kolokwium Katalityczne OKK XLVII (Polish Annual Conference on Catalysis), 16-18 III 2015, Kraków, Polska.
5. M. Gierada, J. Handzlik, P. Michorczyk, **Komunikat ustny:** „Theoretical and experimental investigations of reduced Cr oxide species supported on silica” Ogólnopolskie Kolokwium Katalityczne OKK XLVII (Polish Annual Conference on Catalysis), 16-18 III 2015, Kraków, Polska.
4. M. Gierada, J. Handzlik, **Komunikat ustny:** „Reduced monomeric Cr oxide species on silica surface – cluster and periodic DFT calculations” Konferencja Użytkowników Komputerów Dużej Mocy 2015 (KU KDM'15), 11-13 III 2015, Zakopane, Polska.
3. M. Gierada, **Komunikat ustny:** „Structure of chromium(IV) and chromium(II) oxide species supported on silica. Cluster DFT Studies” Students International Conference in Yuriy Fedkovych National
2. M. Gierada, **Komunikat ustny:** „Structure of reduced chromium oxide species supported on silica. Cluster DFT Studies” Uczelniana Sesja Studenckich Kół Naukowych na Politechnice Krakowskiej; Sesja obcojęzyczna, międzynarodowa, 25 IV 2014, Kraków, Polska.
1. M. Gierada, R. Rachwałik, **Komunikat ustny:** „Rola reakcji ubocznych w procesie izomeryzacji α pinenu” VI Interdyscyplinarna Konferencja Naukowa TYGIEL 2014, 22-23 III 2014, Lublin.